IDENTIFICATION OF A FLUID-BASED MICROGLIAL ACTIVATION-DEPENDENT BIOMARKER PANEL

Ida-Mariette Pesämaa

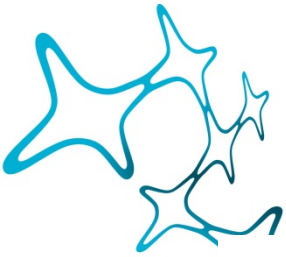

Graduate School of
Systemic Neurosciences

LMU Munich

Dissertation at the
Graduate School of Systemic Neurosciences
at Ludwig-Maximilians-University Munich

Dissertation der Graduate School of Systemic Neurosciences
der Ludwig-Maximilians-Universität München

31.03.2023

Supervisor
Prof. Dr. Dr. h.c. Christian Haass
Biomedizinisches Centrum (BMC), Biochemie, Ludwig-Maximilians-Universität München
Deutsches Zentrum für Neurodegenerative Erkrankungen (DZNE) e.V.

First Reviewer:	Prof. Dr. Dr. h.c. Christian Haass
Second Reviewer:	Prof. Dr. Christian Behrends
Third Reviewer:	Dr. Sabina Tahirovic
External Reviewer	Prof. MD PhD. Ville Leinonen

Date of Submission:	31.03.2023
Date of Defense:	22.09.2023

To my grandma, Varpu Pesämaa.

Popular science summary of the thesis

Alzheimer's disease is the most common cause of dementia, characterized by memory loss and other cognitive functions with a severity that interferes with a patient's everyday life. Today, 55 million people are living with dementia worldwide of which most are older than 65 years. The World Health Organization (WHO) has reported dementia as the seventh leading cause of death and one of the major causes of disability and dependency among elders.

Dementia is caused by a loss of neuronal cells, an irreversible condition known as neurodegeneration. The brain consists of different types of cells, with neurons being the best-known type of brain cell as these cells make up the signaling networks required for the brain to process and store of information. The maintenance of healthy neuronal networks requires a favorable environment for these cells. The aggregation of proteins or the remains of dead brain cells interfere with the brain environment and may become toxic. For example, in Alzheimer's disease two proteins named amyloid and tau are spreading and aggregating throughout the brain. These two toxic processes are the main hallmarks for Alzheimer's disease and are known to start decades before any symptoms become apparent.

The immune cells of the brain, known as microglia, only account for 10% of the brain cells but they carry out vital functions. Microglia use their long processes, covered with sensitive receptors, to constantly search the brain environment for any type of disturbance. Once microglia find an unwanted component in the environment, they change their appearance and adopt an activated signature. This activated signature makes it possible for microglia to respond, for example by surrounding the threat to prevent spreading, releasing inflammatory factors, or by removing the threat from the environment by engulfing it (a process called phagocytosis). Within the last decade, researchers have identified several factors that disturb the activation of microglia as risk factors for the development of late-onset Alzheimer's disease. This suggests that the activation of microglia is protective in Alzheimer's disease, and it has led to the emergence of microglia modulating therapies, with the hope to drive microglia to a protective activated state.

A major challenge for the field is to evaluate the activation states of microglia. To date, there is no easy-accessible and robust method to monitor the activation of microglia, which is urgently needed for the evaluation of microglia modulating therapeutics and to better select patients that would be suitable for clinical trials.

For my thesis, I have used different microglia models (mouse models and cultured microglia) to study the most opposite states of activation: non-activated microglia versus hyperactivated microglia. More specifically, I have used a method to quantitatively detect thousands of proteins and investigated these proteins to find those that are characteristic for the activated microglia. I then studied the proteins detectable in the fluid surrounding the brain (cerebrospinal fluid, CSF) of patients diagnosed with frontotemporal dementia. By comparing all these different proteins, in different conditions, I identified six proteins that appear to increase in dependence to the activation of microglia. Furthermore, I could confirm three of these proteins (FABP3, MDH1, and GDI1) as significantly increased in the CSF of Alzheimer patients as well as in the CSF of non-demented individuals with mild cognitive impairment (MCI) and confirmed amyloid pathology. This suggests that the levels of the three proteins increases in an amyloid-dependent manner.

Taken together, the findings presented in my thesis may be relevant for the evaluation of the microglial activation status in clinical practice and clinical trials modulating microglial activity and amyloid deposition.

Populärwissenschaftliche Zusammenfassung der Dissertation

Die Alzheimer-Krankheit ist die häufigste Form der Demenz. Sie ist zeichnet sich durch Gedächtnisverlust und Einschränkung anderer kognitiver Funktionen aus, wodurch der Alltag der Patienten negativ beeinflusst wird. Heute leben weltweit 55 Millionen Menschen mit Demenz, von denen die meisten älter als 65 Jahre sind. Die Weltgesundheitsorganisation (WHO) hat Demenz als die siebthäufigste Todesursache und eine der Hauptursachen für Behinderung und Abhängigkeit bei älteren Menschen angegeben.

Demenz wird durch den Verlust neuronaler Zellen verursacht, ein irreversibler Zustand, der als Neurodegeneration bekannt ist. Das Gehirn besteht aus verschiedenen Zelltypen, aber Neuronen sind die bekannteste Art Gehirnzellen. Sie bilden ein neuronales Netzwerk, welches für die Verarbeitung und Speicherung von Informationen verantwortlich ist. Die Aufrechterhaltung gesunder neuronaler Netzwerke erfordert eine günstige Umgebung für diese Zellen. Die Aggregation von Proteinen oder totem Zellmaterial stört die Umgebung der Gehirnzellen und kann toxisch werden. Bei der Alzheimer-Krankheit breiten sich beispielsweise zwei Proteine, die Amyloid und Tau genannt werden, aus und aggregieren im ganzen Gehirn. Diese toxische Prozesse sind das Hauptmerkmal der Alzheimer-Krankheit und beginnen bekanntlich Jahrzehnte bevor erste Symptome auftreten.

Die als Mikroglia bezeichneten Immunzellen des Gehirns machen nur 10% der Gehirnzellen aus, erfüllen aber lebenswichtige Funktionen. Mikroglia benutzen ihre langen Fortsätze, die mit empfindlichen Rezeptoren bedeckt sind, um die Umgebung des Gehirns ständig nach Störungen abzusuchen. Sobald Mikroglia einen unerwünschten Fremdkörper in der Umgebung finden, ändern sie ihr Aussehen und wechseln in einen aktivierten Status. Dieser aktivierte Status ermöglicht es Mikroglia zu reagieren, indem sie beispielsweise die Bedrohung umzingeln, um eine Ausbreitung zu verhindern, Entzündungsfaktoren freisetzen oder die Bedrohung aus der Umgebung entfernen, indem sie diese auffrisst, ein Prozess, der als Phagozytose bezeichnet wird. Innerhalb des letzten Jahrzehnts haben Forscher mehrere Faktoren identifiziert, die die Aktivierung von Mikroglia stören und als Risikofaktoren für die Entwicklung einer spät einsetzenden Alzheimer-Krankheit gelten. Dies deutet darauf hin, dass

die Aktivierung von Mikroglia bei der Alzheimer-Krankheit schützend wirkt und hat zur Entwicklung von Mikroglia-modulierenden Therapien geführt, um sie in einen schützenden, aktivierten Zustand zu versetzen.

Eine große Herausforderung für das Forschungsfeld ist die Bewertung der Aktivierungszustände von Mikroglia. Bis heute gibt es keine leicht zugängliche und robuste klinische Methode, um die Aktivierung von Mikroglia zu überwachen. Methoden zur Bewertung der Aktivierungszustände von Mikroglia sind dringen notwendig, um geeignete Mikroglia modulierende Therapien in klinischen Studien zu testen und Patienten, bei denen eine solche Therapie erfolgsversprechend scheint, auszuwählen.

Für meine Doktorarbeit verwendete ich verschiedene Mikrogliamodelle (Mausmodelle und kultivierte Mikroglia), um die gegensätzlichen Aktivierungszustände zu untersuchen: nicht aktivierte Mikroglia versus hyperaktivierte Mikroglia. Genauer gesagt habe ich eine Methode zur quantitativen Erkennung tausender Proteine eingesetzt und diese Proteine untersucht, um herauszufinden, welchen Proteine für aktivierte Mikroglia charakteristisch sind. Anschließend untersuchte ich Proteine im Liquor, einer Flüssigkeit, die das Gehirn umgibt, von Patienten mit diagnostizierter frontotemporaler Demenz. Durch den Vergleich all dieser verschiedenen Proteine unter verschiedenen Bedingungen konnte ich sechs Proteine identifizieren, die in Abhängigkeit von der Aktivierung von Mikroglia zuzunehmen scheinen. Darüber hinaus konnte ich drei dieser Proteine (FABP3, MDH1 und GDI1) als signifikant erhöht im Liquor von Alzheimer-Patienten sowie im Liquor von nicht dementen Personen mit leichten kognitiven Beeinträchtigungen (MCI) und mit bestätigter Amyloid-Aggregation nachweisen.

Zusammen können die beschriebenen Ergebnisse für die Bewertung des Mikroglia-Aktivierungsstatus in der klinischen Praxis und in klinischen Studien zur Modulation der Mikroglia-Aktivität und Amyloid-Ablagerung relevant sein.

Publications

Publications of the thesis

Pesämaa I, Müller SA, Robinson S, Darcher A, Paquet D, Zetterberg H, Lichtenthaler SF, Haass C. *"A microglial activity state biomarker panel differentiates FTD-granulin and Alzheimer's disease patients from controls"*. Mol Neurodegener. doi: 10.1186/s13024-023-00657-w (2023)

Other publications

Reifschneider, A., Robinson, S., van Lengerich, B., Gnörich, J., Logan, T., Heindl, S., Vogt, M. A., Weidinger, E., Riedl, L., Wind, K., Zatcepin, A., **Pesämaa, I.**, Haberl, S., Nuscher, B., Kleinberger, G., Klimmt, J., Götzl, J. K., Liesz, A., Bürger, K., Brendel, M., … Haass, C. "*Loss of TREM2 rescues hyperactivation of microglia, but not lysosomal deficits and neurotoxicity in models of progranulin deficiency"*. The EMBO journal, e109108 (2022)

van Lengerich B, Zhan L, Xia D, Chan D, Joy D, Park JI, Tatarakis D, Calvert M, Hummel S, Lianoglou S, Pizzo ME, Prorok R, Thomsen E, Bartos LM, Beumers P, Capell A, Davis SS, de Weerd L, Dugas JC, Duque J, Earr T, Gadkar K, Giese T, Gill A, Gnörich J, Ha C, Kannuswamy M, Kim DJ, Kunte ST, Kunze LH, Lac D, Lechtenberg K, Leung AW, Liang CC, Lopez I, McQuade P, Modi A, Torres VO, Nguyen HN, **Pesämaa I**, Propson N, Reich M, Robles-Colmenares Y, Schlepckow K, Slemann L, Solanoy H, Suh JH, Thorne RG, Vieira C, Wind-Mark K, Xiong K, Zuchero YJY, Diaz D, Dennis MS, Huang F, Scearce-Levie K, Watts RJ, Haass C, Lewcock JW, Di Paolo G, Brendel M, Sanchez PE, Monroe KM. "*A TREM2-activating antibody with a blood-brain barrier transport vehicle enhances microglial metabolism in Alzheimer's disease models*". Nat Neurosci. doi: 10.1038/s41593-022-01240-0. (2023)

Table of content

Abstract

Common features across several neurodegenerative diseases include microgliosis and astrogliosis. Cellular debris and extracellular protein aggregates are common triggers for the brain's immune system. Microglia, the resident macrophages of the brain, are highly plastic and respond rapidly to pathological changes. These immune cells use a variety of receptors to sense disturbances within the homeostasis of the brain environment. The activation of microglia is very complex and includes a wide repertoire of functions, including the release of inflammatory mediators, enhanced lysosomal function, metabolic capacity, and phagocytosis. With the emergence of microglial modulating therapies, the field is in urgent need of reliable biomarkers to measure microglial activation states, for (1) the stratification of patients for clinical trials, (2) the monitoring of target engagement, as well as for (3) prognostic evaluation.

Thus, I aimed to identify biomarker candidates for the assessment of microglial activation by studying activation-dependent changes in the lysates and secretome of microglia. In this study, I made use of both *in vivo* (mouse) and *in vitro* (human-induced pluripotent stem cell (iPSC)-derived microglia (hiMGL)) models, genetically modified to yield the two most opposite microglial activation phenotypes (*TREM2*-knockout modeling a homeostatic microglial state, versus *GRN*-knockout modeling a hyperactivated microglial state). Mass spectrometry-based proteomic analysis demonstrated that the opposite transcriptomic microglial phenotypes in *Grn*-knockout versus *Trem2*-knockout mice are very well conserved in the microglia proteome and at least in part reflected in the CSF proteome. Analysis of the proteome and secretome of monocultured hiMGL, with the same genotypic comparison, demonstrated that the findings in mice are partly translatable to the proteome and secretome of hiMGL. 33% of the proteins significantly increased in *Grn*-knockout mouse microglia are also appearing as significantly upregulated in the cell lysate of *GRN*-knockout hiMGL.

For further translation to the human microglial proteome, I analyzed the CSF proteome of heterozygous *GRN* mutation carriers suffering from frontotemporal dementia (FTD) (FTD-GRN). Comparing the human CSF proteome with the secretome of *GRN*-knockout hiMGL, I identified an overlap of 26 proteins that were significantly increased in both datasets. Out of

these 26 proteins, I selected a panel of six proteins ("*Panel 6*") as potential biomarkers for microglial activation: fatty acid binding protein 3 (FABP3), malate dehydrogenase 1 (MDH1), GDP dissociation inhibitor-1 (GDI1), macrophage-capping protein (CAPG), CD44, and glycoprotein non-metastatic B (GPNMB). The measured abundances of these six proteins were sufficient to successfully distinguish FTD-GRN patients as well as Alzheimer's (AD) patients from healthy controls. I confirmed elevated CSF levels of three of the Panel 6 proteins (FABP3, MDH1, GDI1) in patients diagnosed with AD as well as in individuals with mild cognitive impairment (MCI). Strikingly, the CSF levels of these three proteins were significantly different between MCI cases with and without detectable amyloid pathology. The separation of MCI patients according to their amyloid status, without the use of traditional AD biomarkers, is highly unique. Furthermore, this separation was statistically significant for each of the three proteins independently from each other, which emphasizes the potential of each of these biomarker candidates for stratification purposes. As an extracellular pathology, amyloid is known to activate microglia, which supports the suggestion of the proteins FABP3, MDH1, and GDI1 as dependent on microglial activation.

Taken together, the identified panel may be relevant for the evaluation of the microglial activation status in clinical practice and clinical trials modulating microglial activity and amyloid deposition.

1. Introduction

1.1. Frontotemporal dementia

Frontotemporal Dementia (FTD) is an umbrella term for several clinical syndromes and it is considered the second most common type of dementia in individuals younger than 65 years old, accounting for 5-15% of all dementia cases. FTD encompasses a heterogenous group of neurodegenerative disorders which vary in symptoms, pathology and heritability. Common for all disorders of FTD is the progressive deterioration of the frontotemporal neural networks, also known as frontotemporal lobar degeneration (FTLD) (Haass & Neumann, 2016; Mackenzie & Neumann, 2016).

FTD was first described in the 1890s by neuropsychiatrist Arnold Pick after characterizing several cases in which patients with progressive language disturbances showed the similar histopathological patterns located in the frontal and temporal brain regions (Pick, 1892). Initially, this combination of clinical and histological characteristics, was termed “Pick’s disease”. However, this was later changed to “dementia of frontal type” - a group of disorders to which include Pick’s disease. Today, FTD is diagnosed via consensus criteria based on clinical features, neuropathological phenotypes and genetical background (Boeve, Boxer, Kumfor, Pijnenburg, & Rohrer, 2022; Goedert, Ghetti, & Spillantini, 2012).

1.1.1. Symptoms and clinical classification of FTD

The frontal lobes perform a multitude of functions mainly associated with executive function and language comprehension, such as working memory, cognitive flexibility, inhibitory control, and basic language comprehension. The various functions of the frontal lobe are reflected in the heterogeneity of symptom characteristics observed in FTD (Seelaar, Rohrer, Pijnenburg, Fox, & van Swieten, 2011). Abnormalities in behavior and cognition is named behavioral variant FTD (bvFTD). A person suffering from bvFTD may come across as socially inappropriate, unreasonable, apathic, impulsive, compulsive, or unsympathetic. bvFTD is diagnosed according to empirically derived diagnostic criteria, which includes “possible bvFTD” and “probable bvFTD” in the diagnostic spectra (Boeve et al., 2022; Goedert et al., 2012; Rascovsky et al., 2011). Symptoms related to speech and language fall under the

diagnosis of primary progressive aphasia (PPA). As the disease progresses, the clinical phenotypes classified as bvFTD or PPA converge (Mackenzie & Neumann, 2016). The characteristic symptoms of PPA can be further distinguished, enabling the classification into clinical variants of PPA: logopenic variant (lv-PPA), semantic variant (sv-PPA), and non-fluent variant (nfv-PPA). In brief, lv-PPA is characterized by repetition and difficulties to retrieve words, while sv-PPA is recognized by fluent speech that lacks meaning, and finally, nfv-PPA is defined by agrammatical or slurred speech (Boeve et al., 2022; Goedert et al., 2012; Gorno-Tempini et al., 2011). Despite the defined clinical criteria for PPA variants, the classification can be challenging. Adding yet another layer of complexity, motorneuron disease (MND) in the form of amyotrophic lateral sclerosis (ALS) or atypical parkinsonism (mainly in the form of corticobasal degeneration (CBD) or progressive supranuclear palsy (PSP)), might be present in combination with bv-FTD or PPA (Boeve et al., 2022; Goedert et al., 2012) (Figure 1.1). About 15% of FTD patients also suffer from ALS (FTD-ALS) (Lomen-Hoerth, Anderson, & Miller, 2002). The common hallmark for all these disorders is the progressive degeneration of functional networks in the frontal and temporal lobes.

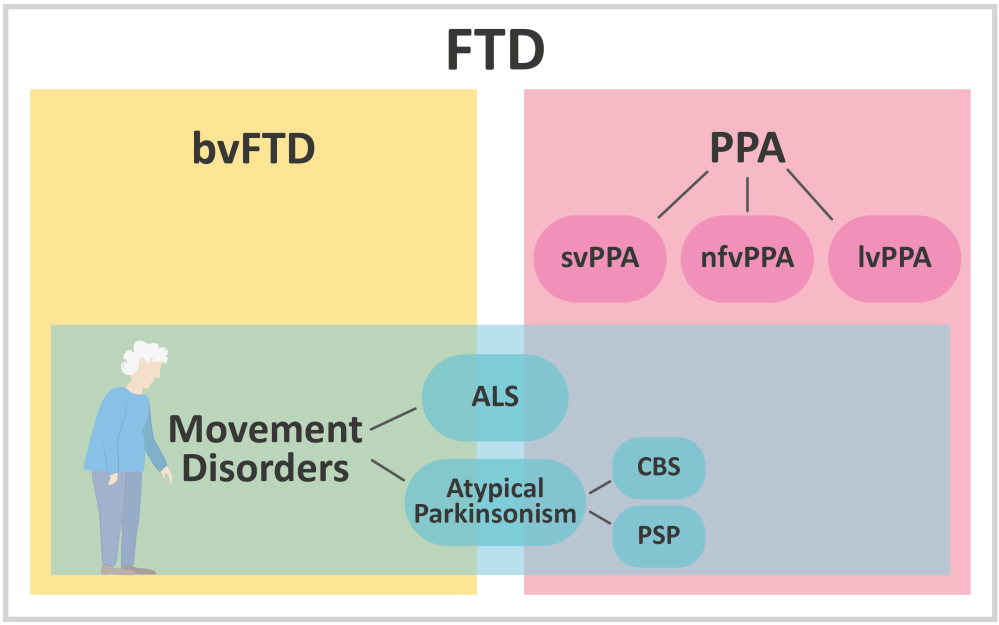

Figure 1.1. Clinical classification of frontotemporal dementia.
Schematic showing the classification of frontotemporal dementia (FTD) according to symptom characteristics: behavioral variant FTD (bvFTD) and primary progressive aphasia (PPA). PPA can be further classified according to semantic variant PPA (svPPA), non-fluent variant PPA (nfvPPA), or logopenic variant (lvPPA), depending on how the speech and language has been impaired. FTD may be accompanied by movement disorders in form of ALS or atypical parkinsonism (mainly corticobasal degeneration (CBD) or progressive supranuclear palsy (PSP)). Modified from Boeve et al. 2022.

1.1.2. Pathological characteristics of FTD

Neuropathologically, FTLD is commonly caused by one of three proteinopathies. The most common proteinopathy observed in FTD, present in approximately 50% of FTD cases, is the intracellular aggregation of transactive response DNA-binding protein 43 (TDP-43), while tau pathology is considered to be the second most common neuropathological cause of FTLD (Bahia, Takada, & Deramecourt, 2013; Haass & Neumann, 2016; Halliday et al., 2012; Mackenzie & Neumann, 2016; Neumann et al., 2006). Only 5-10% of FTD cases are characterized by neuropathological inclusions of the proteins fused in sarcoma (FUS), Ewing's sarcoma (EWS), or TATA-binding protein-associated factor 15 (TAF15) – collectively referred to as FET-positive inclusions (Haass & Neumann, 2016; Halliday et al., 2012; Mackenzie & Neumann, 2016) (Figure 1.2). The exact type of pathology appears to affect the clinical outcome. For example, FTD combined with motorneuron disease (FTD-MND) is associated with TDP-43 pathology, while tau pathology is associated with PSP and CBD (Josephs et al., 2011). Furthermore, in cases of genetic FTD, the type of pathology associates with mutation type (Haass & Neumann, 2016; Mackenzie & Neumann, 2016). According to the neuropathological characteristics, FTLD is classified into three main classes: FTLD-TDP, FTLD-tau, and FTLD-FET (Haass & Neumann, 2016; Mackenzie & Neumann, 2016) (Figure 1.2).

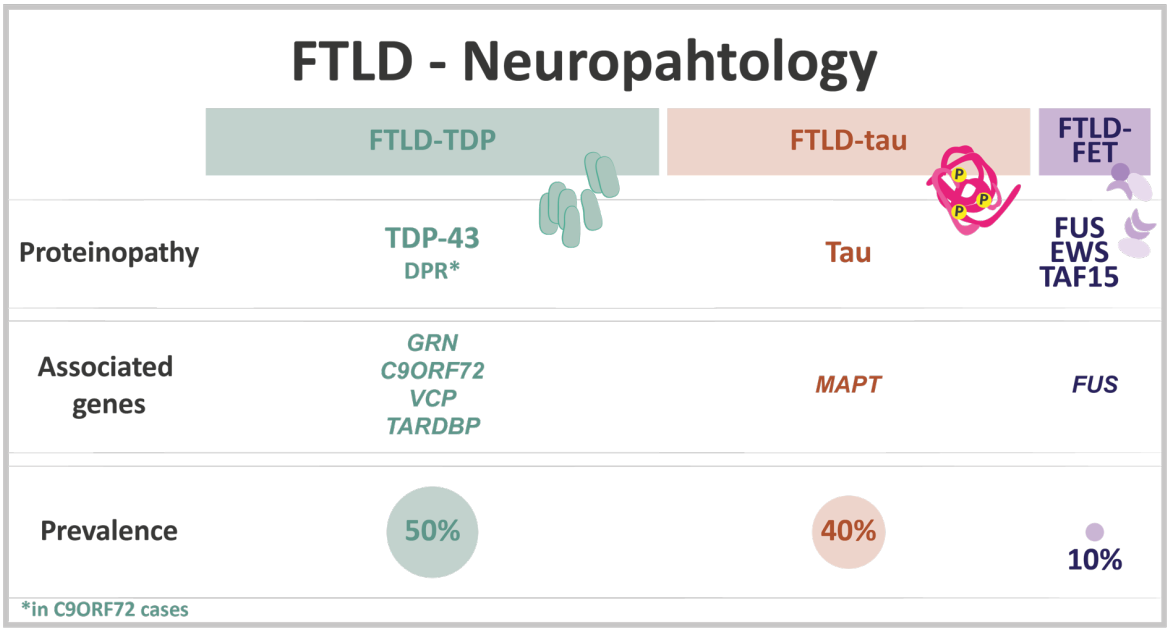

Figure 1.2. Neuropathological characterization of FTLD.
Schematic summarizing the neuropathological classification of frontotemporal lobar degeneration (FTLD). FTLD caused by TDP-43 pathology (FTLD-TDP) is the most common type. In cases of genetic FTLD-TDP where the *C9ORF72* gene is affected, the TDP pathology is accompanied by dipeptide repeat (DPR) pathology. FTLD caused by the accumulation of hyperphosphorylated tau (FTLD-tau) is the second most common type of FTLD. The least common type of FTLD is caused by FET-positive inclusions (including the proteins FUS, EWS, and TAF15) (FTLD-FET). In the genetic forms of FTLD, the type of FTLD is associated with the affected gene.

Abbreviations: TDP-43 = transactive response DNA-binding protein 43; GRN = progranulin (gene); C9ORF72 = chromosome 9 open reading frame 72; VCP = valosin containing protein; TARDBP = transactive response DNA-binding protein; MAPT = microtubule associated protein tau; FUS = fused in sarcoma; EWS = Ewing's sarcoma; TAF15 = TATA-binding protein-associated factor 15. Modified from Haass & Neumann 2016.

1.1.2.1. FTLD-TDP

FTLD-TDP is the most common type of FTLD and is characterized by neuropathology in form of ubiquinated inclusions, which is why this type of FTLD was previously referred to as FTLD-U (Bahia et al., 2013). This type of FTLD shows genetic association to the following genes: progranulin (*GRN)*, chromosome 9 open reading frame 72 (*C9ORF72*), valosin containing protein (*VCP*), as well as the gene encoding for transactive response DNA-binding protein (*TARDBP*) (Haass & Neumann, 2016). Under healthy conditions, TDP-43 shuttles between nucleus and cytoplasm, but is mainly localized within the nucleus where it binds DNA and RNA to regulate a variety of processes, including mRNA transport, splicing and transcription (Bahia et al., 2013). In a pathological context, TDP-43 is mislocalized, meaning that the protein is depleted from the nucleus and instead it accumulates in the cytosol of neurons. In the cytosolic environment, TDP-43 is prone to post-translational modifications (PTMs), such as C-terminal fragmentation, phosphorylation, and ubiquitination – all which affect the biochemical properties of the protein (Keating, San Gil, Swanson, Scotter, & Walker, 2022). TDP-43 has been identified as the major ubiquinated disease protein in FTLD-TDP (Bahia et al., 2013; Neumann et al., 2006). Mechanisms that regulate protein homeostasis are of central importance for the dysfunction and aggregation of TDP-43, such as the ubiquitin proteasome system (UPS), autophagy-lysosome pathway (ALP), heat-shock response (HSR), and chaperone-mediated autophagy (CMA) (Keating et al., 2022).

In both ALS and FTD, hexanucleotide repeat expansion (HRE) mutations within the *C9ORF72* gene cause dipeptide repeat (DPR) pathology. DPRs interfere with key components of the nucleocytoplasmic transport process, which causes mislocalization and cytoplasmic aggregation of TDP-43 (Keating et al., 2022). As a result, TPD-43 inclusion bodies are accompanied by DPR pathology in *C9ORF72* HRE mutation carriers (Keating et al., 2022; Mackenzie & Neumann, 2016) (Figure 1.2).

1.1.2.2. FTLD-FET

FTLD-FET only accounts for 5-10% of the FTLD cases and is characterized by neuropathological accumulation of FET-proteins, which includes the proteins FUS, EWS, and TAF15 (Haass & Neumann, 2016; Mackenzie & Neumann, 2016). Similar to TDP-43, these proteins are mainly localized in the nucleus where they bind to DNA and RNA with the purpose to regulate processes associated to transcription and DNA/RNA metabolism (Mackenzie & Neumann, 2012). In FTLD-FET, the family of FET proteins appear to co-localize in cytoplasmic and intranuclear inclusions in neuronal and glial cells (Mackenzie & Neumann, 2012; Neumann et al., 2011). The cytoplasmic inclusions are suggested to be derived from stress granules that occur due to an impaired nuclear import (Dormann & Haass, 2011). FTLD-FET is primarily considered to be of sporadic nature, although a few FTLD-FET cases have been associated with mutations in the *FUS* (Haass & Neumann, 2016; Mackenzie & Neumann, 2016) (Figure 1.2).

1.1.2.3. FTLD-Tau

Tau, encoded by the *MAPT* gene, is a protein involved in the assembly and maintenance of microtubules, which makes it especially important for axonal stabilization and transport within neurons (G. Lee & Leugers, 2012). Diseases associated with dysfunctional tau are referred as to tauopathies and are characterized by the hyperphosphorylation of tau and the consequential formation of insoluble filaments that accumulate within neuronal and glial cells (Bahia et al., 2013; Mackenzie & Neumann, 2016). FTLD-tau is a primary tauopathy, characterized by the intracellular deposits of hyperphosphorylated tau. The majority of cases are of sporadic nature, although there are mutations within the *MAPT* gene that associate with FTLD-tau (Bahia et al., 2013) (Figure 1.2).

1.1.3. The etiology of FTD

Familial FTD (f-FTD) is estimated to account for 30% of the total FTD cases (https://www.allftd.org/ftld). However, the prevalence of f-FTD varies across diagnostic spectra and is not always associated with genetic status. For instance, 48% of bvFTD cases have been considered familial, while for PPA only 12% were strongly linked to family history (Greaves & Rohrer, 2019; Wood et al., 2013).

Reported by two independent studies, 18-19% of all FTD cases appear to have a monogenic cause, meaning that these cases are caused by an alternation within a single gene (Blauwendraat et al., 2018; Wagner et al., 2021). The most common pathogenic variants, found in 60% of f-FTD cases, occur in one of three genes: *C9ORF72*, *GRN*, or *MAPT* (Baker et al., 2006; Loy, Schofield, Turner, & Kwok, 2014; Olszewska, Lonergan, Fallon, & Lynch, 2016; Takada, 2015). As mentioned, each FTD-associated gene is linked to a certain proteinopathy (Figure 1.2). However, there are a few tau-negative cases that cannot be classified as FTLD-TDP nor FTLD-FET. Exceptional cases include a type of f-FTD caused by mutations in the *CHMP2B* gene, encoding for the protein charged multivesicular body protein 2b (Mackenzie & Neumann, 2016).

The Genetic FTD initiative (GENFI) is a consortium including European and Canadian research centers focusing on f-FTD. Participants are enrolled at a symptomatic or pre-symptomatic stage, with a confirmed mutation in any of the FTD-associated genes. Thus, the GENFI study enables the investigation of FTD in a longitudinal manner, including the earliest stages of FTD (genfi.org). Remarkably, brain abnormalities have been detectable in pre-symptomatic participants of the GENFI cohort >10 years before the expected symptom onset (Bocchetta et al., 2021; Gordon, Rohrer, & Fox, 2016; Sudre et al., 2019).

1.1.4. Biomarkers in FTD

Fluid biomarkers are available to identify FTD with an underlying genetic cause. For *GRN* mutation carriers, a reduction of progranulin levels can be easily detected in cerebrospinal fluid (CSF) or blood (Finch et al., 2009; Ghidoni, Benussi, Glionna, Franzoni, & Binetti, 2008; Meeter, Patzke, et al., 2016; Sleegers et al., 2009). Individuals carrying a *C9ORF72*-mutation can be identified early on by increased CSF levels of poly-GP dipeptide repeats (Gendron et al., 2017; Lehmer et al., 2017). Unfortunately, there are still no biomarkers for the detection TDP-43 pathology, primary tauopathies, or FET proteinopathy, which are the main neuropathological characteristics of FTD (Figure 1.2). As a result, the diagnosis of sporadic FTD is heavily relying on neuropsychological assessments and is very complicated in comparison to the diagnosis of genetically caused FTD (Swift et al., 2021).

Due to the lack of FTD-specific biomarkers, non-specific biomarkers of tau pathology and neurodegeneration are used for the prognosis of FTD and as an exclusionary diagnostic criterion (Swift et al., 2021). AD biomarkers are of special relevance as symptom characteristics of bvFTD and AD may be very similar (Boeve et al., 2022; Swift et al., 2021). For this purpose, plasma levels of phosphorylated tau (p-tau), especially p-tau181 and p-tau217, are used to differentiate FTD from AD as these levels are increased in AD patients but not in FTD (Palmqvist et al., 2020; Thijssen et al., 2020). Without a clear explanation, AD biomarkers in form of different amyloid β (Aβ) species (Aβ38, Aβ40 and sAPPβ) appear as decreased in the CSF of FTD patients, which might complicate the distinction between FTD and AD (Gabelle et al., 2011; Swift et al., 2021).

To distinguish FTD from non-neurodegenerative disorders, markers of neurodegeneration, such as plasma or CSF levels of neurofilament light (NFL), may be used to confirm neurodegeneration (Swift et al., 2021). More specifically, NFL is a marker for neuroaxonal damage, which has been reported to increases three to four-fold at the time of onset of FTD (Meeter, Dopper, et al., 2016; Ntymenou et al., 2021). Furthermore, NFL and may be used as a prognostic marker for evaluating the course of neurodegeneration in FTD (Swift et al., 2021; van der Ende et al., 2019). Neuroimaging can be used to further support the diagnosis of FTD (theaftd.org). Structural magnetic resonance imaging (MRI) may be used to study the pattern of brain atrophy, which is rather defined for each of the clinical and neuropathological variants of FTD (Whitwell, 2019). MRI enables the evaluation of white and gray matter abnormalities, which are detectable 5-10 years before symptom onset in cases with genetic FTD (Panman et al., 2019). If required for further elucidation of the FTD diagnosis, (18F)-fluorodeoxyglucose-positron emission tomography (FDG-PET) may be used to evaluate functional changes within the process of glucose metabolism. This is of relevance as hypometabolism is a commonly observed characteristic in FTD-patients and have been reported to appear already at pre-symptomatic stages before any brain abnormalities are detectable with MRI (Panman et al., 2019; Swift et al., 2021; Whitwell, 2019).

1.2. Alzheimer's disease

In 1901 German physician Alois Alzheimer took on the case of 51-year-old Auguste Deter. Alzheimer conducted several detailed interviews with Mrs. Deter and documented the progressive cognitive impairment, the hallucinations and delusions that he observed. "I have lost myself" were the famous words that Mrs. Deter herself used to describe her condition. After Mrs. Deters death in April 1906, Alzheimer carefully studied and described both the clinical and histopathological characteristics of the disease that now is known as Alzheimer's disease (AD) (Alzheimer, Stelzmann, Schnitzlein, & Murtagh, 1995).

AD is a progressive neurodegenerative disease and the most common cause of dementia with an estimation of 60-70% of all dementia cases. Age is the greatest risk factor for AD and as the global population is aging the cases of dementia is expected to rise tremendously, which will challenge the world's social and economic systems (Alzheimer Association 2022; World Health Organization 2022). By 2030, the worldwide care costs are projected to rise to a total of 2 trillion USD, an increase of >40% compared to the 181 billion USD that were spent on dementia care in 2015. With no cure available, these data and predictions suggest that dementia should be considered a public health priority (WHO, 2017).

1.2.1. Symptoms of AD

Signs of dementia may appear as disorientation of time and place, personality changes, memory and language impairments, all which may complicate a person's daily routine (Alzheimer et al., 1995) (Alzheimer's Association 2022). Symptoms become apparent when functional brain networks are disrupted and neurons start to degenerate, with the degree of atrophy correlating with the severity of the symptoms (Ashton et al., 2021; C. R. Jack et al., 2010; Lewczuk et al., 2018; Mouton PR, 1998; Sanchez-Valle et al., 2018). Early symptoms of AD may be very subtle and difficult to notice. In some cases, symptoms are only recognized by the individual affected and their family members, cognitive impairments that are prominent enough to be evaluated but not severe enough to be classified as dementia. These characteristics are usually described as mild cognitive impairment (MCI) (Petersen et al., 2017) (Alzheimer Association 2022 (MCI)). When subjects raise concern regarding their memory but no abnormalities in memory or cognition can be measured, this may be referred to as subjective cognitive impairment (SCI) or subjective memory complaint (SMC) (Reisberg &

Gauthier, 2008; Reisberg et al., 2008). For cross sectional studies SCI/SMC and MCI are often included as representations of very early stages of dementia, which is of particular importance for biomarker studies with the aim to identify or characterize early biomarkers.

1.2.2. Neuropathological characteristics of AD

AD is mainly defined by two neuropathological features: amyloid plaques and hyperphosphorylated tau forming intracellular neurofibrillary tangles (NFTs). These two characteristics were part of the histopathological findings described by Alois Alzheimer more than 100 years ago and are still considered the main pathological hallmarks of Alzheimer's disease, of which today's diagnostic tools are based on (Alzheimer et al., 1995; Jack CR Jr, 2016).

1.2.2.1. Amyloid β-peptide

The pathological amyloid plaques are formed by progressive accumulation of amyloid β (Aβ) peptides in the extracellular space (De Strooper & Karran, 2016; Haass, 2004; Haass & Selkoe, 1993; M. P. Lambert et al., 1998). The pathological mechanism underlying the formation of amyloid plaques (the core-signature of AD) is the proteolytic processing of amyloid precursor protein (APP). Consecutive cleavages of APP yield either the AD-causing Aβ fragment or a non-detrimental fragment called p3 (Haass, Koo, Mellon, Hung, & Selkoe, 1992; Haass, Schlossmacher, et al., 1992; Haass & Selkoe, 1993, 2007). The proteolytic processing of APP can therefore be described according to two pathways, the amyloidogenic and the non-amyloidogenic (Figure 1.3). The key players in the APP cleavage are three secretases: α, β, and γ. Cleavage by α-secretase yields the non-amyloidogenic fragments: sAPPα, p3, and APP intracellular domain (AICD). In the amyloidogenic pathway, APP is first proteolytically processed by β-secretase (generating sAPPβ), whereupon, the remaining C99 fragment is processed by γ-secretase to yield Aβ peptides (Figure 1.3) (De Strooper & Karran, 2016; Haass, Kaether, Thinakaran, & Sisodia, 2012; Haass & Selkoe, 1993; Selkoe, 2001). The generated Aβ peptides are at least 37 amino acids long, with the length depending on the exact site where γ-secretase cleaves the C99 fragment. The Aβ peptide composed of 40 amino acids (Aβ40) is the most common of all Aβ species (80-90%), while the slightly longer fragment, Aβ42, accounts for 5-10% of the total Aβ species (Murphy & LeVine, 2010). The Aβ42 species is of hydrophobic nature, thus prone to deposit as oligomers, fibrils and ultimately plaques. In fact,

Aβ42 is the most common Aβ species found in the neurotoxic Aβ plaques (Haass, 2004; Haass & Selkoe, 1993; Murphy & LeVine, 2010). Shorter Aβ peptides, such as Aβ40 and Aβ38, are less hydrophobic than Aβ42 and are therefore these Aβ species tend to remain soluble in the interstitial fluid (Mawuenyega et al., 2010). Recently, a study investigating the CSF levels of Aβ38 revealed a protective effect of this peptide, independently of Aβ42 levels. In AD patients from two independent cohorts, high Aβ38 levels in CSF correlated with a slower cognitive decline (Cullen et al., 2022).

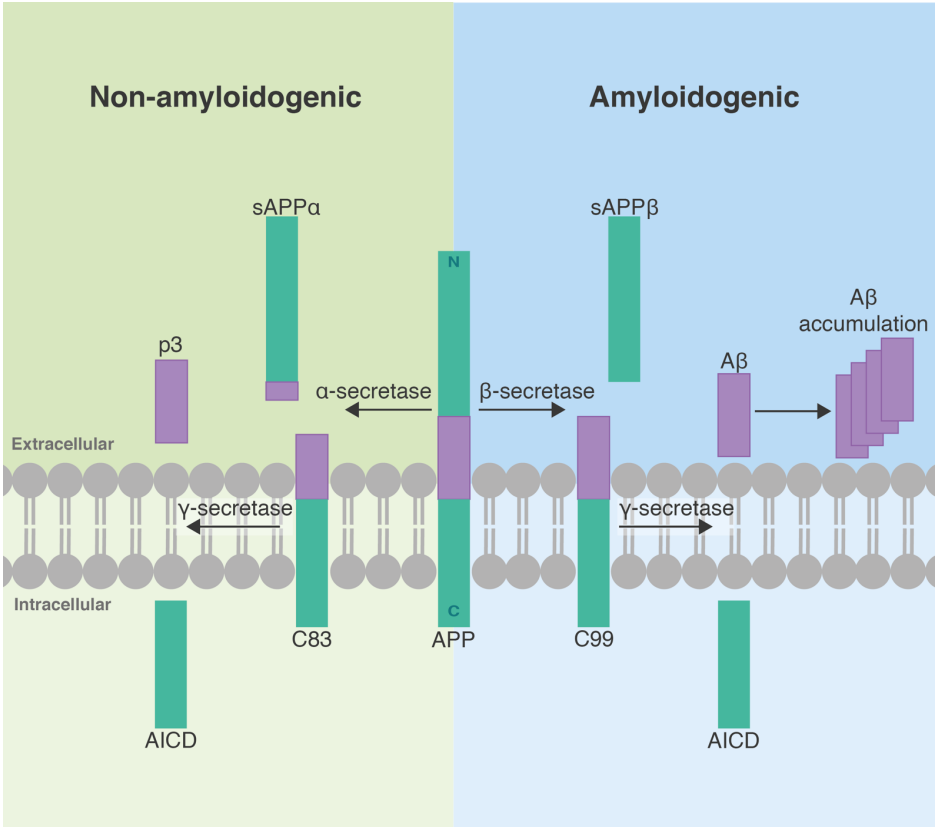

Figure 1.3. Proteolytic processing of amyloid precursor protein (APP).
Schematic representation of the proteolytic processing of amyloid precursor protein (APP), following either the non-amyloidogenic (left) or amyloidogenic (right) pathway. APP is a type-1 transmembrane protein with cytoplasmic C- and exoplasmic N-terminus. In the non-amyloidogenic pathway, APP is first cleaved by α-secretase, followed by an intramembranous cleavage by γ-secretase. While in the amyloidogenic pathway APP is first proteolytically processed by β-secretase, and then cleaved within the transmembrane domain by γ-secretase. This will generate aggregation prone Aβ species. Abbreviations: sAPPα/β = soluble APPα/β, AICD = APP intracellular domain, Aβ = amyloid β. Modified from Haass et al. 2012.

1.2.2.2. Tau

The extracellular accumulation of Aβ is followed by hyperphosphorylation and intracellular aggregation of tau and eventually neuronal death (C. R. Jack et al., 2010). Through alternative splicing of the MAPT gene, tau is expressed in six isoforms and depending on the isoform tau

will have either three (3R) or four (4R) repeats of microtubule binding domains (Goedert, Spillantini, Jakes, Rutherford, & Crowther, 1989; Goedert, Spillantini, Potier, Ulrich, & Crowther, 1989). In a healthy state, tau is one of three neuronal microtubule-associated proteins with the role to stabilize microtubules and the tau-microtubule interaction is dynamically regulated by phosphorylation of tau. In AD, tau becomes dysfunctional and hyperphosphorylated due to causes that are not yet fully understood. The hyperphosphorylation of tau destabilizes the tau-microtubule complex and instead the protein becomes misfolded and aggregates into insoluble tau tangles (Virgilio et al., 2022).

1.2.2.3. The amyloid cascade hypothesis

This order of pathological sequences: the formation of extracellular amyloid plaques, then the intracellular aggregation of tau, followed by neurodegeneration, is known as the amyloid cascade hypothesis (ACH) (J. Hardy & Selkoe, 2002; J. A. Hardy & Higgins, 1992; Selkoe & Hardy, 2016). The underlying mechanisms for the relationship between amyloid and tau are yet to be unraveled. Several studies, including both *in vivo* and *in vitro* models, suggest that a reduction or depletion of tau impedes Aβ-induced neuronal dysfunctions (Chang, Shao, & Mucke, 2021; Ittner et al., 2010; Roberson et al., 2007). Recently reported, tau abnormalities in form of tau phosphorylated at threonine 231 (p-tau231) was observed at even earlier stages than the detection aggregation of amyloid (Ashton et al., 2022). The phosphorylation of tau adds yet another layer of complexity to the ACH, as the different tau species may differ depending on disease stage and in regards to other disease characteristics (such as amyloid and cortical atrophy) (Barthelemy et al., 2020).

As the traditional outline of the ACH did not address the immune responses of the brain, an updated version, including microglial responses for each step throughout the cascade, has recently been proposed (Haass & Selkoe, 2022). It is well known that microglia react to extracellular pathology, like Aβ aggregates, by initiating an activation repertoire (Paolicelli et al., 2022). This suggests that microglial changes are present at the time of amyloid abnormalities, which has been detected decades before symptom onset (Buchhave et al., 2012; C. R. Jack et al., 2010). In fact, there is already substantial evidence supporting the proposal of microglial activation as an early response to neuropathology (Morenas-Rodriguez et al., 2022).

1.2.3. Etiology of AD

Following the amyloidogenic pathway, amyloid aggregation depends on the equilibrium of Aβ production, Aβ clearance, and the rate of transition from soluble Aβ to insoluble fibrils. This mechanistic interplay, with Aβ accumulating over time, explains age as the main risk factor for developing AD (Haass, 2004). The majority (90-95%) of AD cases are considered to be sporadic (Harman, 2006; Masters et al., 2015). In sporadic AD, symptoms become apparent at an age of 65 years or older, which defines late-onset AD (LOAD). In contrast, 5-10% of AD patients may develop symptoms before an age of 65 years and are therefore diagnosed with early-onset AD (EOAD) (Dai, Zheng, Zeng, & Zhang, 2018). Age of symptom onset is not the only feature that is different between LOAD and EOAD, but the two categories are also distinguishable by genetics, clinical condition and disease progression (Mendez, 2017). In regard to genetics, LOAD is a highly polygenic disease with the involvement of a several genetic factors and an estimated non-Mendelian heritability of 60-80%. The most common gene associated with LOAD is *APOE,* encoding for the protein apolipoprotein E (Raulin et al., 2022). Other genes associated with an increased risk of LOAD include *BIN1* (encoding for bridging integrator 1), *PICALM* (encoding for phosphatidylinositol binding clathrin assembly protein), *TREM2* (encoding for triggering receptor expressed on myeloid cells 2)*, and SORL1* (encoding for sortilin-related receptor 1) – all of central importance for the clearance of pathological amyloid via functions associated with the brain-residence macrophages known as microglia (Guerreiro et al., 2013; Hansen, Hanson, & Sheng, 2018; Jonsson et al., 2013). In general, the risk of developing AD is 3.5 times greater for individuals with a first-degree relative suffering from AD (van Duijn et al., 1991). Importantly, familial diseases are not completely based on common genetics (not considering autosomal dominant transmission), instead the observed correlation is likely to be affected by complex combinations of several genes as well as the lifestyles that are often very similar between first degree relatives (Loy et al., 2014). In contrast to LOAD, the heritability for EOAD is estimated to reach 92-100% (Mol et al., 2022). To date, three genes have been identified as causative genes for EOAD, namely: *APP*, *PSEN1* (encoding for presenilin 1), and *PSEN2* (encoding for presenilin 2) (Y.-w. Zhang, Thompson, Zhang, & Xu, 2011). While LOAD is likely to be affected by age-related processes, EOAD appears to have stronger genetic causes, which is likely to explain the faster disease-progression that is observed in EOAD cases compared to LOAD cases (Tellechea et al., 2018).

1.2.3.1. Genetics affecting the APP processing

Less than 1% of all AD cases are considered to be mendelian AD, caused by autosomal dominant mutations in one of the three causative genes: *APP*, *PSEN1*, or *PSEN2* (Bekris, Yu, Bird, & Tsuang, 2010; Blennow, de Leon, & Zetterberg, 2006; Campion et al., 1999; Loy et al., 2014; Pavisic et al., 2020). In the context of autosomal dominant AD (ADAD), several missense mutations have been reported within the *APP* gene, of which 31 mutations have been proven to be pathogenic. All the reported APP mutations are all located within or in close proximity to the α-, β-, and γ-secretase cleavage sites, which play a central role in APP proteolysis (Bateman et al., 2011; Bi, Bi, & Li, 2019; Tomiyama & Shimada, 2020; Weggen & Beher, 2012). One of the most studied mutations located within the *APP* gene is the KM670/671NL mutation, which is commonly referred to as the Swedish mutation. The Swedish mutation is a double mutation, consisting of two amino acid substitutions (lysine to asparagine and methionine to leucine) located at the cleavage site of β-secretase (Haass et al., 2012; Mullan et al., 1992). This exchange in amino acids increases the affinity of APP as a substrate to β-secretase, which ultimately causes an increased production of total Aβ (Citron et al., 1992; Haass et al., 2012). Other APP mutations, such as the "Arctic" E693G mutation, is closer located to the α-secretase cleavage site and increases the aggregation properties of Aβ (Nilsberth et al., 2001).

The presenilins, PSEN1 and PSEN2, are known as the catalytic core of γ-secretase. As a consequence, mutations within the *PSEN1* or *PSEN2* genes affect the ability of γ-secretase to perform intramembrane hydrolysis, which interferes with the proteolytic processing of APP and consequently increases the generation of longer amyloidogenic peptides such as Aβ42 (De Strooper, 2007; De Strooper, Iwatsubo, & Wolfe, 2012; Weggen & Beher, 2012). The fact that all three AD-deterministic genes are key players in Aβ generation, emphasizes the pivotal role of APP processing in the development of AD and strongly supports the ACH.

1.2.3.2. The genetic implications of APOE in AD

APOE is the most common genetic risk factor for the development of LOAD and it is estimated to affect more than 50% of all AD cases (Raulin et al., 2022). *APOE* is polymorphic and has three common alleles: *APOE* ε2 is the least common and appears to be protective against AD, *APOE* ε3 is the most common and does not affect the risk of developing AD, and *APOE* ε4

which significantly increases risk of AD although the prevalence estimates are highly diverse (Corder et al., 1993; Loy et al., 2014; Ward et al., 2012) (Alzheimer Association 2022 (AD Genetics)). Although the mechanism is not entirely clear, APOE appears to be of importance for the process of plaque compaction, probably carried out in order to reduce spreading of the soluble and most likely neurotoxic forms of Aβ (Bales et al., 1999; Holtzman, Bales, et al., 2000; Holtzman, Fagan, et al., 2000; Mahan et al., 2022; Parhizkar et al., 2019).

1.2.4. Biomarkers in AD

Despite the heterogeneity between and within the groups of LOAD and EOAD, all forms of AD share the neurological characteristics of amyloid pathology. Thus, amyloid is of central importance for the diagnosis of AD.

1.2.4.1. Fluid biomarkers in AD

The degree of Aβ aggregation in the brain parenchyma can be measured by using immunoassays to determine the levels of free Aβ in the CSF. As Aβ aggregates into fibrils and plaques in the brain, less amyloid is to be measured in the CSF, which is why a reduction of certain Aβ species ($A\beta_{42}$ or ratio of $A\beta_{42}$ /$A\beta_{40}$) in CSF reflects an increase of Aβ aggregation in the brain (Blennow & Zetterberg, 2015a, 2015b; Doecke et al., 2020; C. R. Jack, Jr. & Vemuri, 2018; Shaw et al., 2009). Abnormal levels of CSF Aβ can be detected up to 24 years before symptoms become apparent (McDade et al., 2018). In addition, tau-based measures are used for a more reliable diagnosis and prognosis of AD and the degree of neurodegeneration. Total tau (t-tau) can be measured in CSF and plasma as a marker neurodegeneration, meaning that t-tau does not show any AD-specific correlation but rather correlates with cognitive decline (C. R. Jack, Jr. & Vemuri, 2018; Marks et al., 2021; Mielke et al., 2017; Wirth et al., 2013). Instead, different p-tau species are measured in both CSF and plasma (commonly p-tau181), which may be AD specific (depending on the p-tau species) (Karikari, Ashton, Zetterberg, & Blennow, 2022; Palmqvist et al., 2021). As mentioned, increased levels of CSF p-tau231 can be measured prior to amyloid abnormalities (Ashton et al., 2022). For prognostic purposes and to confirm a neurodegenerative status, NFL levels may be measured in CSF or plasma (Lewczuk et al., 2018; Zetterberg, 2016). Even though NFL is a robust marker for neurodegeneration it is not specific for AD (Zetterberg, 2016; Zetterberg & Blennow, 2021).

1.2.4.2. Imaging-based biomarkers in AD

As an alternative to the evaluation of CSF-Aβ levels, amyloid pathology may also be assessed and monitored using amyloid-PET. The assessment of amyloid pathology using CSF- versus PET-based modalities (with amyloid ligands [18F] florbetapir, Pitsburgh compound-B (PiB), or flutemetamol) have been evaluated in many studies, revealing a generally high diagnostic ability for each method as well as a high concordance between CSF and PET (Blennow, Mattsson, Scholl, Hansson, & Zetterberg, 2015). In addition to amyloid-PET, tau-PET may be used to evaluate intracellular tau inclusions. Similar to CSF t-tau, tau-PET alone is not intended for a definite AD diagnosis. However, tau-PET provide complementary information regarding disease state and stage, which is highly important for the prognostic evaluation of AD (Schöll et al., 2019). Complimentary information regarding disease state and stage may also be provided by evaluating the status of brain atrophy (using MRI) or brain metabolism (using FDG-PET). Both MRI and FDG-PET are useful for prognostic purposes, but neither of them is specific for AD (Blennow et al., 2006).

1.2.5. Diagnosis of AD

In 2016, the "A/T/N" framework was introduced for the diagnosis of AD, novel in the sense that it did not rely on cognitive tests or neuropsychological evaluation. The system uses a binary evaluation ("+" or "-") to address each of the core pathophysiologies of AD: "A" = amyloid (measured as amyloid-PET intensity or CSF $A\beta_{42}$ levels), "T" = tau (measured as tau-PET intensity or p-tau levels in CSF or plasma), and "N" = neurodegeneration or neuronal injury (FDG-PET, MRI, or t-tau) (Blennow et al., 2015; Blennow & Zetterberg, 2015a; Jack CR Jr, 2016) (Figure 1.4). This systematic strategy for AD diagnosis, with the neuropathological characteristics in focus, turned out to be very efficient and resulted in an updated definition of AD (C. R. Jack, Jr. & Vemuri, 2018). Since then the A/T/N framework has been widely used to diagnose AD and to stratify patients for clinical studies.

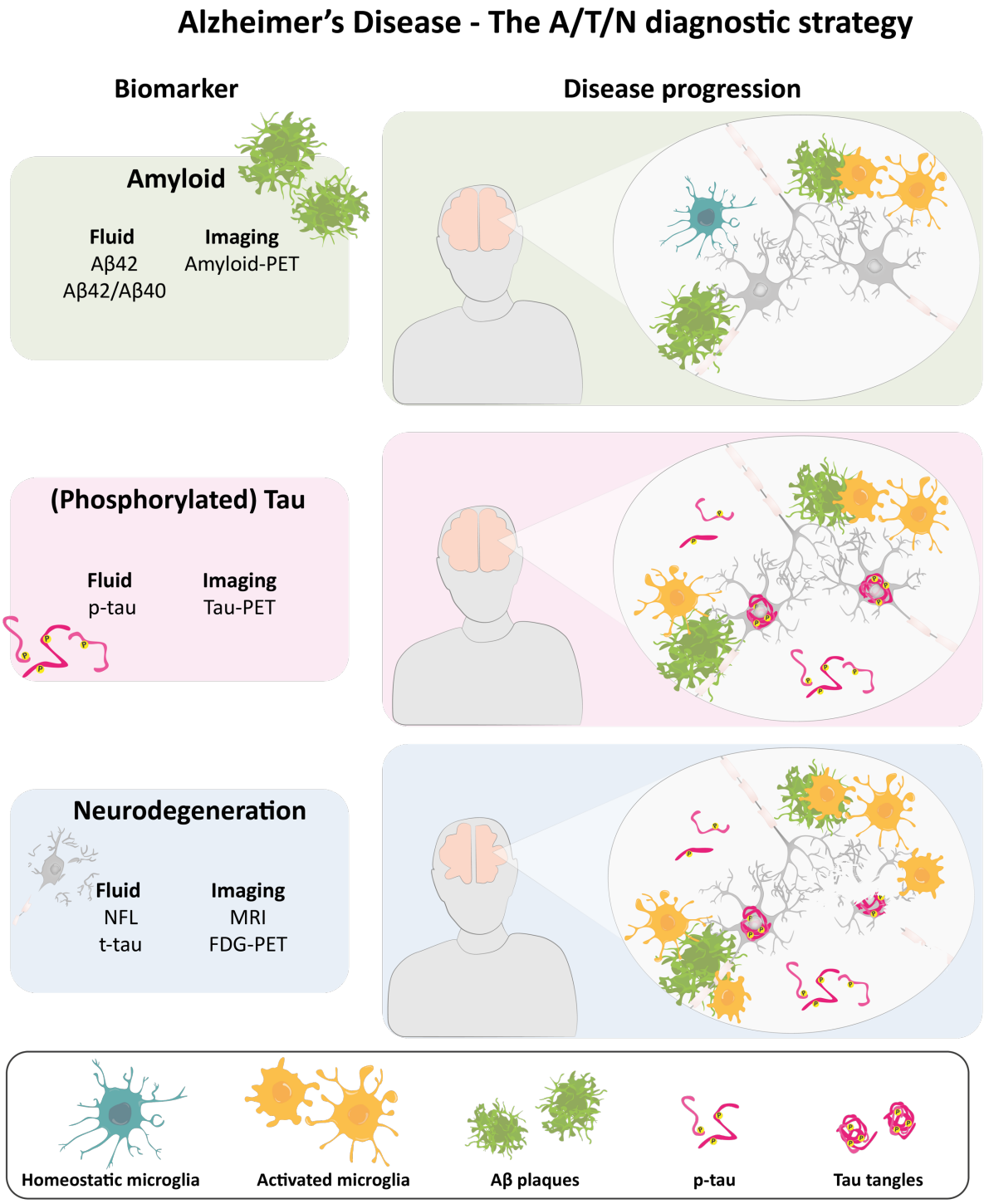

Figure 1.4. The A/T/N framework for diagnosis of Alzheimer's disease.

The current strategy for diagnosis of AD based on amyloid pathology (A), tau pathology (T), and neurodegeneration (N), with the addition of the expected microglial activation status throughout the course of the disease. Abbreviations: Aβ42/Aβ40 = ratio: amyloid β 42 amino acids long/ amyloid β 40 amino acids long; PET = positron emission tomography; p-tau = phosphorylated-tau; NFL = neurofilament light; t-tau = total-tau; MRI = magnetic resonance imaging; FDG-PET = [18F]-fluorodeoxyglucose-PET.

1.3. The role of microglia in neurodegeneration

As the innate immune cells of the central nervous system (CNS), microglia are essential for the maintenance of CNS homeostasis and play a pivotal role in development, health and disease (Lewcock et al., 2020; Prinz, Masuda, Wheeler, & Quintana, 2021; Prinz & Priller, 2014). Microglia account for approximately 10% of the total cell population in a healthy brain, a context in which microglia are ramified and use a multitude of fine processes to survey the brain environment (Colonna & Butovsky, 2017; Deczkowska, Amit, & Schwartz, 2018; Nimmerjahn, Kirchhoff, & Helmchen, 2005; Prinz et al., 2021; Ransohoff & El Khoury, 2015; Salter & Stevens, 2017).

For over a decade, genome-wide association studies (GWAS) have been used to identify several LOAD-related risk variants located within genes that are highly or selectively expressed by microglia (Hansen et al., 2018; Jonsson et al., 2013; J. C. Lambert et al., 2013; McQuade & Blurton-Jones, 2019; Ulrich, Ulland, Colonna, & Holtzman, 2017) (Table 1.1). In addition, a protective variant (P522R) has been identified within the *PLCG2* gene (encoding for phospholipase C-γ2) (Sims et al., 2017). This protective variant enhances microglial functions such as phagocytosis and inflammatory response, including increased secretion of cytokines and enhanced antigen presentation (Claes et al., 2022; Takalo et al., 2020). This genetic evidence revealed the critical involvement of microglia in disease progression and broadened the previously neuro-centric perspective (De Strooper & Karran, 2016). Thus, the importance of microglia in healthy aging and disease is no longer questioned. In fact, the modulation of microglial functions is considered as an innovative therapeutic approach and microglial modulating therapies have already demonstrated very promising potential in preclinical trials (Lewcock et al., 2020). Lastly, microglial activation is no longer considered to be a binary switch, but a complex and dynamic combination of processes that are context-, disease-, and disease stage-dependent, all which is to be considered when determining the beneficial versus detrimental effects of microglial activation, (Paolicelli et al., 2022).

Microglia and AD - The genetic evidence

Gene	Microglial function	Genetic variant
TREM2	Receptor important for cell survival and phagocytic function	R47H, R62H, T66M, H157Y
ABI3	Part of ABI/WAVE complex regulating actin polymerization, most likely linked to cytoskeletal changes	S209F
SORL1	Receptor involved in lipid metabolism	rs2298813, rs2070045, Y141C
CR1	Complement receptor regulating the complement cascade	non-coding SNP rs679515, rs3818361
MS4A6A/ MS4A6E	Transmembrane protein, likely involved in microglial receptor complex	non-coding SNP
INPP5D	Phosphatase interacting with DAP12, important for phagocytosis and lipid signaling	non-coding rs35349669
CD33	Receptor important for phagocytosis	rs3865444 A14G, A14V (rs12459419)
SPI1	Transcription factor regulating cell development and function	rs1057233
PICALM	Adaptor protein involved in endolysomal trafficking	non-coding rs3851179
APOE	Apolipoprotein involved in lipid metabolism and inflammatory response	Isoforms: ε2, ε3, and ε4
BIN1	Adaptor protein important for membrane and cytoskeletal dynamics	rs6733839, rs744373
CLU (APOJ)	Apolipoprotein involved in lipid transport and metabolism	T203I
ABCA7	Lipid transporter important for lipid efflux and phagocytosis	non-coding rs3764650
CD2AP	Adaptor protein involved in endolysosomal trafficking and phagocytosis	rs9349407, rs9296559

Table 1.1. AD risk genes highly expressed by microglia.

Microglia relevant genes with reported variants associated with an increased risk of late onset AD (LOAD). Abbreviations: TREM2 = triggering receptor expressed on myeloid cells 2; ABI3 = abscisic acid intensive 3; SORL1 = sortilin related receptor 1; CR1 = complement receptor 1; MS4A6A/MS4A6E = membrane-spanning 4-domains subfamily A6A/ membrane-spanning 4-domains subfamily A6E; INPP5D = inositol polyphosphate-5-phosphatase D; SPI1 = transcription factor PU.1; PICALM = phosphatidylinositol binding clathrin assembly protein; APOE = apolipoprotein E; BIN1 = myc box-dependent-interacting protein 1; CLU (APOJ) = clusterin (apolipoprotein J); ABCA7 = ATP-binding cassette transporter A7; CD2AP = CD2 associated protein; DAP12 = DNAX activation protein of 12kDa. Modified from Hansen et al. 2018 and Lewcock et al. 2020, with additions from uniport.org (obtained on November 24th 2022).

1.3.1. Microglial states and dynamics

Microglia are highly plastic and respond rapidly to any challenges, such as extracellular protein aggregates and neuronal damage (W. M. Song & Colonna, 2018). They use receptors, such as Triggering receptor expressed on myeloid cells 2 (TREM2), to detect any factors causing a disturbance in the homoeostasis of the brain environment (Kober & Brett, 2017; Poliani et al., 2015; W. Song et al., 2017; Takahashi, Rochford, & Neumann, 2005; Turnbull et al., 2006; Ulrich et al., 2017; Y. Wang et al., 2015; Xiang et al., 2016; Xiang et al., 2021; Zhong et al., 2018). In a healthy brain, microglia use their long processes to survey the brain environment, a microglial state referred to as "resting" or more commonly "homeostatic" (Q. Li & Barres, 2018; Paolicelli et al., 2022). The ramified processes of homeostatic microglia show high expression of P2Y purinoceptor 12 (P2RY12), a protein that is important for the polarization, migration and elongation of the microglia branches (Casali & Reed-Geaghan, 2021; Haynes et al., 2006; Moore et al., 2015).

1.3.1.1. The activation signature of microglia

There is a wide repertoire of microglia functions, as these cells do not only to detect disturbances within the brain environment, but they also respond by adapting a refined activation program. Upon activation, microglia take on an amoeboid morphology, release proinflammatory molecules, and activate pathways involved in proliferation, phagocytosis, lysosomal function, and lipid metabolism (Kleinberger et al., 2014; Lewcock et al., 2020; Spittau, 2017; Ulland et al., 2017). Within the field of microglia research, "disease-associated microglia" (DAM), or "microglial neurodegenerative phenotype" (MGnD) are the most commonly used terms to describe activated microglia, with characteristic upregulation of genes associated with phagocytosis, lysosomal function, and the complement cascade, and with TREM2 as a central player required for the full activation (Butovsky & Weiner, 2018; Cox et al., 2014; Deczkowska, Keren-Shaul, et al., 2018; Gotzl et al., 2019; Keren-Shaul et al., 2017; Krasemann et al., 2017; Mazaheri et al., 2017; Paolicelli et al., 2022) (Figure 1.5). The DAM and MGnD signatures are both associated with AD and were first identified in mouse models for amyloid pathology (5xFAD (Keren-Shaul et al., 2017) and APPPS1 (Krasemann et al., 2017) (Figure 1.5). A third microglia signature, named activated response microglia (ARM), was identified in yet another mouse model for amyloid pathology (APP^{NL-G-F}) (Sala Frigerio et al., 2019). The transcriptomic profile of ARM is very similar to the transcriptomic signature of DAM

and MGnD (Paolicelli et al., 2022) (Figure 1.5). In addition to amyloid mouse models, several states for microglial activation have been observed and described in different species, models, and contexts. For example, proliferative-region-associated microglia (PAM) have been identified in the developing brains of young mice (postnatal day 7). PAM exhibit an amoeboid morphology and share characteristics with DAM (Q. Li et al., 2019) (Figure 1.5). The DAM gene signature is also reflected in microglia isolated from the white matter of aged mice (18-20 months old), referred to as white matter-associated microglia (WAM) (Safaiyan et al., 2021) (Figure 1.5). Activated microglia within the demyelinated white matter of mice with experimental autoimmune encephalomyelitis (EAE, a common model for multiple sclerosis), have been described as microglia inflamed in MS (MIMS). Although described as a novel glial phenotype, the transcriptional profile of the MIMS population shares characteristics of the DAM gene signature, including Trem2, Apoe, Lpl, and Cd68 (Absinta et al., 2021) (Figure 1.5).

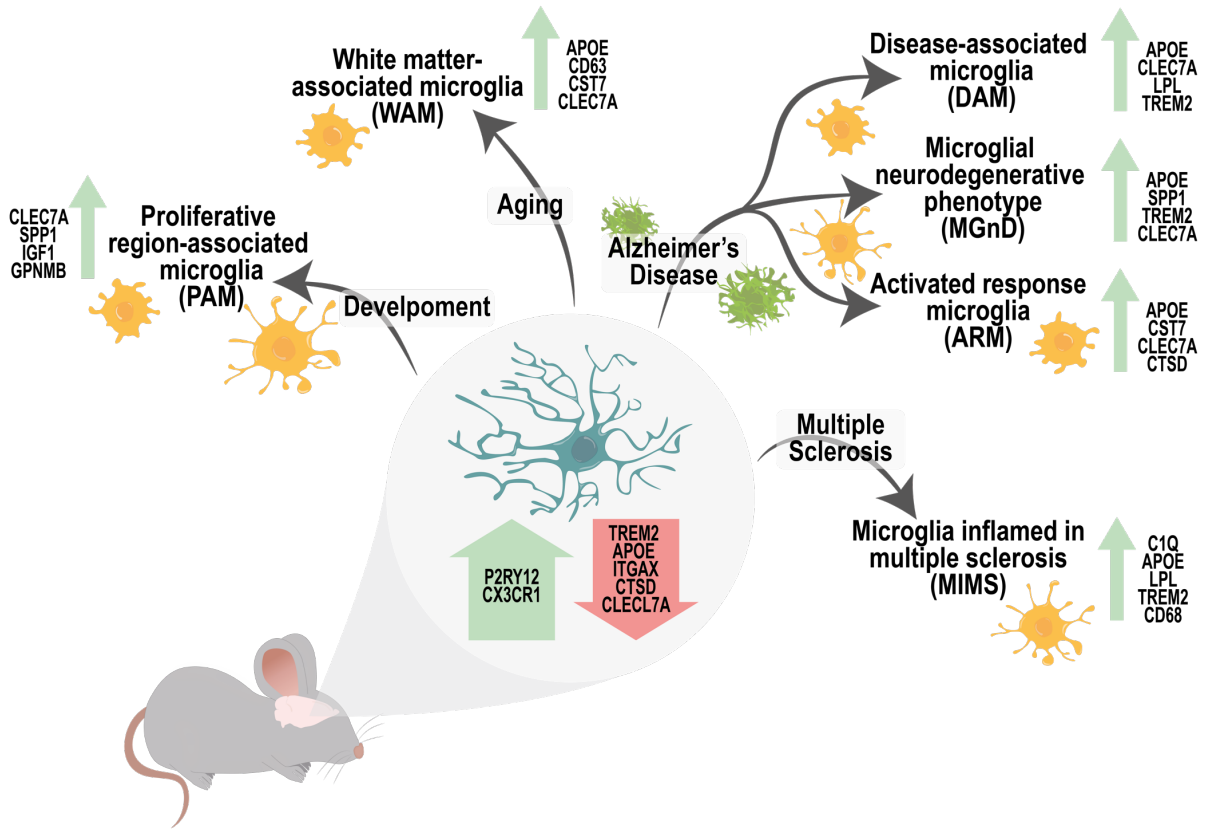

Figure 1.5. Microglial activation signatures in mice.

An overview of transcriptomic profiles identified in activated microglia. The typical transcriptomic profile of homeostatic microglia is depicted in the center (encircled). The homeostatic markers, such as P2RY12 and CX3CR1, are downregulated in the activated microglia. Modified from Paolicelli et al. 2022.

As mentioned, the nature of microglia is very complex and dynamic, which is why a binary classification (such as “rested” versus “activated”) may be restricting and confusing. However, the overwhelming number of activation profiles termed “...-associated microglia” may also become confusing and misleading. As a result, when comparing microglial signatures across species, models, and contexts, the highly dynamic and responsive characteristics of microglia should always be taken into consideration as microglia respond in a context-dependent manner (Hammond et al., 2019; Paolicelli et al., 2022; Pettas et al., 2022).

1.3.1.1.1. TREM2 mediates the complete activation of microglia

As mentioned, microglial activation should not be considered as a binary on/off-switch, going from resting to activated. The characterization of microglial activation as TREM2-independent (DAM1) and TREM2-dependent (DAM2), adds a layer of information to the microglial activation profile, which surely is more complex (Keren-Shaul et al., 2017; Krasemann et al., 2017; Paolicelli et al., 2022). The TREM2-dependent activation is considered to be the stage of full (or mature) microglial activation (Keren-Shaul et al., 2017; Krasemann et al., 2017; Mazaheri et al., 2017). Several ligands have been reported to stimulate TREM2, among those are anionic phospholipids, nucleotides, and APOE (Atagi et al., 2015; Brown & St George-Hyslop, 2021; Daws et al., 2003; Gratuze, Leyns, & Holtzman, 2018; Kober & Brett, 2017; Painter et al., 2015; Y. Wang et al., 2015). Upon ligand binding, TREM2 signaling relies on the coupling to DNAX activation protein of 12 kDA (DAP12), a signaling adaptor protein that further relays the signal to the intracellular side. The formation of the TREM2-DAP12 signaling complex is possible due to the electrostatic interactions between a positively charged lysine and a negatively charged aspartic acid residue, located within the transmembrane domains of TREM2 and DAP12, respectively (Deczkowska, Weiner, & Amit, 2020; Gratuze et al., 2018; Turnbull & Colonna, 2007). Downstream signaling of DAP12 includes phosphorylated SYK, activating signaling cascades involving phosphatidylinositol 3-kinases (PI3K), phospholipase C-γ (PLCG), and extracellular-signal-regulated kinase (ERK) (Figure 1.6) (Deczkowska et al., 2020; Hansen et al., 2018; Lewcock et al., 2020; Turnbull & Colonna, 2007). Ultimately resulting in Ca^{2+} mobilization, as well as functional adaptations necessary for macrophage function including the proliferation, survival and clustering of microglia, as well as phagocytic and metabolic functions (Figure 1.6) (Colonna & Wang, 2016; Deczkowska et al., 2020; Gratuze et al., 2018; Kleinberger et al., 2014; Nugent et al., 2020; Ulland & Colonna, 2018; Ulland et al.,

2017). The signaling cascades initiated by TREM2 activation are thought to be regulated by shedding of TREM2, mediated by a disintegrin and metalloproteinase domain-containing protein 10 (ADAM10) and -17 (ADAM17) (Schlepckow et al., 2017; Thornton et al., 2017). Supporting this idea, the prevention of TREM2 cleavage enhances TREM2 signaling and microglial activation (Kleinberger et al., 2014; Lewcock et al., 2020; Schlepckow et al., 2020; S. Wang et al., 2020). Following the extracellular processing by ADAM10/17, the transmembrane domain, TREM2 is proteolytically processed by γ-secretase (Wunderlich et al., 2013). It is still unclear whether the extracellular fragment, soluble TREM2 (sTREM2), has cell non-autonomous properties (Brown & St George-Hyslop, 2021) (Figure 1.6).

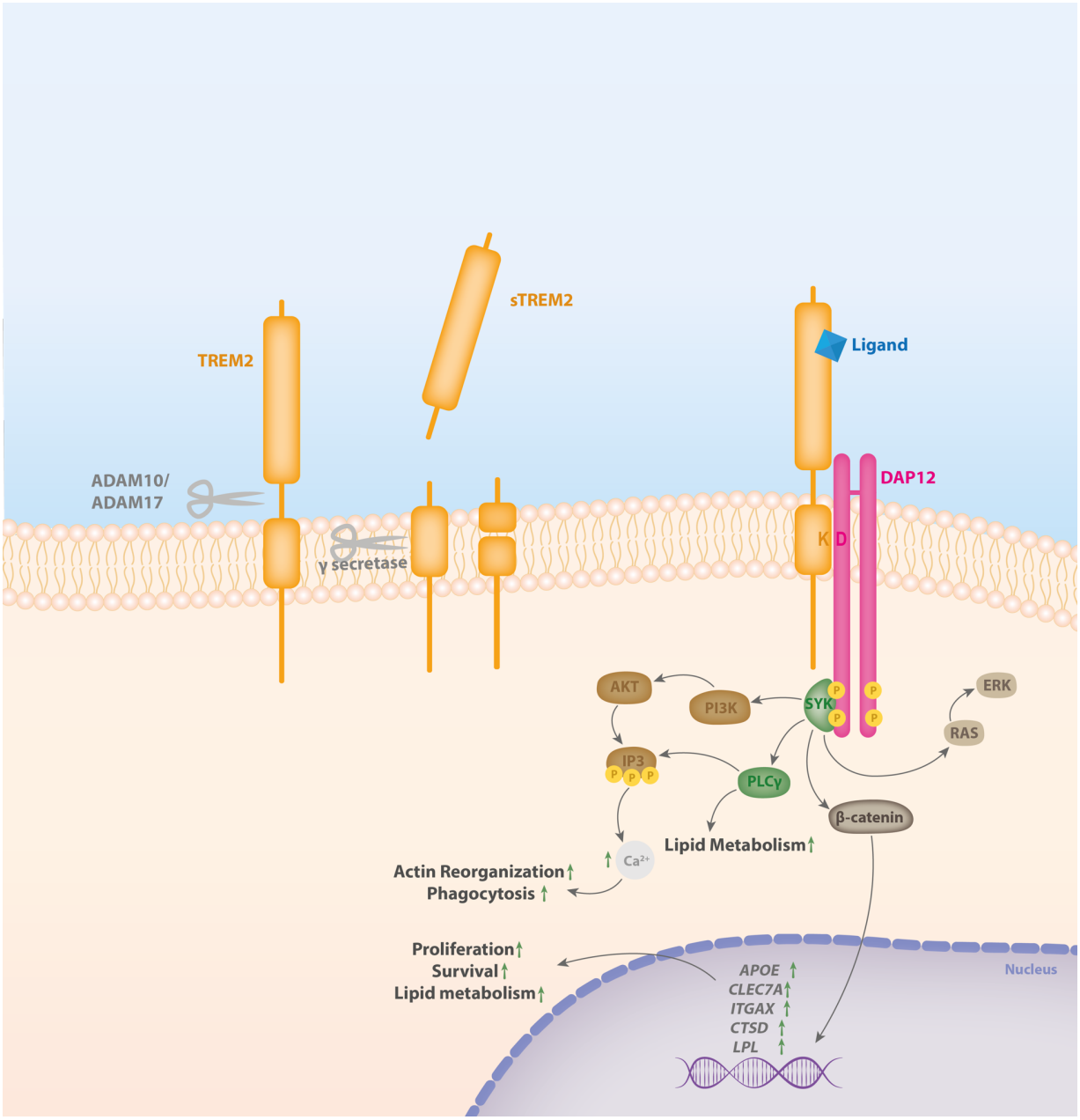

Figure 1.6. TREM2 signaling – an overview.

The signaling function of TREM2 is completely dependent on signaling adaptor protein DAP12, with which an interaction is possible via the charged amino acids in TREM2 (lysine, K (+)) and in DAP12 (aspartic acid, D (-)), located within the transmembrane domains of each protein. Upon signaling, the intracellular ITAM of DAP12 gets phosphorylated, followed by SYK recruitment and downstream signaling, which promotes proliferation, survival and lipid metabolism. Abbreviations: TREM2 = triggering receptor expressed on myeloid cells 2; DAP12 = to DNAX activation protein of 12 kDa; PI3K = phosphatidylinositol 3-kinases; PLCγ = phospholipase C-γ (also known as PLCG); ERK = extracellular-signal-regulated kinase; Ca^{2+} = calcium ions; ITAM = immunoreceptor tyrosine-based activation motif; APOE = apolipoprotein E; ITGAX = integrin subunit alpha X; CTSD = cathepsin D; LPL = lipoprotein lipase; SYK = tyrosine-protein kinase; AKT = protein kinase B; RAS = ; IP3 = inositol trisphosphate.

In context of AD, TREM2 has been reported as both beneficial and detrimental. In mouse with AD pathology, TREM2 signaling has been reported to reduce plaque load, tau spreading, and axonal dystrophy (Meilandt et al., 2020; Nugent et al., 2020; Price et al., 2020; Schlepckow et al., 2020; Ulrich et al., 2014), while others report a worsening tau pathology in animals where TREM2 signaling has been boosted (Jain & Ulrich, 2022).

When depleting TREM2 in mice, microglia are locked in a homeostatic state and can no longer respond to challenges in the brain environment (Keren-Shaul et al., 2017; Krasemann et al., 2017; Mazaheri et al., 2017; Nugent et al., 2020). This is reflected in human AD cases harboring a partial TREM2 loss-of-function (LOF) mutation, where microglia with dysfunctional TREM2 show reduced clustering around amyloid plaques as well as reduced secretion of APOE for plaque compaction, both are processes that are likely to prevent further spreading of the amyloid pathology (Parhizkar et al., 2019). Homozygous LOF variants in either the TREM2 or DAP12 gene, have been identified as a definite cause for a rare disease called Nasu-Hakola Disease (NHD) also known as Polycystic lipomembranous osteodysplasia leukoencephalopathy (PLOSL) (Kaneko, Sano, Nakayama, & Amano, 2010). NHD is a devastating disease with symptoms of bone fractures (due to progressive osteoporosis), personality changes, memory impairment and eventually premature death (Paloneva et al., 2001). This genetic evidence suggests that the TREM2-DAP12 signaling is of outer most importance for skeletal and brain functions. In addition, heterozygous LOF variants in TREM2 have been reported to significantly increase the risk for AD, which further supports the pivotal role of TREM2 and microglia in AD onset and progression (Guerreiro et al., 2013; Hansen et al., 2018; Jonsson et al., 2013; Lewcock et al., 2020). As a further association to AD, TREM2 expression is closely accompanied by the expression of the amyloid plaque associated protein APOE (Keren-Shaul et al., 2017; Krasemann et al., 2017). Like TREM2, APOE is one of the key players in the microglia activation signature of the DAM and the TREM2-APOE pathway has been proven to play a central role in microglial activation and response (Ulrich et al., 2018).

1.3.1.1.2. Progranulin and the hyperactivation of microglia

In addition to TREM2 and APOE, progranulin (PGRN) encoded by the granulin gene (*GRN*) has been recognized as a highly important for the activation of microglia, via its lysosomal and neuroinflammatory function (Abella et al., 2017; Rhinn, Tatton, McCaughey, Kurnellas, &

Rosenthal, 2022). PGRN consists of seven granulin domains, named A-G, and one half-domain referred to as the paragranulin domain (P) (Abella et al., 2017) (Figure 1.7). PGRN is a secreted protein with neurotrophic properties regulating neurite outgrowth (Van Damme et al., 2008). PGRN is capable of entering the lysosome via prosaposin (PSAP), mannose 6-phosphate receptor (M6PR), low-density lipoprotein receptor-related protein 1 (LRP1), and sortilin (SORT1) (Hu et al., 2010; Rhinn et al., 2022; X. Zhou et al., 2015). Within the acidic environment of endolysosomal compartments, progranulin is cleaved into granulins by various cathepsins (Mohan et al., 2021) (Figure 1.7).

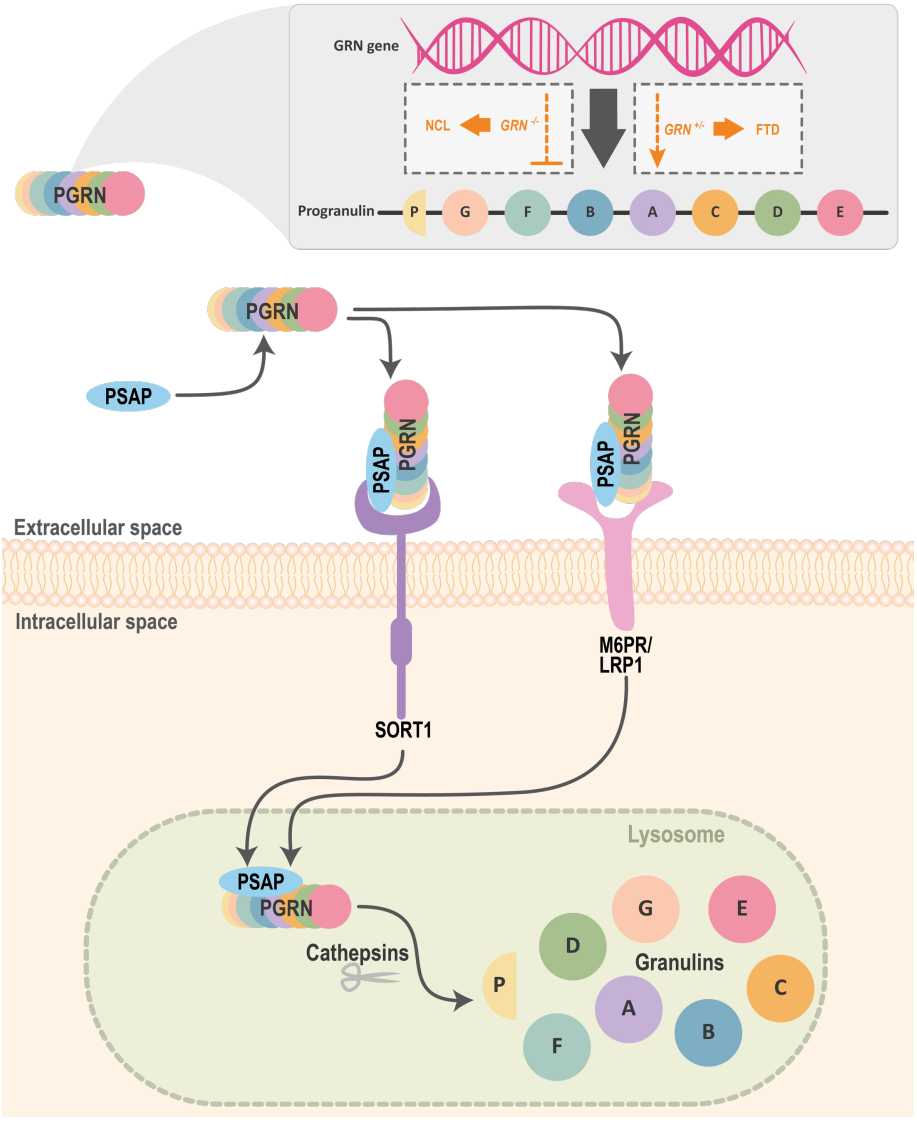

Figure 1.7. Proteolytic processing of progranulin to granulins.

The *GRN* gene encodes for the protein progranulin, which consists of seven granulin domains (A-G) and one half-domain (P). PGRN can enter the lysosome via interaction with prosaposin (PSAP), mannose-6-phosphate receptor (M6PR), low-denisty lipoprotein receptor-related protein 1 (LRP1), and sortilin (SORT1). In the lysosome, progranulin is proteolytically processed by cathepsins to generate granulins. Homozygous loss of function mutations in the *GRN* gene cause a rare lysosomal storage disorder known as neuronal ceroid lipofuscinosis (NCL), while heterozygous loss of function within the *GRN* gene is associated with frontotemporal dementia (FTD). Modified from Abella et al. 2017 and Swift et al. 2021.

Homozygous variants in GRN gene, causing a complete loss of function of the protein, have been reported to cause a rare lysosomal storage disorder known as neuronal ceroid lipofuscinosis (NCL) (Huin et al., 2020; Kamate, Detroja, & Hattiholi, 2019; Smith et al., 2012) (Figure 1.7). As previously mentioned, heterozygous LOF mutations in the *GRN* gene results in FTD with TDP-43 pathology (Baker et al., 2006; Haass & Neumann, 2016) (Figure 1.7).

Homozygous depletion of *GRN* in mice and human-induced pluripotent stem cell (iPSC)-derived microglia (hiMGL) results in a hyperactivated microglial signature. This hyperactivated signature is characterized by an upregulation of genes associated to microglial activation, such as: *APOE*, *CLEC7A* (encoding the C-type lectin domain family 7 member A)*, ITGAX* (encoding the integrin subunit alpha X), *SPP1* (encoding for osteopontin), *CTSD* (encoding the protein cathepsin D), and *TREM2.* In contrast, genes associated to the homeostatic signature, such as *P2RY12* and *CX3CR1* (encoding the CX3C chemokine receptor 1), are downregulated (Gotzl et al., 2019; Reifschneider et al., 2022).

1.3.2. Biomarkers for microglial activation states

With a rapidly growing awareness of the relevance and complexity of microglial activation, there is now a considerable interest to investigate the characteristics and effects of microglial activation in different neurological disorders, as well as in the models used to study these disorders. To enable for such characterization, biomarkers for microglial activation are needed. In addition, the emergence of microglia-modulating therapies requires robust and reliable biomarkers to evaluate the target engagement and treatment effects. Ultimately, addressing the microglial activation state could potentially facilitate the prognostic evaluation and patient stratification, both of highly relevant in clinical studies and clinical trials.

1.3.2.1. TSPO-PET

To date, the clinical assessment of neuroinflammation, including microglia activity, mainly relies on PET-imaging targeting translocator protein (TSPO), a receptor expressed on the outer mitochondrial membrane where it is involved in various processes such as cholesterol transport, apoptosis, and oxidative stress (Y. Lee, Park, Nam, Lee, & Yu, 2020; Notter et al., 2018). TSPO depletion in mice lead to metabolically impaired microglia incapable of adapting an activated phenotype (Yao et al., 2020). Unfortunately, there are limitations that raise

concerns regarding the reliability of this measure. A recent study underscores the differences between TSPO expression and signal in rodents and humans (Erik Nutma et al., 2022). In addition, the TSPO signal is detected throughout the brain, which interferes with the methodology as an area of no signal is required for reference (Guilarte, Rodichkin, McGlothan, Acanda De La Rocha, & Azzam, 2022). TSPO is expressed throughout the body and within the brain the expression is not microglia specific (Notter et al., 2018), it has even been argued that astrocytes and endothelial cells, as well as neuronal activity, may contribute to the TSPO signal (Guilarte et al., 2022; Rupprecht et al., 2010). Nevertheless, the signal obtained from TSPO-PET can, at least as a major part, be related to microglial activation, as the signal intensity has been reported to depend on TREM2 levels and the presence of microglia (Rauchmann et al., 2022; Xiang et al., 2021). This leads to the question if the detected signal reflects microglia activation or proliferation (E. Nutma et al., 2021). Thus, for proper and reliable interpretations of TSPO-PET data, the abovementioned uncertainties should be taken into consideration. In addition, fluid-based microglial activation markers would be of great use to address the origin of the TSPO-PET signal.

1.3.2.2. sTREM2

The levels of soluble TREM2 (sTREM2) are quantifiable in mouse and human CSF, and is considered to be a proximity marker reflecting the levels of TREM2 available at the surface of microglia and has therefore been suggested as a biomarker for TREM2-dependent microglial activation (Brown & St George-Hyslop, 2021; Kleinberger et al., 2014; Morenas-Rodriguez et al., 2022; Schlepckow et al., 2017; Suarez-Calvet, Araque Caballero, et al., 2016). Levels of CSF sTREM2 appear as a very promising measure across several neurodegenerative diseases (Piccio et al., 2008; Piccio et al., 2016; Suarez-Calvet, Kleinberger, et al., 2016; van der Ende et al., 2021; Wilson et al., 2020). Recent studies suggest that sTREM2 measured in serum, which is much easier to access compared to CSF, can be used as a marker for early or mild cognitive impairment (Jiahuan et al., 2022; Tanaka et al., 2022). However, sTREM2 appears to be very dynamic, with level variability across disease types and stages (Brown & St George-Hyslop, 2021; Knapskog et al., 2020; Ma et al., 2020). Initial studies suggested sTREM2 to be a marker of microglial activation in AD. In these studies, the increased levels of sTREM2 did not correlate with the decrease of CSF $A\beta_{42}$, but instead the correlation was observed with the increased levels of t-tau and p-tau. These studies suggested, that the TREM2-dependent microglial

activation is initiated approximately 5 years before symptom onset, but after the occurrence amyloid deposition and neuronal injury. (Ma et al., 2020; Suarez-Calvet, Araque Caballero, et al., 2016; Suarez-Calvet, Kleinberger, et al., 2016; Suarez-Calvet et al., 2019). However, this suggestion was challenged by a longitudinal AD-study, taking the rate of change into account, instead of absolute levels as previously compared in a cross-sectional manner (Morenas-Rodriguez et al., 2022). This longitudinal approach led to the insight that the sTREM2 levels may vary between individuals, but the rate of sTREM2 increase correlates with amyloid pathology. Moreover, the rate of increased sTREM2 levels in CSF, shows a close association with slower cognitive decline, further supporting the protective function of TREM2-dependent microglial activation in AD. In addition, this study used a novel assay to measure sTREM2 and managed to detect changes 21 years before expected symptom onset. This discovery supports the idea of microglia as very plastic and rapidly reacting cells, which (in the context of AD) are likely to cluster around and react to the very early forms of amyloid seeds and thereby hinder the spreading and growth of the amyloid pathology (Morenas-Rodriguez et al., 2022; Parhizkar et al., 2019). Studies of sTREM2 highlight the importance of longitudinal studies, as cross-sectional studies do not to allow for the investigation of the rate of change. This also emphasizes the need of more robust microglial activation markers, measurable in a cross-sectional manner with high reliability and reproducibility. Furthermore, biomarkers capturing the TREM2-independent signatures of microglial activation may be useful to cover a wider range of the activation spectra. Finally, TREM2-independent markers will become highly relevant in the context of evaluating the effects of TREM2 agonistic therapies, which boost the activation of microglia by preventing the cleavage of TREM2 and consequently reduces the levels of the otherwise measurable sTREM2 (Lewcock et al., 2020). Taken together, it is very likely that sTREM2 and TSPO-PET, as biomarkers for microglial activity, would benefit by the addition of further markers, in order to capture the complex and dynamic nature of microglia.

2. Aims of the thesis

Mice lacking either *Trem2* or *Grn*, display extremely divergent transcriptomic and functional phenotypes in regards of microglial activation. While the loss of *Trem2* enhances the expression of genes associated with a non-activated phenotype, sometimes referred to as "homeostatic", the microglia isolated from *Grn*-knockout mice appear as hyperactivated. In this thesis, I have further investigated these divergent microglial phenotypes and the differences within the microglial proteome and secretome. The ultimate aim of my Ph.D. research was to identify biomarker candidates for microglial activation, which are measurable in human CSF. During my Ph.D. research, the following aims were addressed to enable the identification of biomarker candidates for microglia activation in human CSF:

1. Investigating the opposite microglial phenotypes in the *Trem2*-knockout and *Grn*-knockout mouse models on a proteome level, in microglia and CSF.

2. Address the translatability of the findings in mouse to human systems using hiMGL of the same genotypic comparison; *TREM2*-knockout versus *GRN*-knockout.

3. Identify biomarker candidates by investigating potential overlaps between our mouse models and hiMGL models with the human CSF proteome of patients suffering of FTD with heterozygous progranulin deficiency (FTD-GRN).

4. Confirming the detection and change of potential candidates within the human CSF proteome by analyzing proteomic data obtained from human CSF of a second cohort.

The aims were approached using mass spectrometry-based discovery proteomics. With our cross-validation approach candidates were not only confirmed across *in vivo* and *in vitro* systems, but also investigated in regard of a translational assurance by comparing proteomic data generated from mice, human models, and patient CSF.

3. Materials and methods

3.1. Materials

3.1.1. Laboratory equipment and consumables

Instruments and consumables	Company
Accu-jet pro pipette controller	BrandTech
Analytical balance (0.0001-200g)	Denver Instrument
Balance (0.01-2000g)	Sartorius
Cell scraper	Sigma Aldrich
Centrifuge 5417R	Eppendorf
Centrifuge 5810R Eppendorf	Thermo Fisher Scientific
Centrifuge Megafuge 16 Centrifuge Series	Thermo Fisher Scientific
Centrifuge Megafuge 40R	Thermo Fisher Scientific
Class II Biological Safety Cabinet Safe2020	Thermo Fisher Scientific
Conical centrifugation tubes (15 and 50 ml) Falcon	Fisher Scientific
Dissection microscope (SZ61)	Olympus
DNA electrophoresis gel system	Bio-Rad
Dumont #2, Laminectomy Forceps	Fine Science Tools (FST)
Dumont #5, straight fine forceps	Fine Science Tools (FST)
Freezer -80°C - Herafreeze Basic	Thermo Fisher Scientific
Hardened fine scissors straight	Fine Science Tools (FST)
Heating and stirring plate	IKA RH
Incubator	Heraeus, Thermo Fisher
Incubator Heracell 150i CO2 with Stainless-Steel Chambers	Thermo Fisher Scientific
Large spatula, double, one round end	Heathrow Scientific
Light source KL 1600 LED	Olympus
Liquid Nitrogen - Cryo technology	Biostore System
Magnetic Stirrer with Heating, Heidolph instruments MR Hei-Tec	Fisher Scientific
Microcentrifuge Heraeus Frisco 17	Thermo Fisher Scientific

Microcentrifuge Heraeus Frisco 21	Thermo Fisher Scientific
Microcentrifuge Heraues Pico 17	Thermo Fisher Scientific
Milli-Q plus Water Purification System	Merck Millipore
NanoPhotometer N60/N50	Implen
pH meter (Seven easy)	Mettler Toledo
Pipette set	Gilson, Eppendorf
Plate reader for protein quantification NanoQuant Infinite M200 PRO	TECAN
Serological pipettes (2, 5, 10 and 25ml)	Sarstedt
Thermomixer compact	Eppendorf
ThermomixerC	Eppendorf
Thin spatula, double, one round end	Heathrow Scientific
Vortex mixer (Vortex-2 genie)	Scientific Industries
Cell culture dishes Nunc (6 and 10ml)	Thermo Fisher Scientific
Parafilm "M" roll Bemis	Thermo Fisher Scientific
PCR caps, VersiCap Mat, 96-well, flat cap strips	Thermo Fisher Scientific
PCR tubes, VersiPlate PCR Strip Tube Plate, 96-well, low profile	Thermo Fisher Scientific
Pipette tips (10, 200, 300 and 1000µl)	Sarstedt
Protein LoBind tubes (0.5ml)	Eppendorf
Protein LoBind tubes (1.5ml)	Eppendorf
Tubes (0.5, 1.5, 2, 15, and 50ml)	Sarstedt

Table 3.1. List of general laboratory instruments, equipment and consumables used in this study.

3.1.2. Reagents, solutions and buffers

Reagent	Company
Agarose Ultrapure	Life Technologies
Deoxyribonucleotides (dNTPs)	Roche
DNA Ladder 1kb Plus	Invitrogen
DNA Polymerase (GoTaq G2)	Promega
GelRed Nucleic Acid Gel Stain	Biotium
GoTaq buffer (5x)	Promega

NaOH (1M)	Millipore
Proteinase K [100µg/ml]	Roche
Tris base	AppliChem
Triton X-100	Merck

Table 3.2. List of general reagents used in this study.

Abbreviations: DNA = deoxyribonucleic acid; dNTPs = deoxynucleoside triphosphates

Solution	Composition	Storage	Purpose
Agarose gel [1.5%]	Agarose 1.5 g TAE buffer (1x) 100 ml GelRed Stain 4 µl	Heated and poured while liquid, solidified in RT	Used for genotyping
BSA solution [5%]	BSA 5 g Ultrapure H_2O 100 ml	- 20°C	Used for MACS buffer
Denaturation mix (10ml)	Urea 3.6 g Thiourea 1.52 g HEPES 23.83 mg H_2O Mass Spec Grade NaOH to reach pH 8.0 Ultrapure H_2O 73 ml	Centrifuged at 5000 x g for 10 min. Aliquoted and stored at - 80°C	Used for in-solution digestion
Digestion buffer: Ammonium bicarbonate (ABC) [50mM]	Ammonium bicarbonate (ABC) 40 mg Mass Spec Grade H_2O 10ml	Stored dark at RT	Used for in-solution digestion
HBSS supplemented with HEPES	HBSS 500 ml HEPES [1 M] 3.5 ml	+ 4°C	Used for microglial isolation using MACS protocol
MACS buffer	BSA Solution [5%] 5 ml PBS 100 ml	Filtered via SteriCup, in laminar flow hood. Stored at + 4°C for max. 1 week	Used for microglial isolation using MACS protocol
Mouse tail lysis buffer (1L)	Tris [1.0 M, pH 8.0] 100 ml EDTA [0.5 M] 10 ml SDS [20%] 10 ml NaCl [2.5 M] 80 ml	RT	Proteinase K added upon use2.5µl per tail biopsy (equivalent to 500µl Mouse tail lysis buffer)

	Ultrapure H_2O 1 L		
	Proteinase K [100µg/ml]	+ 4°C	
PBS (10x) (1L)	NaCl 80g	RT	General use
	$NaHPO_4$ x 2 H_2O 17.8g		
	KH_2PO_4 2.4g		
	KCl 2g		
	Ultrapure H_2O filled up to 1 L		
Reduction buffer (10ml)	Dithiothreitol (DTT) [1M] 100 µl	Aliquoted and stored at - 20°C	Used for in-solution digestion
	Digestion buffer 9.9 ml		
RIPA lysis buffer (100ml)	NaCl [5M] 3 ml	RT	Lysis of hiMGL cells
	EDTA [0.5M, pH 8.0] 1 ml		
	Tris [0.5M, pH 8.0] 10 ml		
	Triton X-100 1ml		
	Sodium deoxycholate [5%] 10 ml		
	SDS [5%] 2 ml		
	Ultrapure H_2O 73 ml		
SDS [5%]	SDS 5 g	Dissolves better when heated. Stored at RT	General use
	Ultrapure H_2O 100 ml		
SDS [20%]	SDS 20 g	Dissolves better when heated. Stored at RT	General use
	Ultrapure H_2O 100 ml		
STET lysis buffer (1L)	NaCl [5M] 30 ml	+ 4°C	Lysis of hiMGL cells
	EDTA [0.5M, pH 8.0] 4 ml		
	Tris [1M, pH 7.5] 50 ml		
	Triton X-100 10 ml		
	Ultrapure H_2O 906 ml		
TAE buffer (50x) (5L)	Tris [121.14 g/mol] 1210 g	RT	General use
	Acetic Acid 285.5 ml		
	EDTA [0.5M, pH 8.0] 500 ml		
	Ultrapure H_2O		
Tris [0.1M, pH 8.0] (1L)	Tris [121.14 g/mol] 12.1 g	RT	General use
	Ultrapure H_2O 800 ml		

	HCl to adjust pH to 8.0		
	Ultrapure H_2O filled up to 1 L		
Tris [0.1M, pH 8.5] (1L)	Tris [121.14g/mol] 12.1 g	RT	General use
	Ultrapure H_2O 800 ml		
	HCl to adjust pH to 8.5		
	Ultrapure H_2O filled up to 1 L		
Tris [0.5M, pH 8.0] (1L)	Tris [121.14g/mol] 60.57 g	RT	General use
	Ultrapure H_2O 800 ml		
	HCl to adjust pH to 8.0		
	Ultrapure H_2O filled up to 1 L		
Tris [1.0M, pH 7.5] (1L)	Tris [121.14 g/mol] 121.14 g	RT	General use
	Ultrapure H_2O 800 ml		
	HCl to adjust pH to 7.5		
	Ultrapure H_2O filled up to 1 L		
Urea buffer A (UA buffer) [8M, pH 8.5] (10ml)	Urea 4.8 g	Prepared fresh upon use	Used for filter aided sample preparation
	Tris [0.1M, pH 8.5] 6.5 ml		
Urea buffer B (UB buffer) [8M, pH 8.0] (10ml)	Urea 4.8 g	Prepared fresh upon use	Used for filter aided sample preparation
	Tris [0.1M, pH 8.0] 6.5 ml		

Table 3.3. List of solutions and buffers used in this study.
Abbreviations: RT = room temperature; BSA = bovine serum albumin; RIPA = radioimmunoprecipitation assay; STET = sodium chloride-Tris-Cl-EDTA-Triton X-100; EDTA = ethylenediaminetetraacetic acid; SDS = sodium dodecyl sulfate; PBS = phosphate-buffered saline; MACS = magnetic-activated cell sorting; HBSS = Hank's balanced salt solution; HEPES = N-2-hydroxyethylpiperazine-N-2-ethane sulfonic acid; DTT = dithiothreitol; ABC = ammonium bicarbonate.

3.1.3. Mice

Designation	Gene alteration	Reference	Identifier	Additional information
C57BL/6J	No genetic modifications	The Jackson Laboratory (JAX)	RRID:IMSR_JAX:000664	Assigned as wild-type (Wt) control and used for the cross breeding of the *Grn*- and *Trem2*-knockout lines
C57BL/6J *Grn*-knockout	Deletion of exon 2-13 of the *GRN* gene	Kayasuga et al. 2007	N/A	
C57BL/6J *Trem2*-knockout	Deletion of exon 3 and 4 of the *TREM2* gene	Turnbull et al. 2006	N/A	

Table 3.4. List of mouse strains used in this study.
Abbreviations: Wt = wild-type; Grn = progranulin (gene); Trem2 = triggering receptor expressed on myeloid cells 2; N/A = not applicable.

3.1.3.1. Genotyping of mouse strains

Mouse strain	Primer	Primer sequence (5' to 3')
Grn-knockout	Neo forward	CCAATATGGGATCGGCCATTGAAC
	Neo reverse	CGCTCGATGCGATGTTTCGCTTGG
	GRN-forward primer	TGGATTCCCCTGAGCCCATA
	GRN-reverse primer	TCGCACTTCACCTCCTTCAC
Trem2-knockout	Primer-FW 1	CCCTAGGAATTCCTGGATTCTCCC
	Primer-FW 2	TTACACAAGACTGGAGCCCTGAGGA
	Primer-Rev	TCTGACCACAGGTGTTCCCG

Table 3.5. List of primers used for genotyping of mouse strains.
Abbreviations: Grn = progranulin (gene); Trem2 = triggering receptor expressed on myeloid cells 2.

PCR mixture (one reaction)	
Component	**Volume [µl]**
5x Go Taq Buffer [1.5 mM $MgCl_2$]	4
dNTPs [10mM]	0.4
Primer-FW1 [10µM]	1.5
Primer-FW2 [10µM]	1.5
Primer-Rev [10µM]	1.5
GoTaq G2 [5U/µl]	0.1
DNA template [<100ng/µl]	1
dH_2O	10

PCR Program		
Cycle	**Temperature [°C]**	**Time**
1	94	2 min
2	94	15 sec
3	55	30 sec
4	72	1 min
5	Repeat cycle 2-4 30 times	
6	72	5 min
7	10	Hold

Table 3.6. PCR conditions used for the genotyping of the Trem2-knockout mouse line.
Abbreviations: PCR = polymerase chain reaction; min = minutes; sec = seconds.

PCR mixture (one reaction)		PCR mixture (one reaction)	
Component	**Volume [µl]**	**Component**	**Volume [µl]**
5x Go Taq Buffer [1.5 mM $MgCl_2$]	4	5x Go Taq Buffer [1.5 mM $MgCl_2$]	4
dNTPs [10mM]	0.5	dNTPs [10mM]	0.5
GRN-forward primer [10µM]	1	Primer: Neo forward [10µM]	1
GRN-reverse primer [10µM]	1	Primer: Neo Reverse [10µM]	1
GoTaq G2 [5U/µl]	0.2	GoTaq G2 [5U/µl]	0.2
DNA template [<100ng/µl]	1	DNA template [<100ng/µl]	1
dH_2O	14.1	dH_2O	14.1
PCR Program			
Cycle	**Temperature [°C]**	**Time**	
1	94	2min	
2	94	15sec	
3	55	30sec	
4	72	1min	
5	Repeat cycle 2-4 30 times		
6	72	5min	
7	10	Hold	

Table 3.7. PCR conditions used for the genotyping of the Grn-knockout mouse line.

Abbreviations: PCR = polymerase chain reaction; min = minutes; sec = seconds; GRN = progranulin (gene).

3.1.3.2. CSF collection from mouse

Component	Company
CSF capillaries o.d. 1.00mm, i.d. 0.75mm, 10cm length, Fire Polished	Sutter Instrument
Flex-arm stand with table clamp and mountable focus arm	Leica Microsystems
Inclined binocular tube 45° M-series	Leica Microsystems
Injection arm (Electrode holder) Model 1770 Standard Electrode Holder	Kopf Instruments
Leica Eyepiece 10x/23B, adjustable, 3d gen	Leica Microsystems
Leica M80 Stereomicroscope	Leica Microsystems
Mouse non-rupture earbars, Model 1922, 45° 0.8mm radius	Kopf Instruments
Objective achromat 0.8x, WD = 114mm	Leica Microsystems
SOMNI Scientific Animal Temperature Heating Pad with PID controller	Fischer Scientific
Stereotaxic frame Model 963 Ultra Precise Small Animal Stereotaxic Instrument	Kopf Instruments

Table 3.8. List of instruments used for the collection of CSF from mouse.

Abbreviations: CSF = cerebrospinal fluid; i.d. = inner diameter; o.d. = outer diameter.

3.1.4. Microglia isolation from mouse using MACS

Component	Company
CD11b MicroBeads (microglia)	Miltenyi Biotec
Counting chambers	Bio-rad
Falcon Cell Strainers (40µm)	Thermo Fisher Scientific
GentleMACS C tubes	Miltenyi Biotec
GentleMACS Dissociator	Miltenyi Biotec
HBSS No Phenolred, supplemented Ca^{2+} and Mg^{2+}	Thermo Fisher Scientific
HEPES [1M] Gibco	Thermo Fisher Scientific
LS Columns MACS	Miltenyi Biotec
MACS Neural Tissue Dissociation Kit (P)	Miltenyi Biotec
QuadroMACS separator	Miltenyi Biotec
Stericup filter bottle (250ml)	Millipore

Table 3.9. List of instruments used for the isolation of microglia from mouse.

Abbreviations: MACS = magnetic-activated cell sorting; HBSS = Hank's balanced salt solution; HEPES = N-2-hydroxyethylpiperazine-N-2-ethane sulfonic acid.

3.1.5. Material used for the differentiation and maintenance of hiMGL

3.1.5.1. Cell lines, constructs and plasmids

Cell lines	Company
Female iPSC line A18944	Thermo Fisher

Table 3.10. Cell line used for the generation of human-iPSC-derived microglia (hiMGL).
Abbreviations: iPSC = induced pluripotent stem cell.

Constructs and plasmids	Source	Sequence
Cas9 (pSpCas9(BB)-2A-Puro (PX459) V2.0	Gift from Feng Zhang (Addgene plasmid #62988) (Ran et al. 2013)	
GRN gRNA	In house	GCTGGGAGGCCTCAAAATCATGG
MLM3636 plasmid	Gift from Keith Joung (Addgene plasmid #43860)	
TREM2 gRNA	In house	ACTGGTAGAGACCCGCATCATGG

Table 3.11. gRNA constructs and plasmids used for the generation of human-iPSC-derived microglia (hiMGL).
Abbreviations: GRN = progranulin (gene); TREM2 = triggering receptor expressed on myeloid cells 2; gRNA = guide ribonucleic acid.

3.1.5.2. Equipment

Component	Company
70% Ethanol	In house
Accutase (A1110501)	Thermo Fisher
Agarose	Serva
BTXpress electroporation solution (732-1285)	VWR International GmbH
Cell culture plates (6, 12, 24 and 96-wells)	Corning
Cryopreservation medium BamBanker	FUJIFILM Wako Chemicals
DMEM - Dulbecco's Modified Eagle Medium, high glucose, GlutaMAX Supplement	Thermo Fisher Scientific
dNTP mix [10mM]	Invitrogen
EDTA	Invitrogen
Electroporation buffer BTXpress High Performance Electroporation Solution	BTX/Fisher Scientific
Electroporation Cuvettes Plus 1mm BTX	BTX/Fisher Scientific
Electroporator BTX Gemini X2	BTX/Fisher Scientific
Essential 8 Flex Medium (A2858501)	Thermo Fisher
Fetal Bocine Serum (FBS) for freezing of iPSCs	Thermo Fisher Scientific

Fluoromount-G	Thermo Fisher
Geltrex LDEV-Free, hESC-Qualified, Reduced Growth Factor Basement Membrane Matrix (A1413302)	Thermo Fisher
Gibco StemFlex Medium (A3349401)	Thermo Fisher
HPC differentiation kit	StemCell Technologies
IL-34	Peprotech
Incubator	Eppendorf CellXpert C170i
M-CSF	Peprotech
Microscope	Zeiss Axio Observer Z1
Multiwell plates (6x)	Thermo Fisher Scientific
MwoI enzyme	NEB
Paraformaldehyd (PFA) 4%, in PBS pH 7,2	Morphisto
PBS	Sigma
Penicillin/Streptomycin (5000U/ml)	Thermo Fisher Scientific
Precision cover glasses thickness No. 1.5H (tol. ± 5 µm), Ø12mm	Marienfeld
Puromycin dihydrochloride, Ultra Pure Grade	VWR International GmbH
Random hexamers [50µM]	Invitrogen
RNA Preparation Kit, RNeasy Mini Kit (74104)	Qiagen
RNaseOut Rnase Inhibitor	Invitrogen
ROCK inhibitor (S1049)	Selleckchem
SuperFrost Plus Adhesion microscope slides	VWR
Superscript IV, Reverse Transcriptase	Invitrogen
TAE Buffer (Tris-acetate-EDTA) (50X)	Thermo Fisher
Taqman Buffer - PrimeTime® Gene Expression Master Mix	IDT
Taqman Primer	IDT
TGF-β	Peprotech
UltraPure™ DNase/RNase-Free Distilled Water	Thermo Fisher
Vitronectin (VTN-N) Recombinant Human Protein, Truncated (A14700)	Thermo Fisher

Table 3.12. Equipment used for the generation of human-iPSC-derived microglia (hiMGL).
Abbreviations: GRN = progranulin (gene); TREM2 = triggering receptor expressed on myeloid cells 2; gRNA = guide ribonucleic acid; TGF-β = ; qPCR = quantitative polymerase chain reaction; PBS = ; EDTA = ethylenediaminetetraacetic acid; RFLP = restriction fragment length polymorphism; RNA = ribonucleic acid; M-CSF = macrophage colony-stimulating factor; IL-34 = interleukin 34; HPC = hematopoietic progenitor cell; dNTPs = deoxynucleotide triphosphates; FBS = fetal bovine serum; DEPC = diethyl pyrocarbonate.

3.1.5.3. Antibodies

Antibody	Company	Purpose
Donkey anti-Mouse IgG (H+L) Highly cross-adsorbed secondary antibody, Alexa Fluor Plus 488 (A32766)	Thermo Fisher	Secondary antibody for the detection of TRA-1-60
Donkey anti-Rabbit IgG (H+L) Highly Cross-Adsorbed Secondary Antibody, Alexa Fluor 568 (A10042)	Thermo Fisher	Secondary antibody for the detection of Oct4 and Nanog
Nanog antibody (4903S)	Cell Signaling	Primary antibody for the detection of Nanog
Oct4 antibody (09-0023)	Tebubio/StemGent	Primary antibody for the detection of Oct4
Ssea4 antibody (ab16287)	Abcam	Primary antibody for the detection of Ssea4
TRA-1-60 antibody	Millipore	Primary antibody for the detection of TRA-1-60

Table 3.13. Antibodies used for immunofluorescence analysis of pluripotency markers.
Abbreviations: Ssea4 = stage-specific embryonic antigen 4; TRA-1-60 = podocalyxin.

3.1.6. Mass spectrometry – instruments, equipment and reagents

3.1.6.1. Mass spectrometry instruments

Instrument	Company
Centrifuge, Benchtop model, Tomy Tip-Centrifuge	Sonation lab solution
Ion source NanoFlex with PRSO-V1 column oven	Sonation, Germany
Ionization Source, Nano Electrospray Source, Thermo Proxeon	Thermo Fisher Scientific
Liquid Chromatograph EASY-nLC 1000/1200 (Proxeon)	Thermo Fisher Scientific
Mass Spectrometer Q-Exactive	Thermo Fisher Scientific
Mass Spectrometer Q-Exactive HF	Thermo Fisher Scientific
Mass Spectrometer TimsTOF PRO	Bruker Daltonics
Ultrasonic bath, Sonorex Super Sonicator	Brandelin
Vacuum centrifuge, ScanSpeed MaxiVac	ScanVac

Table 3.14. List of instruments used for mass spectrometry analysis and sample preparation.

3.1.6.2. Mass spectrometry equipment

Component	Company
C18 columns (in-house packed), 30 cm, i.d.: 75 µm. ReproSil-Pur 120 C18-AQ, 1.9 µm	Dr. Maisch GmbH, Germany
C18 Empore disks, Supelco	Merck

Filter Columns, Corning-Costar-Spin-X (0.22 µm cut-off)	Merck
Magnetic Rack, DynaMag-2 Magnet	Thermo Fisher Scientific
Pierce BCA Protein Assay Kit	Thermo Fisher Scientific
RNA Preparatin Kit, Rneasy Mini Kit (74104)	Qiagen
Vivacon spin filters (30kDa cut-off)	Sartorius

Table 3.15. List of equipment used for mass spectrometry analysis and sample preparation.
Abbreviations: BCA = Bicinchoninic acid; kDa = kilodaltons; i.d. = inner diameter; RNA = ribonucleic acid.

3.1.6.3. Mass spectrometry reagents

Reagent	Company
Acetic Acid	Fluka
Acetonitrile 100%, UHPLC Grade	Biosolve
Acetonitrile 80%	Thermo Fisher Scientific
Ammoniumbicarbonate (ABC)	Thermo Fisher Scientific
Benzonase	Sigma Aldrich
Bovine Serum Albumin (BSA)	Sigma Aldrich
$CaCl_2$	Merck
Dimethylsulfidoxid (DMSO)	Roth
Dithiothreitol (DTT)	Biomol, Germany
EDTA	Merck
Ethanol, 100%	Roth
Ethanol, 80%	Merck
Formic Acid (FA) 0.1%	Sigma Aldrich, Germany
Formic Acid (FA) 8%	Sigma Aldrich, Germany
H_2O LC-MS Grade	Thermo Fisher Scientific
HCl 32%	Merck
Iodoacetamide (IAA)	Sigma Aldrich, Germany
Isopropanol	Thermo Fisher Scientific
$MgCl_2$	Merck
$MnCl_2$	Sigma Aldrich
NaCl	Roth

Protease Inhibitor cocktail (Pi) (P8340)	Sigma Aldrich
rLys-C, Mass Spec Grade	Promega
SeraMag beads A	Thermo Fisher Scientific
SeraMag beads B	Thermo Fisher Scientific
Sodium azide	Merck
Sodium deoxycholate	Sigma Aldrich
Sodium dodecyl sulfate	Sigma Aldrich
Thiourea	Sigma Aldrich
Trypsin, Sequencing Grade Modified	Promega
Urea	Merck

Table 3.16. List of reagents used for mass spectrometry analysis and sample preparation.
Abbreviations: UHPLC = Ultra-High-Performance Liquid Chromatography; ABC = ammonium bicarbonate; BSA = bovine serum albumin; DMSO = dimethylsulfidoxid; DTT = dithiothreitol; EDTA = ethylenediaminetetraacetic acid; FA = formic acid; LC-MS = liquid chromatography–mass spectrometry; IAA = iodoacetamide; Pi = protease inhibitor.

3.1.7. Software

Software	Version	Source
Adobe Illustrator	2020	Adobe Systemts Inc., USA
CRISPOR (online tool)	N/A	crispor.tefor.net (Concordet & Haeussler 2018)
DIANN	1.8	github.com/vdemichev/DiaNN
GraphPad Prism	9.3.1	GraphPad, Dotmatics
Maxquant	1.6.1.0	maxquant.org/maxquant, Max-Planck Institute Munich (Cox et al. 2014)
Maxquant	1.6.3.3	maxquant.org/maxquant, Max-Planck Institute Munich (Cox et al. 2014)
Perseus	1.6.15.0	maxquant.org/perseus, Max-Planck Institute Munich (Tayanova et al. 2016)
Spectronaut	15.0.210615.50606	Biognosys, Switzerland
Spectronaut	14.10.201222.47784	Biognosys, Switzerland
Spectronaut	12.0.20491.14.21367	Biognosys, Switzerland

Table 3.17. List of software used for this study.

3.2. Methods

3.2.1. Mice

All mice were housed in standard sized individually ventilated cages (IVC), with enriched environment and ad libitum access to food and water. Mice were maintained in a specific pathogen-free facility with a 12-hour light/dark cycle. All experiments and handling of mice was performed in compliance with the German animal welfare law and with approval from the Government of Upper Bavaria. CSF was sampled under the animal license: ROB 55.2-2532.Vet_02-15-69. Mice were sacrificed by cervical dislocation followed by brain harvest. CSF and brain tissue were collected from mice of the following mouse strains: C57BL/6J, C57BL/6J *Grn*-knockout (Kayasuga et al., 2007), and C57BL/6J *Trem2*-knockout (Turnbull et al., 2006) (Table 3.4). Both male and female mice were used for the experiments.

3.2.1.1. Genotyping of mice

Mouse biopsies from tail or ear were submerged in mouse tail lysis buffer (pH 8.5), supplemented with Proteinase K. Samples were then incubated at 55 °C and shaking (750 rpm) until tissue is completely dissolved (minimum 3 hours). Genomic DNA was precipitated and purified using isopropanol and several centrifugation and ethanol washing steps. The locus harboring the *Trem2* gene was amplified by polymerase chain reaction (PCR) using two forward primers and one reverse primer (Table 3.5). PCR reactions were carried out as follows: denaturation at 94 °C for 2 minutes, followed by 30 amplification cycles of 94 °C for 15 seconds, 55 °C for 30 seconds, 72 °C for 1 minute, then final extension at 72 °C for 5 minutes (Table 3.6). As the *Grn*-knockout mouse line was previously generated by replacing exons 2-13 of the *Grn* gene with a neomycin resistance gene (Kayasuga et al., 2007) the knockout status was determined using Neo-forward primer and Neo-reverse primer yielding a fragment of 424 base pairs (bp). The wild-type gene was determined using GRN-forward primer and GRN-reverse primer, resulting in a fragment of 555 bp (Table 3.5). PCR reactions were carried out as follows: denaturation at 95 °C for 5 minutes, followed by 30 amplification cycles of 95 °C for 30 seconds, 62 °C for 30 seconds, 72 °C for 30 seconds, then final extension at 72 °C for 5 minutes (Table 3.7). Fragments were separated and detected by gel electrophoresis (1.5% agarose gel), whereupon the genotype of each mouse could be determined. For quality control purposes, each mouse was genotyped twice, with two separate biopsies (ear and tail).

3.2.1.2. Mouse CSF sampling

Mice were deeply anesthetized using a mix of medetomidine [0.5 mg/kg], midazolam [5 mg/kg], and fentanyl [0.05 mg/kg] (MMF). The MMF-mix was dosed according to bodyweight of each mouse and administrated via intraperitoneal injection. To avoid hypothermia, mice were kept on a heating pad (37 °C) throughout the whole procedure. CSF was collected from the cisterna magna by a single stereotactic puncture of the dura using a glass capillary (inner diameter of 0.75 mm). Immediately after collection, the CSF was ejected to a Protein LoBind tube and stored on ice until further processing. In total, the procedure, from injection of MMF to cervical dislocation, lasted 15-20 minutes. The collected CSF samples were centrifuged at 2000 x g for 10 minutes, visually controlled for blood contamination, aliquoted to Protein LoBind tubes in volumes of 5 µl, snap-frozen in liquid nitrogen and finally stored at -80 °C (Figure 3.1). A very similar procedure for CSF sampling has previously been documented and published (Lim et al., 2018).

1 Skin incision

Position the mouse in the stereotaxic frame, using rounded ear bars, positioned well that the head can only move in a smooth vertical manner when pulling the tail. Separate the the fur (gray arrows) to generate a midline stretching from the top of the head to the neck. Water or ointment like Bepanthen® can be used to keep the hair in place. Use surgical scissors of appropriate size to make an incision, following the vertical midline (black arrow), through the superficial layers of the skin (epidermis and dermis).

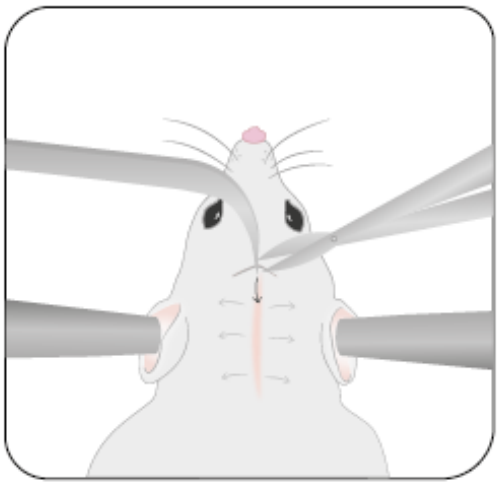

2 Subcutaneous incision

Starting at the top of the head, where you can see and feel the partly exposed skull, gently slide the tip of sharp point forceps in a vertical direction from the skull towards the neck. Find and grip the subcutaneous layer with the forceps and insert a vertical incision, following the bright midline.

Tip: Before making the incision, a larger area will be exposed if lifting up the skin and cutting off fibers of connective tissue attached to the suncutanous layer.

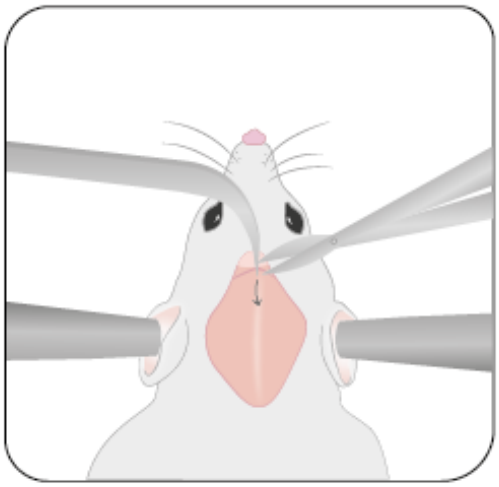

3 Parting the muscle tissue

Use very gentle and vertical movements to part the muscle tissue, layer by layer, one forcep in front of the other. It is very important to cautiosly use the sharp point forceps and avoid horisontal movements, as this would cause the muscles to rupture and later on impede the hooking of the muscles.

Tip: Before parting the muscle tissue, stop and clean all bleedings. This will reduce the risk of blood reaching the dura and potential contamination.

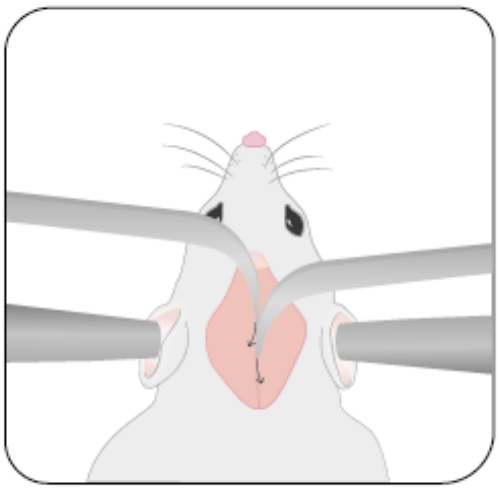

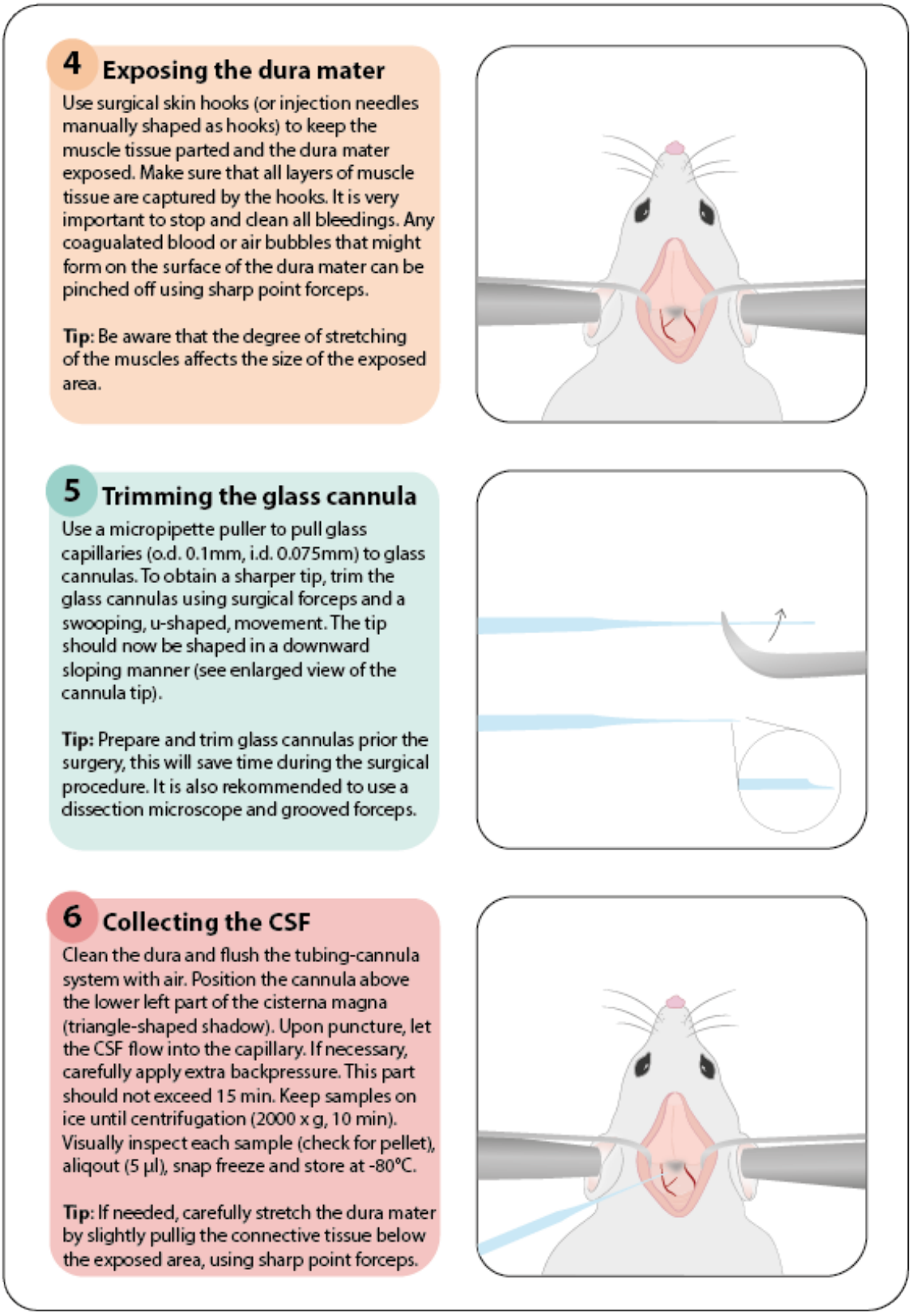

Figure 3.1. The procedure of CSF collection from mouse.

Six-step summary for the collection of CSF from mouse. Abbreviations: CSF = cerebrospinal fluid; min = minutes; o.d. = outer diameter; i.d. = inner diameter.

3.2.1.3. Microglia isolation from mouse brain using MACS

Mouse brains were isolated immediately after CSF sampling, transferred to a 3 cm petri dish, and completely covered with Hank's Balanced Salt Solution (HBSS; containing Ca^{2+} and Mg^{2+}), supplemented with 1 M HEPES. Microglia were isolated using the magnetic-activated cell sorting (MACS) technique, following the manufactures instructions (Neural Tissue Dissociation Kit (P), MACS Miltenyi Biotec), with slight modifications similarly to a previously published protocol (Sebastian Monasor et al., 2020). In brief, cerebellum, olfactory bulb, and meninges were removed, and each hemisphere was cut into pieces. Dissected brains were homogenized using an automatic (gentleMACS Dissociator) and enzymatic (Enzyme A (10 µl) + Enzyme P (50 µl)) dissociation process. The homogenates were rinsed through a cell strainer (cut-off 40 µm). Filtered samples were pelleted, washed and resuspended in HBSS. After washing, cells were magnetically labeled with CD11b (Microglia) Microbeads, diluted in 90 µl MACS buffer. The magnetically labeled cell suspension was loaded onto a MACS LS-column, washed with MACS buffer, and eluted into a Protein LoBind tube. The eluted microglia fraction was pelleted and washed with HBSS to remove any remains of bovine serum albumin (BSA) from the MACS buffer. Then all liquid was aspirated and the remaining cell pellet was snap-frozen and stored at -80°C.

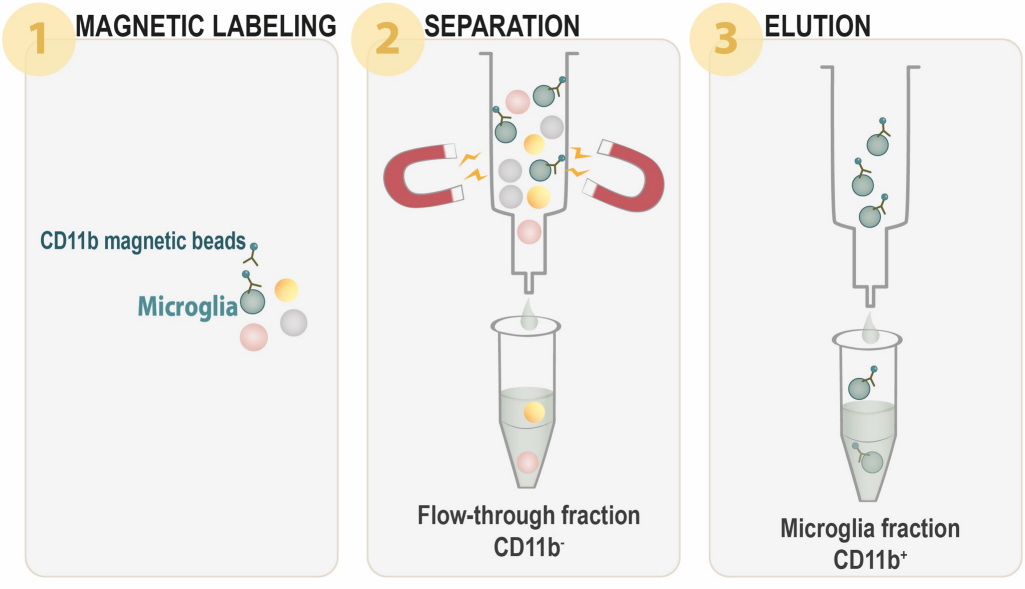

Figure 3.2. The principle of microglia isolation using the MACS technique.

Illustration depicting the principle of the magnetic-activated cell sorting (MACS) technique. (1) Magnetic labeling of microglia by incubating brain homogenates with magnetic beads coupled to antibodies targeting CD11b. (2) Separation of cells by retaining the magnetically bound microglia to the LS-column, allowing the non-labeled cells to elute yielding a microglia-depleted flow-through fraction. (3) Elution of microglia by removing the magnets.

3.2.2. hiGML

For this thesis three hiMGL cell lines have been used: *GRN*-knockout, *TREM2*-knockout, and wild-type. The generation and quality control of the *GRN*-knockout hiMGL line has already been published (Reifschneider et al., 2022). Therefore, the generation and quality control of the *TREM2*-knockout hiMGL line is presented here.

3.2.2.1. Generation of iPSC lines

All experiments including iPSCs were performed in compliance with all applicable guidelines and regulations. Cells from the female iPSC line A18944 (ThermoFisher) were cultured on Vitronectin-coated plates in Essential 8 Flex Medium at 37 °C with 5% CO_2. Two times per week, iPSCs were incubated in PBS/EDTA (EDTA (Invitrogen) diluted 1:1000 (to 0.5 mM) in PBS (Sigma)) for 5 minutes then split in form of minor clusters. Prior to transfection via electroporation, iPSCs were incubated in PBS/EDTA for 10 minutes, then split to single cells onto plates coated with Geltrex and cultured for two days in StemFlex Medium supplemented with 10mM ROCK inhibitor. Transfection was performed according to a previously published protocol (Kwart, Paquet, Teo, & Tessier-Lavigne, 2017), with modifications as previously described (Reifschneider et al., 2022). In short, 2 million cells were detached using Accutase. Following detachment, cells were resuspended in 100 ml cold BTXpress electroporation solution, supplemented with 20 mg Cas9 (pSpCas9(BB)-2A-Puro (PX459) V2.0 (gift from Feng Zhang; Addgene plasmid #62988; http://n2t.net/addgene:62988; RRID: Addgene_62988 (Ran et al., 2013)) and 5 mg sgRNA cloned into the BsmBI restriction site of the MLM3636 plasmid (gift from Keith Joung, Addgene plasmid #43860; http://n2t.net/addgene:48360; PRID: Addgene_43860). Cells were transferred to a 1 mm cuvette and the electroporation was performed using double pulses, each pulse at 65 mV for 20 ms. Post electroporation, cells were cultured on Geltrex-coated 10 cm plates in StemFlex Medium supplemented with 10 mM ROCK inhibitor until cell colonies became visible. One day post electroporation, selection of Cas9 expressing cells was performed by incubating cells with Puromycin dihydrochloride [350 ng/ml] for three consecutive days (Steyer et al., 2018). Single-cell colonies were picked and analyzed using Restriction fragment length polymorphism technique (RFLP). For the analysis with RFLP, the MwoI enzyme was used for the *GRN* ko line, while the NEB enzyme SfaNI was used for the *TREM2* KO. The analysis using RFLP and Sanger Sequencing was performed according to a previously published protocol (Kwart et al., 2017). The CRISPR/Cas9-

based genome editing, iPSC quality control measures and differentiation of hiMGL were previously described for the GRN ko line (Reifschneider et al., 2022).

3.2.2.2. Genome editing with CRISPR/Cas9

CRISPOR (http://crispor.tefor.net (Concordet & Haeussler, 2018) was used to select guide RNAs and to evaluate potential off-target loci (Figure 3.3). Successful knockout was confirmed in RIPA cell lysates by measuring mRNA levels using qPCR. In conditioned media, successful knockout was confirmed using ELISA (Figure 3.4).

Figure 3.3. Genetic design of the TREM2-knockout hiMGL line.

The genome editing strategy of *TREM2*-knockout in hiMGL: the *TREM2* locus was targeted in exon 2 by a sgRNA (target and PAM sequence indicated), leading to a one base pair insertion in the *TREM2*-knockout line. The resulting frameshift exposes a nearby stop codon.

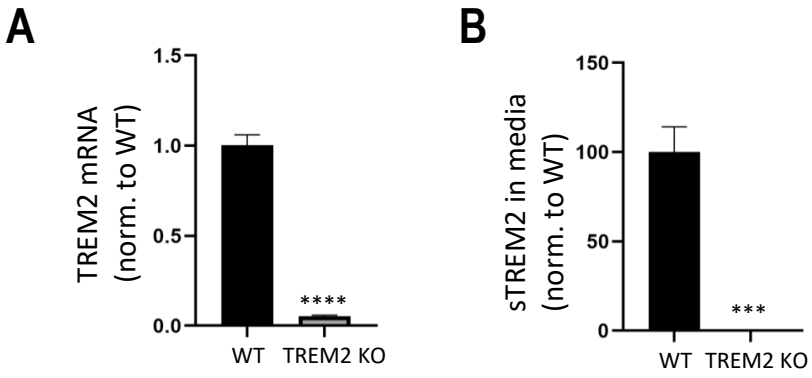

Figure 3.4. TREM2 mRNA transcript and sTREM2 levels in wild-type and TREM2-knockout hiMGL lysate and media.

(A) mRNA levels of *TREM2* in WT and *TREM2*-knockout hiMGL, normalized to WT levels, measured by qPCR, showing that *TREM2* is not expressed on the RNA level in the *TREM2*-knockout (mean, SD). (B) sTREM2 concentration in conditioned media of WT and *TREM2*-knockout hiMGL, normalized to WT levels, measured by ELISA, showing no sTREM2 in the media of the *TREM2*-knockout. Abbreviations: mRNA = messenger ribonucleic acid; WT = wild-type; KO = knock-out; norm. = normalized; sTREM2 = soluble TREM2.

For quality control purposes, the absence of off-target effects within the edited iPSC clones was confirmed using PCR amplification and Sanger sequencing with the top five hits based on MIT and CFD scores on CRISPOR (Table 3.18).

Gene	ID	Sequence	Mismatch Position	Mismatch Count	MIT Score	CFD Score	Location	Location Description	Indels detected
TREM2	gRNA	ACTGGTAGAGACCCGCATCATGG							
TREM2	CFD OT 1	ACTGGTAGAGACCTGAAAAAGGG	.....*.*.**	4	0.002	0.210	2:74495899:74496421:-1	intergenic:TTC31-LBX2	None
TREM2	CFD OT 2	ACTGGTAGAAAACCACAGCATGG	.....*.*..*..	4	0.032	0.209	8:117315826:117316348:1	intergenic:SNORA31-MED30	None
TREM2	CFD OT 3	ACGGGGAGAGAACCACATCAAGG	..*..*....*.*....	4	0.118	0.192	8:73680166:73680688:1	intergenic:RP11-463D19.1-STAU2/RP11-463D19.2	None
TREM2	MIT OT 1	ACAGGTACAAAACCGCATCATGG	..*....*.**.....	4	0.639	0.293	X:33061394:33061916:-1	intron:DMD	None
TREM2	MIT OT 2	TCTGTGAGAGACCCGCATCTGGG	*...**.....*	4	0.422	0.103	7:27943174:27943696:-1	intron:JAZF1	None
TREM2	MIT OT 3	CATGGTAAAGACCCTCATCATGG	**.....*.....*.....	4	0.403	0.089	3:73654765:73655287:1	intergenic:PDZRN3/CTD-2006M22.2/PDZRN3-AS1-RP11-20B7.1	None
TREM2	MIT OT 4	ACTGGCAGAGACCCGCTTCCTGG	.....*.....*..*	3	0.306	0.028	20:35899369:35899891:-1	exon:PHF20	None
TREM2	MIT OT 5	AATGGAAGAGACCAGCATCATGG	.*...*.....*.....	3	0.268	0.221	13:77120497:77121019:-1	intergenic:MYCBP2/MYCBP2-AS1-MYCBP2	None

Table 3.18. Confirmed absence of potential off-target effects.

Top five most similar off-target loci ranked by MIT and CFD prediction scores. No off-target effects were detected by Sanger sequencing. Abbreviations: CFD = cutting frequency determination; gRNA = guide RNA.

The absence of on-target effects, including large deletion and loss of heterozygosity, was evaluated by qPCR and nearby SNP sequencing (Weisheit et al., 2021) (Figure 3.5). The pluripotency was confirmed with immunofluorescence staining for pluripotency markers: PCT4, NANOG, SSEA4, and TRA160 (Figure 3.6). As a final step of quality control, chromosomal integrity was ensured by molecular karyotyping (LIFE & BRAIN GmbH) (Figure 3.7). The whole procedure, including the design and preparation of editing reagents and quality control of edited iPSCs, has been previously described elsewhere (Weisheit et al., 2020; Weisheit et al., 2021). Only when passing all the described quality controls, one clonal cell line was used for further differentiation into hiMGL.

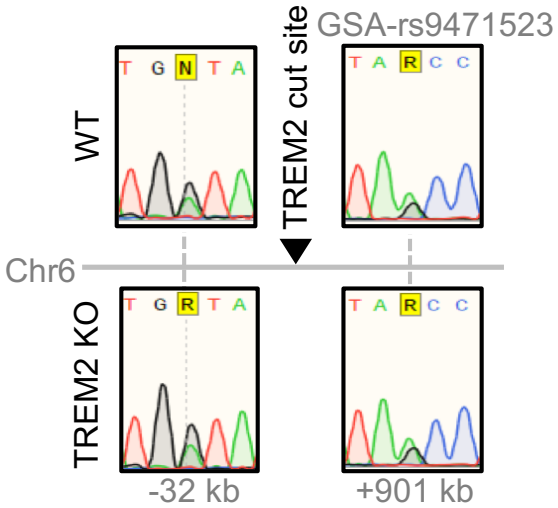

Figure 3.5. Quality control of hiMGL generation.

Analysis of on-target effects mediated by CRISPR editing through Sanger sequencing of SNPs near the edited locus in WT and *TREM2*-knockout lines, showing maintenance of both alleles. Abbreviations: KO = knock-out; WT = wild-type.

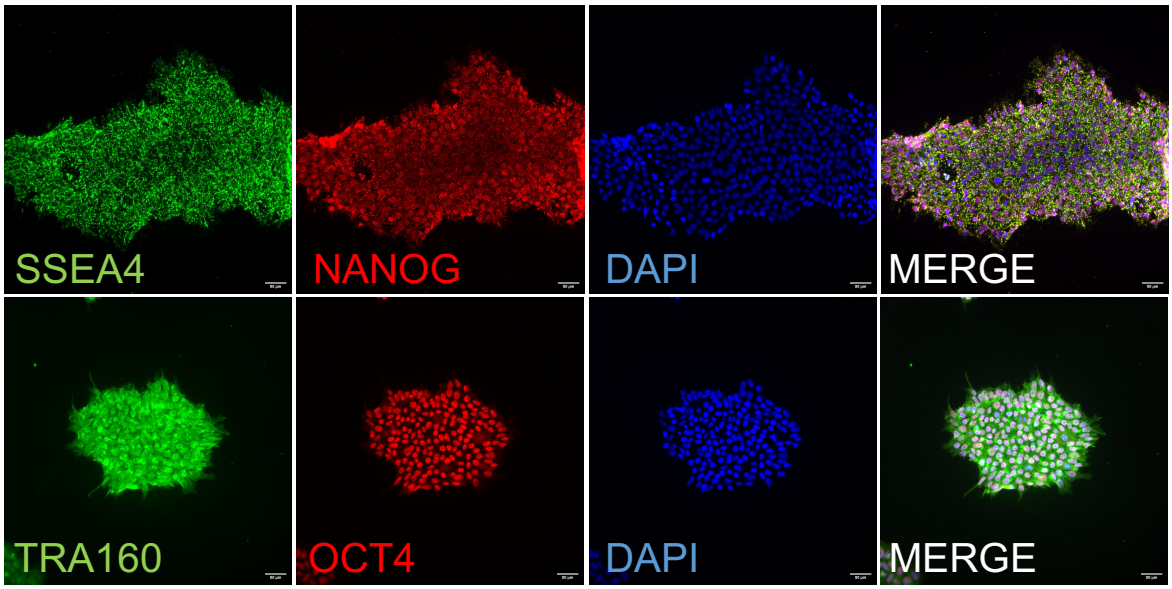

Figure 3.6. Immunofluorescence analysis of pluripotency.

Immunofluorescence image of the pluripotency markers SSEA4, NANOG, TRA160, and OCT4 with DAPI in *TREM2*-knockout iPSCs. Scalebars = 100 µm. Abbreviations: SSEA4 = stage-specific embryonic antigen-4; DAPI = DNAX activation protein of 12kDa; TRA160 = podocalyxin.

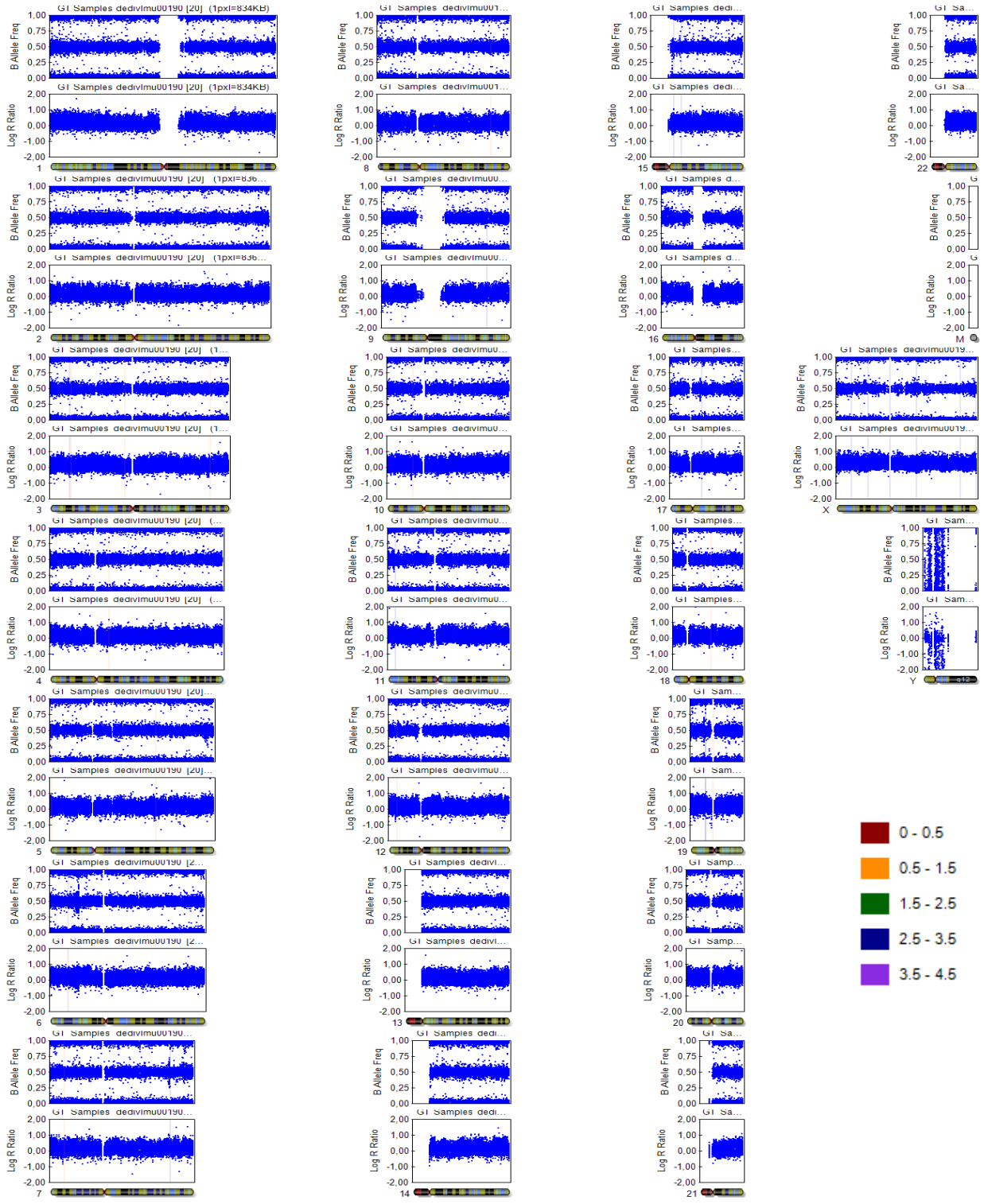

Figure 3.7. Molecular karyotyping of TREM2-knockout iPSC line

Log R ratios and B allele frequencies (BAF) for each chromosome in the *TREM2*-knockout iPSC line. The blue dots indicate measured SNPs. Normal zygosities on all chromosomes are indicated by BAF values and absence of detectable insertions and deletions are confirmed by the Log R ratios. There are no chromosomal aberrations shown by the karyotyping.

3.2.2.3. Differentiation of iPSC-derived microglia (hiMGL)

The clonal lines that passed all quality controls were selected for differentiation from iPSCs to hiMGL, following a previously described procedure (Abud et al., 2017) with modifications improving efficiency and yield (similar protocol published elsewhere (McQuade et al., 2018)). In brief, iPSCs were split 1:100-200 once a confluency of 70-90% was reached, then transferred to GelTrex-coated six-well plates for the hematopoietic cell (HPC) differentiation using EDTA to yield approximately 20 small colonies per well. On day 0, cells were fed with 2 ml HemA medium (HPC differentiation kit, StemCell technologies). On day 2, cells where half-fed with 1 ml HemA. On day 3, media was switch from HemA to HemB, with half-feeds on days 5 and 7 and 1 ml HemB was added on day 10. HPCs were collected as non-adherent cells on day 12 and frozen at 1 million cells per 1 ml in cryopreservation medium BamBanker. Upon thawing, 1 million HPCs were evenly distributed among all wells of a GelTrex-coated six-well plate. Each well contained 2 ml iMGL media, freshly supplemented with 25 ng/ml M-CSF, 100 ng/ml IL-34, and 50 ng/ml TGF-β. Throughout the process of microglia differentiation, 1 ml media was added every other day and cells were split in a 1:2 ratio every 6-8 days according to cell confluency. CD200 and CX3CL1 were not used for final differentiation, as this did not affect the hiMGL gene expression profile analyzed with NanoString. On day 16 of the hiMGL differentiation, cells were used for experiments.

3.2.2.4. Harvesting of hiMGL

Throughout the harvesting procedure, cells and PBS were kept on ice. In total, two 6-well plates from each experimental group (wild-type, *GRN*-knockout, and *TREM2*-knockout) were used, with 200 000 cells per well. The cells were carefully dissociated from the plate using a cell scraper, washed with their media, and subsequently transferred to conical centrifuge tubes (15 ml). The cells collected from each well were pooled pairwise, yielding n = 6 for each experimental group. The tubes were centrifuged at 300 x g for 6 min at 4 °C and the conditioned media was transferred to a new conical centrifuge tube (15 ml). Each well of the plates were washed with 0.5 ml PBS. The PBS was pooled following the same order as the pooling of the collected cells, resulting in a total volume of 1 ml and n = 6 per experimental group. The 1 ml of PBS with the resuspended cells was transferred to a 1.5 ml Protein LoBind tube. All tubes were centrifuged: centrifugation tubes containing the supernatant at 300 x g for 20 minutes and LoBind tubes with the cell pellet and PBS-wash at 300 x g for 6 minutes.

From each centrifugation tube, the supernatant was aliquoted to 3 x 1 ml, snap-frozen in liquid nitrogen and stored at -80 °C (media fraction). From the Protein LoBind tubes, each cell pellet was isolated by removal and disposal of the supernatant. The cell pellet was snap-frozen and stored at -80 °C (microglia fraction).

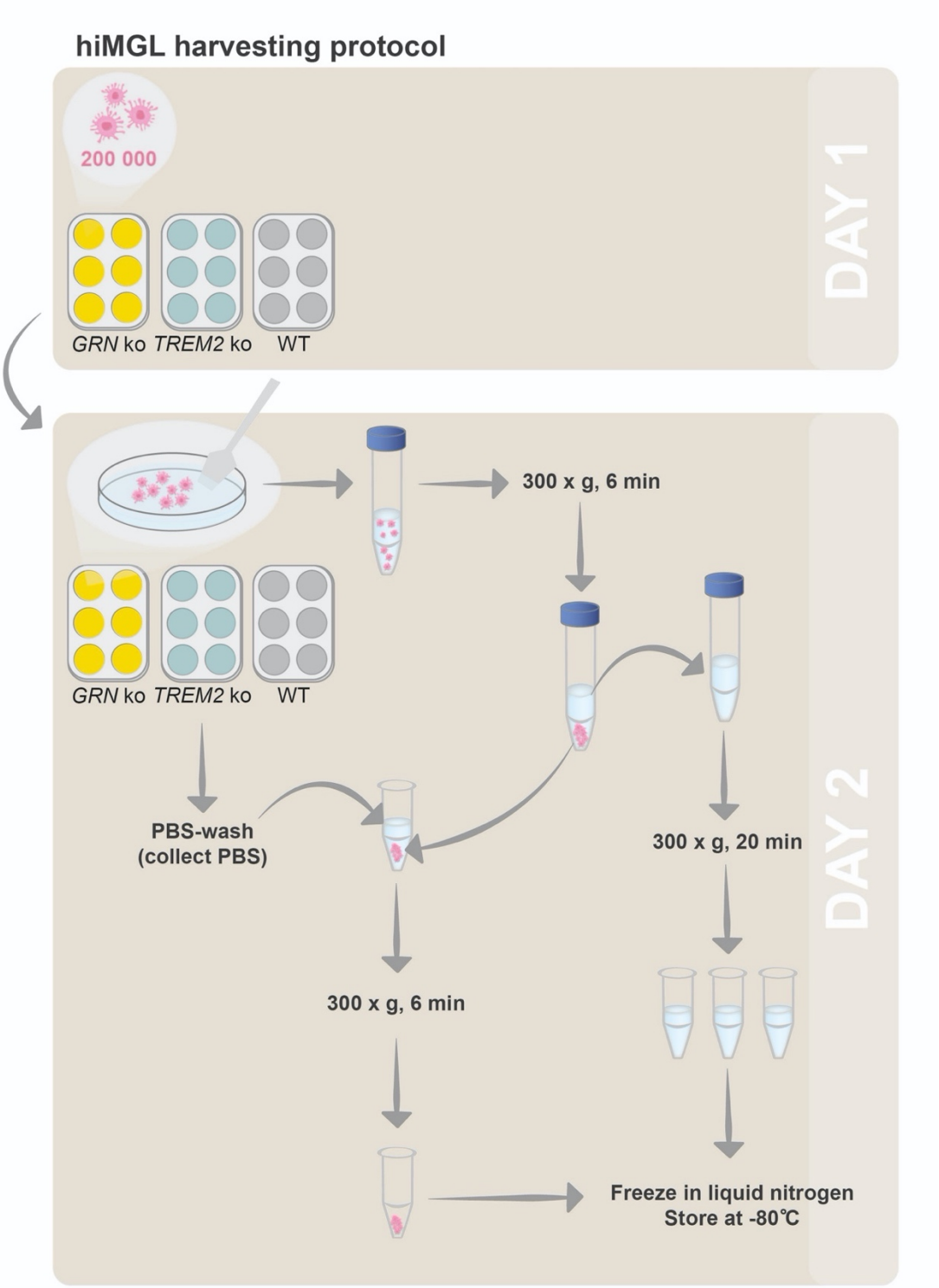

Figure 3.8. Summary of procedure for the harvesting of hiMGL cells and media.

Abbreviation: min = minutes; PBS = phosphate-buffered saline.

3.2.3. Human CSF samples

3.2.3.1. Study Participants

In total, CSF of 12 heterozygous *GRN* mutation carriers with symptomatic FTD (FTD-GRN) and 12 non-symptomatic non-carriers (CON) were analyzed. Data from one *GRN* mutation carrier was excluded as this participant was not fulfilling the criteria of symptomatic FTD, resulting in a comparison of 11 FTD-GRN and 12 CON. All participants were enrolled in ARTFL (U54NS092089) or LEFFTDS (U01AG045390), together ALLFTD, which is a North American research consortium to study sporadic and familiar FTD. All CSF from the ALLFTD consortium were approved and provided by the National Centralized Repository for Alzheimer's Disease and Related Dementias (NCRAD). CSF obtained from ALLFTD was collected following NCRAD standard operating procedure. In brief, CSF was collected in the morning between 8.00 am – 10.00 am, preferably fasted or following a low-fat diet. Lumbar puncture was performed in a sterile field using an atraumatic technique. Within 15 minutes of collection, CSF samples were centrifuged at 2000 x g for 10 minutes at room temperature. Post centrifugation the CSF was aliquoted into pre-cooled aliquot tubes. Within 60 minutes of CSF collection aliquots are snap frozen on dry ice and stored at -80 °C.

ALLFTD cohort

	Non-symptomatic Non-carriers (n = 12)	Symptomatic mutation carriers (n = 11)
SEX		
Male	6 (50.0%)	3 (27.3%)
Female	6 (50.0%)	8 (72.7%)
AGE		
45 - 49	1 (8.3%)	0 (0.0%)
50 - 54	2 (16.7%)	1 (9.1%)
55 - 59	3 (25.0%)	1 (9.1%)
60 - 64	3 (25.0%)	3 (27.3%)
65 - 69	2 (16.7%)	3 (27.3%)
70 - 74	1 (8.3%)	3 (27.3%)

Table 3.19. Demographics of the ALLFTD cohort.

3.2.4. Sample preparation for mass spectrometry

3.2.4.1. Sample overview

In total, 14 sets of samples have been collected, prepared and analyzed with liquid chromatography tandem mass spectrometry (LC-MS/MS) using a label-free quantification (LFQ) method. The mouse cohort consists out of three mouse lines: wild-type (wt), *Grn* knockout (ko), and *Trem2* ko – all sacrificed when 12 months old. Prior to scarification and subsequent microglia isolation, each mouse was deeply anaesthetized and CSF was collected. In total, we analyzed CSF from 14 mice (n (wt) = 6; n (*Grn* ko) = 4; n (*Trem2* ko) = 4) and microglia from 19 mice (n (wt) = 7; n (*Grn* ko) = 4; n (*Trem2* ko) = 8). The hiMGL samples included both cell lysates and conditioned media, each collected from three different iPSC lines: WT, *GRN* ko, and *TREM2* ko, with a sample size of n = 6 for each sample type and line. For human CSF, the CSF of 11 FTD-GRN patients and 12 non-symptomatic non-carriers (CON) was analyzed. All samples were prepared and analyzed together according to sample type: mouse CSF, mouse microglia, hiMGL media, hiMGL cell lysates, and human CSF (hCSF). Mouse CSF was prepared using in-solution digestion. Mouse microglia and hiMGL media were prepared using filter aided sample preparation (FASP) (Wisniewski, Zougman, & Mann, 2009), while hiMGL cell lysates and hCSF were prepared using Single-pot, solid-phase-enhanced sample preparation (SP3) (Hughes, Sorensen, & Morin, 2019) (Figure 3.9).

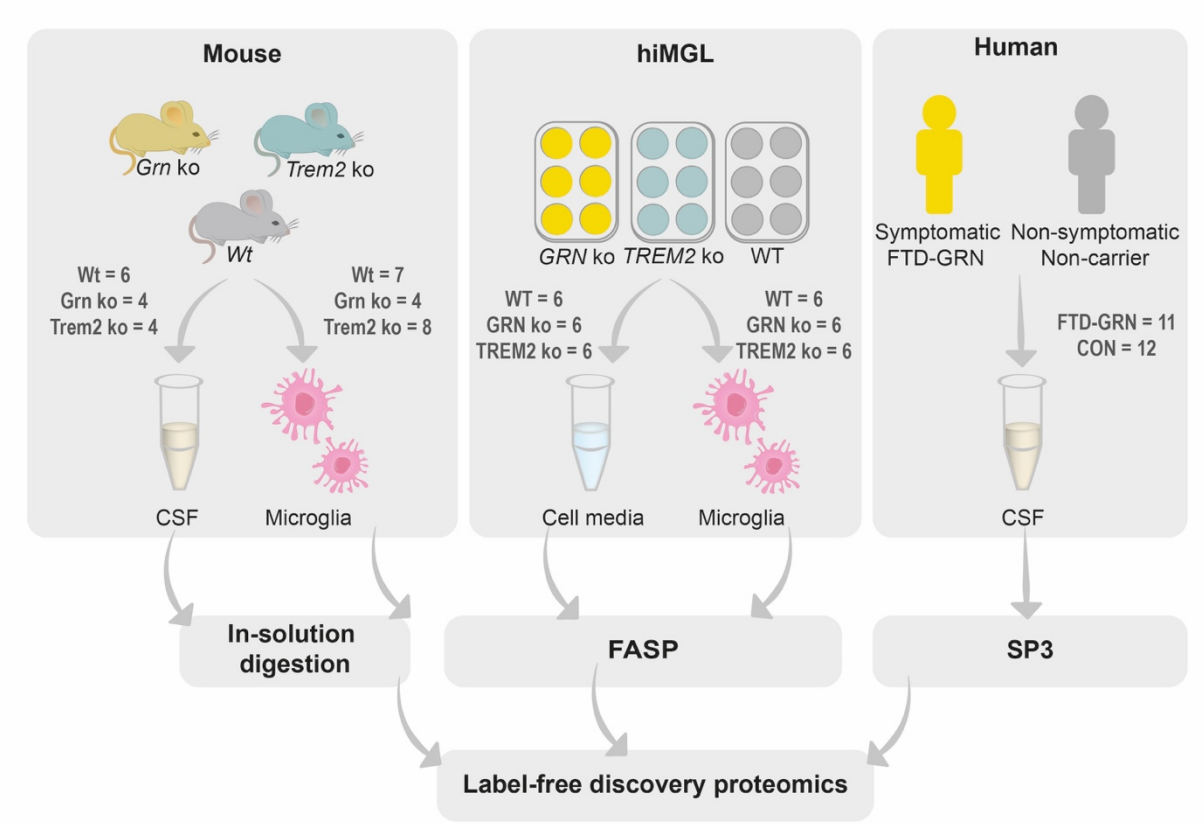

Figure 3.9. Graphical abstract summarizing all samples prepared and analyzed with mass spectrometry. Overview of samples used for this study. Number of samples is indicated in dark gray. Abbreviations: WT = wild-type; hiMGL = human-iPSC-derived microglia; CSF = cerebrospinal fluid; FASP = filter aided sample preparation; SP3 = single-pot, solid-phase-enhanced sample preparation.

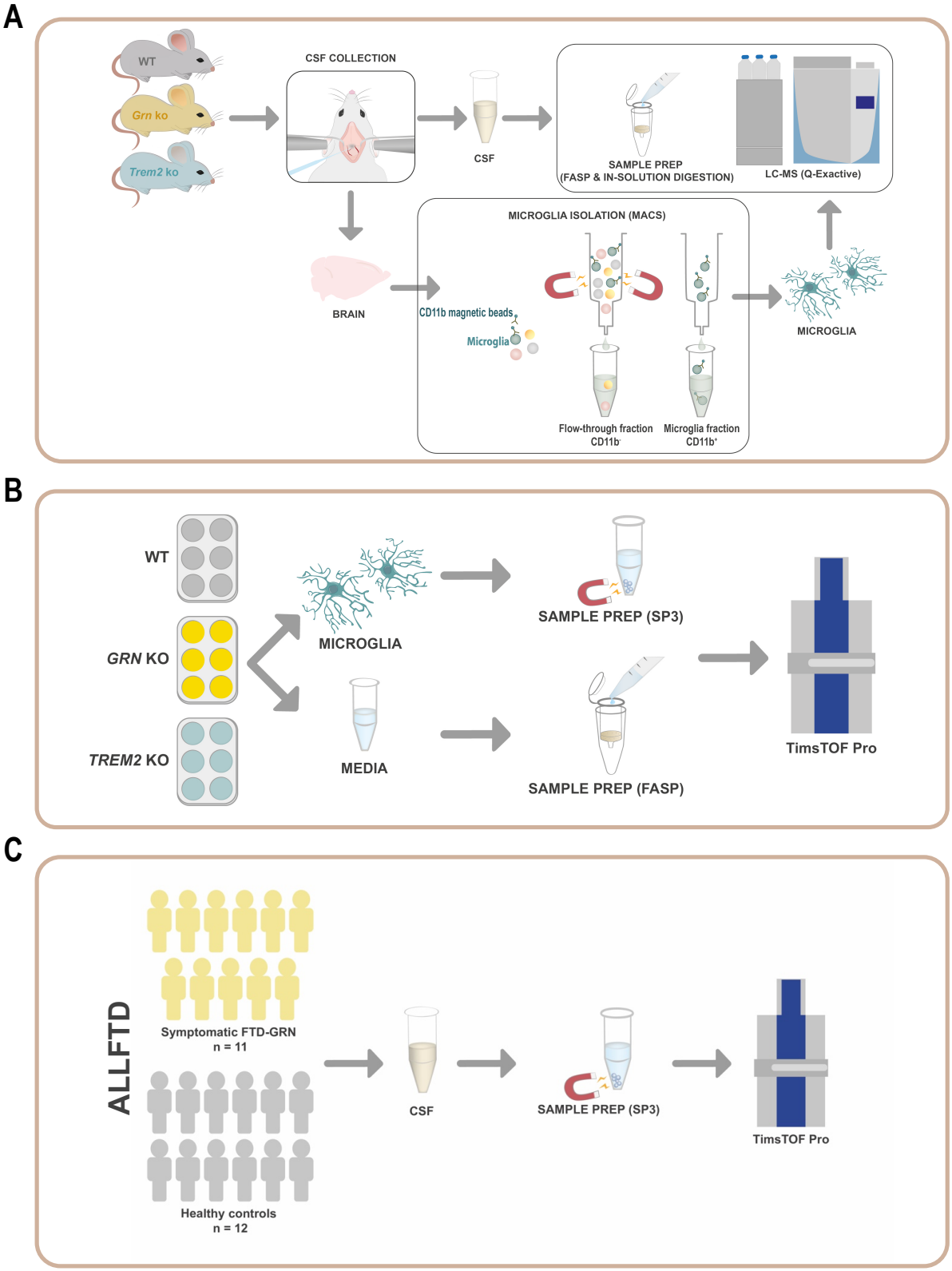

Figure 3.10. Graphical abstract summarizing sample type and sample preparation.
Overview of sample type and sample preparation for samples originating from (A) mice, (B) hiMGL, and (C) human. Abbreviations: WT = wild-type; GRN = progranulin (gene); TREM2 = triggering receptor expressed on myeloid cells 2; CFS = cerebrospinal fluid; FTD-GRN = frontotemporal dementia caused by heterozygous mutation in the *GRN* gene; hiMGL = human-iPSC-derived microglia; LC-MS = liquid chromatography–mass spectrometry; FASP = filter aided sample preparation; SP3 = single-pot, solid-phase-enhanced sample preparation.

3.2.4.2. In-solution digestion

From each sample of mouse CSF, a volume of 5 µl was used for in-solution digestion, corresponding to approximately 1.5-2 µg of protein. Denaturation of proteins was performed by adding a mix of 6 M urea, 2 M thiourea and 10 mM HEPES (pH = 8.0) to each CSF sample (15 µl denaturation mix per 5 µl CSF). For the reduction of disulfide bonds, 2 µl of reduction buffer (dithiothreitol (DTT)) and 50 mM ammonium bicarbonate (ABC) was added to each sample, followed by an incubation for 30 minutes at room temperature. To alkylate cysteine residues, 2 µl of alkylation buffer (55 mM iodoacetamide (IAA)) in 50 mM ABC was added to each sample, followed by a second addition of 2 µl reduction buffer and subsequent incubation for 30 minutes at room temperature. Then the samples were subjected to proteolytic digestion by adding 0.1 µg LysC for 3 hours and 0.1 µg trypsin for 16 hours at room temperature. Following incubation, the process of protein digestion was terminated by acidification using 8% formic acid (FA) to reach a pH < 2.5 (approximately 6 µl FA per 50 µl). Samples were collected by centrifugation and then desalted by stop and go extraction (STAGE) with C18-packed pipetting tips (Rappsilber, Ishihama, & Mann, 2003).

3.2.4.3. Single-pot, solid-phase-enhanced sample preparation - SP3

15 µl of human CSF was mixed with 15 µl STET lysis buffer with 2% Triton X-100 to inactivate potential viruses. For hiMGL, cell pellets were resuspended in 100 µl STET lysis buffer supplemented with protease inhibitors (Protease Inhibitor Cocktail, Sigma Aldrich, Product P8340) and incubated on ice for 20 minutes with intermediate mixing. Following incubation, cells were centrifuged at 16 000 x g for 10 minutes at 4 °C with subsequent isolation of the supernatant in which the protein concentration was determined using the Pierce 660 nm protein assay (Thermo Fisher Scientific) according to the manufacturer instructions. Protein LoBind tubes were used for storage and handling of samples throughout the protocol. The SP3 sample preparation was performed according to a previously published protocol (Hughes et al., 2019). In brief, a mixture consisting of two types of carboxylate-modified paramagnetic beads (SeraMag beads (Thermo Fisher Scientific)) was prepared in a ratio 1:1 (v/v). The beads were washed and resuspended in LC-MS grade water to a final bead concentration of 20 µg/µl. hiMGL cell lysates (35 µl [10-20 µg protein]) were supplemented with a 12.5 units Benzonase-$MgCl_2$ mix to degrade nucleic acid contaminations and incubated for 30 minutes at 37 °C. Samples were reduced using 4 µl dithiothreitol (DTT) [200 mM] with an incubation at 37 °C

for 30 minutes. Then samples were alkylated with 8 µl iodoacetamide (IAA) [400 mM] and incubated for 30 minutes at room temperature in the dark. The reaction was quenched by adding 4 µl DTT [200 mM]. Once reduced and alkylated, 10 µl of the paramagnetic bead stock was added to each sample. Proteins were bound to the beads by adding acetonitrile (ACN) to a final concentration of 70% (v/v) and incubated on a Thermomixer at room temperature and 600 rpm. Beads were washed four times with 200 µl 80% ethanol, using a magnetic rack to retain the beads. The digestion procedure was performed with 0.3 µg trypsin (Promega) and 0.3 µg Lys C (Promega) in 40 µl 50 mM ammonium bicarbonate, followed by incubation at 37 °C with shaking (1000 rpm) for 30 minutes. After the initial incubation, samples were further incubated at room temperature for 16 hours. Costar Spin-X filters with a 0.22 µm cut-off were washed with 200 µl 0.1% formic acid (FA) and placed in collection tubes. To collect the samples, the tubes were placed on a magnetic rack for 2 minutes to retain the beads. The supernatant was transferred to the prepared Spin-X columns. The aggregated beads were washed with 20 µl 0.1% FA, followed by brief sonication and collection by centrifugation. The tubes were placed again on the magnetic rack and the supernatant was transferred to the same equilibrated Spin-X filters (0.22 µg cut-off). Samples were acidified with 2 µl 8% FA and filtered into a collection tube by centrifugation at 2000 x g for 2 minutes. For final peptide isolation and storage, samples were dried by vacuum centrifugation and stored at -20 °C. Prior to tandem mass spectrometry analysis, samples were resuspended in 20 µl 0.1% FA.

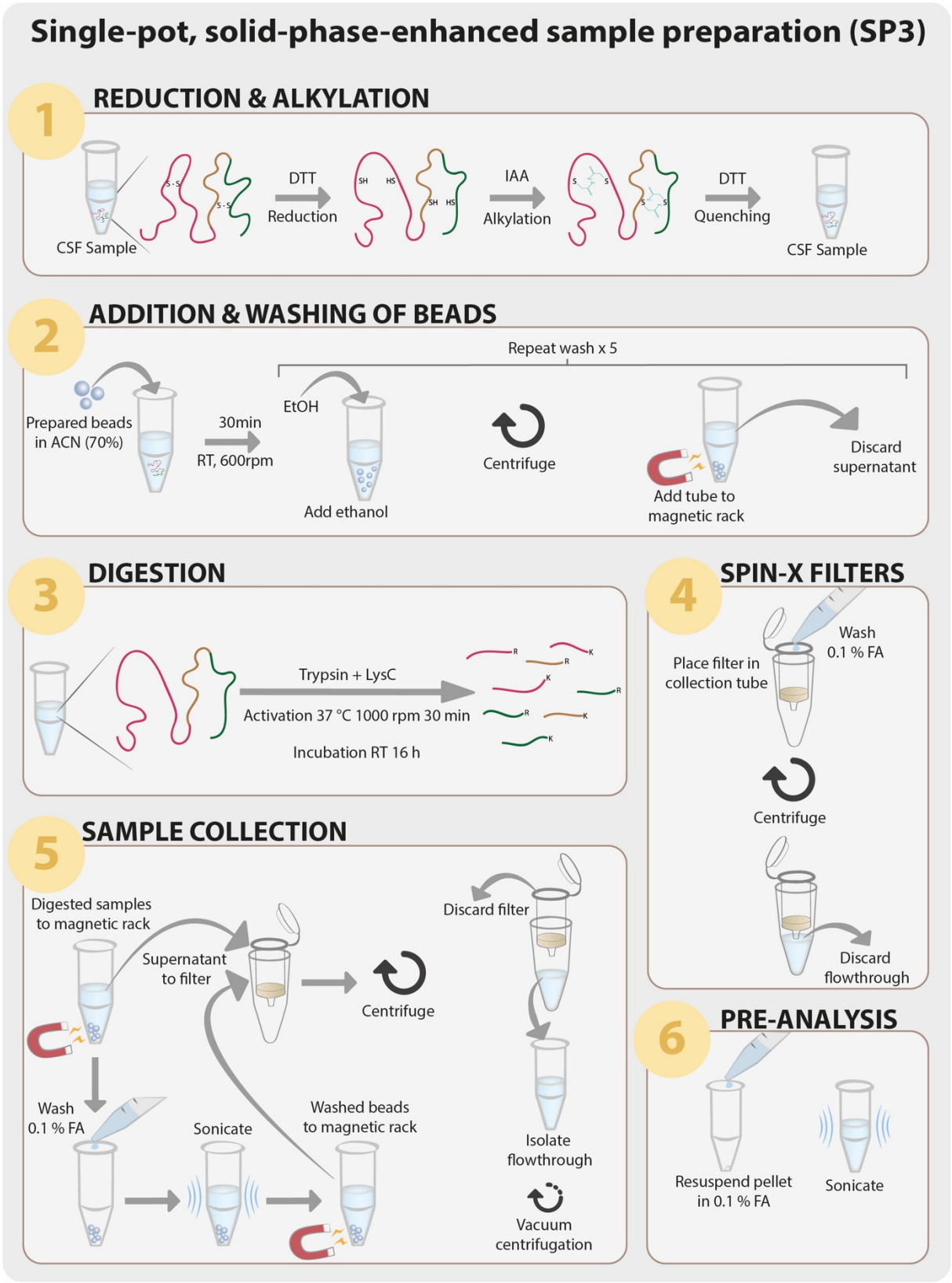

Figure 3.11. Single-pot, solid-phase-enhanced sample preparation (SP3).
Illustration summarizing the workflow of SP3 sample preparation. Abbreviations: CSF = cerebrospinal fluid; DTT = dithiothreitol; IAA = iodoacetamide; EtOH = ethanol; RT = room temperature; FA = formic acid.

3.2.4.4. Sample preparation for mass spectrometry – FASP

Protein LoBind tubes were used for storage and handling of samples throughout the procedure and samples were digeted using filter aided sample preparation (FASP) as previously described (Wisniewski et al., 2009). Samples were added to Vivacon spin filters (cut-off: 30 kDa for cell lysates and 10 kDa for conditioned media (500 µl)) with assigned collection tube. Samples were mixed with 200 µl 8 M urea buffer A (UA buffer: 8 M urea in 0.1 M Tris/HCl pH 8.5) with 100 mM DTT and proteins were reduced for 30 minutes on a thermomixer at 37 °C and 600 rpm. Afterwards, each sample was concentrated by centrifugation at 14 000 x g for 30 minutes, followed by the addition of 200 µl UA buffer and a second centrifugation step at 14 000 x g for 30 minutes. Then, 100 µl 50 mM IAA (in UA buffer) was added to each sample and samples were incubated for 5 minutes in the dark. Afterwards, samples were concentrated by centrifugation at 14000 x g for 30 minutes, followed by three subsequent additions of 200 µl 8 M urea buffer B (UB buffer: 8 M urea in 0.1 M Tris/HCl pH 8.0) and concentration by centrifugation (each step 14 000 x g for 30 minutes). Protein digestion was performed in two steps, for initial digestion LysC (Promega) (dissolved in 50 mM ABC) was added to each sample with an enzyme-protein ratio of 1:50 and then incubated at 37 °C for 16 hours in a wet chamber. For the second round of digestion, trypsin (Promega) (dissolved in 50 mM ABC) was added to each sample with an enzyme-protein ratio of 1:100 followed by incubation at 37 °C for 4 hours in a wet chamber. Peptides were eluted into clean collection tubes by centrifugation at 14 000 x g for 50 minutes. For improved peptide recovery, 50 µl of 0.5 M NaCl was added to each filter and samples were centrifuged at 14 000 x g for 20 minutes. Then, samples were acidified using 8% FA to reach a pH < 2.5 (approximately 6 µl FA per 50 µl). Samples were then desalted using the Stop and Go Extraction (STAGE) (Rappsilber et al., 2003).

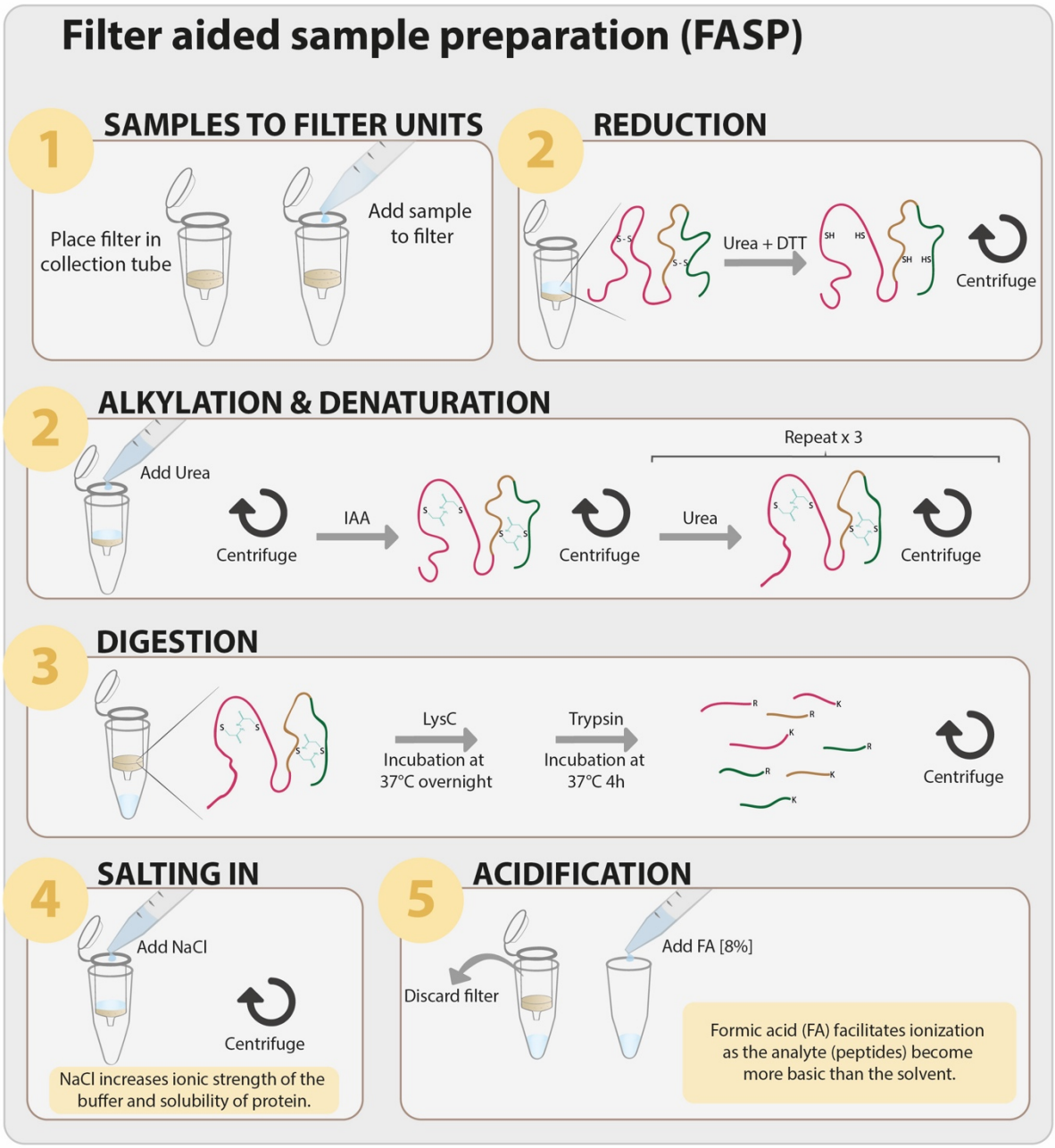

Figure 3.12. Filter aided sample preparation (FASP).
Illustration summarizing the workflow of FASP. Abbreviations: DTT = dithiothreitol; IAA = iodoacetamide; FA = formic acid; h = hours.

3.2.4.5. Stop and Go Extraction – STAGE

Peptides were desalted using Stop and Go Extraction (STAGE) with pipetting tips packed with C18 membrane disks (Empore Disks) (Rappsilber et al., 2003). The tips were manually packed with four C18 membrane layers in each tip, then conditioned by adding 100 µl methanol and centrifuging the tips without drying the membranes. After conditioning the tips and visually controlling for any leakage, 100 µl 0.1% FA was added to wash and remove the remaining methanol. Samples were added to tips, centrifuged, then washed three times with 100 µl 0.1%

FA, before eluted to Protein LoBind tubes using 60% ACN supplemented with 0.1% FA. For final peptide isolation and storage, samples were dried by vacuum centrifugation and stored at -20 °C. Prior to tandem mass spectrometry analysis, samples were resuspended in 20 µl 0.1% FA.

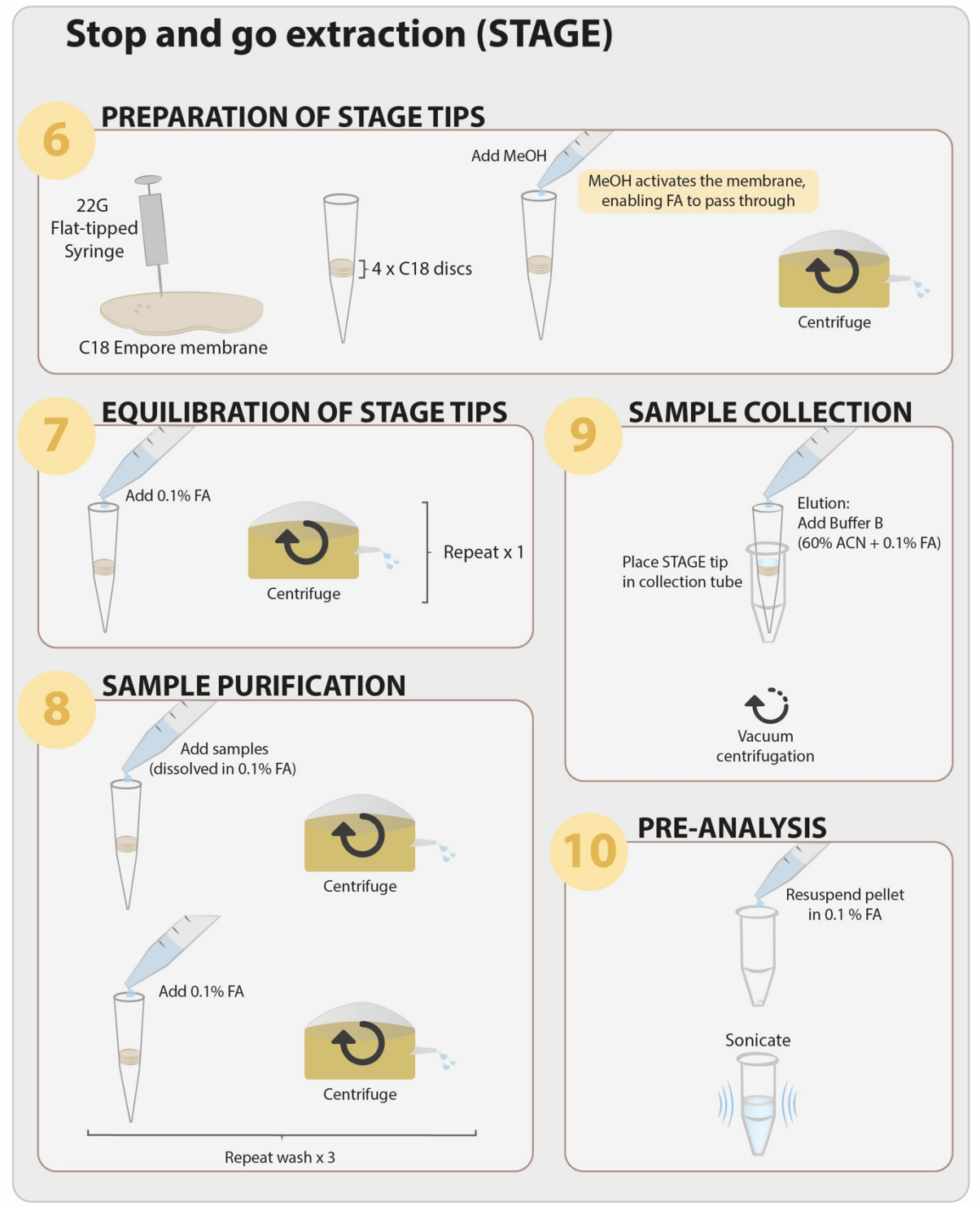

Figure 3.13. Stop and go extraction (STAGE).
Illustration summarizing the workflow STAGE as a part of sample preparation prior to analysis using mass spectrometry. Abbreviations: DTT = dithiothreitol; IAA = iodoacetamide; FA = formic acid; MeOH = methanol; ACN = acetonitrile.

3.2.5. Mass spectrometry using LC-MS/MS

As mentioned, LC-MS/MS was used for label-free quantification (LFQ) of the proteolytic peptides. Two setups were used for the peptide separation and analysis. For mouse samples, separation was carried out on a nanoLC system (Easy-nLC, Proxeon – part of Thermo Scientific, Waltham, MA, US) equipped with a PRSO-V1 column oven (Sonation, Germany) using in-house packed C18 columns (30 cm x 75 µm ID, ReproSil-Pur 120 C18-AQ, 1.9 µm, Dr. Maisch GmbH, Germany) applying a binary gradient of water and ACN (UHPLC grade, Biosolve, NL) supplemented with 0.1% FA (Sigma Aldrich, Germany) (0 minutes, 2% ACN; 3:30 minutes, 5% ACN; 137:30 minutes, 25% ACN; 168:30 minutes, 35% ACN; 182:30, 60% ACN) with a column temperature of 50 °C. The nanoLC system was online coupled to a Q-Exactive HF mass spectrometer (Thermo Scientific, Waltham, MA, US), via a Nanospray Flex Ion Source (Proxeon – part of Thermo Scientific, Waltham, MA, US). Samples were analyzed using data independent acquisition (DIA). For DIA, MS spectra were acquired at a resolution of 120 000 (m/z range: 300-1400: automatic gain control (AGC) target: 3E+6) followed by 25 or 30 MS/MS scans covering a range of 300-1400 m/z with variable m/z windows (resolution 30 000; AGC target: 3E+6 ions; normalized collision energy (NCE): 26%; maximum trapping time: “auto”). For human derived samples (hiMGL and human CSF (hCSF)), peptides were separated using a NanoElute nano high-performance liquid chromatography (HPLC) equipped with either 30 cm (hCSF samples) or 15 cm (hiMGL samples) columns (75 µm ID, packed with ReproSil-Pur 120 C18-AQ, 1.9 µm stationary phase, Dr. Mais GmbH, Germany), applying a 120 minute gradient for hiMGL cell lysates or a 70 minute gradient for hiMGL conditioned media and hCSF. The NanoElute nano HPLC system was online coupled to a TimsTOFpro mass spectrometer (Bruker, Germany). Samples were analyzed using DIA parallel accumulation serial fragmentation. For hCSF samples, one scan cycle induced one MS1 full scan followed by 2 rows of 50 sequential DIA windows with 18 m/z width for peptide fragment ion spectra with an overlap of 1 m/z covering a scan range of 350 to 1200 m/z. The ramp time was fixed to 166 ms and 5 windows were scanned per ramp. This resulted in a total cycle time of 3 seconds. For hiMGL samples, one scan cycle included one MS1 full scan followed by 2 rows of 40 sequential DIA windows with 22 m/z width for peptide fragment ion spectra with an overlap of 1 m/z covering a scan range of 350 to 1200 m/z. The ramp time was fixed to 100 ms and 4 windows were scanned per ramp. This resulted in a total cycle time of 2.1 seconds.

3.2.6. Analyses

3.2.6.1. Mass spectrometry data analysis and label free quantification

Database search and label free quantification was performed using the MaxQuant software package (maxquant.org, Max-Planck Institute Munich) (Cox et al., 2014) for data dependent acquisition (DDA) and Spectronaut (Biognosys, CH) or DIANN (https://github.com/vdemichev/DiaNN, Version 1.8) (Demichev, Messner, Vernardis, Lilley, & Ralser, 2020). The analysis of hCSF samples of the ALLFTD study was performed together with CSD samples of other origin than the ALLFTD, for which the data is not presented here. In total, 43 samples were analyzed using the DIA-NN (https://github.com/vdemichev/DiaNN, Version 1.8, Version 1.8) (Demichev et al., 2020), with which the normalization and library generation was performed. For the purpose of this study, of which FTD and especially the effect of *GRN* mutations on the human CSF proteome was of focus, only the data obtained from the ALLFTD was further investigated. The MS data were searched against canonical fasta databases including one protein per gene of *Mus musculus* and *Homo sapiens* from UniProt. For visualizations, unless stated otherwise, proteins are denoted with the gene name. For DIA of mouse microglia, a spectral library generated with samples of microglia with APPPS1 mice (Sebastian Monasor et al., 2020) was used for data analysis with Spectronaut. DIA-PASEF data from human CSF and iPSC derived human microglia were analyzed with DIA-NN using a library free search. Trypsin was defined as a protease with cleavage specificity for C-terminal of K and R. Acetylation of protein N-termini and oxidation of methionines were defined as variable modifications. Carbamidomethylation of cysteines was defined as fixed modification. For the database search, two missed cleavages were allowed. False discovery rate (FDR) for both proteins and peptides was adjusted to 1%.

3.2.6.2. Statistical analysis

LFQ values were used for relative quantification, log2 transformed and statistically analyzed using Perseus (Version 1.6.15.0) (Tyanova et al., 2016) and GraphPad Prism (Version 9.3.1). Proteins were considered quantifiable when LFQ intensities could be detected in at least three biological replicates per experimental group. No data imputation was performed to replace missing LFQ values. Unless stated otherwise, an unpaired two-tailed Student's *t*-test was applied to evaluate the significance of proteins with changed abundance. In addition, multiple hypothesis correction was performed using a permutation-based FDR estimation (Tusher,

Tibshirani, & Chu, 2001) (FDR = 0.05, $s_0 = 0.1$) or the method of Benjamini, Krieger and Yekutieli (Benjamini, Krieger, & Yekutieli, 2006) (threshold: FDR = 0.05). Unless stated otherwise, the FDR correction was not considered for the visualization of the data nor the selection of candidates. For correlation analysis Spearman correlation was used (two-tail, confidence interval = 95%), with the criteria that each selected protein was detected in at least three participants. For multiple comparison (comparing more than two groups), ordinary one-way ANOVA and Tukey's test were used. Significance was indicated accordingly: "*" = $p < 0.05$, "**" = $p < 0.01$, "***" = $p < 0.001$; "n.s." = non-significant.

R. Acetylation of protein N-termini and oxidation of methionines were defined as variable modifications. Carbamidomethylation of cysteines was defined as fixed modification. For the database search, two missed cleavages were allowed. False discovery rate (FDR) for both proteins and peptides was adjusted to 1%.

3.2.6.3. Prediction analysis

To test if the measured CSF abundances of the six identified candidates could be used to predict mutation status in the ALLFTD cohort, we used a machine learning approach based on logistic regression (sklearn.linear_model.LogisticRegression at scikit-learn.org) (Fabian Pedregosa, Peter Prettenhofer, & Duchesnay, 2011). Prediction performance was assessed via stratified cross-validation (sklearn.model_selection.StratifiedKFold at scikit-learn.org) (Fabian Pedregosa et al., 2011), in which the CSF abundance dataset was split into 5 different test and train sets with a similar distribution of classes. Statistical significance was established via a permutation testing procedure (Ojala & Garriga, 2009) in which the mutation status labels of the test set were shuffled, and the model prediction was performed for the shuffled labels. The score for a given permuted model was the averaged prediction performance across the 5 cross-validation splits. This procedure was repeated 1000 times, providing a baseline performance for the model pipeline. The p-value was defined as the number of permuted models with a higher score than the ground-truth, non-permuted model divided by the total number of permutations.

Based on sample estimators (Baeza-Delgado et al., 2022; Hsieh, Bloch, & Larsen, 1998), the number of patients per outcome necessary for a robust validation of the predictive capacity

of the protein panel is at least 30. Due to the relative rarity of GRN-mutations associated with FTD, and the constraints of obtaining clinical data, it is difficult to reach the sample size needed to develop a sufficiently consistent and reproducible model. For these reasons, we employ this model as a companion to conventional tests to provide further evidence of the protein panel's involvement, but not as exclusive evidence of the predictive capacities of this panel.

4. Results

4.1. Microglial activity state dependent proteomic signatures in Trem2-knockout and Grn-knockout mice

The first aim of my thesis was to investigate the opposite microglial phenotypes in the *Trem2*-knockout and *Grn*-knockout mice on the proteome level. As previously reported, *Trem2*-knockout microglia appear as homeostatic and incapable of responding to triggers (Gotzl et al., 2019; Keren-Shaul et al., 2017; Krasemann et al., 2017; Mazaheri et al., 2017; Reifschneider et al., 2022), while *Grn*-knockout microglia appear as hyperactivated (Gotzl et al., 2019; Reifschneider et al., 2022). A mass spectrometry-based approach was used to compare the proteome of microglia isolated from 12 months old *Grn*-knockout (Kayasuga et al., 2007) and *Trem2*-knockout mice (Turnbull et al., 2006) and their corresponding age-matched control (wild-type mice) (Figure 3.9 A). The 12 months old *Grn*-knockout mice showed an upregulation of markers associated with disease-associated microglia (DAM), such as Apoe, Lgals3, Lyz2, and Clec7a. In contrast, these DAM markers were downregulated in the age-matched *Trem2*-knockout mice (Figure 4.1 A-B).

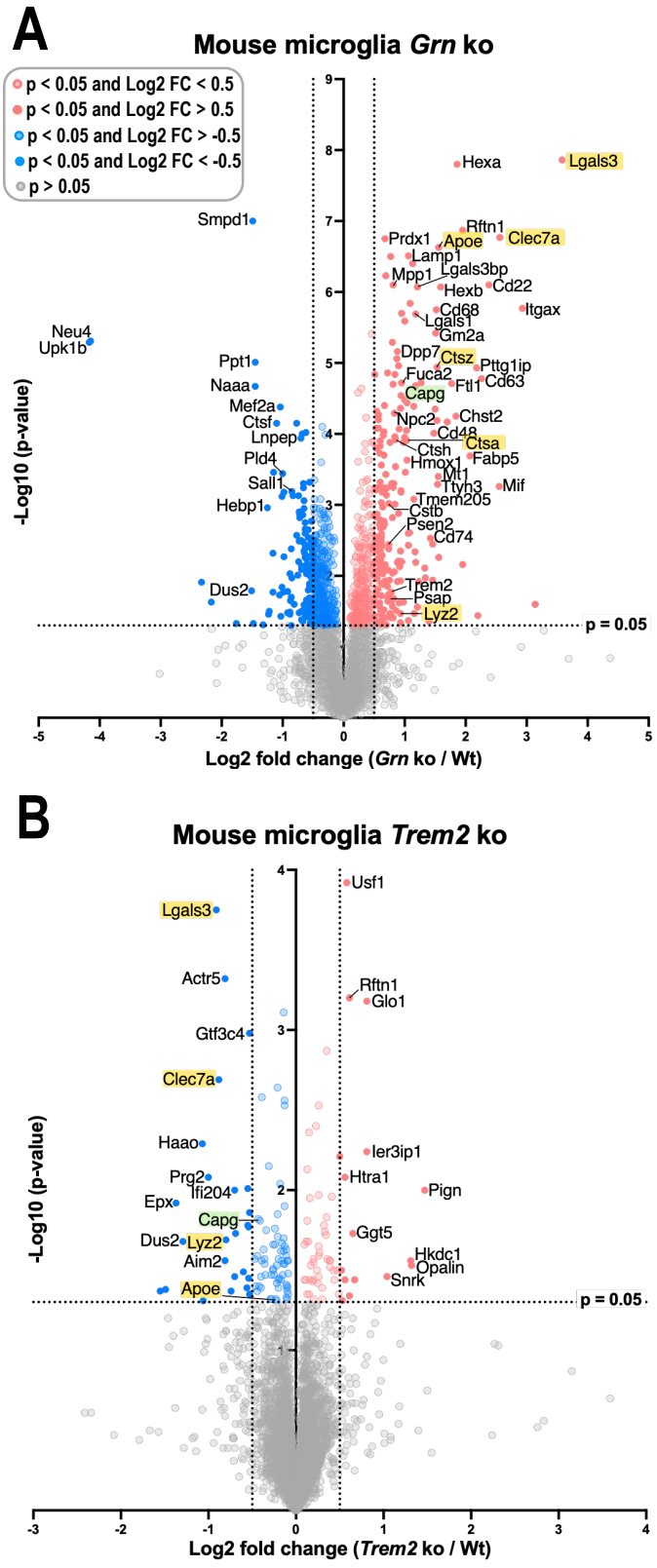

Figure 4.1. The proteomic signature of hyperactivated and non-activated microglia isolated from Grn-knockout and Trem2-knockout mice.

Comparing upregulated (red) and downregulated (blue) proteins in microglia isolated from mice with the following genotypic comparisons: (A) *Grn*-knockout versus Wt and (B) *Trem2*-knockout versus wild-type. Example of markers for activated microglia are highlighted in yellow (Lgals3, Clec7a, Lyz2, Apoe). X-axis represent the Log2 fold change and the Y-axis represent the -log10 p-value. Selected cut-off values: $p < 0.05$ and $-0.5 > \text{Log2 fold change} > 0.50$.

The proteome of the isolated microglia matched very well the previously published transcriptomic signatures of the *Grn*-knockout and *Trem2*-knockout mice (Gotzl et al., 2019). The most prominent proteomic changes in the *Grn*-knockout microglia, including the upregulation of Clec7a, Apoe, Ctsz, Cd63, and Cd68, are well reflected the transcriptomic signature. In contrast, these markers are downregulated in the microglia of *Trem2*-knockout mice, in both the transcriptome and the proteome (Figure 4.2).

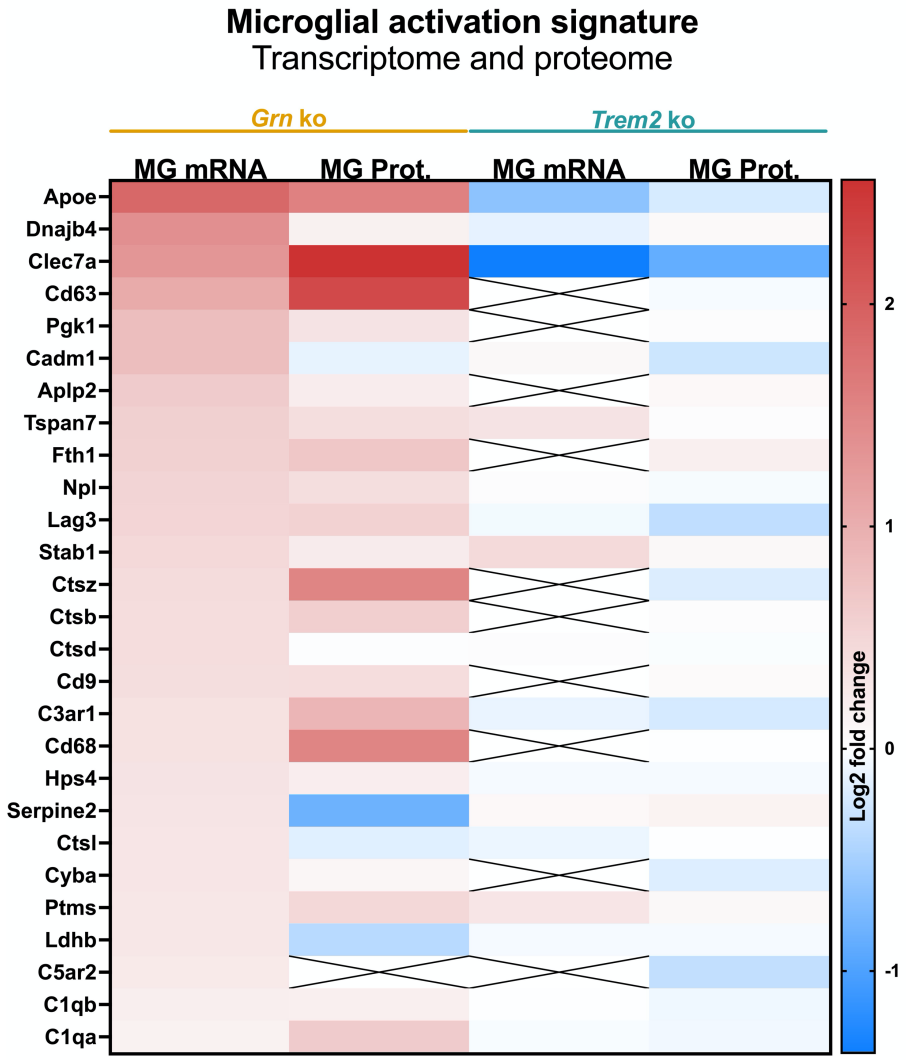

Figure 4.2. The transcriptomic and proteomic signatures of hyperactivated microglia in mice.

Changes observed in the *Grn*-knockout and *Trem2*-knockout mice (each compared to age-matched wild-type) reveal an overlap between transcriptomic and proteomic changes related to microglial activation. Protein and mRNA signatures were generated from Cd11b-positive microglia isolated from *Grn*-knockout and *Trem2*-knockout mice, respectively. Mice used for proteomic analysis (liquid chromatography–mass spectrometry (LC-MS)) were aged for 12 months before sacrificed, while the already published transcriptomic (NanoString) data was obtained by using 5.5 months old mice (Gotzl et al., 2019). Abbreviations: MG = microglia; mRNA = messenger RNA; Prot. = protein.

The homeostatic signature observed in the *Trem2*-knockout microglia was not only verified by the downregulation of activation markers, but also by the upregulation of P2ry12, a marker significant for the homeostatic signature. In contrast, P2ry12 was downregulated in the transcriptome and proteome of *Grn*-knockout microglia (Figure 4.3). The panels used for the activated and homeostatic signatures (Figure 4.2 and 4.3) were adopted from a previously published study (Gotzl et al., 2019).

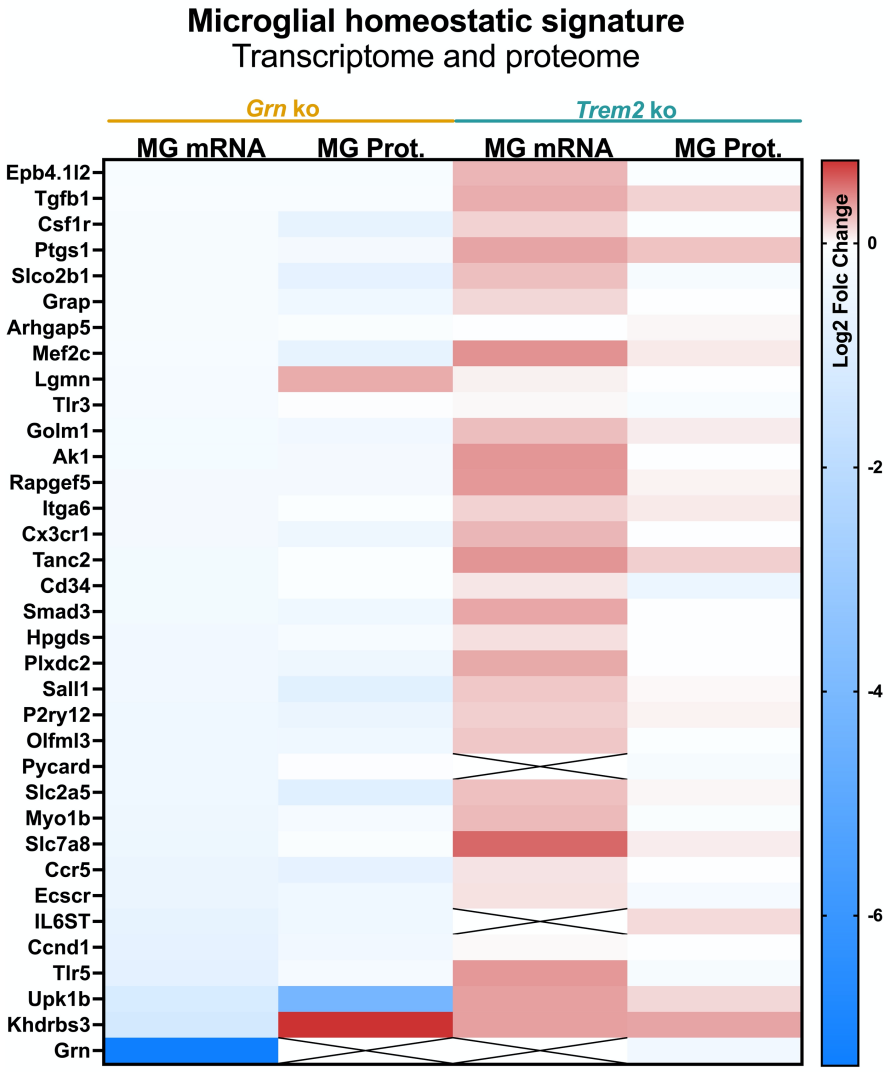

Figure 4.3. The transcriptomic and proteomic signatures of homeostatic microglia in mice.

Changes in the *Grn*-knockout and *Trem2*-knockout mice (each compared to age-matched wild-type). Protein and mRNA signatures were generated from Cd11b-positive microglia isolated from *Grn*-knockout and *Trem2*-knockout mice, respectively. Mice used for proteomic analysis (liquid chromatography–mass spectrometry (LC-MS)) were aged for 12 months before sacrificed, while the already published transcriptomic (NanoString) data was obtained by using 5.5 months old mice (Gotzl et al., 2019). Abbreviations: MG = microglia; mRNA = messenger RNA; Prot. = protein.

To further confirm the hyperactivated signature observed in *Grn*-knockout microglia, I performed a comparison of the proteins and genes that are considered significantly changed (selection criteria: p-value > 0.05). The generated overlaps provide information of which proteins/genes are consistently representing the signature. In *Grn*-knockout mice, the signature is characterized by a significant upregulation of 13 markers (Clec7a, Cd63, Apoe, Ctsz, Cd68, C3ar1, Fth1, C1qa, Ctsb, C1qb, Lag3, and Cd9) on both mRNA and proteome level (Figure 4.4 A). Comparing the significantly downregulated genes and proteins, resulted in an overlap of 14 markers (Ak1, Golm1, Grap1, Smad3, Plxdc2, Cx3cr1, P2ry12, Mef2c, Csf1r, Slco2b1, Ccr5, Sall1, Slc2a5, Upk1b) (Figure 4.4 B). Of note, Cx3cr1, P2ry12, and Sall1 are all significantly downregulated on both mRNA and protein level in the *Grn*-knockout microglia, these markers have been reported as part of the homeostatic microglial signature (Holtman, Skola, & Glass, 2017; Keren-Shaul et al., 2017; Mazaheri et al., 2017).

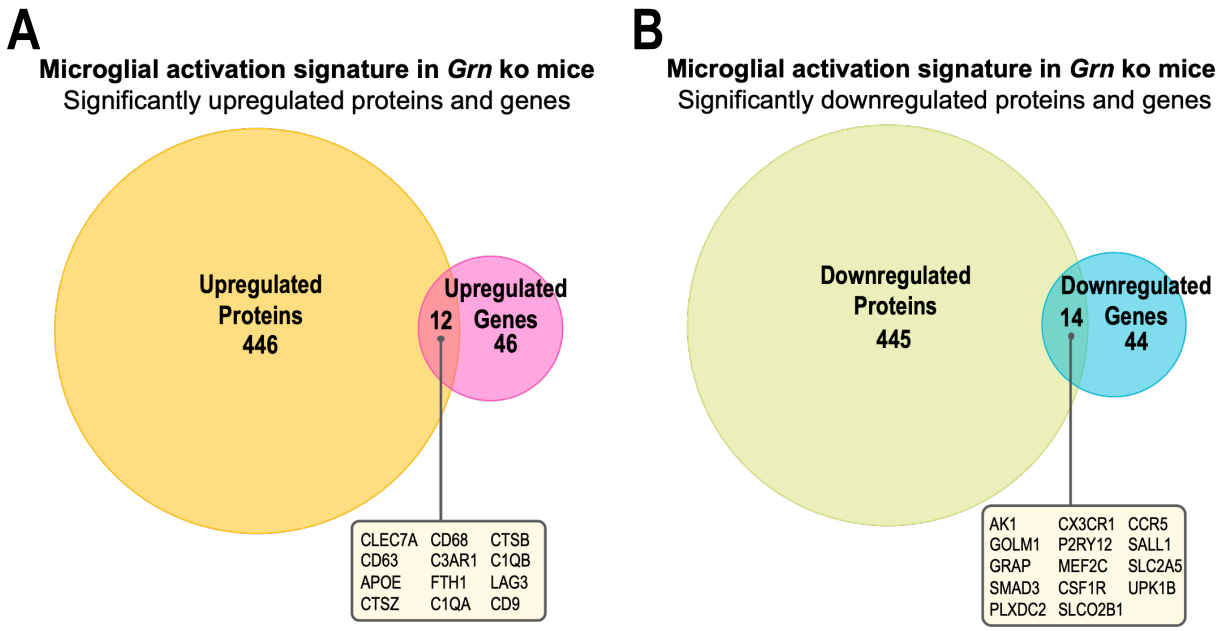

Figure 4.4. Overlapping proteomic and transcriptomic signatures in microglia of Grn-knockout mice.

Comparison of the proteomic and transcriptomic signature of microglia isolated from *Grn*-knockout mice. (A) Significantly upregulated proteins (orange) versus significantly upregulated genes (pink), with an overlap of 12 markers that are significantly upregulated on both protein and mRNA level (text box). (B) Significantly downregulated proteins (green) versus significantly downregulated genes (blue), with an overlap of 14 markers significantly downregulated on both protein and mRNA level (text box). Selected cut-off values: $p < 0.05$.

Investigating the significantly changed genes and proteins in the *Trem2*-knockout microglia, no overlap was observed as significantly upregulated (Figure 4.5 A). However, Lgals3, Apoe, and Clec7a, were significantly downregulated on both mRNA and proteome level (Figure 4.5

B). These three markers are all part of the activated microglial signature and their significant downregulation in the *Trem2*-knockout microglia further confirms that Trem2 is required for the microglial activation. Furthermore, it also confirms Lgals3, Apoe, and Clec7a as markers for the activation repertoire.

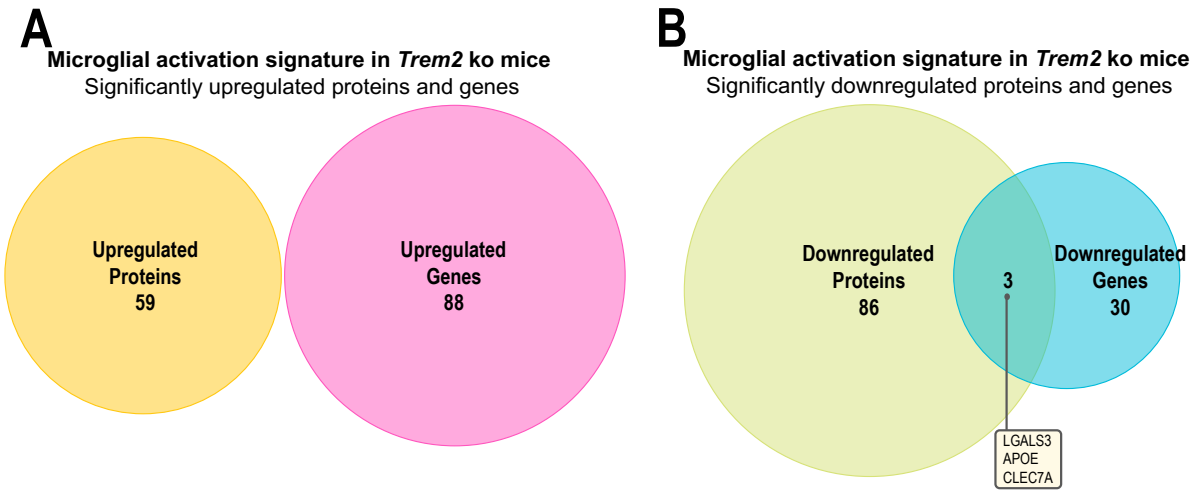

Figure 4.5. Microglia activation markers LGALS3, APOE and CLEC7A are significantly downregulated in the proteomic and transcriptomic signatures of Trem2-knockout mice.

Comparison of the proteomic and transcriptomic signatures of microglia isolated from *Trem2*-knockout mice: (A) Significantly upregulated proteins (orange) versus significantly upregulated genes (pink). No overlap of common markers was detected as significantly upregulated on both protein and mRNA level. (B) Significantly downregulated proteins (green) versus significantly downregulated genes (blue), with an overlap of 3 markers significantly upregulated on both protein and mRNA level (text box). Selected cut-off values: $p < 0.05$.

4.2. The microglial activation signature is partially reflected in the CSF proteome of Grn-knockout mice

CSF was collected pre-mortem from the same mice from which the microglia were isolated. The CSF proteome of the *Grn*-knockout mice showed several significant changes compared to age-matched wild-type. The most significantly changed proteins within the CSF proteome of the *Grn*-knockout included: Ctsb, Ctsd, Apoe, and Lyz2 (Figure 4.6 A), which are a known to be increased on the mRNA level in the DAM signature (Gotzl et al., 2019; Keren-Shaul et al., 2017). In contrast, the homeostatic signature observed in the *Trem2*-knockout mouse microglia did not show pronounced changes in the CSF proteome compared to age-matched wild-type mice (Figure 4.6 B).

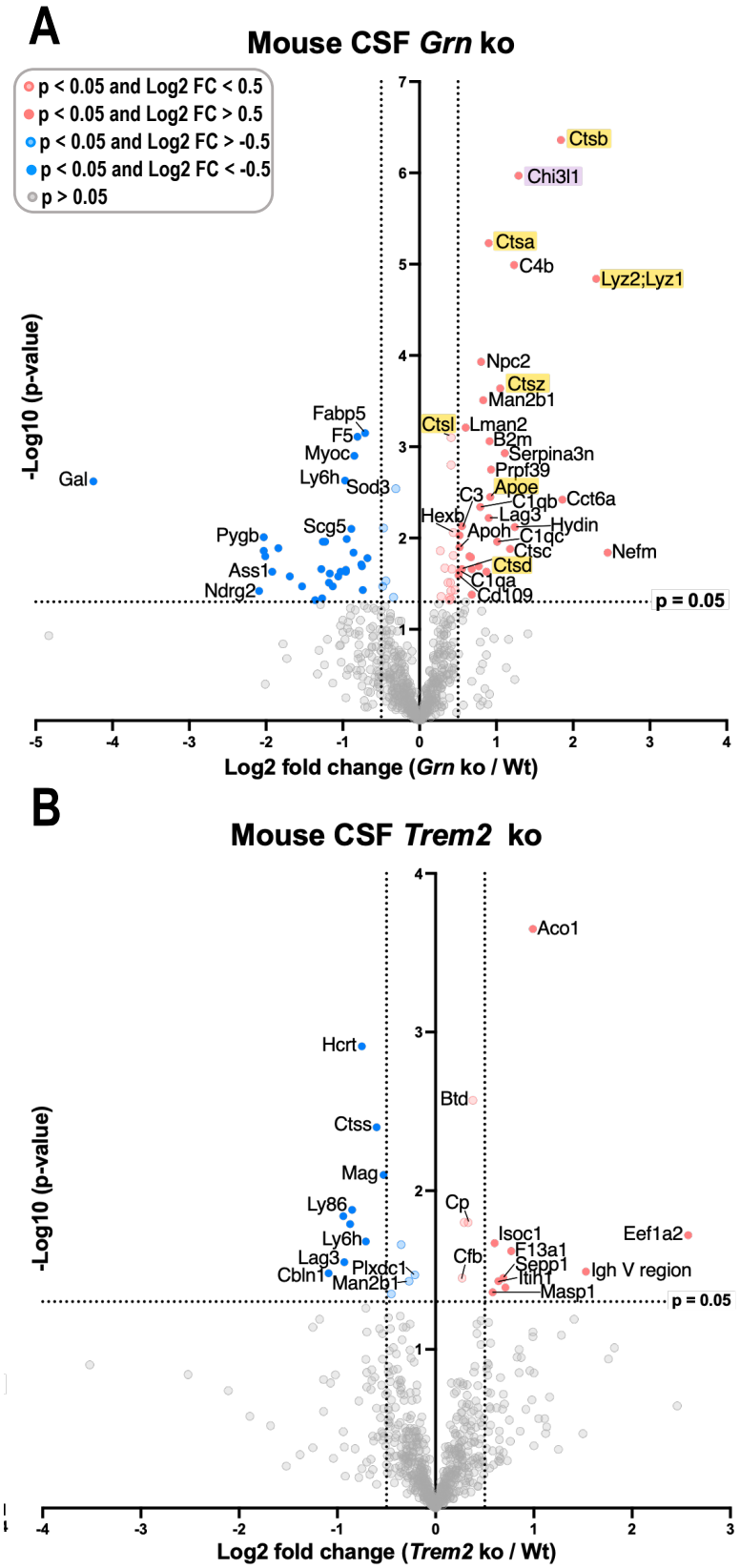

Figure 4.6. The CSF proteome of Grn-knockout and Trem2-knockout mice.

Comparing upregulated (red) and downregulated (blue) proteins in the CSF from mice with the following genotypic comparisons: (A) *Grn*-knockout versus wild-type and (B) *Trem2*-knockout versus wild-type. Example of markers for activated microglia are highlighted in yellow (Apoe, Ctsb, Ctsd, Lyz2). X-axis represent the Log2 fold change and the Y-axis represent the -log10 p-value. Selected cut-off values: p < 0.05 and -0.5 > Log2 fold change > 0.50.

By comparing the significantly upregulated proteins in microglia and CSF isolated from *Grn*-knockout mice, I identified an overlap of 13 proteins; Hexb, Apoe, Ctsz, Ctsa, Npc2, C1qa, Ctsb, C1qb, Lag3, C1qc, Creg1, Ctsc, and Lyz2 (Figure 4.7 A). Of note, peptides matching the sequence of both lysozyme 1 and 2 (Lyz1 and Lyz2, respectively) were detectable and quantified as significantly upregulated in the CSF of *Grn*-knockout mice. As Lyz2 is part of the DAM signature and significantly increased in proteome of *Grn*-knockout mouse microglia, I considered the detected peptides assigned as Lyz1/Lyz2 as Lyz2 only. With this assumption, Lyz2 can be added to the list of overlapping proteins (Figure 4.7 A). No overlap was observed when comparing the significantly upregulated proteins in the CSF and microglia isolated from *Trem2*-knockout mice (Figure 4.7 B). This suggests that the signature of homeostatic microglia is not as well reflected in the CSF as the signature of activated microglia.

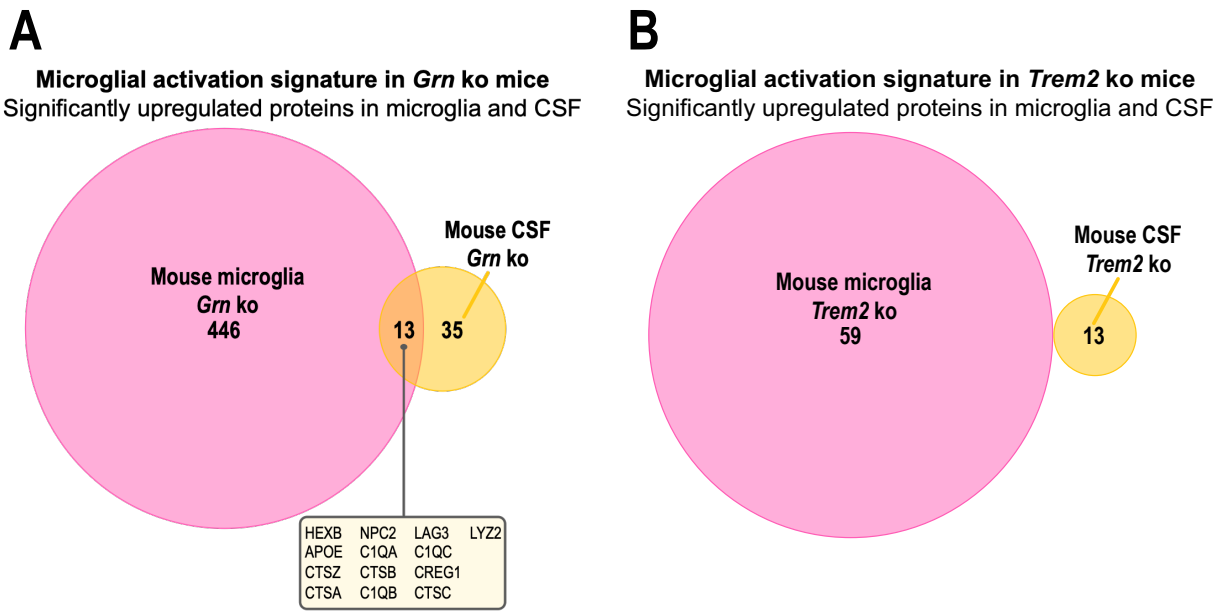

Figure 4.7. Overlapping microglial signatures detected in the CSF of Grn-knockout mice, but not in Trem2-knockout mice.

Comparison of the microglial proteome (pink) and the CSF proteome (orange) in (A) *Grn*-knockout mice and (B) *Trem2*-knockout mice. Selected cut-off values: $p < 0.05$.

The observed increase of Apoe, Ctsb, Ctsz, and Lyz2 indicates that DAM-associated changes can be detected in the CSF and microglial proteome of *Grn*-knockout mouse models (Figure 4.8). This is in line with previously published data generated from amyloid burden mouse models with confirmed microglial activation (Eninger et al., 2022).

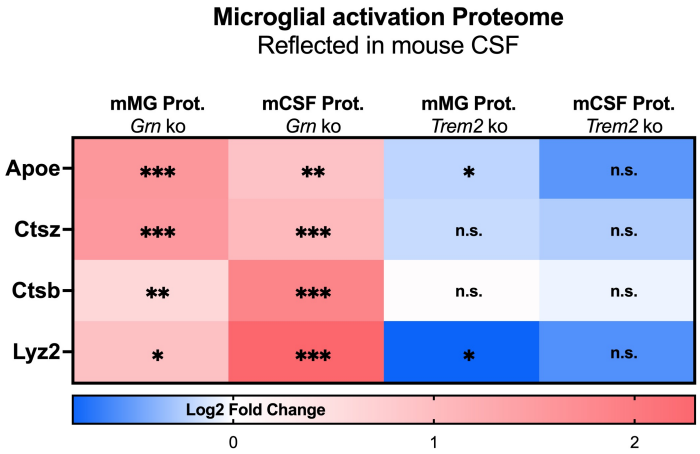

Figure 4.8. Apoe, Ctsz, Ctsb, and Lyz2 are significantly increased in both microglia and CSF of Grn-knockout mice.

Changes (relative to age-matched wild-type) of Apoe, Ctsz, Ctsb, and Lyz2 are consistent in the proteome of isolated microglia and in the proteome of CSF sampled from the very same mice; *Grn*-knockout and *Trem2*-knockout mice. Statistical differences were calculated using Student's t-test. Crosses indicate missing values. "*" = $p < 0.05$, "**" = $p < 0.01$, "***" = $p < 0.001$; "n.s."= non-significant. False discovery rate (FDR) was not considered for the presented visualizations. Abbreviations: mMG = mouse microglia; mCSF = mouse cerebrospinal fluid; Prot. = protein.

4.3. The proteomic signatures observed in mice are comparable with those identified in human iPSC derived microglia

To further confirm the proteomic datasets derived from mouse microglia and CSF, the proteome of human-induced pluripotent stem cell (iPSC)-derived microglia (hiMGL) was investigated, with the same genotypic comparison: *GRN*-knockout and *TREM2*-knockout (each compared to wild-type control).

As expected, the *GRN*-knockout hiMGL showed more prominent proteomic changes compared to *TREM2*-knockout hiMGL (Figure 4.9 A-B). Cathepsins (CTS) including CTSA, CTSB, and CTSZ were significantly upregulated in the *GRN*-knockout hiMGL compared to wild-type control, which is in line with our findings in the microglia proteome of *Grn*-knockout mouse (Figure 4.1 A and Figure 4.9 A).

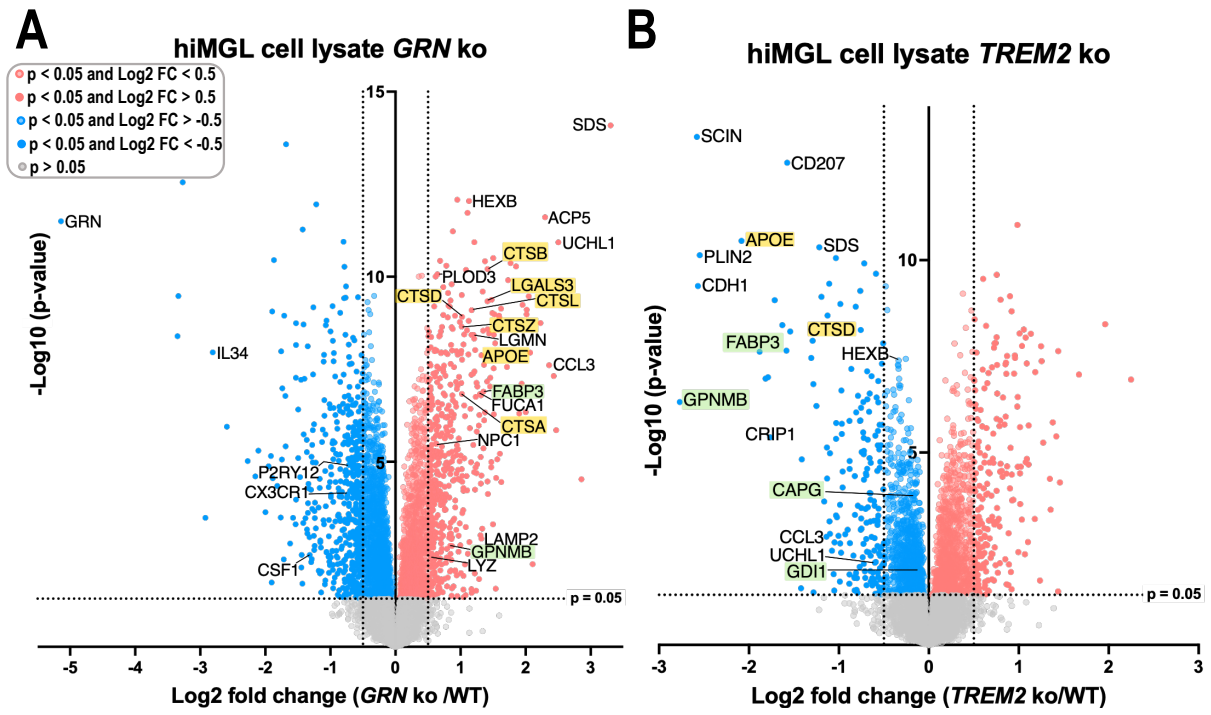

Figure 4.9. The proteomic signatures of GRN-knockout and TREM2-knockout hiMGL.

Comparing upregulated (red) and downregulated (blue) proteins in human-induced pluripotent stem cell (iPSC)-derived microglia (hiMGL) with the following genotypic comparisons: (A) *GRN*-knockout versus wild-type and (B) *TREM2*-knockout versus wild-type. Cathepsins are highlighted in yellow (CTSA, CTSB, CTSD, CTSL, CTSZ). X-axis represent the Log2 fold change. Y-axis represent the -log10 p-value. Selected cut-off values: $p < 0.05$ and $-0.5 >$ Log2 fold change > 0.50. Abbreviations: KO = knockout; WT = wild-type.

The hiMGL models showed significant consistency between the microglia transcriptome and proteome. For example, proteins with strong association to microglial activation, such as TREM2, APOE and CTSD were all upregulated on both mRNA (measured by qPCR) and protein level in the *GRN*-knockout hiMGL compared to wild-type control. Consistent with the activation state of *GRN*-knockout hiMGL, levels of the homeostatic marker P2RY12 were significantly reduced in *GRN*-knockout hiMGL transcriptome and proteome. In contrast, P2RY12 levels are increased in the *TREM2*-knockout hiMGL, which are locked in a homeostatic state (Figure 4.10 and 4.11 A-D).

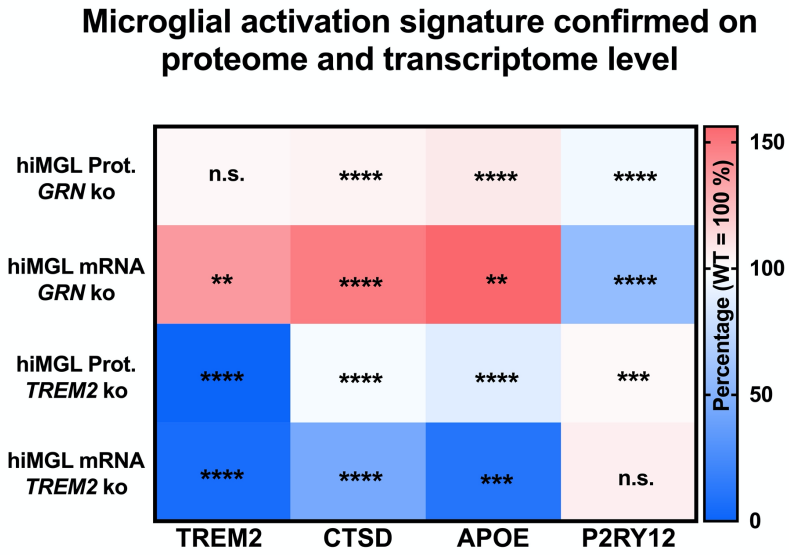

Figure 4.10. Levels of TREM2, CTSD, APOE and P2RY12 confirms the opposite activation phenotypes observed in GRN-knockout and TREM2-knockout hiMGL.

Known microglia markers showed significant consistency between the proteome (top row) and transcriptome (bottom row) in hiMGL cell lysates. Proteomic data was obtained by liquid chromatography–mass spectrometry (LC-MS), while mRNA data were obtained by qPCR. Abbreviations: KO = knockout; WT = wild-type; Prot. = protein. "*" = $p < 0.05$, "**" = $p < 0.01$, "***" = $p < 0.001$; "****" = $p < 0.0001$ "n.s."= non-significant.

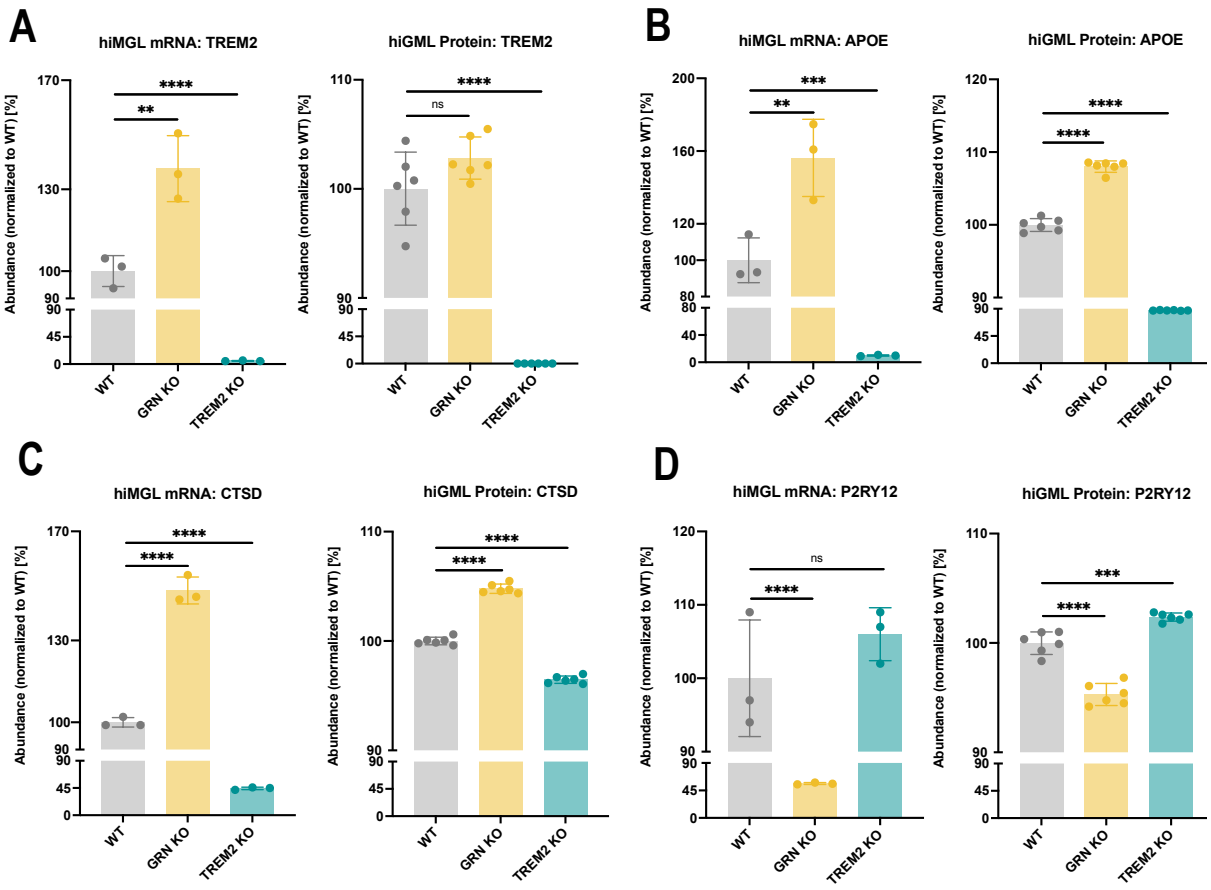

Figure 4.11. Levels of TREM2, CTSD, APOE and P2RY12 confirms the opposite activation phenotypes observed in GRN-knockout and TREM2-knockout hiMGL.

Comparing proteomic and transcriptomic signatures of wild-type, *GRN*-knockout, and *TREM2*-knockout hiMGL. Confirming the activated signature in *GRN*-knockout hiMGL on a proteome level, a signature confirmed to be absent in the *TREM2*-knockout hiMGL: (A) TREM2, (B) APOE, (C) CTSD, (D) P2RY12. Abbreviations: KO = knockout; WT = wild-type. "*" = $p < 0.05$, "**" = $p < 0.01$, "***" = $p < 0.001$; "****" = $p < 0.0001$ "n.s."= non-significant.

The proteomic signature observed in microglia isolated from *Grn*-knockout mice were comparable with the changes measured in *GRN*-knockout hiMGL. In total, 33% of proteins significantly upregulated in *Grn*-knockout mouse microglia were also significantly upregulated in the proteome of *GRN*-knockout hiMGL (Figure 4.12 A). As observed in our mouse models, the changes in the *TREM2*-knockout hiMGL model are more subtle than those in the *GRN*-knockout hiMGL. The number of significantly upregulated proteins in lysates of *GRN*-knockout hiMGL accounts for 1675 proteins (Figure 4.12 A), while the significantly upregulated proteins in lysates of *TREM2*-knockout hiMGL accounts for 1247 proteins (Figure 4.12 B). This indicates that the *GRN*-knockout hiMGL significantly upregulate ~25% more proteins than the *TREM2*-knockout hiMGL. Out of the 59 proteins that were significantly increased in *Trem2*-knockout

mouse microglia, only 5 proteins (8.5%) (GLO1, PRPS2, HPRT1, SORT1, and DHX36) were also significantly increased in the *TREM2*-knockout hiMGL cell lysates (Figure 4.12 B).

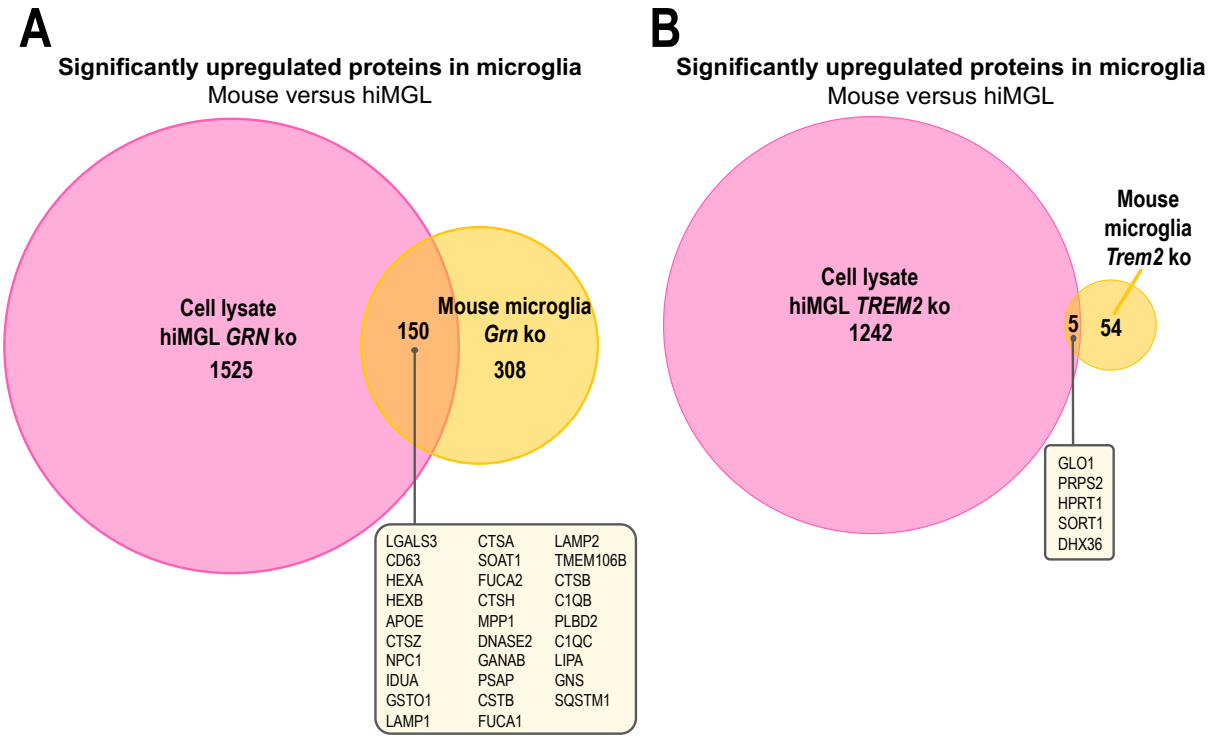

Figure 4.12. The proteomic signature of activated mouse microglia is comparable with GRN-knockout hiMGL.

Comparison of the significantly increased proteins in hiMGL and mice. (A) Significantly increased proteins in *GRN*-knockout hiMGL (pink) and *Grn*-knockout mice (orange), with an overlap of 150 proteins (example of overlapping proteins in text box). (B) Significantly increased proteins in *TREM2*-knockout hiMGL (pink) and *Trem2*-knockout mice (orange), with an overlap of 5 proteins (text box). Selected cut-off values: $p < 0.05$.

The main aim of my thesis was to identify fluid-based biomarker candidates reflecting the microglial activation states in humans. Therefore, I compared the hiMGL cell proteome (cell lysate) with the hiMGL secretome (conditioned media). The proteomic signature observed in *GRN*-knockout hiMGL was well reflected in the media of *GRN*-knockout hiMGL. For example, several cathepsins (CTSA, CTSB, CTSD, CTSL, and CTSZ) were significantly upregulated in lysates and media of *GRN*-knockout hiMGL (Figure 4.13 A).

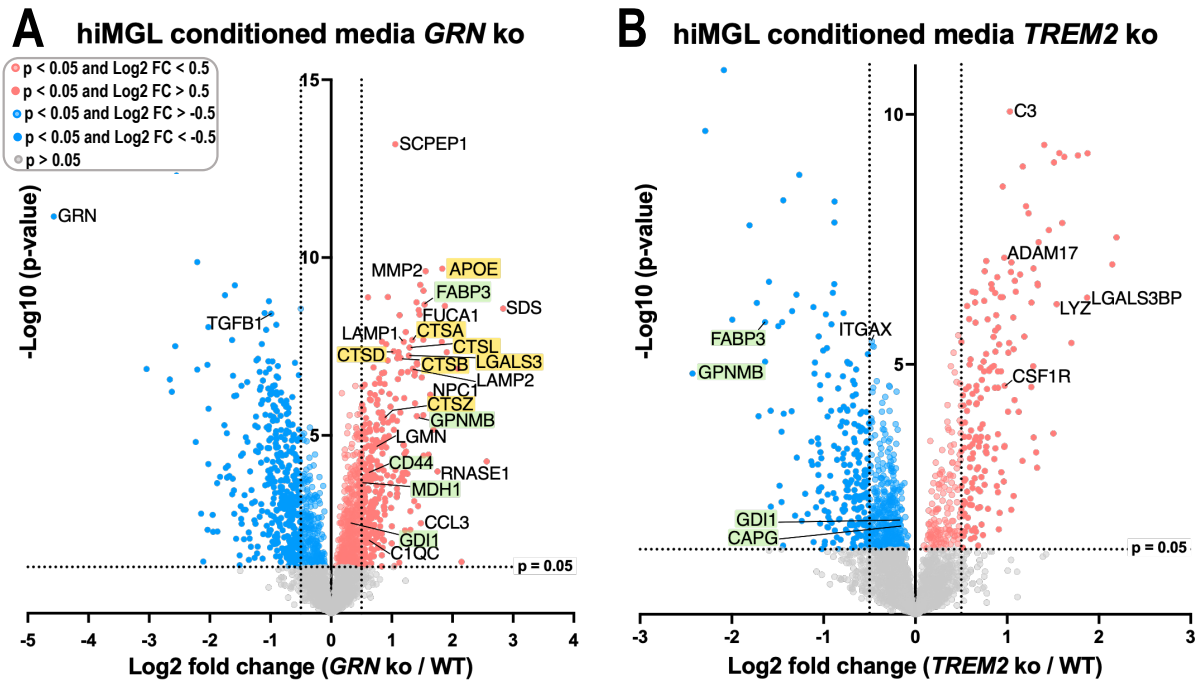

Figure 4.13. The secretome of GRN-knockout and TREM2-knockout hiMGL.

Comparing upregulated (red) and downregulated (blue) proteins in the conditioned media of human-induced pluripotent stem cell (iPSC)-derived microglia (hiMGL) with the following genotypic comparisons: (A) *GRN*-knockout versus wild-type and (B) *TREM2*-knockout versus wild-type. Cathepsins are highlighted in yellow (CTSA, CTSB, CTSD, CTSL, CTSZ). X-axis represent the Log2 fold change. Y-axis represent the -log10 p-value. Selected cut-off values: $p < 0.05$ and $-0.5 > \text{Log2 fold change} > 0.50$.

In the CSF of *Grn*-knockout mice, 47 proteins were significantly increased compared to wild-type. Out of these 47 proteins, 20 proteins (> 42%) were also significantly upregulated in the conditioned media of *GRN*-knockout hiMGL (Figure 4.14 A). This suggests that the proteomic signature for microglial activation that we capture with our mouse model is at least in part (33% in microglia and >42% in secretome) conserved from mouse to human (Figure 4.12 A and Figure 4.14 A). Of note, no proteins overlapped when comparing the 13 significantly upregulated proteins in the *Trem2*-knockout mouse CSF versus the 316 significantly upregulated proteins in the media of *TREM2*-knockout hiMGL (Figure 4.14 B).

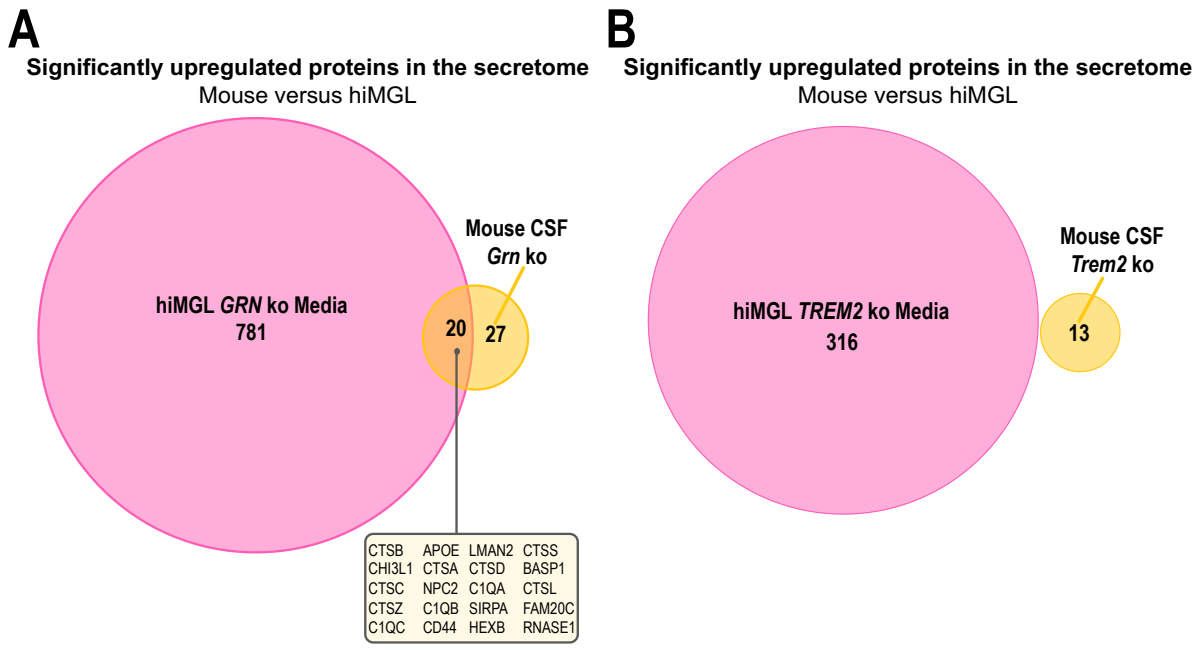

Figure 4.14. The proteomic signature of activated microglia associates well between mouse CSF and the hiMGL secretome.
Significantly increased proteins in the conditioned media of hiMGL (pink) and CSF sampled from 12 months old mice. (A) Significantly increased proteins in *GRN*-knockout hiMGL (pink) and *Grn*-knockout mice (orange), with an overlap of 20 proteins (text box). (B) Significantly increased proteins in *TREM2*-knockout hiMGL (pink) and *Trem2*-knockout mice (orange), with no overlap observed. Selected cut-off values: $p < 0.05$.

4.4. Common microglia-enriched changes detected in the CSF of symptomatic GRN mutation carriers and in the GRN-knockout hiMGL secretome

The third aim of my thesis was to identify biomarker candidates by investigating the changes observed in our proteomic datasets derived from our models for microglia activation with the CSF of proteome of human *GRN* mutation carriers. For this comparison, the CSF proteome of symptomatic heterozygous *GRN* mutation carriers and healthy non-carriers was analyzed using label-free LC-MS/MS. In total, the cohort included 11 symptomatic heterozygous *GRN* mutation carriers (FTD-GRN), of which 3 patients were diagnosed with mild cognitive impairment (MCI) at the timepoint of CSF sampling. In addition, the CSF of 12 non-symptomatic non-carriers (CON) was included as a control (Table 3.19).

As expected, GRN was significantly decreased in the CSF of FTD-GRN patients compared to healthy controls, which is in line with previously reported characteristics for FTD-GRN patients (Finch et al., 2009; Ghidoni et al., 2008; Meeter, Kaat, Rohrer, & van Swieten, 2017; Sleegers

et al., 2009). Furthermore, levels of neurofilament light (NFL), a marker for neurodegeneration (Zetterberg & Blennow, 2021), were significantly increased in the CSF of FTD-GRN patients compared to the control group (Figure 4.15).

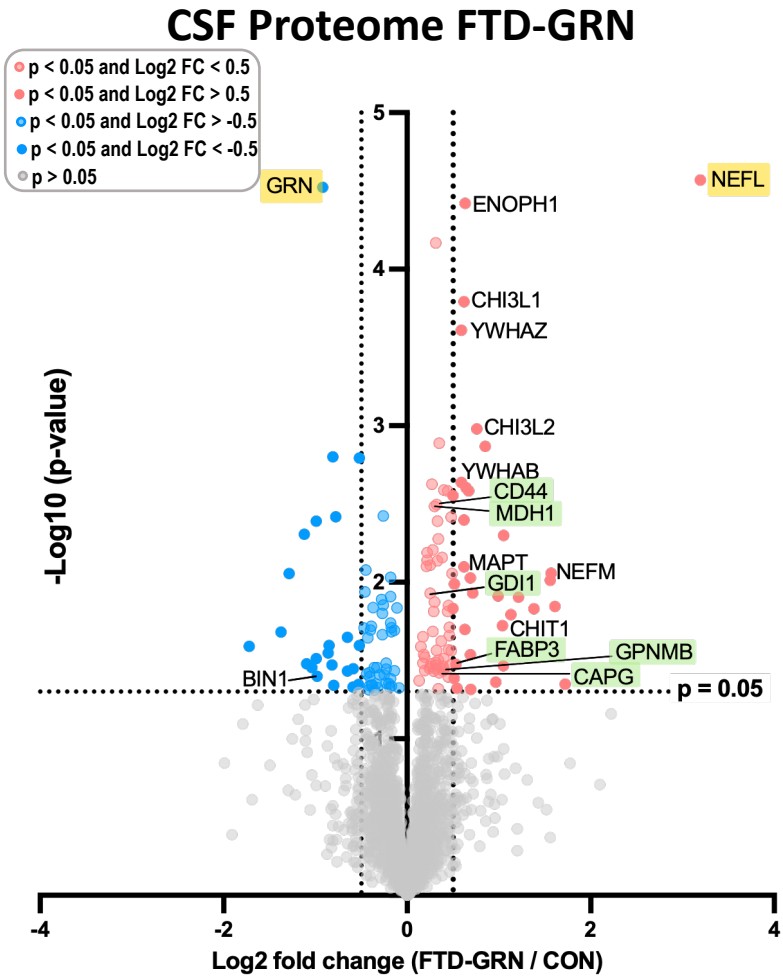

Figure 4.15. The CSF proteome of FTD-GRN patients.

Comparing the CSF proteome of symptomatic heterozygous *GRN* mutation-carriers (FTD-GRN) and healthy controls (CON). Significantly upregulated proteins (red) versus significantly downregulated proteins (blue). X-axis represent the Log 2 fold change. Y-axis represent the -log10 p-value. Selected cut-off values: $p < 0.05$ and $-0.5 < \text{Log2 fold change} > 0.50$.

Comparison of the CSF proteome of FTD-GRN patients to the proteome data obtained from conditioned media of *GRN*-knockout hiMGL media allowed the identification of 26 proteins that were significantly increased in both fluids ($p < 0.05$, not considering FDR-correction) (Figure 4.16).

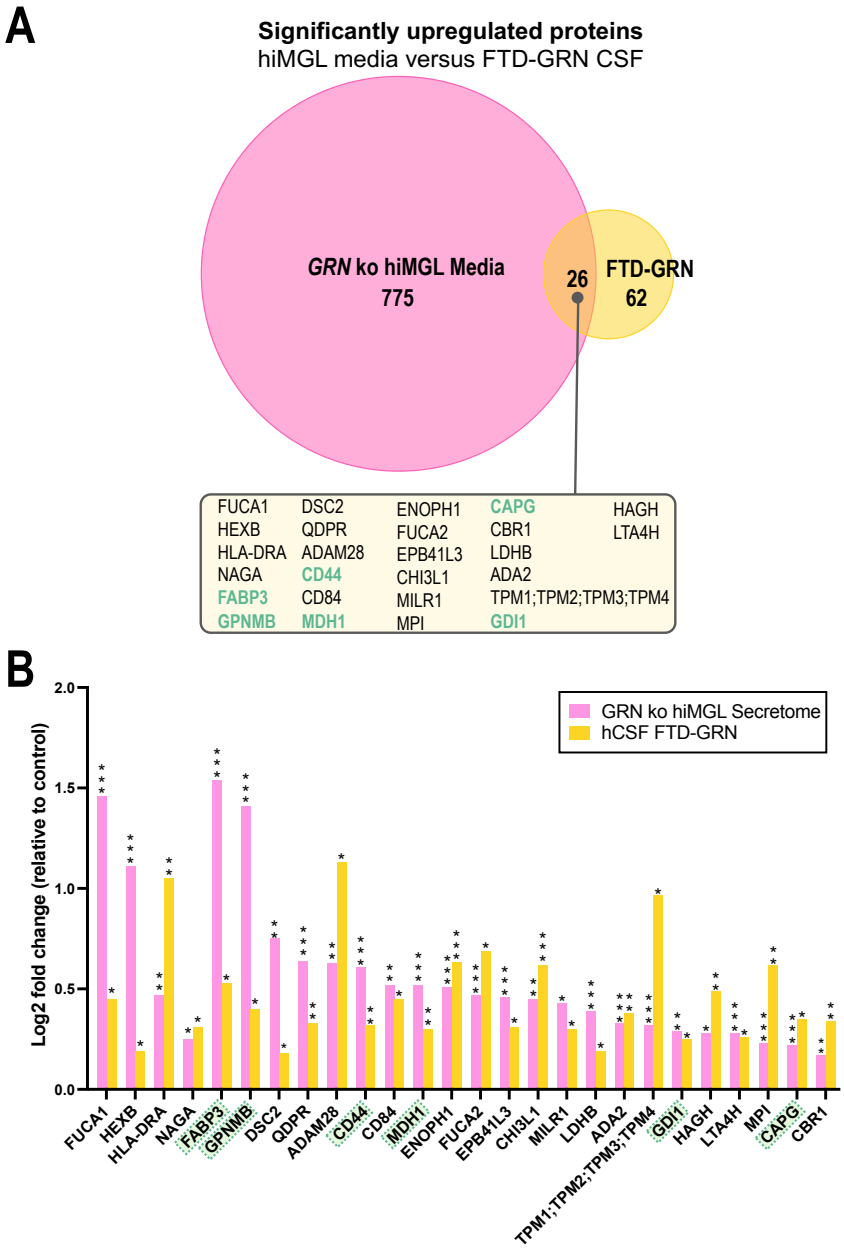

Figure 4.16. Common microglia-enriched changes in the CSF proteome of FTD-GRN patients and in the conditioned media of GRN-knockout hiMGL.

Identification of microglia state-dependent proteins, by comparing the significantly upregulated proteins in human CSF of FTG-GRN patients (orange) to the significantly upregulated proteins detected in the media of *GRN*-knockout hiMGL (pink). (A) In the CSF of FTD-GRN patients 88 proteins were significantly upregulated compared to healthy non-carriers, 26 (30%) of these proteins were also detected as significantly upregulated in the media of monocultured hiMGL lacking *GRN* (compared to media of wild-type hiMGL). (B) Quantitative comparison of the 26 proteins detected as significantly upregulated in both the human CSF (hCSF) of FTD-GRN patients (orange) and the media of monocultured *GRN*-knockout hiMGL (pink). Statistical differences were calculated using Student's t-test. Crosses indicate missing values. "*" = $p < 0.05$, "**" = $p < 0.01$, "***" = $p < 0.001$.

When comparing these 26 proteins with our proteomic data derived from the *Grn*-knockout mouse microglia, a statistically significant upregulation is only observed for four proteins: FUCA1, HEXB, FUCA2, and CAPG. In the CSF of *Grn*-knockout mice, the increased levels of three proteins reached a statistical significance: HEXB, CD44, and CHI3L1 (Figure 4.17).

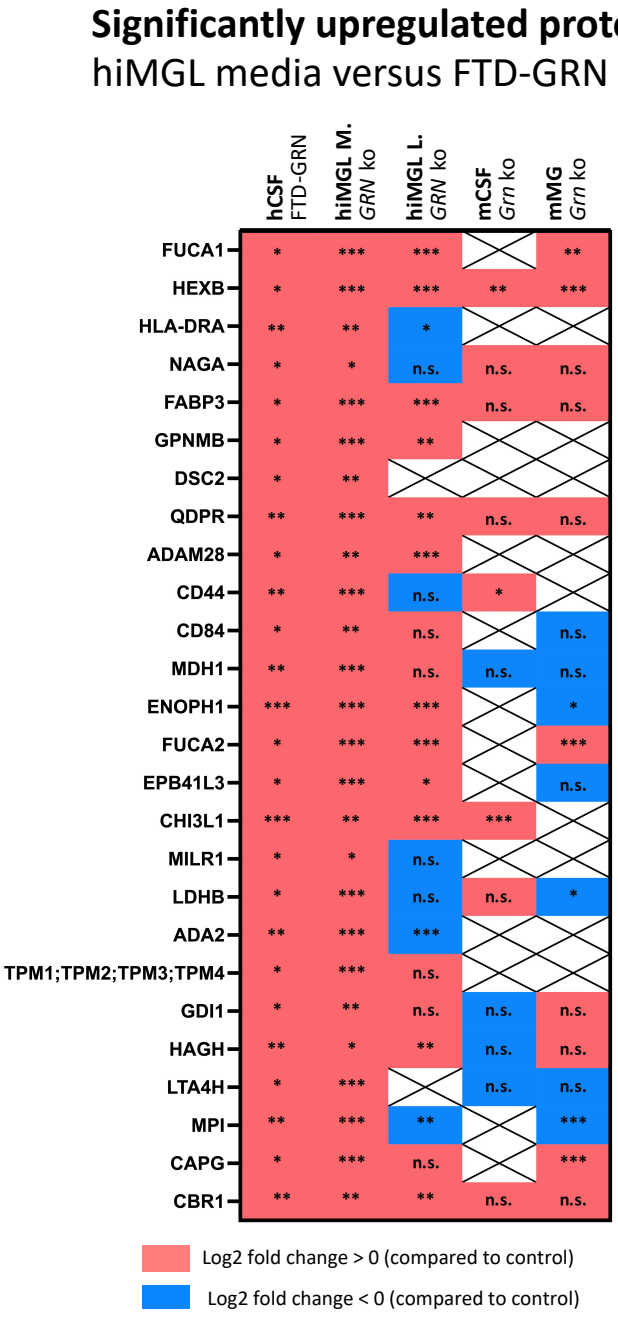

Figure 4.17. The 26 overlapping proteins: from mouse to hiMGL to human.

A binary comparison of the 26 proteins significantly upregulated in *GRN*-knockout hiMGL secretome and FTD-GRN CSF with the up- (red) or downregulation (blue) of each protein indicated for cell lysates of *GRN*-knockout hiMGL, CSF of *Grn*-knockout mice, and in cell lysates of microglia isolated from *Grn*-knockout mice. Statistical differences were calculated using Student's t-test. Crosses indicate missing values. "*" = $p < 0.05$, "**" = $p < 0.01$, "***" = $p < 0.001$, "n.s." = non-significant. Abbreviations: hCSF = human CSF; hiMGL M. = hiMGL conditioned media; hiMGL L. = hiMGL cell lysate; mCSF = mouse CSF; mMG = mouse microglia.

4.5. Identification of microglia activation-dependent biomarkers successfully distinguishing patients with FTD-GRN from healthy controls

By comparing the 26 proteins that were significantly upregulated in both the secretome of *GRN* ko hiMGL and in the CSF of FTD-GRN patients (Figure 4.16 and Figure 4.17), I identified six proteins, which I refer to as *Panel 6*, including fatty acid binding protein 3 (FABP3), malate dehydrogenase 1 (MDH1), GDP dissociation inhibitor-1 (GDI1), macrophage-capping protein (CAPG), CD44, and glycoprotein NMB (GPNMB). The selection of these six proteins was mainly based on a combination of the information available at UniProt (Table 4.1) as wells as the results of a more extensive screening of the literature, which are described in the discussion on page 127.

Significantly upregulated proteins in hiMGL Media and hCSF FTD-GRN		
Gene	**Protein ID**	**Function (uniprot.org)**
FUCA1	P04066	Alpha-L-fucosidase is responsible for hydrolyzing the alpha-1,6-linked fucose joined to the reducing-end N-acetylglucosamine of the carbohydrate moieties of glycoproteins.
HEXB	P07686	Hydrolyzes the non-reducing end N-acetyl-D-hexosamine and/or sulfated N-acetyl-D-hexosamine of glycoconjugates, such as the oligosaccharide moieties from proteins and neutral glycolipids, or from certain mucopolysaccharides (PubMed:11707436, PubMed:9694901, PubMed:8672428, PubMed:8123671).
HLA-DRA	P01903	An alpha chain of antigen-presenting major histocompatibility complex class II (MHCII) molecule.
NAGA	P17050	Removes terminal alpha-N-acetylgalactosamine residues from glycolipids and glycopeptides. Required for the breakdown of glycolipids.
FABP3	P05413	FABP are thought to play a role in the intracellular transport of long-chain fatty acids and their acyl-CoA esters.
GPNMB	Q14956	Could be a melanogenic enzyme.
DSC2	Q02487	Component of intercellular desmosome junctions.
QDPR	P09417	Catalyzes the conversion of quinonoid dihydrobiopterin into tetrahydrobiopterin.
ADAM28	Q9UKQ2	May play a role in the adhesive and proteolytic events that occur during lymphocyte emigration or may function in ectodomain shedding of lymphocyte surface target proteins, such as FASL and CD40L.
CD44	P16070	Cell-surface receptor that plays a role in cell-cell interactions, cell adhesion and migration, helping them to sense and respond to changes in the tissue microenvironment (PubMed:16541107, PubMed:19703720, PubMed:22726066).
CD84	Q9UIB8	Self-ligand receptor of the signaling lymphocytic activation molecule (SLAM) family. In macrophages enhances LPS-induced MAPK phosphorylation and NF-kappaB activation and modulates LPS-induced cytokine secretion; involving ITSM 2 (By similarity).
MDH1	P40925	Plays essential roles in the malate-aspartate shuttle and the tricarboxylic acid cycle, important in mitochondrial NADH supply for oxidative phosphorylation (PubMed:31538237).
ENOPH1	Q9UHY7	Bifunctional enzyme that catalyzes the enolization of 2,3-diketo-5-methylthiopentyl-1-phosphate (DK-MTP-1-P) into the intermediate 2-hydroxy-3-keto-5-methylthiopentenyl-1-phosphate (HK-MTPenyl-1-P), which is then dephosphorylated to form the acireductone 1,2-dihydroxy-3-keto-5-methylthiopentene (DHK-MTPene).
FUCA2	Q9BTY2	Alpha-L-fucosidase is responsible for hydrolyzing the alpha-1,6-linked fucose joined to the reducing-end N-acetylglucosamine of the carbohydrate moieties of glycoproteins.
EPB41L3	Q9Y2J2	Tumor suppressor that inhibits cell proliferation and promotes apoptosis.
CHI3L1	P36222	Carbohydrate-binding lectin with a preference for chitin. Has no chitinase activity. May play a role in tissue remodeling and in the capacity of cells to respond to and cope with changes in their environment.
MILR1	Q7Z6M3	Immunoglobulin-like receptor which plays an inhibitory role in degranulation of mast cells.
LDHB	P07195	Interconverts simultaneously and stereospecifically pyruvate and lactate with concomitant interconversion of NADH and NAD+.
ADA2	Q9NZK5	Adenosine deaminase that may contribute to the degradation of extracellular adenosine, a signaling molecule that controls a variety of cellular responses.
TPM1;TPM2; TPM3;TPM4	P06753;P07951; P09493;P67936	Binds to actin filaments in muscle and non-muscle cells.
GDI1	P31150	Regulates the GDP/GTP exchange reaction of most Rab proteins by inhibiting the dissociation of GDP from them, and the subsequent binding of GTP to them.
HAGH	Q16775	Thiolesterase that catalyzes the hydrolysis of S-D-lactoyl-glutathione to form glutathione and D-lactic acid.
LTA4H	P09960	Bifunctional zinc metalloenzyme that comprises both epoxide hydrolase (EH) and aminopeptidase activities. Acts as an EH to catalyze the conversion of LTA4 to the pro-inflammatory mediator leukotriene B4 (LTB4) (PubMed:11917124, PubMed:12207002, PubMed:15078870, PubMed:18804029, PubMed:1897988, PubMed:1975494, PubMed:2244921).
MPI	P34949	Involved in the synthesis of the GDP-mannose and dolichol-phosphate-mannose required for a number of critical mannosyl transfer reactions.
CAPG	P40121	Calcium-sensitive protein which reversibly blocks the barbed ends of actin filaments but does not sever preformed actin filaments. May play an important role in macrophage function.
CBR1	P16152	NADPH-dependent reductase with broad substrate specificity.

Table 4.1. UniProt description of the 26 overlapping proteins.
Description of the 26 proteins significantly upregulated in both CSF of FTD-GRN patients and in the conditioned media of *GRN*-knockout hiMGL. Function obtained from UniProt (uniprot.org on 21.07.2022).

By comparing the Log2 fold changes (relative to the respective controls; wild-type in hiMGL and heathy non-carriers in the human CSF comparison), FABP3 and GPNMB show the most prominent increase of the Panel 6 proteins (Figure 4.18).

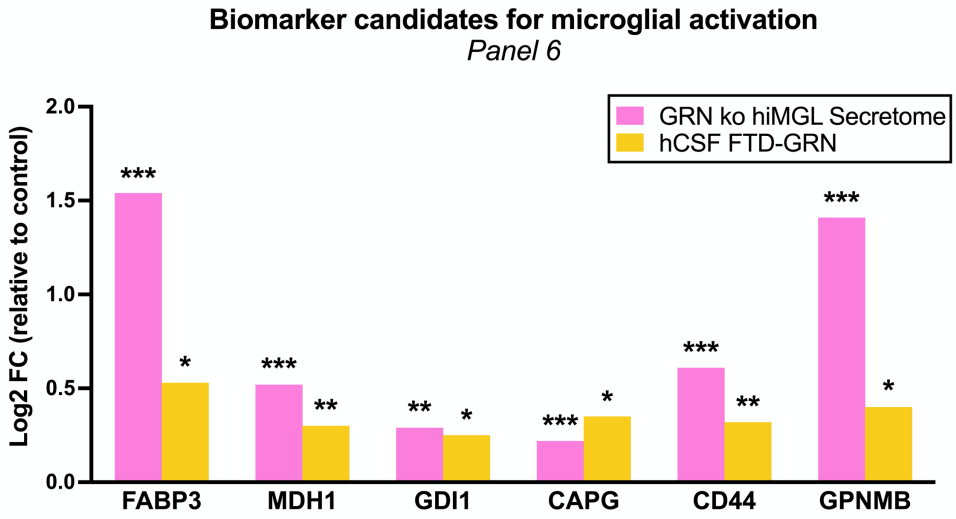

Figure 4.18. The Panel 6 proteins in the CSF of FTD-GRN patients and in the conditioned media of GRN-knockout hiMGL.

Abundances of Panel 6 proteins (FABP3, MDH1, GDI1, CAPG, CD44, and GPNMB) in secretome of *GRN*-knockout hiMGL (pink) and in CSF of symptomatic FTD-GRN patients (orange). The abundance of each group is normalized to the abundances measured in control groups; secretome of wild-type hiMGL and CSF levels in healthy controls), respectively. Abbreviations: hCSF = human CSF; FC = fold change. "*" = $p < 0.05$, "**" = $p < 0.01$, "***" = $p < 0.001$.

Interestingly, FABP3 and GPNMB are the only proteins that were also significantly upregulated in the cell lysate of the *GRN*-knockout hiMGL (Figure 4.19 A and B). Comparisons with the proteome data derived from *Grn*-knockout mice revealed that CD44 was the only protein within Panel 6 that was significantly upregulated in CSF, while CAPG was the only protein significantly upregulated in mouse microglia (Figure 4.19 A and B). FAB3 was the only protein of the Panel 6 proteins that showed a Log2 fold change > 0.5 throughout all systems (Figure 4.19 B).

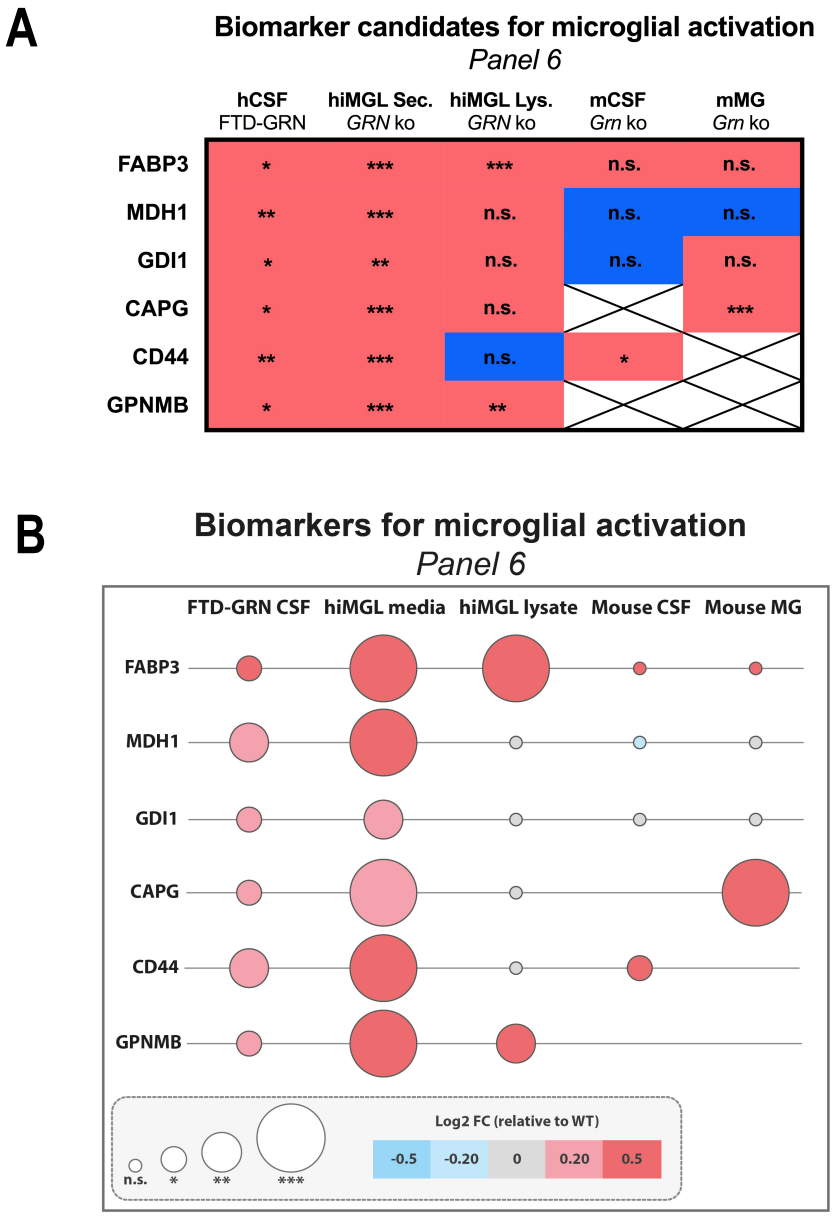

Figure 4.19. The abundances of Panel 6 proteins in models with confirmed microglial activation.

(A) Binary representation of the up- (red) and downregulation (blue) of the Panel 6 proteins in the CSF of FTD-GRN patients, media and cell lysates of *GRN*-knockout hiMGL, as well as in CSF and microglia from *Grn*-knockout mice. Crosses indicate missing values. (B) Comparison of abundance of Panel 6 proteins in: CSF from FTD-GRN patients, media and cell lysates from *GRN*-knockout hiMGL, CSF and microglia from *Grn*-knockout mice. Circle size indicate statistical significance based on p-value obtained from Student's t-test. Color intensity indicate the degree of up- (red) or downregulation (blue). Non-changed abundances are indicated in gray and are defined by -0.5 < Log2 Fold change < 0.5. Statistical differences were calculated using Student's t-test. "*" = $p < 0.05$, "**" = $p < 0.01$, "***" = $p < 0.001$, "n.s." = non-significant. Abbreviations: hCSF = human CSF; hiMGL M. = hiMGL conditioned media; hiMGL L. = hiMGL cell lysate; mCSF = mouse CSF; mMG = mouse microglia.

I then compared the Panel 6 proteins with already published data obtained from studies using various models for the triggering of microglia. In 2017, Keren-Shaul et al. identified the microglia subtypes that we today know as disease-associated microglia (DAM), which may be

further characterized to subtypes according to their TREM2-indeoendent (DAM1) and TREM2-dependent (DAM2) activation signatures (Keren-Shaul et al., 2017). Out of the six selected candidates, Cap and Gpnmb were significantly increased on a transcriptomic level in the microglia defined as DAM (Figure 4.20).

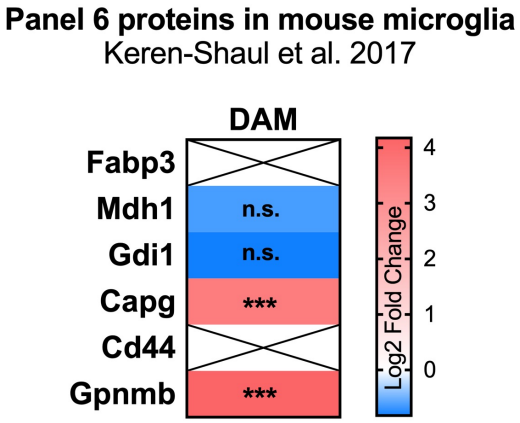

Figure 4.20. The abundance of Panel 6 proteins in DAM microglia.

The abundances of Panel 6 proteins in previously published data obtained from disease-associated microglia DAM (Keren-Shaul et al., 2017).Crosses indicate missing values. "*" = $p < 0.05$, "**" = $p < 0.01$, "***" = $p < 0.001$, "n.s." = non-significant.

To compare the Panel 6 proteins with microglial activation signatures reported on a proteome level, I made use of previously published proteomic data (Sebastian Monasor et al., 2020) obtained from microglia isolated from amyloid burden mice (APPPS1 and APP-KI, respectively) of ages 3, 6, and 12 months. Interestingly, two of the Panel 6 proteins, namely Fabp3 and Capg, appear as significantly increased in both mouse models. Capg is significantly increased in both APP-KI and APPPS1 microglia (Sebastian Monasor et al., 2020) already at an age of 3 months, this increase remains significant and appears to further increase with age. The levels of Fabp3 show no or less prominent changes at early ages (1 and 3 months), but with a significant increase at 6 and 12 months in both models (Sebastian Monasor et al., 2020) (Figure 4.21).

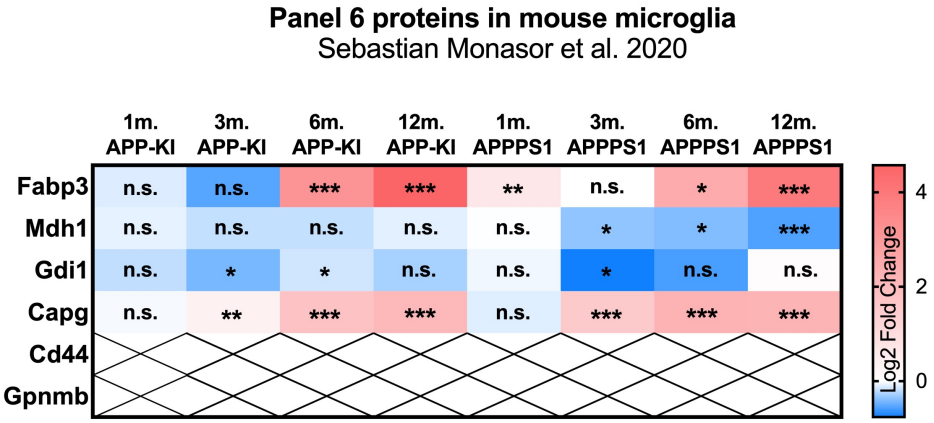

Figure 4.21. The abundance of Panel 6 proteins in microglia isolated from amyloid burden mice.

The abundances of Panel 6 proteins in previously published data obtained from microglia isolated from APPPS1 and APP-KI mice respectively (Sebastian Monasor et al., 2020). Crosses indicate missing values. "*" = $p < 0.05$, "**" = $p < 0.01$, "***" = $p < 0.001$, "n.s." = non-significant.

To investigate the abundance of the Panel 6 proteins in the CSF of models with known microglial activation, I made use of proteomic data that was recently published in a study reporting glia related changes in the CSF proteome of APPPS1 mice (Eninger et al., 2022). This data revealed increased levels of three of the six selected proteins: Fabp3, Mdh1, and Gdi1. However, none of these changes reached a statistical significance, except the CSF levels of Gdi1 when comparing 18 months wild-type with 3 months wild-type. Furthermore, the CSF levels of Cd44 appear as increased, but only when comparing the effect of aging (18 months versus 3 months) within each genotype (Figure 4.22).

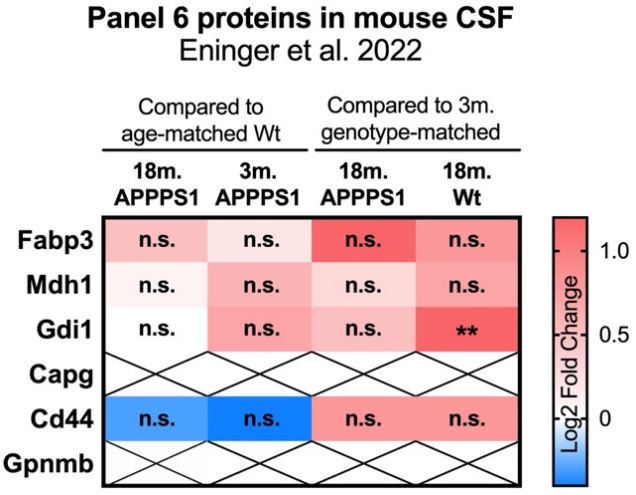

Figure 4.22. The abundance of Panel 6 proteins in the CSF of amyloid burden mice.

The abundances of Panel 6 proteins in previously published data obtained from CSF sampled from APPPS1 mice (Eninger et al., 2022). Crosses indicate missing values. "*" = $p < 0.05$, "**" = $p < 0.01$, "***" = $p < 0.001$, "n.s." = non-significant.

4.6. Panel 6 proteins distinguish FTD-GRN patients from controls in the ALLFTD cohort

Using a machine learning approach, the abundances of FABP3, MDH1, GDI1, CAPG, CD44, and GPNMB (as measured in the CSF samples of the ALLFTD cohort, using mass spectrometry) could be used to successfully distinguish FTD-GRN patients from healthy controls. The used model is based on logistic regression (sklearn.linear_model.LogisticRegression) (Fabian Pedregosa et al., 2011), where mutation status was predicted solely based on the CSF abundances of the Panel 6 proteins. In brief, the CSF abundance dataset was split into 5 different test and train sets with a similar distribution of classes. To test the statistical significance a permutation testing procedure was used, in which the mutation status labels of the test set were shuffled, and the model prediction was performed for the shuffled labels (Ojala & Garriga, 2009). The score for a given permuted model was the averaged prediction performance across the 5 cross-validation splits. This procedure was repeated 1000 times, providing a baseline performance for the model pipeline. The p-value was defined as the number of permuted models with a higher score than the ground-truth, non-permuted model divided by the total number of permutations. The average prediction performance was 81.0% (chance level prediction was 54%), with statistical significance of p = 0.03 (Figure 4.23).

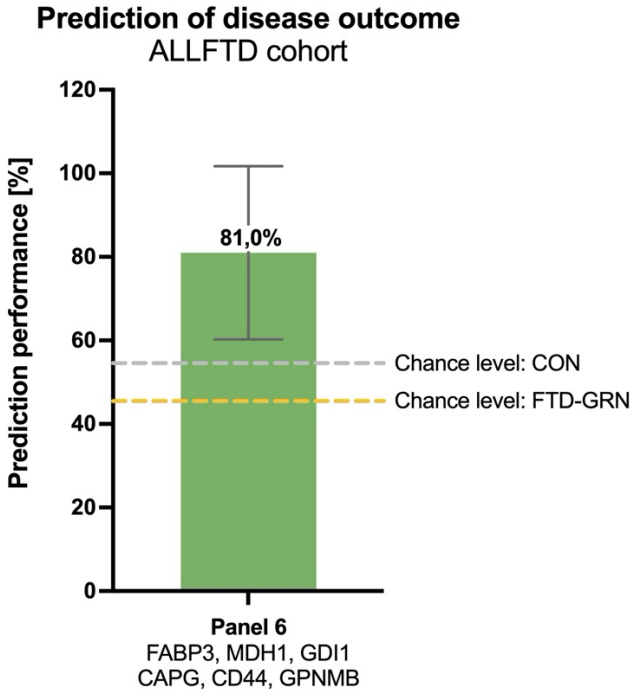

Figure 4.23. Panel 6 proteins successfully distinguishing FTD-GRN patients from controls.

The panel 6 proteins could be used to reliably predict a cohort participants mutation status as being healthy non-carrier control (CON) or symptomatic *GRN* mutation carrier (FTD-GRN), with a prediction efficiency of 81.0%.

4.7. CSF levels of FABP3, MDH1 and GDI1 are significantly elevated in Alzheimer's disease and amyloid-positive MCI cases

The fourth and final aim of my thesis was to confirm promising candidates in human CSF originating from a second cohort. Therefore, as a final confirmation, I investigated the abundances of the six selected proteins in a previously published dataset from the European Medical Information Framework Alzheimer's Disease Multimodal Biomarker Discovery (EMIF-AD MBD) (Weiner et al., 2022).

The studied EMID-AD MBD cohort was stratified according to diagnosis, yielding four participant groups: cognitively normal controls (CNC), subjective cognitive impairment (SCI), mild cognitive impairment (MCI), and Alzheimer's disease (AD) (Figure 4.24 A). Due to the relevance of amyloid in the context of microglial activation, I further stratified these groups according to the amyloid status of each individual: amyloid abnormalities detected (A+) versus no amyloid abnormalities detected (A-) (Figure 4.24 B). The presence or absence of amyloid abnormalities for the participants of the EMIF-AD MBD cohort was based on levels of $A\beta_{1-42}$, as previously assessed by Tijms et al. (Tijms et al., 2020).

Figure 4.24. The EMIF-AD MBD cohort.
The EMIF-AD MBD cohort panel stratified according to (A) diagnosis only and (B) diagnosis and amyloid status.

Within the EMID-AD MBD cohort three of the Panel 6 proteins were significantly altered between cohort groups, namely FABP3, MDH1, and GDI1. Of note, the CSF levels of these

three proteins were not only significantly elevated in participants diagnosed with AD, but a significant increase was also observed in MCI group compared to CNC (Figure 4.25 A-C).

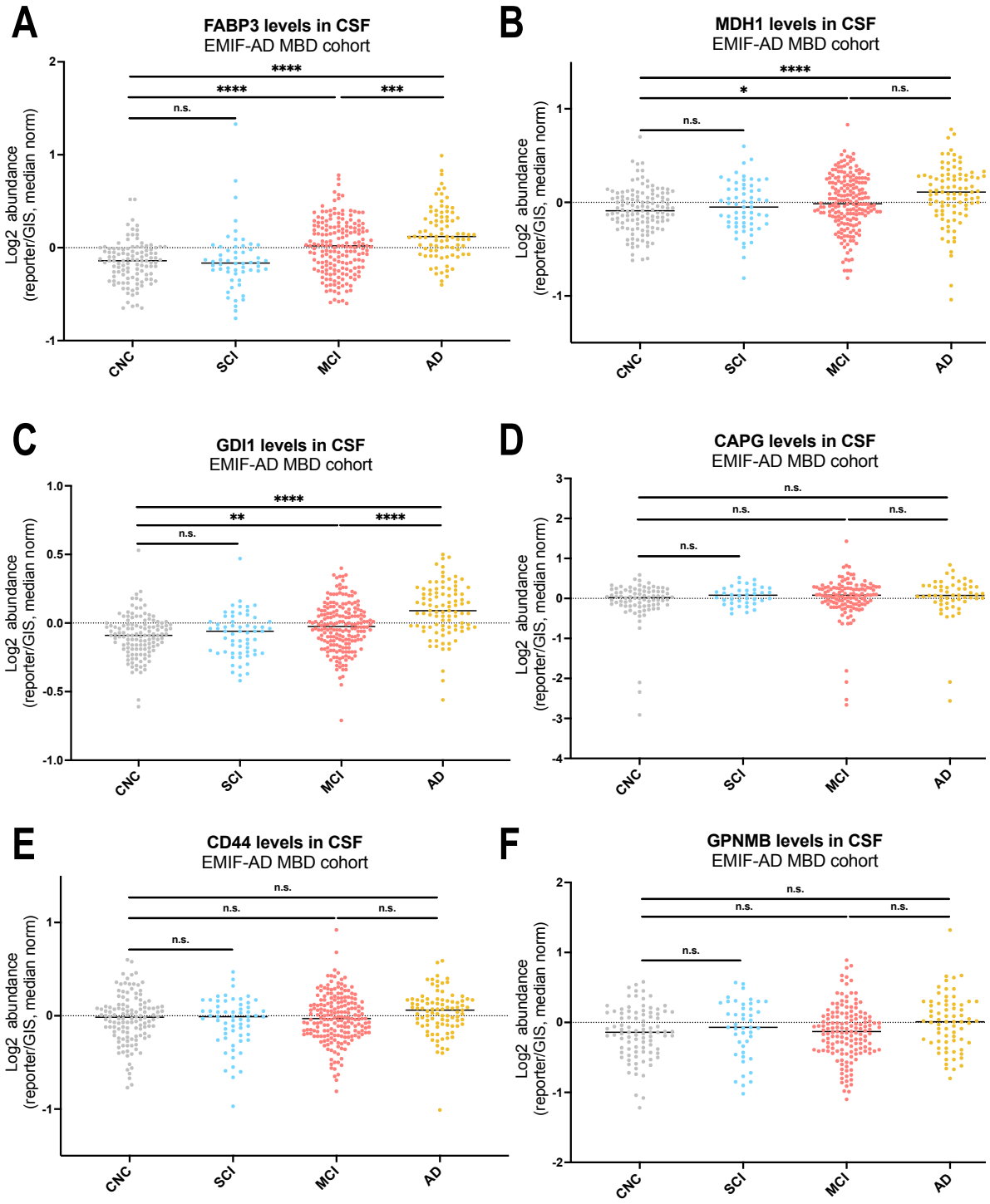

Figure 4.25. Levels of FABP3, MDHI1, and GDI1 are significantly elevated in the CSF of individuals diagnosed with MCI and AD.

CSF levels of (A) FABP3, (B) MDH1, (C) GDI1, (D) CAPG, (E) CD44, and (F) GPNMB in controls (CNC) (gray), SCI (blue), MCI (pink), and AD (yellow). Ordinary one-way ANOVA (alpha = 0.05). CSF levels are defined by log2 abundances, normalized to the abundance measured in a technical control (reporter/GIS) and the median of each individual (median norm.). "*" = $p < 0.05$, "**" = $p < 0.01$, "***" = $p < 0.001$, "n.s." = non-significant.

Stratification according to amyloid status allowed for further separation of within the MCI and AD group. CSF levels of FABP3, MDH1, and GDI1 were significantly different within the MCI group, with a highly significant elevation in MCI cases with amyloid abnormalities compared to amyloid normal MCI cases (Figure 4.26 A-F). Intriguingly, CSF levels of MDH1 was significantly different within the AD group, when stratifying this group according to amyloid status (Figure 4.26 B).

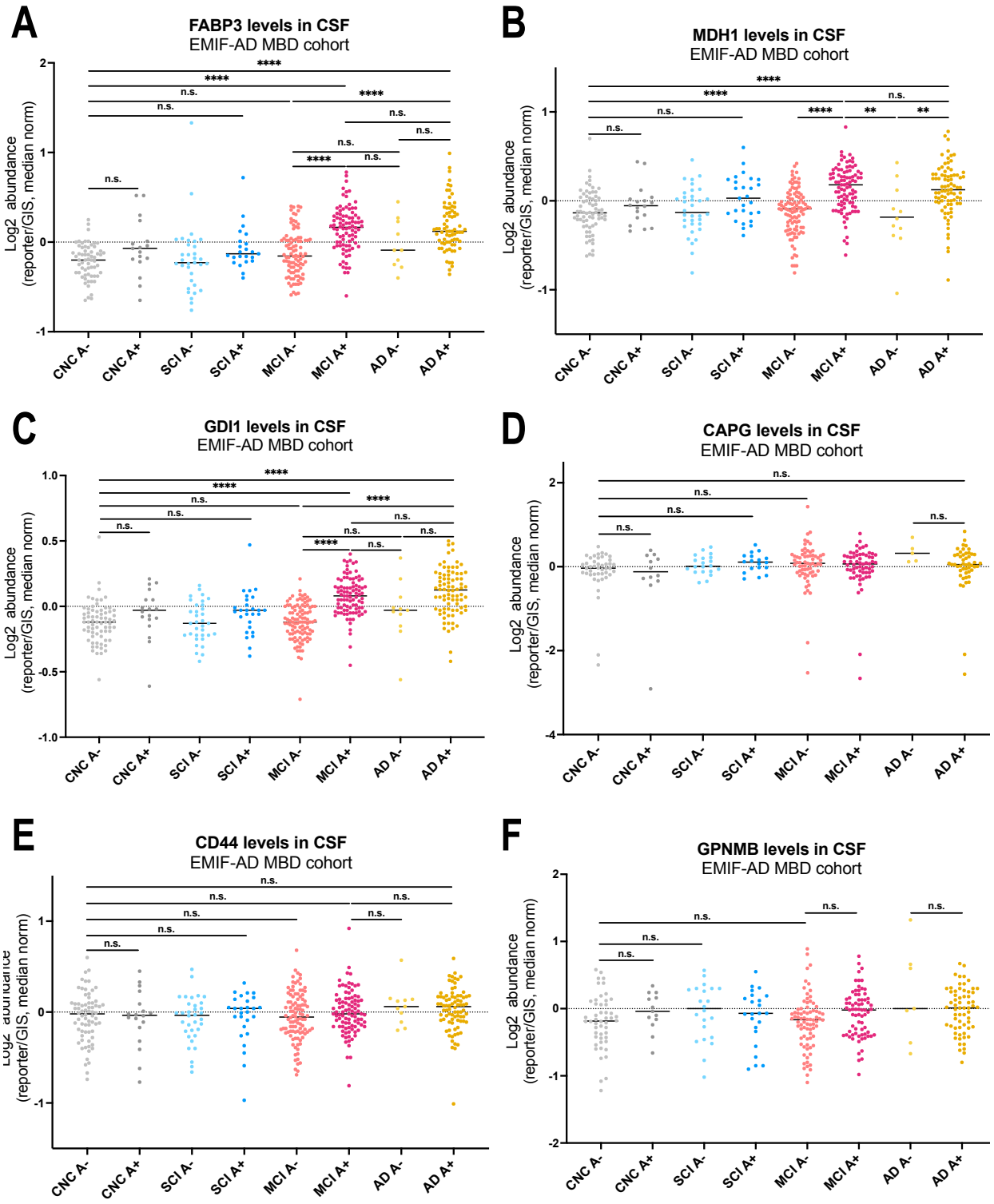

Figure 4.26. Levels of FABP3, MDH1, and GDI1 are significantly increased in an amyloid-dependent manner.

CSF levels of (A) FABP3, (B) MDH1, (C) GDI1, (D) CAPG, (E) CD44, and (F) GPNMB in CNC A- (light gray), CNC A+ (dark gray), SCI A- (light blue), SCI A+ (dark blue), MCI A- (light pink), MCI A+ (dark pink), AD A- (light yellow), and AD A+ (dark yellow). "A-" = amyloid normal, "A+" = amyloid abnormal. Ordinary one-way ANOVA (alpha = 0.05). CSF levels are defined by log2 abundances, normalized to the abundance measured in a technical control (reporter/GIS) and the median of each individual (median norm.). "*" = $p < 0.05$, "**" = $p < 0.01$, "***" = $p < 0.001$, "n.s." = non-significant.

4.8. CSF levels of FABP3, MDH1, and GDI1 correlate with each other and with neuroinflammatory marker CHI3L1

To further elucidate the role of Panel 6 proteins in the context of neuroinflammation, I investigated the correlation between each of the six proteins within the ALLFTD cohort (Figure 4.27), as well as within each group of the ALLFTD cohort: healthy non-carriers and FTD-GRN patients (Figure 4.28). For this analysis, I included known markers for microgliosis (TREM2), astrogliosis (GFAP), and neuroinflammation (CHI3L1, also known as YKL-40). A significant correlation was observed between FABP3, MDH1, and GDI1(Figure 4.27). The levels of these proteins also significantly correlated with the levels of CHI3L1 (Figure 4.27). In general, the observed correlations were weaker in the healthy controls compared to the FTD-GRN patients (Figure 4.28 A versus Figure 4.28 B). Strong correlations (defined by Spearman $r > 0.5$) were observed between GPNMB-CHI3L1, GDI1-GPNMB, GDI1-CHI3L1, FABP3-MDH1, FABP3-CHI3L1, MDH1-CHI3L1, CD44-CHI3L1, and MDH1-GDI1 (Figure 4.27). Very strong correlations (defined by Spearman $r > 0.75$) were observed between FABP3-MDH1 and MDH1-CHI3L1 in the FTD-GRN group (Figure 4.28 B). Notably, no correlation could be observed between GPNMB and TREM2 in the CSF of healthy controls (Figure 4.28 A), while in the CSF of FTD-GRN patients these proteins show a strong and significant correlation (Spearman $r = 0.67$) (Figure 4.28 B).

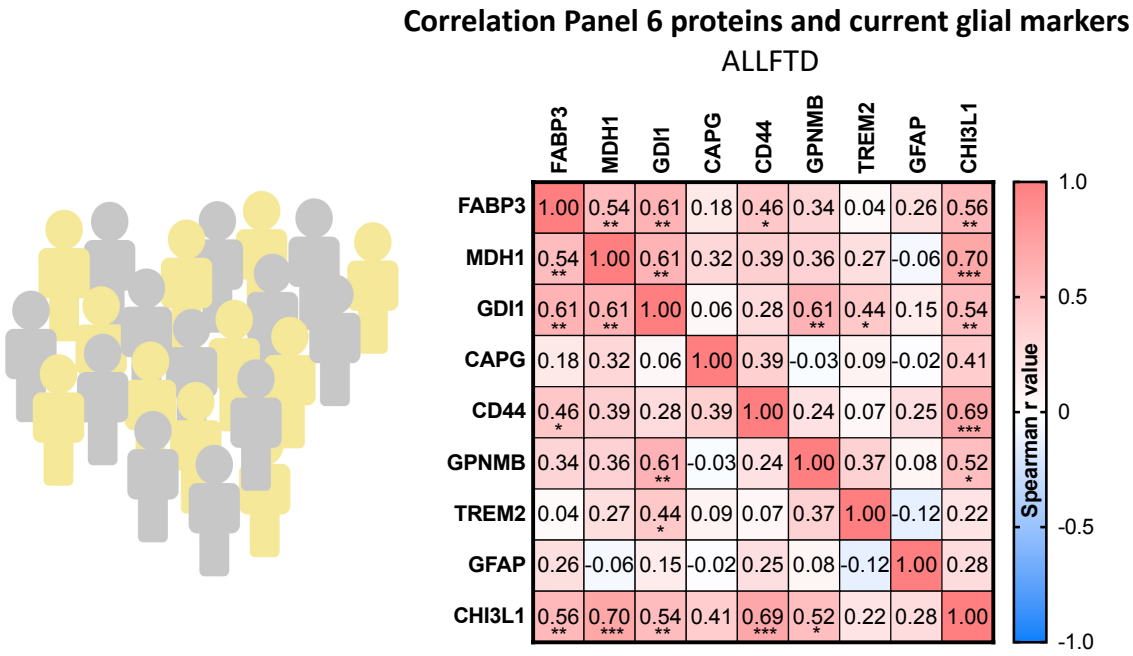

Figure 4.27. Correlation between FABP3, MDH1, GDI1, and CHI3L1 in the ALLFTD cohort.

Correlation analysis of Panel 6 proteins and known markers: TREM2 (microgliosis), GFAP (astrogliosis), and CHI3L1 (also known as YKL-40, neuroinflammation). Each cell is colored and labeled according to Spearman r value. "*" = $p < 0.05$, "**" = $p < 0.01$, "***" = $p < 0.001$, "n.s." = non-significant.

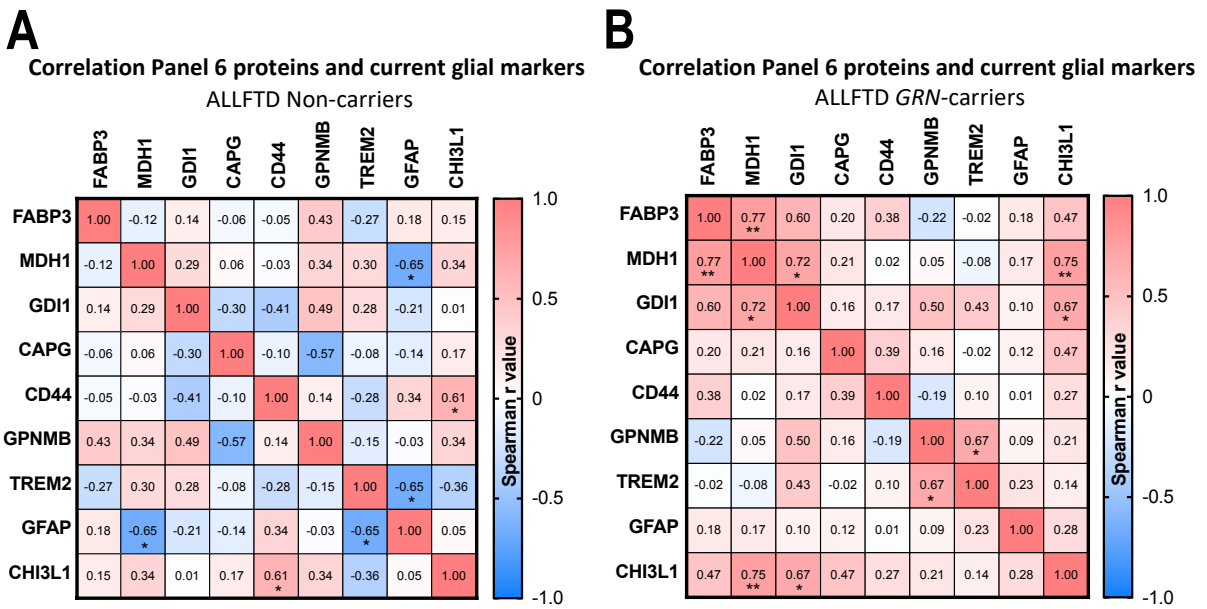

Figure 4.28. The correlation between FABP3, MDH1, and GDI1 is stronger in FTD-GRN patients than controls.

Correlation analysis of Panel 6 proteins and known markers: TREM2 (microgliosis), GFAP (astrogliosis), and CHI3L1 (also known as YKL-40, neuroinflammation). Each cell is colored and labeled according to Spearman r value. "*" = $p < 0.05$, "**" = $p < 0.01$, "***" = $p < 0.001$, "n.s." = non-significant.

The correlation between FABP3, MDH1, and GDI1, as observed in the ALLFTD cohort (Figure 4.27) was also confirmed in the AD group of the EMIF-AD MBD cohort (Figure 4.29 A). Of note, this correlation was considerably weaker within the CNC group of the EMIF-AD MBD cohort (Figure 4.29 B). Further confirming the relevance of these three markers in a neuroinflammatory setting, all three markers showed a significant correlation with neuroinflammatory marker CHI3L1 within the AD group (Figure 4.29 A).

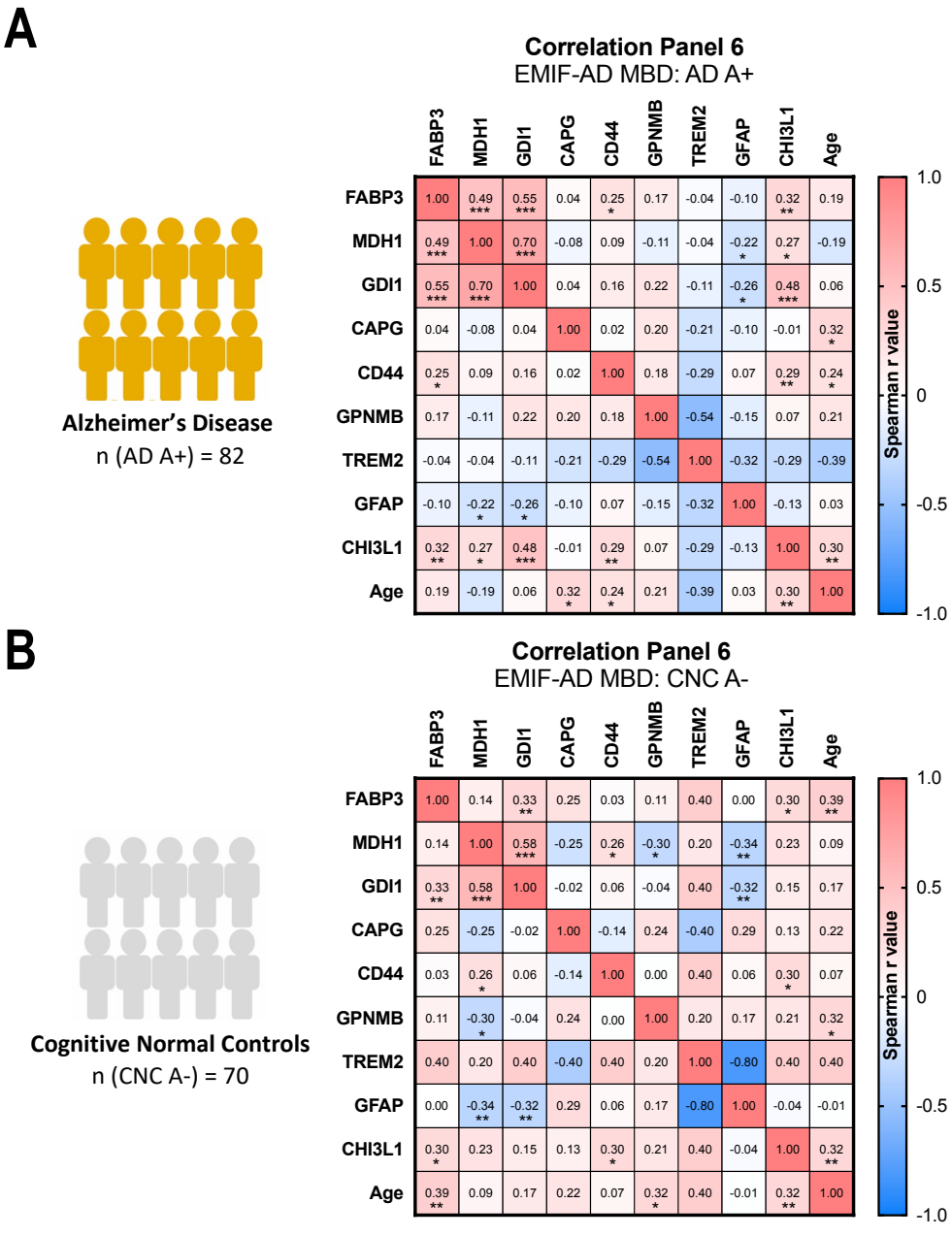

Figure 4.29. The correlation between FABP3, MDH1, and GDI1 is stronger in AD patients than controls.

Correlation analysis of Panel 6 proteins and known markers: TREM2 (microgliosis), GFAP (astrogliosis), and CHI3L1 (also known as YKL-40, neuroinflammation). Each cell is colored and labeled according to Spearman r value. "*" = $p < 0.05$, "**" = $p < 0.01$, "***" = $p < 0.001$, "n.s." = non-significant. FDR was not considered for the presented visualizations.

5. Discussion

The main objective of my thesis was to study the microglial proteome and secretome to identify biomarker candidates for the evaluation of microglial activation in humans. In the presented study, I have performed an in-depth characterization of the microglial proteome and secretome, including a translational aspect to address the relevance in humans. Based on the generated data and the results of a literature screening, I selected a panel of six proteins: FABP3, MDH1, GDI1, CAPG, CD44, and GPNMB. Three of the six proteins (FABP3, MDH1, and GDI1) were further confirmed in a second cohort, regarding a different disease, in a completely independent dataset derived from the EMIF-AD MBD cohort (Weiner et al., 2022).

5.1. The activation signature in mouse microglia

The characterization of microglial activation in various mouse models is largely based on transcriptomic data. This has resulted in several classifications of microglia, so-called "…-associated microglia" (commonly abbreviated "…AM"), including proliferative-region-AM (PAM) (Q. Li et al., 2019), white matter-AM (WAM) (Safaiyan et al., 2021), as well as disease-AM (DAM) (Keren-Shaul et al., 2017) (Figure 1.5). These activation signatures share common characteristics, which especially includes the upregulation of the gene encoding for the microglia receptor Trem2. When referring to the microglial activation signature, the DAM signature (Keren-Shaul et al., 2017) and the MGnD signature (Krasemann et al., 2017) are most commonly used.

The divergent microglial activation phenotypes observed in microglia isolated from mice lacking either Trem2 (reported to model homeostatic microglia) or the lysosome-associated protein Grn (reported to model hyperactivated microglia), have previously been characterized with transcriptional and functional analysis (Gotzl et al., 2019; Mazaheri et al., 2017). The proteomic analysis of these mouse models, as presented in this thesis, confirms the opposite microglial activation phenotypes also on a level of the proteome (Figure 4.1-4.3). The activation signature observed in the *Grn* ko mice shows considerable overlap with microglial activation signatures previously reported by several other groups. Common characteristics across the activation signatures include the upregulation of lysosomal proteins (such as

cathepsins (CTS), especially CTSD), transmembrane receptors (including CLEC7A, ITGAX, and TREM2), and lipid-interacting proteins (especially APOE) (Butovsky et al., 2014; Holtman et al., 2015; Keren-Shaul et al., 2017; Krasemann et al., 2017). Further confirming the activated signature observed in *Grn*-knockout microglia, the homeostatic marker P2RY12 is significantly reduced in both the transcriptome (analyzed with NanoString) and proteome (analyzed with mass spectrometry) of these mice (Figure 4.4 B). These frequently observed features of microglial activation indicate that there are some central components of the microglial response that are rather robust (such as the TREM2-pathway), despite the different strategies and models used to trigger the activation of microglia.

The hyperactivated signature observed in microglia isolated form *Grn*-knockout mice is more prominent than the homeostatic signature observed in the *Trem2*-knockout microglia, as indicated by the number of significantly upregulated proteins: 458 proteins in *Grn*-knockout microglia (Figure 4.4 A) versus 59 proteins in *Trem2*-knockout microglia (Figure 4.5 A). Surprisingly, the 59 significantly upregulated proteins in microglia isolated from *Trem2*-knockout mice, did not show any overlap with the CSF proteome isolated from the exact same mice (Figure 4.7 B). This accentuates the plastic nature of microglia and the perplexity of the homeostatic signature, which is more reliably addressed by the reduced levels of activation markers in the CSF rather than elevated levels of markers specific for the homeostatic signature.

5.1.1. Limitations of my study regarding the modeling of microglial activation in mice

As proposed by world-leading experts in the field of microglia research, different microglial states should be described according to a conceptual framework, in order to capture the wide repertoire of microglial functions and the potential coexistence of multiple microglial states (Paolicelli et al., 2022). Considering this, the commonalities observed between the activated microglia investigated in this study and in studies by others, are likely to reflect the specific functions that are relevant for microglial activation, including the enhancement of pattern recognition receptors (PRRs) required for the downstream signaling and subsequent microglial response, the upregulation of lysosomal proteins relevant for the enhancement of inflammatory cascades, as well as metabolic reprogramming (Paolicelli et al., 2022; Van Acker, Perdok, Bretou, & Annaert, 2021). According to the proposed framework for the

nomenclature of microglia (Paolicelli et al., 2022), one should consider the potential effects of the experimental design as well as the strategy used to activate microglia. For this study, I made use of the *Grn* ko mouse model, in which the microglia experience a lysosomal impairment. As a result of lysosomal impairment, the degradation process of undesired material (such as misfolded proteins and extracellular aggregates) is affected, with the initiation of sequential intracellular stress responses, which may be present throughout the lifetime of these mice. Notably, this lysosomal deficit cannot be rescued by a loss or diminution of TREM2 (Reifschneider et al., 2022). In amyloid mouse models (such as APPPS1 and 5xFAD) microglia are triggered by extracellular amyloid, which accumulates with time. The effects of intracellular versus extracellular triggers are not yet clear, but it might be a cause for the differences observed across different models for microglial activation.

Furthermore, the mouse microglia investigated in this study were acutely isolated from mouse brains post CSF collection. To collect CSF, mice were deeply anesthetized using MMF. The anesthetic was dosed according to bodyweight and delivered interperitoneally, whereupon the mice were anesthetized for approximately 15-20 minutes. Although the specific anesthetic and duration used in this study have not been reported to affect microglia, it has previously been reported that other anesthetics may affect the microglial morphology and responsiveness (W. Sun et al., 2019; Xu et al., 2023). As I did not analyze microglia from non-anesthetized mice, I cannot rule out that some of the observed changes are related to the anesthetic.

Following CSF collection, mice were sacrificed by cervical dislocation and the brains were immediately harvested. The isolated brains were dissected with only the cerebrum remaining, from which meninges were removed and microglia were isolated. Unfortunately, this dissection strategy (including the removal of the olfactory bulb and cerebellum) might cause regional biases as only microglia of the cerebrum were isolated and analyzed.

The CD11b protein, also known as integrin alpha M (ITGAM) or complement receptor 3 alpha (CR3A), is a commonly used marker for both homeostatic and activated microglia, although the expression has been reported to increase upon activation (Hopperton, Mohammad, Trepanier, Giuliano, & Bazinet, 2018; Jurga, Paleczna, & Kuter, 2020). As a result, the

potentially diluted effect of the homeostatic signature cannot be ruled out. Furthermore, CD11b is not exclusively expressed by microglia. To evaluate the purity of the isolated microglia fraction, the absence/low abundance of CD45 (as a common marker for leukocytes), CD206, and CD163 (both considered as markers for perivascular macrophages) may be used to confirm the microglia purity (Jurga et al., 2020). As presented in this study, the proteomic data of mouse microglia (sorted as a CD11b-enriched fraction) reached a depth of > 5000 proteins with label-free LC-MS/MS. In this dataset of > 5000 proteins, none of the abovementioned markers (CD45, CD206, and CD163) could be detected. This further confirms the high purity and microglia-specificity of this isolation protocol, as previously addressed by others (Sebastian Monasor et al., 2020).

Taken together, as microglia are extremely plastic cells, we cannot rule out potential alterations due to the procedure of CSF collection (including anesthesia) nor the procedure of microglial isolation. These limitations were not possible to circumvent for this study and therefore additional studies, with the aim to investigate if and how the microglial activation signature may be affected by the experimental design.

5.2. The microglial activation signature in mouse CSF

CSF is a body fluid directly in contact with the brain, supporting the brain with nutrients, assists with waste removal, and protects the brain from mechanical injury (Telano & Baker, 2022). Studying the CSF proteome brings insights to molecular mechanisms involved in brain function and disease, as well as the ability to identify and measure biomarkers (Zetterberg & Bendlin, 2021). The CSF proteome includes proteins originating from all cell types in the CNS, which is why a careful confirmation of potential biomarker candidates are of high relevance. As presented here, changes within the CSF proteome are compared with changes observed in the microglial proteome, isolated from the very same mice (Figure 3.9 and 3.10 A).

The proteomic changes commonly associated with the microglial activation in mice were partially reflected in the mouse CSF. Most strikingly, the clear divergence of APOE levels in *Grn*-knockout and *Trem2*-knockout mice (each compared to wild-type) is not only significant in microglia, but also strongly altered in the CSF of both genotypes (Figure 4.8). Other features

of the microglial activation signature that are reflected in the CSF proteome of *Grn*-knockout mice include the upregulation of cathepsins (CTSA, CTSD, CTSZ), proteins of the complement system (C1QA and C1QB), and the frequently observed lysozyme 2 (LYZ2) (Figure 4.1 A, 4.6 A, and 4.7 A). However, to exclude a GRN-biased effect, the proteomic signatures observed in microglia and CSF of *Grn*-knockout mice should be confirmed in mouse models where the microglial activation is triggered by extracellular factors (such as Aβ). It is therefore corroboratory that the microglial activation signature observed in the CSF of *Grn*-knockout mice aligns with the findings of a recent study where the glial activation signature was studied in the CSF of amyloid burden mice (Eninger et al., 2022).

Proteins may be released into the CSF through a variation of processes, including proteolytic processing of the extracellular domain, secretion via vesicles (endosomes, exosomes, secretory lysosomes, microvesicles), membrane translocation or membrane rupture (Sitia & Rubartelli, 2020). Once released into the CSF, proteins have different turnover rates, which may be dynamic and context-dependent. Furthermore, the proteins released into the CSF may or may not be relevant for cell non-autonomous functions. Hence, one should consider that once these proteins are present in the CSF they may interact with each other and/or other components, which may or may not affect cellular functions. As a consequence, further studies are required to address questions regarding how and why certain biomarker candidates are released from microglia into the CSF.

5.3. The microglial activation signature in hiMGL

The activated signature of *GRN*-knockout hiMGL have previously been assessed using transcriptomic analysis (Nanostring) and by measuring the catalytic activity of CTSD (Reifschneider et al., 2022). However, with the data presented here the activated signature observed in the *GRN*-knockout hiMGL is also confirmed on a proteome level, with a deeper characterization than previously reported (> 8000 proteins detected, compared to the customized NanoString panel consisting of 90 genes). In addition, this study also addresses the phenotypic signature of *TREM2*-knockout hiMGL, which could be confirmed as locked in a homeostatic state. To complement the proteomic analysis, qPCR was used to assess the cellular levels of three major markers for microglial activation (TREM2, CTSD and APOE), for

which the expression was increased in the *GRN*-knockout hiMGL and decreased in *TREM2*-knockout hiMGL. The qPCR data further confirmed a downregulation of the homeostatic marker P2RY12 in the *GRN*-knockout hiMGL (Figure 4.10 and 4.11). Taken together, the data presented here provides strong evidence for the opposite microglial activation phenotypes of *GRN*-knockout and *TREM2*-knockout hiMGL, respectively.

As the aim of this thesis is to identify potential biomarker candidates for the assessment of microglial activation in humans, the differences and commonalities between mouse and human models are highly relevant. Previously reported by several groups, microglial activation profiles may differ substantially between mouse and human models, especially in the context of amyloid-induced responses (Hasselmann et al., 2019; Mancuso et al., 2019; Y. Zhou et al., 2020). The data presented here, allow for translational comparisons of not only the microglial activation states, but also the microglial secretome. Translational comparisons are needed to fully characterize and understand the models of interest. In addition, mouse-to-human translation is necessary to determine which mechanisms and pathways are possible to model in mice. By comparing the proteomic signature of hiMGL with the proteome data obtained from mouse microglia, a rather well-conserved activation profile between the two systems was revealed. In microglia isolated from *Grn*-knockout mice, 458 proteins were significantly upregulated. Strikingly, 33% (150) of these proteins were also significantly upregulated in the proteome of monocultured *GRN*-knockout hiMGL (total of 1675 significantly increased proteins). The overlap of 150 proteins, include a significant increase of activation markers such as APOE, LGALS3, as well as various cathepsins (CTSA, CTSB, CTSH, CTSZ) (Figure 4.12 A). To conclude, the opposite microglial activation signatures observed in *Grn*-knockout and *Trem2*-knockout mice are well translatable to the human *in vitro* model using *GRN*-knockout and *TREM2*-knockout hiMGL.

5.3.1. Limitations of my study regarding the modeling of microglial activation in hiMGL

For this study, iPSCs were genetically altered to generate three hiMGL lines: *GRN*-knockout, *TREM2*-knockout, and wild-type. From the genetically modified iPSCs, only one clone per genotype was selected to generate hiMGL, from which all technical replicates (n = 6 per genotype) originated. Despite very careful and extensive quality control, one should be aware that there might be clone-specific changes. To allow for complete assurance, selected markers

would have to be analyzed in a setting where different clones have been selected for the differentiation of hiMGL.

5.4. The microglial activation state in the hiMGL secretome

The activated signature observed in *GRN*-knockout hiMGL was partly reflected in the conditioned media, in a similar manner as the microglial activation signature detected in the CSF of *Grn*-knockout mice. As observed in the cell lysates of *GRN*-knockout hiMGL, the cathepsin signature (CTSA, CTSB, CTSD, CTSL, CTSS, and CTSZ) appear as significantly upregulated in the secretome of *GRN*-knockout hiMGL. Similarly, APOE and proteins of the complement system (C1QB and C1QC) were also significantly upregulated in both cell lysates and conditioned media of *GRN*-knockout hiMGL (Figure 4.9 A and 4.13 A). Intriguingly, all of the listed proteins (CTSA, CTSB, CTSD, CTSL, CTSS, CTSZ, APOE, C1QB, and C1QC) were significantly upregulated in also in the CSF of *Grn*-knockout mice (Figure 4.14 A). The activation signature observed in the *GRN*-knockout models are much more distinguishable than the homeostatic signature of the *TREM2*-knockout models, which is more similar to the wild-type control. In the CSF of *Trem2*-knockout mice, only 13 proteins were significantly elevated, none of these proteins were significantly upregulated in the secretome of *TREM2*-knockout hiMGL (Figure 4.14 B). Instead, the most relevant changes confirming a homoeostatic signature in the media of *TREM2*-knockout hiMGL is the down regulation of markers associated with microglial activation (including ITGAX and GPNMB) (Figure 4.13 B). Of note, levels of lysozyme (LYZ) were significantly elevated in the conditioned media of *TREM2*-knockout hiGML compared to wild-type (Figure 4.13 B), which give indication that further characterization of these cells is necessary. However, this limitation is not a major concern for this study as the *GRN*-knockout model, with the confirmed and well consistent activation signature, is of focus. Nevertheless, when using the hiMGL model, any findings related to microglial activation should be carefully controlled and confirmed in additional systems.

5.5. The overlapping signature in human CSF and models of microglial activation

To further investigate the microglial activation signature in a human context, I analyzed the CSF proteome of FTD-GRN patients. In the CSF of these patients, one of the most significant changes was the reduction of GRN, which confirms the expected phenotype. Elevated levels of the neuroinflammatory marker CHI3L1 (also known as YKL-40) were observed in the CSF of FTD-GRN patients, but not in healthy controls. In corroboration with the expected neurodegenerative state of the FTD-GRN patients, neurofilament light (NEFL) appeared as the most significantly elevated protein within the CSF proteome of these patients (Figure 4.15). In total, 88 proteins were significantly elevated in the CSF of FTD-GRN patients compared to the healthy non-carriers (Figure 4.16 A).

To identify potential microglial-dependent alterations within the CSF proteome of these patients, I compared the CSF profile of FTD-GRN patients with the data obtained from *GRN*-knockout hiMGL media. Intriguingly, > 30% (26 proteins) of the significantly elevated proteins detected in the CSF of FTD-GRN patients were also significantly increased in the media of *GRN*-knockout hiMGL (Figure 4.16 A). Closer investigation of these 26 proteins revealed commonalities across the models investigated in this study (mouse and hiMGL), including FUCA1, HEXB, FABP3, QDPR, FUCA2, CHI3L1, CAPG, and CBR1. However, our data also revealed changes of the proteome that are not translatable across the investigated models, such as protein levels of MDH1, ENOPH1, CD84, and EPB41L3; all that are upregulated in the hiMGL model and in FTD-GRN CSF but downregulated in mice (Figure 4.17). The translational commonalities and differences reported here may be of great use when selecting models for future studies.

5.6. The discovery of FABP3, MDH1, GDI1, CAPG, CD44, and GPNMB as possible markers for microglial activation

The main finding of this study was the identification of six microglial activation-dependent markers, referred to as Panel 6, namely: FABP3, MDH1, GDI1, CAPG, CD44, and GPNMB. These proteins are significantly increased in the conditioned media of *GRN*-knockout hiMGL, as well as in the CSF of FTD-GRN patients (Figure 4.18). Importantly, I decided to avoid referring to

these changes as microglia-*specific*, as these six proteins are expressed by other cell types as well. For example, expression of FABP3, MDH1, and CAPG have been reported in neurons (Hassan et al., 2020; Kawahata, Bousset, Melki, & Fukunaga, 2019; Kwon et al., 2023), and the expression of GDI1 and CD44 has been reported in astrocytes (Neal, Boyle, Budge, Safadi, & Richardson, 2018; Potokar et al., 2017), while GPNMB has been reported to be expressed by both neurons and astrocytes (Nakano et al., 2014). Nevertheless, the fact that the hiMGL lines were grown in isolation, with an activated signature confirmed exclusively in the *GRN*-knockout line, implies that the significantly elevated levels of the Panel 6 proteins are indeed microglial activation-*dependent* and not driven by other cell types.

A limitation when studying the proteome in humans, is the restriction to CSF and the lack of isolated microglia. Ideally, a consistent workflow would be maintained for all of the studied subjects (mouse, hiMGL, and human), as this would enable the possibility of correlating the observed changes in the CSF proteome to the microglial activation status in patients. However, the comparison with the microglial activation status observed in our models (Figure 4.19) and in models by others (Figure 4.20-4.22) (Eninger et al., 2022; Keren-Shaul et al., 2017; Sebastian Monasor et al., 2020), support the idea of altered levels of the Panel 6 proteins (FABP3, MDH1, GDI1, CAPG, CD44, GPNMB) as dependent on the microglial activation state. This holds especially true for FABP3, CAPG, and GPNMB (Figure 4.20-4.22).

Interestingly, with the CSF levels of the Panel 6 proteins (as measured with mass spectrometry) FTD-GRN patients were successfully distinguished from the healthy controls. The used model for this prediction analysis was a logistic regression model. The prediction efficiency reached a score of 81.0% and was only possible when using the combination of all six proteins (Figure 4.23). Unfortunately, the small sample size and the restricted cohort data (such as age defined as a categorical variable of 5 years intervals) are limiting factors for the prediction analysis. Consequently, the prediction analysis presented here is only conclusive for this dataset and not for a general differentiation of FTD-GRN patients and healthy individuals.

5.7. CSF levels of FABP3, MDH1 and GDI1 increase in an amyloid-dependent manner

With the final aim of my thesis being the confirmation of potential biomarker candidates in the CSF proteome derived from a validation cohort, I made use of completely independent and already published data from the EMIF-AD MBD cohort (Weiner et al., 2022). There are several reasons as to why the EMIF-AD MBD cohort is suitable as a validation cohort for this study: (1) the proteomics data is already available, which is ethically defendable as this optimizes the use of patient data and reduces the use of patient samples, (2) the data was generated and analyzed independently from this study, which reduces any potential bias due to invariable study design, (3) the data was generated using a different methodology (tandem mass tag (TMT) mass spectrometry), which reduces any potential bias due to invariable experimental design, (4) the validation cohort (EMIF-AD MBD) consists of participants with different disease and pathological focus than the discovery cohort (ALLFTD), and finally, (5) the validation cohort (EMIF-AD MBD) provides information regarding amyloid pathology, which is an extracellular pathology known to activate microglia even before symptom become apparent (Morenas-Rodriguez et al., 2022).

Out of the six selected proteins, three proteins could be confirmed in the dataset of the EMIF-AD MBD cohort. CSF levels of FABP3, MDH1, and GDI1, were significantly elevated in MCI and AD patients (Figure 4.25). Importantly, CSF levels of these three candidates were elevated, with a strong statistical significance, in MCI cases with detectable amyloid abnormalities compared to amyloid-negative MCI cases (Figure 4.26). The highly significant elevation of these three proteins in amyloid-positive MCI cases, is in complete agreement with previous studies where increased sTREM2 up levels are detectable to 21 years before the estimated year of onset following immediately the deposition of amyloid (Morenas-Rodriguez et al., 2022). Together, these findings support the idea that microglia respond to the earliest amyloid related threat, before any symptoms become apparent.

5.8. The correlation between FABP3, MDH1 and GDI1 accentuates the advantageous use of biomarkers in a panel format

With a deeper investigation of the Panel 6 proteins, I discovered significant correlation between CSF levels of FABP3, MDH1, and GDI1 in the FTD cohort (ALLFTD) as well as in the AD cohort (EMIF-AD MBD) (Figure 4.27-4.29). The correlation between these three proteins was most prominent in the patient groups of the two cohorts (FTD-GRN: Figure 4.28, and AD: Figure 4.29). The CSF levels of FABP3, MDH1, and GDI1 also correlated with the neuroinflammatory marker CHI3L1 (also known as YKL-40), again with the strongest correlation observed in the patient groups of the two cohorts (Figure 4.28-4.29). The correlation with CHI3L1 provides further evidence that the levels of these markers are indeed linked to an immune response. The correlation analysis also revealed a correlation between GPNMB and TREM2, a correlation that is significant in FTD-GRN patients but not in healthy controls (Figure 4.28). This correlation supports the microglial activation-dependency, especially as the correlation can only be seen in the FTD-GRN patients where the microglia are expected to be activated (in contrast to the healthy control where the microglia are expected to be closer to the homeostatic signature). The Panel 6 proteins, with especial notice of FABP3, MDH1, and GDI1, appear as very promising biomarker candidates. However, to understand the function and nature of these proteins and thereby optimize a potential future use of these biomarker candidates, further studies addressing the molecular mechanisms are required.

5.9. Literature screening and the potential involvement of Panel 6 proteins in lipid metabolism in microglia

To get a better understanding about the identified biomarker candidates, I screened the literature to investigate the possibility of common mechanism(s) that could explain the observed correlations between FABP3, GDI1, and MDH1.

5.9.1. FABP3 – Crucial factor for the uptake and intracellular distribution of lipids

As the name reveals, Fatty acid-binding protein 3 (FABP3), also known as heart FABP (H-FABP or FABPH), is a lipid binding protein that binds n-6 fatty acids, such as arachidonic acid (Furuhashi & Hotamisligil, 2008; Hanhoff, Lucke, & Spener, 2002; Mallick, Basak, & Duttaroy, 2021) (uniprot.org/uniprotkb/P05413/entry). FABP3 was initially isolated from heart tissue,

hence the nomenclature H-FABP and FABPH. However, the name heart FABP is rather misleading as this protein has now been isolated from several tissues in addition to heart tissue, including brain tissue (Furuhashi & Hotamisligil, 2008; Mallick et al., 2021).

FABP3 is a cytosolic protein that works as an intracellular chaperon protein, binding and transporting lipids to sites of lipid metabolism. This function of FABP3 has been reported in heart tissue (Zhuang et al., 2021), in skeletal muscle (Debard et al., 2004), and in cancer cells (Bensaad et al., 2014), where FABP3 is specifically involved in the uptake of lipids and the transport to the mitochondria for subsequent β-oxidation (Furuhashi & Hotamisligil, 2008; Munir, Lisec, Swinnen, & Zaidi, 2019). Further supporting the role of FABP3 in lipid uptake, FABP3-knockout mice show a decrease in lipid uptake, accompanied with increased plasma levels of long-chain fatty acids (Binas, Danneberg, McWhir, Mullins, & Clark, 1999). FABP3 has also been reported to be involved in the formation of lipid droplets, a process that is considered very important for microglial response (Bensaad et al., 2014; Gouna et al., 2021; Munir et al., 2019; Nugent et al., 2020). In adipocytes and hepatocytes, cellular levels of FABPs are increased when exposed to high lipid concentrations in a chronic manner. Lipid exposure-dependent increase has been reported specifically for FABP3, in both *in vivo* and *in vitro* models (Furuhashi & Hotamisligil, 2008). The function of FABP3 in the brain is less studied, although there are studies suggesting an association between FABP3 and the accumulation of α-synuclein (Oizumi et al., 2021; Shioda et al., 2014). Behavioral characteristics observed in FABP3-knockout mice including impaired social memory and thinking, further supports the importance of FABP3 function within the brain (Mallick et al., 2021; Shimamoto et al., 2014). As presented, levels of FABP3 appear to increase with age in microglia of amyloid burden mice (Sebastian Monasor et al., 2020).

In humans, blood levels of FABP3 have previously been reported to associate with peripheral artery disease (PAD) (B. Li, Syed, Khan, Singh, & Qadura, 2022) and acute myocardial infarction (AMI) (Moon et al., 2021). Of note, elevated levels of FABP3 in CSF have been associated with neurodegenerative diseases, including AD (Chiasserini et al., 2017; Dulewicz, Kulczynska-Przybik, Slowik, Borawska, & Mroczko, 2021; Higginbotham et al., 2020), Parkinson's disease with dementia (PDD), and dementia with Lewy bodies (DLB) (Chiasserini et al., 2017). Furthermore, FABP3 has previously been associated with insulin, lipid and cardiovascular

phenotypes (Y. Zhang et al., 2013). Interestingly, levels of FABPs are increased in skeletal muscles of diabetic patients compared to healthy individuals (Furuhashi & Hotamisligil, 2008). In pre-diabetic patients, characterized by an impaired glucose metabolism, fatty acids constitute an extremely important energy source, which has been suggested to explain the overexpression of FABP3 that has been associated with the disease (Karbek et al., 2011; Mallick et al., 2021). With the gathered evidence, it is very plausible that the observed increase of FABP3 in microglia, reflects an increased lipid-associated burden that microglia are facing in diseased conditions (Colombo et al., 2021; Munoz Herrera & Zivkovic, 2022). In line with this hypothesis, FABP3, together with APOE, has recently been proposed as biomarkers for lipid-metabolism in AD patients (Dulewicz et al., 2021). However, the study presented here appears to be the first study that links the elevated levels of FABP3 in CSF to the microglial activation status. Personally, I think it is tempting to speculate about the link between FABP3 and diabetes in relation to diabetes-related AD. The function of FABP3 in brain and disease will need to be investigated in further studies, which considers different cell types and diseases.

5.9.2. MDH1 – part of the malate-aspartate shuttle and a potential support for microglia in metabolically demanding contexts

Malate dehydrogenase 1 (MDH1), is a cytosolic enzyme catalyzing the NAD/NADH-dependent oxidation of malate to oxaloacetate, as part of the malate-aspartate shuttle and a final step of the tricarboxylic acid (TCA) cycle (Broeks et al., 2019; Friedrich, Morizot, Siciliano, & Ferrell, 1987; Kim et al., 2012; Minarik, Tomaskova, Kollarova, & Antalik, 2002) (uniprot.org/uniprotkb/P40925/entry). With its central role in the malate-aspartate shuttle and the TCA cycle, MDH1 has a clear link to cellular metabolism. The expression of MDH1 correlates with the demand of aerobic metabolism, with highest expression in heart, skeletal muscle, and in brain (Broeks et al., 2019). Furthermore, the enzymatic activity of MDH1 appears to be induced by acetylation and may play a role in fatty acid synthesis (Kim et al., 2012).

According to a recently reported study, the microglial response to lipopolysaccharide (LPS)-treatment, which is known to activate the microglia, is highly dependent on the malate-aspartate shuttle (C. Zhou, Shang, Yin, Shi, & Ying, 2021). The processes related to microglial

activation are very energy demanding, which might explain the increased levels of MDH1 as the expression of MDH1 correlates with the demand of aerobic metabolism (Broeks et al., 2019; Churchward, Tchir, & Todd, 2018). Under energy intensive conditions, where glucose is insufficient or not present, microglia are capable of utilizing alternative energy sources, such as lipids (Churchward et al., 2018). Although very hypothetical, the need of alternative energy sources could result in increased de novo lipogenesis, a glial function that is considered essential for the maintenance of the lipid homeostasis within the CNS (Folick, Koliwad, & Valdearcos, 2021). In line with this hypothesis, the enzymatic activity of MDH1 has indeed been linked to fatty acid synthesis (Kim et al., 2012), which could be an alternative explanation for the increased levels of MDH1 in microglia. However, these ideas remain as pure speculations as the role of MDH1 needs to be further studied context of microglial activation, especially to address whether the increased MDH1 levels are part of a process of metabolic reprograming or if it is a consequence to a disturbed energy metabolism.

In humans, a pathogenic homozygous MDH1 mutation (c.413C-T, NM_001199111) was recently identified in two cousins (age 2.5 and 4 years) with developmental and epileptic encephalopathy. Both patients showed clear neurological symptoms, including developmental delay, epilepsy and progressive microcephaly (Broeks et al., 2019). Further supporting the important role of MDH1 within the CNS, MDH1 has been suggested as a biomarker for Creutzfeldt-Jakob disease (CJD), as MDH1 levels in CSF increase in CJD cases of sporadic (sCJD) and genetic (gCJD) nature (Schmitz et al., 2016; Zerr et al., 2019).

5.9.3. GDI1 – important for vesicle trafficking and a potential key player in the transportation of lipid droplets

GDP dissociation inhibitor 1 (GDI1), also known as GDIα, regulates the activation of Rab proteins by inhibiting the dissociation of GDP, which is required for the Rab-GTP interaction and the subsequent activation of Rab proteins. Due to the inhibited dissociation of GDP, Rab proteins are kept in the cytosol as their interaction with the cell membrane is hindered. As a result, GDI1 is indirectly involved in intracellular vesicle trafficking (Stenmark, 2009). Further supporting this, GDI1 was recently identified as a mediator involved in vesicle trafficking and intracellular lipid homeostasis, via the actin-network and heat shock factor 1 (HSF-1) (Watterson et al., 2022).

To my knowledge, no concrete link between GDI1 and microglia has been studied, although GDI1 was significantly increased in the CSF of aged mice, in a study investigating the glial activation signature in mouse CSF (Eninger et al., 2022) (Figure 4.22). Interestingly, GDI1-knockout mice show an increased signal in FDG-PET, indicating an induced glucose uptake and a relevant function regarding cellular metabolism (D'Adamo et al., 2021). Based on the interactions and functions of GDI1 as reported in the literature, it might be possible that GDI1 plays a role in microglial activation via its interactions with TMEM59 (H. Wang & Wen, 2022) and Rab10 (Chen et al., 2009). Upon insulin stimulation, GDI1 preferentially interacts with Rab10 (Chen et al., 2009), which has been reported to play a role in the formation of lipid droplets (Jin et al., 2021). With this hypothesis, potentially linking GDI1 to microglia via lipid droplet formation, the depletion of GDI1 would likely cause an impaired distribution of lipid droplets and therefore interfere with the use of fatty acids as a source of energy. With impaired lipid metabolism, it is plausible that the glucose uptake and metabolism would be boosted in order to maintain the energy demand of the cell. Although highly hypothetical, this might explain the induced glucose uptake observed in GDI1-knockout mice (D'Adamo et al., 2021). However, as GDI1 has not been studied in a microglia-specific context, this hypothesis should be carefully investigated before any conclusions can be made.

In humans, elevated GDI1 levels have previously been reported in the CSF of AD patients (Higginbotham et al., 2020), which is in line with our findings using available proteomic data from the EMIF-AD MBD cohort (Figure 4.25 C and 4.26 C). Mutations in the GDI1 gene have been identified to cause X-linked intellectual disability (XLID), which further indicates the important role of GDI1 in the CNS (D'Adamo et al., 2021).

5.9.4. CAPG – Promotes macrophage motility

Macrophage-capping protein (CAPG) is an actin capping protein involved in the regulation of actin polymerization and cell motility in macrophages. Increased levels of CAPG promotes cell locomotion through a mechanism involving the activation of PLC-γ, which in turn has been associated to protective microglial functions via TREM2 (H. Q. Sun, Kwiatkowska, Wooten, & Yin, 1995; Takalo et al., 2020).

Increased cellular levels of CAPG have previously been observed in activated microglia (Keren-Shaul et al., 2017; Nugent et al., 2020; Sebastian Monasor et al., 2020) (Figure 4.20-4.22), supporting the idea of CAPG as a potential biomarker for microglial activation. In humans, altered levels of CAPG in CSF has previously been reported in sporadic and genetic amyotrophic lateral sclerosis (ALS) (Oeckl et al., 2020).

5.9.5. CD44 – A regulator of the inflammatory response in microglia

CD44 is a transmembrane adhesion receptor, located at the cell surface of various cell types; including B-cells, granulocytes, and macrophages (Naor, Nedvetzki, Golan, Melnik, & Faitelson, 2002). In astrocytes, the activation of CD44 initiates intracellular signaling that downregulates inflammatory factors such as interleukin-6 (IL-6) and reactive oxygen species (ROS), while levels of anti-inflammatory mediators are induced (Neal et al., 2018; Saade, Araujo de Souza, Scavone, & Kinoshita, 2021). In hepatocytes and adipocytes, the activation of CD44 is enabling de novo lipogenesis, via signaling a pathway involving PI3K-AKT-mTORC1-SREBP1C (Kuang & Lin, 2019).

According to the reported data, no significant change of the CSF levels of CD44 could be observed across the groups of the EMIF-AD MBD cohort (CNC, SCI, MCI, and AD). However, increased CSF levels of CD44 have previously been reported in AD patients of another AD-cohort (Higginbotham et al., 2020).

5.9.6. GPNMB – Associated with microglia regeneration and proliferation in the CNS

Glycoprotein non-metastatic melanoma protein B (GPNMB), sometimes referred to as Osteactivin, DC-HIL or HGFIN, is a type I transmembrane glycoprotein. GPNMB is expressed by various tissues and cell types, with microglia as the main GPNMB-expressing cell type within the brain (Saade et al., 2021). The cellular levels of GPNMB have previously been reported as altered by the microglial activation state. However, the exact function of GNPMB in regard to inflammation is still debatable as there is evidence that speak for both a pro-inflammatory and anti-inflammatory role, although within the CNS the function of GPNMB appears to be anti-inflammatory and regenerative (Huttenrauch et al., 2018; Saade et al., 2021). According to a recent study, GPNMB is upregulated upon lysosomal stress, a context in which GPNMB plays a protective role for the maintenance of lysosomal integrity (Suda et al. 2022). In mice,

GPNMB has been linked to activated and proliferative microglia (Holtman et al., 2015; Keren-Shaul et al., 2017; Krasemann et al., 2017; Paolicelli et al., 2022). Using transcriptomic analysis, *GPNMB* has previously been reported as one of the most upregulated genes in APPPS1 mice, an amyloid-burden mouse model with confirmed microgliosis (Lopez-Rodriguez et al., 2021), compared to age-matched wild-type (Weissmann et al., 2016).

In humans, the microglial expression of GPNMB appears to be higher in white matter compared to gray matter. In addition, GPNMB was identified as one of the most differentially expressed genes in microglia isolated from normal-appearing gray matter of multiple-sclerosis (MS) patients (van der Poel et al., 2019). A white matter-specific increase of microglial GPNMB has also been reported in patients diagnosed with Nasu-Hakola disease (NHD) and AD, in a study where the abundance of the GPNMB protein was evaluated using immunohistochemistry (Satoh, Kino, Yanaizu, Ishida, & Saito, 2019). Notably, NHD, also known as polycystic lipomembranous osteodysplasia with sclerosing leukoencephalopathy (PLOSL), is a rare autosomal recessive disease, caused by homozygous loss of function mutations in the *TREM2* or *DAP12* gene (Dardiotis et al., 2017).

The extracellular domain of GPNMB is proteolytically processed by ADAM10, generating soluble GPNMB, which has been reported as a ligand for CD44 (Neal et al., 2018; Saade et al., 2021). The downstream signaling of CD44 is associated with anti-inflammatory responses, as well as de novo lipogenesis (Kuang & Lin, 2019; Neal et al., 2018; Saade et al., 2021). Notably, GPNMB-positive microglia can be found in two different microglial populations: one population surrounding the amyloid plaques (similar to the DAM microglia), while the other GPNMB-positive microglial population appear as amoeboid and lipid-rich (Huttenrauch et al., 2018). The potential role of GPNMB in lipogenesis, could provide a possible link to the microglial GPNMB-expression and the white-matter specificity as reported in MS, AD, and NHD patients (Satoh et al., 2019; van der Poel et al., 2019). The functions linking GPNMB to lipid storage, and potentially lipid metabolism, need to be further investigated. In this context, CD44 should be investigated to confirm or exclude a potential interaction between the two proteins.

The soluble version of GPNMB has previously been reported as a possible CSF-based biomarker for ALS (Oeckl et al., 2020) and AD (Huttenrauch et al., 2018). An Aβ-driven elevation of CSF GPNMB has already been linked to microglial activation, with evidence including the clustering of GPNMB-positive microglia around Aβ-plaques as well as an increased expression of GPNMB upon Aβ-treatment *in vitro* (Huttenrauch et al., 2018).

5.10. The association of Panel 6 proteins and various neurodegenerative diseases

Further supporting our findings, abnormal CSF levels of the Panel 6 proteins have all been previously reported individually in various neurodegenerative diseases: (1) FABP3 in AD (Chiasserini et al., 2017; Dulewicz et al., 2021; Higginbotham et al., 2020), PDD, and DLB (Chiasserini et al., 2017), (2) MDH1 sporadic and genetic CJD (Schmitz et al., 2016; Zerr et al., 2019), (3) GDI1 in AD (Higginbotham et al., 2020), (4) CAPG in in sporadic and genetic ALS (Oeckl et al., 2020), (5) CD44 in AD (Higginbotham et al., 2020), and (6) GPNMB in ALS and AD (Huttenrauch et al., 2018; Oeckl et al., 2020).

With the data presented here, I suggest that the levels of these markers in CSF do not reflect a specific disease, despite the previously published disease-dependent alterations. Instead, I propose, with support of the data presented here, that the observed changes reflect processes and pathways that are commonly occurring across the various diseases. Furthermore, in the case of the proteins FABP3, MDH1, GDI1, CAPG, CD44, and GPNMB, I propose that the involved processes are associated to, and most likely driven by, microglial activation.

5.11. CSF levels of FABP3, MDH1, GDI1, CD44 and GPNMB – a possible indication of metabolic reprogramming within activated microglia

According to the literature, the majority of the Panel 6 proteins appear to play a role in lipid metabolism. More specifically, I found functions associated with the uptake, synthesis, storage, transport, and metabolism of lipids (Figure 5.1). Lipids are more than just an energy source. These molecules are important for inter- and intracellular signaling with the capacity

to effect gene expression, cellular growth and proliferation, as well as inflammatory and metabolic responses (Furuhashi & Hotamisligil, 2008). Processes like lipid processing, trafficking, and lipid availability versus removal, are complex and dynamic and need to be carefully balanced. Apart from adipocytes (fat cells), macrophages are considered to be a major cell type facing a high demand of lipid trafficking, storage and signaling (Furuhashi & Hotamisligil, 2008). It is therefore very plausible that microglia, as the brain resident macrophages, are forced to deal with lipid-related burdens that come with disease or metabolic impairments within the CNS.

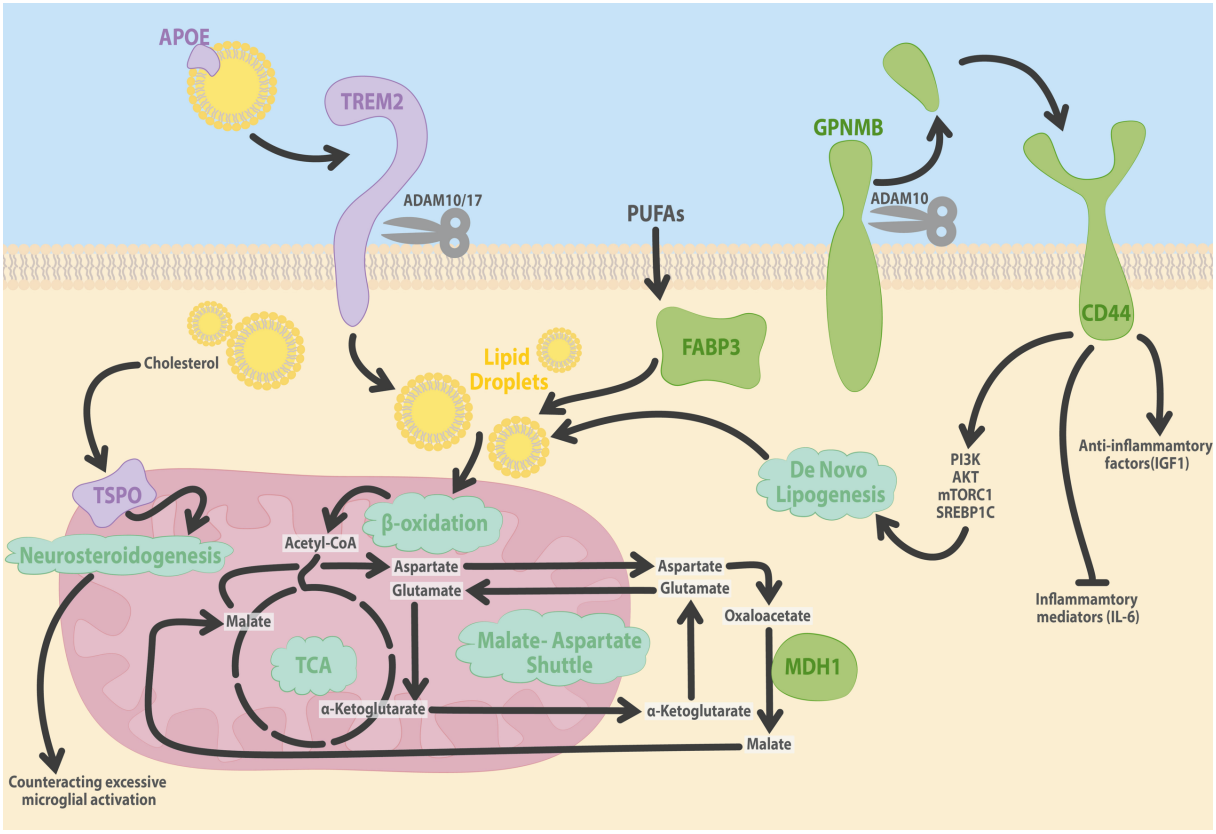

Figure 5.1. The potential link between biomarker candidates for microglial activation and lipid metabolism.
Illustration summarizing the reported functions of FABP3, MDH1, GPNMB and CD44. In purple: proteins already associated with microglial activation (APOE, TREM2, and TSPO). In dark green: proteins that are included in Panel 6 (FABP3, MDH1, GPNMB, and CD44). Metabolic processes are indicated and labeled in bright green.

Recently, several studies brought attention to the metabolic reprogramming present in microglia upon their activation (Blank, Enzlein, & Hopf, 2022; Chausse, Kakimoto, & Kann, 2021; Kleinberger et al., 2017; Kunkle et al., 2019; Leyrolle, Laye, & Nadjar, 2019; Loving & Bruce, 2020; Marschallinger et al., 2020; Paolicelli et al., 2022). Lipid homeostasis may also be

linked to microglia via TREM2. TREM2-dependent processes, including the sensing, binding, uptake, and metabolism of lipids, are crucial for the microglial response and the activation capacity of these cells (Gouna et al., 2021; Nugent et al., 2020; Poliani et al., 2015; Ulland et al., 2017; Y. Wang et al., 2015).

5.11.1. The microglial imaging-based biomarker TSPO – a measure of cholesterol metabolism

The currently used method for assessing microglial activation status, TSPO-PET, is based on the expression of TSPO. Of note, TSPO is not microglia-*specific*, but appears to be microglia activation-*dependent* (Beckers et al., 2018; Gotzl et al., 2019; Kleinberger et al., 2017; Pozzo et al., 2019; Xiang et al., 2021). Interestingly, the main function of TSPO is to transport cholesterol across the mitochondrial membrane, where it can be further metabolized (Papadopoulos & Miller, 2012). The fact that the main function of TSPO regards lipid metabolism further supports my idea of biomarkers associated to lipid metabolism and lipid homeostasis in microglia as biomarkers for microglia activation.

6. Conclusions

The data presented in this thesis confirmed the microglial activation repertoire of hyperactivated *GRN*-knockout models at a proteome level. This hyperactivated signature appears to be comparable between mice and hiMGL and partly reflected in the secretome (CSF from mice and conditioned media from hiMGL).

By comparing the significantly increased proteins in the conditioned media of *GRN*-knockout hiMGL with proteins significantly increased in the CSF of FTD-GRN patients, I identified an overlap of 26 proteins. With a deeper investigation of these proteins, I selected six proteins (FABP3, MDH1, GDI1, CAPG, CD44, and GPNMB) as the most promising biomarker candidates for microglial activation.

Three of these candidate markers (FABP3, MDH1, and GDI1) were confirmed in the CSF of AD and MCI cases that were analyzed independently to this study. The levels of these three proteins appeared to increase in an amyloid-dependent manner. Furthermore, these three proteins show strong correlation with each other and with the neuroinflammatory marker CHI3L1.

To conclude, our panel of six proteins, with the most promising candidates being FABP3, MDH1, and GDI1, may be of great use for the evaluation of the microglial activation status, with potential value for clinical routine work, tracking of disease progression, or as a measurable parameter for clinical trials.

References

Abella, V., Pino, J., Scotece, M., Conde, J., Lago, F., Gonzalez-Gay, M. A., . . . Gualillo, O. (2017). Progranulin as a biomarker and potential therapeutic agent. *Drug Discov Today, 22*(10), 1557-1564. doi:10.1016/j.drudis.2017.06.006

Absinta, M., Maric, D., Gharagozloo, M., Garton, T., Smith, M. D., Jin, J., . . . Reich, D. S. (2021). A lymphocyte-microglia-astrocyte axis in chronic active multiple sclerosis. *Nature, 597*(7878), 709-714. doi:10.1038/s41586-021-03892-7

Abud, E. M., Ramirez, R. N., Martinez, E. S., Healy, L. M., Nguyen, C. H. H., Newman, S. A., . . . Blurton-Jones, M. (2017). iPSC-Derived Human Microglia-like Cells to Study Neurological Diseases. *Neuron, 94*(2), 278-293 e279. doi:10.1016/j.neuron.2017.03.042

Alzheimer, A., Stelzmann, R. A., Schnitzlein, H. N., & Murtagh, F. R. (1995). An English translation of Alzheimer's 1907 paper, "Uber eine eigenartige Erkankung der Hirnrinde". *Clin Anat, 8*(6), 429-431. doi:10.1002/ca.980080612

Ashton, N. J., Benedet, A. L., Pascoal, T. A., Karikari, T. K., Lantero-Rodriguez, J., Brum, W. S., . . . Rosa-Neto, P. (2022). Cerebrospinal fluid p-tau231 as an early indicator of emerging pathology in Alzheimer's disease. *EBioMedicine, 76*, 103836. doi:10.1016/j.ebiom.2022.103836

Ashton, N. J., Leuzy, A., Karikari, T. K., Mattsson-Carlgren, N., Dodich, A., Boccardi, M., . . . Hansson, O. (2021). The validation status of blood biomarkers of amyloid and phospho-tau assessed with the 5-phase development framework for AD biomarkers. *Eur J Nucl Med Mol Imaging, 48*(7), 2140-2156. doi:10.1007/s00259-021-05253-y

Atagi, Y., Liu, C. C., Painter, M. M., Chen, X. F., Verbeeck, C., Zheng, H., . . . Bu, G. (2015). Apolipoprotein E Is a Ligand for Triggering Receptor Expressed on Myeloid Cells 2 (TREM2). *J Biol Chem, 290*(43), 26043-26050. doi:10.1074/jbc.M115.679043

Baeza-Delgado, C., Cerda Alberich, L., Carot-Sierra, J. M., Veiga-Canuto, D., Martinez de Las Heras, B., Raza, B., & Marti-Bonmati, L. (2022). A practical solution to estimate the sample size required for clinical prediction models generated from observational research on data. *Eur Radiol Exp, 6*(1), 22. doi:10.1186/s41747-022-00276-y

Bahia, V. S., Takada, L. T., & Deramecourt, V. (2013). Neuropathology of frontotemporal lobar degeneration: a review. *Dement Neuropsychol, 7*(1), 19-26. doi:10.1590/S1980-57642013DN70100004

Baker, M., Mackenzie, I. R., Pickering-Brown, S. M., Gass, J., Rademakers, R., Lindholm, C., . . . Hutton, M. (2006). Mutations in progranulin cause tau-negative frontotemporal dementia linked to chromosome 17. *Nature, 442*(7105), 916-919. doi:10.1038/nature05016

Bales, K. R., Verina, T., Cummins, D. J., Du, Y., Dodel, R. C., Saura, J., . . . Paul, S. M. (1999). Apolipoprotein E is essential for amyloid deposition in the APP(V717F) transgenic mouse model of Alzheimer's disease. *Proc Natl Acad Sci U S A, 96*(26), 15233-15238. doi:10.1073/pnas.96.26.15233

Barthelemy, N. R., Li, Y., Joseph-Mathurin, N., Gordon, B. A., Hassenstab, J., Benzinger, T. L. S., . . . Dominantly Inherited Alzheimer, N. (2020). A soluble phosphorylated tau signature links tau, amyloid and the evolution of stages of dominantly inherited Alzheimer's disease. *Nat Med, 26*(3), 398-407. doi:10.1038/s41591-020-0781-z

Bateman, R. J., Aisen, P. S., De Strooper, B., Fox, N. C., Lemere, C. A., Ringman, J. M., . . . Xiong, C. (2011). Autosomal-dominant Alzheimer's disease: a review and proposal for

the prevention of Alzheimer's disease. *Alzheimers Res Ther, 3*(1), 1. doi:10.1186/alzrt59
Beckers, L., Ory, D., Geric, I., Declercq, L., Koole, M., Kassiou, M., . . . Baes, M. (2018). Increased Expression of Translocator Protein (TSPO) Marks Pro-inflammatory Microglia but Does Not Predict Neurodegeneration. *Mol Imaging Biol, 20*(1), 94-102. doi:10.1007/s11307-017-1099-1
Bekris, L. M., Yu, C. E., Bird, T. D., & Tsuang, D. W. (2010). Genetics of Alzheimer disease. *J Geriatr Psychiatry Neurol, 23*(4), 213-227. doi:10.1177/0891988710383571
Benjamini, Y., Krieger, A. M., & Yekutieli, D. (2006). Adaptive linear step-up procedures that control the false discovery rate. *Biometrika, 93*(3), 491-507. doi:10.1093/biomet/93.3.491
Bensaad, K., Favaro, E., Lewis, C. A., Peck, B., Lord, S., Collins, J. M., . . . Harris, A. L. (2014). Fatty acid uptake and lipid storage induced by HIF-1alpha contribute to cell growth and survival after hypoxia-reoxygenation. *Cell Rep, 9*(1), 349-365. doi:10.1016/j.celrep.2014.08.056
Bi, C., Bi, S., & Li, B. (2019). Processing of Mutant β-Amyloid Precursor Protein and the Clinicopathological Features of Familial Alzheimer's Disease. *Aging Dis, 10*(2), 383-403. doi:10.14336/ad.2018.0425
Binas, B., Danneberg, H., McWhir, J., Mullins, L., & Clark, A. J. (1999). Requirement for the heart-type fatty acid binding protein in cardiac fatty acid utilization. *FASEB J, 13*(8), 805-812. doi:10.1096/fasebj.13.8.805
Blank, M., Enzlein, T., & Hopf, C. (2022). LPS-induced lipid alterations in microglia revealed by MALDI mass spectrometry-based cell fingerprinting in neuroinflammation studies. *Sci Rep, 12*(1), 2908. doi:10.1038/s41598-022-06894-1
Blauwendraat, C., Wilke, C., Simon-Sanchez, J., Jansen, I. E., Reifschneider, A., Capell, A., . . . Synofzik, M. (2018). The wide genetic landscape of clinical frontotemporal dementia: systematic combined sequencing of 121 consecutive subjects. *Genet Med, 20*(2), 240-249. doi:10.1038/gim.2017.102
Blennow, K., de Leon, M. J., & Zetterberg, H. (2006). Alzheimer's disease. *Lancet, 368*(9533), 387-403. doi:10.1016/S0140-6736(06)69113-7
Blennow, K., Mattsson, N., Scholl, M., Hansson, O., & Zetterberg, H. (2015). Amyloid biomarkers in Alzheimer's disease. *Trends Pharmacol Sci, 36*(5), 297-309. doi:10.1016/j.tips.2015.03.002
Blennow, K., & Zetterberg, H. (2015a). Amyloid and Tau Biomarkers in CSF. *J Prev Alzheimers Dis, 2*(1), 46-50. doi:10.14283/jpad.2015.41
Blennow, K., & Zetterberg, H. (2015b). The past and the future of Alzheimer's disease CSF biomarkers-a journey toward validated biochemical tests covering the whole spectrum of molecular events. *Front Neurosci, 9*, 345. doi:10.3389/fnins.2015.00345
Bocchetta, M., Todd, E. G., Peakman, G., Cash, D. M., Convery, R. S., Russell, L. L., . . . Genetic Frontotemporal dementia, I. (2021). Differential early subcortical involvement in genetic FTD within the GENFI cohort. *Neuroimage Clin, 30*, 102646. doi:10.1016/j.nicl.2021.102646
Boeve, B. F., Boxer, A. L., Kumfor, F., Pijnenburg, Y., & Rohrer, J. D. (2022). Advances and controversies in frontotemporal dementia: diagnosis, biomarkers, and therapeutic considerations. *Lancet Neurol, 21*(3), 258-272. doi:10.1016/S1474-4422(21)00341-0
Broeks, M. H., Shamseldin, H. E., Alhashem, A., Hashem, M., Abdulwahab, F., Alshedi, T., . . . Alkuraya, F. S. (2019). MDH1 deficiency is a metabolic disorder of the malate-aspartate shuttle associated with early onset severe encephalopathy. *Hum Genet, 138*(11-12), 1247-1257. doi:10.1007/s00439-019-02063-z

Brown, G. C., & St George-Hyslop, P. (2021). Does Soluble TREM2 Protect Against Alzheimer's Disease? *Front Aging Neurosci, 13*, 834697. doi:10.3389/fnagi.2021.834697

Buchhave, P., Minthon, L., Zetterberg, H., Wallin, A. K., Blennow, K., & Hansson, O. (2012). Cerebrospinal fluid levels of beta-amyloid 1-42, but not of tau, are fully changed already 5 to 10 years before the onset of Alzheimer dementia. *Arch Gen Psychiatry, 69*(1), 98-106. doi:10.1001/archgenpsychiatry.2011.155

Butovsky, O., Jedrychowski, M. P., Moore, C. S., Cialic, R., Lanser, A. J., Gabriely, G., . . . Weiner, H. L. (2014). Identification of a unique TGF-beta-dependent molecular and functional signature in microglia. *Nat Neurosci, 17*(1), 131-143. doi:10.1038/nn.3599

Butovsky, O., & Weiner, H. L. (2018). Microglial signatures and their role in health and disease. *Nat Rev Neurosci, 19*(10), 622-635. doi:10.1038/s41583-018-0057-5

Campion, D., Dumanchin, C., Hannequin, D., Dubois, B., Belliard, S., Puel, M., . . . Frebourg, T. (1999). Early-onset autosomal dominant Alzheimer disease: prevalence, genetic heterogeneity, and mutation spectrum. *Am J Hum Genet, 65*(3), 664-670. doi:10.1086/302553

Casali, B. T., & Reed-Geaghan, E. G. (2021). Microglial Function and Regulation during Development, Homeostasis and Alzheimer's Disease. *Cells, 10*(4). doi:10.3390/cells10040957

Chang, C. W., Shao, E., & Mucke, L. (2021). Tau: Enabler of diverse brain disorders and target of rapidly evolving therapeutic strategies. *Science, 371*(6532). doi:10.1126/science.abb8255

Chausse, B., Kakimoto, P. A., & Kann, O. (2021). Microglia and lipids: how metabolism controls brain innate immunity. *Semin Cell Dev Biol, 112*, 137-144. doi:10.1016/j.semcdb.2020.08.001

Chen, Y., Deng, Y., Zhang, J., Yang, L., Xie, X., & Xu, T. (2009). GDI-1 preferably interacts with Rab10 in insulin-stimulated GLUT4 translocation. *Biochem J, 422*(2), 229-235. doi:10.1042/BJ20090624

Chiasserini, D., Biscetti, L., Eusebi, P., Salvadori, N., Frattini, G., Simoni, S., . . . Parnetti, L. (2017). Differential role of CSF fatty acid binding protein 3, alpha-synuclein, and Alzheimer's disease core biomarkers in Lewy body disorders and Alzheimer's dementia. *Alzheimers Res Ther, 9*(1), 52. doi:10.1186/s13195-017-0276-4

Churchward, M. A., Tchir, D. R., & Todd, K. G. (2018). Microglial Function during Glucose Deprivation: Inflammatory and Neuropsychiatric Implications. *Mol Neurobiol, 55*(2), 1477-1487. doi:10.1007/s12035-017-0422-9

Citron, M., Oltersdorf, T., Haass, C., McConlogue, L., Hung, A. Y., Seubert, P., . . . Selkoe, D. J. (1992). Mutation of the beta-amyloid precursor protein in familial Alzheimer's disease increases beta-protein production. *Nature, 360*(6405), 672-674. doi:10.1038/360672a0

Claes, C., England, W. E., Danhash, E. P., Kiani Shabestari, S., Jairaman, A., Chadarevian, J. P., . . . Davtyan, H. (2022). The P522R protective variant of PLCG2 promotes the expression of antigen presentation genes by human microglia in an Alzheimer's disease mouse model. *Alzheimer's & Dementia, 18*(10), 1765-1778. doi:https://doi.org/10.1002/alz.12577

Colombo, A., Dinkel, L., Muller, S. A., Sebastian Monasor, L., Schifferer, M., Cantuti-Castelvetri, L., . . . Tahirovic, S. (2021). Loss of NPC1 enhances phagocytic uptake and impairs lipid trafficking in microglia. *Nat Commun, 12*(1), 1158. doi:10.1038/s41467-021-21428-5

Colonna, M., & Butovsky, O. (2017). Microglia Function in the Central Nervous System During Health and Neurodegeneration. *Annu Rev Immunol, 35*, 441-468. doi:10.1146/annurev-immunol-051116-052358

Colonna, M., & Wang, Y. (2016). TREM2 variants: new keys to decipher Alzheimer disease pathogenesis. *Nat Rev Neurosci, 17*(4), 201-207. doi:10.1038/nrn.2016.7

Concordet, J. P., & Haeussler, M. (2018). CRISPOR: intuitive guide selection for CRISPR/Cas9 genome editing experiments and screens. *Nucleic Acids Res, 46*(W1), W242-W245. doi:10.1093/nar/gky354

Corder, E. H., Saunders, A. M., Strittmatter, W. J., Schmechel, D. E., Gaskell, P. C., Small, G. W., . . . Pericak-Vance, M. A. (1993). Gene dose of apolipoprotein E type 4 allele and the risk of Alzheimer's disease in late onset families. *Science, 261*(5123), 921-923. doi:10.1126/science.8346443

Cox, J., Hein, M. Y., Luber, C. A., Paron, I., Nagaraj, N., & Mann, M. (2014). Accurate proteome-wide label-free quantification by delayed normalization and maximal peptide ratio extraction, termed MaxLFQ. *Mol Cell Proteomics, 13*(9), 2513-2526. doi:10.1074/mcp.M113.031591

Cullen, N., Janelidze, S., Palmqvist, S., Stomrud, E., Mattsson-Carlgren, N., Hansson, O., & Alzheimer's Disease Neuroimaging, I. (2022). Association of CSF Abeta(38) Levels With Risk of Alzheimer Disease-Related Decline. *Neurology, 98*(9), e958-e967. doi:10.1212/WNL.0000000000013228

D'Adamo, P., Horvat, A., Gurgone, A., Mignogna, M. L., Bianchi, V., Masetti, M., . . . Zorec, R. (2021). Inhibiting glycolysis rescues memory impairment in an intellectual disability Gdi1-null mouse. *Metabolism, 116*, 154463. doi:10.1016/j.metabol.2020.154463

Dai, M. H., Zheng, H., Zeng, L. D., & Zhang, Y. (2018). The genes associated with early-onset Alzheimer's disease. *Oncotarget, 9*(19), 15132-15143. doi:10.18632/oncotarget.23738

Dardiotis, E., Siokas, V., Pantazi, E., Dardioti, M., Rikos, D., Xiromerisiou, G., . . . Hadjigeorgiou, G. M. (2017). A novel mutation in TREM2 gene causing Nasu-Hakola disease and review of the literature. *Neurobiol Aging, 53*, 194 e113-194 e122. doi:10.1016/j.neurobiolaging.2017.01.015

Daws, M. R., Sullam, P. M., Niemi, E. C., Chen, T. T., Tchao, N. K., & Seaman, W. E. (2003). Pattern recognition by TREM-2: binding of anionic ligands. *J Immunol, 171*(2), 594-599. doi:10.4049/jimmunol.171.2.594

De Strooper, B. (2007). Loss-of-function presenilin mutations in Alzheimer disease. Talking Point on the role of presenilin mutations in Alzheimer disease. *EMBO Rep, 8*(2), 141-146. doi:10.1038/sj.embor.7400897

De Strooper, B., Iwatsubo, T., & Wolfe, M. S. (2012). Presenilins and gamma-secretase: structure, function, and role in Alzheimer Disease. *Cold Spring Harb Perspect Med, 2*(1), a006304. doi:10.1101/cshperspect.a006304

De Strooper, B., & Karran, E. (2016). The Cellular Phase of Alzheimer's Disease. *Cell, 164*(4), 603-615. doi:10.1016/j.cell.2015.12.056

Debard, C., Laville, M., Berbe, V., Loizon, E., Guillet, C., Morio-Liondore, B., . . . Vidal, H. (2004). Expression of key genes of fatty acid oxidation, including adiponectin receptors, in skeletal muscle of Type 2 diabetic patients. *Diabetologia, 47*(5), 917-925. doi:10.1007/s00125-004-1394-7

Deczkowska, A., Amit, I., & Schwartz, M. (2018). Microglial immune checkpoint mechanisms. *Nat Neurosci, 21*(6), 779-786. doi:10.1038/s41593-018-0145-x

Deczkowska, A., Keren-Shaul, H., Weiner, A., Colonna, M., Schwartz, M., & Amit, I. (2018). Disease-Associated Microglia: A Universal Immune Sensor of Neurodegeneration. *Cell, 173*(5), 1073-1081. doi:10.1016/j.cell.2018.05.003

Deczkowska, A., Weiner, A., & Amit, I. (2020). The Physiology, Pathology, and Potential Therapeutic Applications of the TREM2 Signaling Pathway. *Cell, 181*(6), 1207-1217. doi:10.1016/j.cell.2020.05.003

Demichev, V., Messner, C. B., Vernardis, S. I., Lilley, K. S., & Ralser, M. (2020). DIA-NN: neural networks and interference correction enable deep proteome coverage in high throughput. *Nat Methods, 17*(1), 41-44. doi:10.1038/s41592-019-0638-x

Doecke, J. D., Perez-Grijalba, V., Fandos, N., Fowler, C., Villemagne, V. L., Masters, C. L., . . . Group, A. R. (2020). Total Abeta(42)/Abeta(40) ratio in plasma predicts amyloid-PET status, independent of clinical AD diagnosis. *Neurology, 94*(15), e1580-e1591. doi:10.1212/WNL.0000000000009240

Dormann, D., & Haass, C. (2011). TDP-43 and FUS: a nuclear affair. *Trends Neurosci, 34*(7), 339-348. doi:10.1016/j.tins.2011.05.002

Dulewicz, M., Kulczynska-Przybik, A., Slowik, A., Borawska, R., & Mroczko, B. (2021). Fatty Acid Binding Protein 3 (FABP3) and Apolipoprotein E4 (ApoE4) as Lipid Metabolism-Related Biomarkers of Alzheimer's Disease. *J Clin Med, 10*(14). doi:10.3390/jcm10143009

Eninger, T., Muller, S. A., Bacioglu, M., Schweighauser, M., Lambert, M., Maia, L. F., . . . Kaeser, S. A. (2022). Signatures of glial activity can be detected in the CSF proteome. *Proc Natl Acad Sci U S A, 119*(24), e2119804119. doi:10.1073/pnas.2119804119

Fabian Pedregosa, G. V., Alexandre Gramfort, Vincent Michel, Bertrand ¨ Thirion, Olivier Grisel, Mathieu Blondel,, Peter Prettenhofer, R. W., Vincent Dubourg, Jake Vanderplas, Alexandre Passos, David Cournapeau, Matthieu Brucher,, & Duchesnay, M. P. a. E. (2011). Scikit-learn: Machine Learning in Python. *Journal of Machine Learning Research, 12*(85), 2825-2830. Retrieved from http://jmlr.org/papers/v12/pedregosa11a.html

Finch, N., Baker, M., Crook, R., Swanson, K., Kuntz, K., Surtees, R., . . . Rademakers, R. (2009). Plasma progranulin levels predict progranulin mutation status in frontotemporal dementia patients and asymptomatic family members. *Brain, 132*(Pt 3), 583-591. doi:10.1093/brain/awn352

Folick, A., Koliwad, S. K., & Valdearcos, M. (2021). Microglial Lipid Biology in the Hypothalamic Regulation of Metabolic Homeostasis. *Front Endocrinol (Lausanne), 12*, 668396. doi:10.3389/fendo.2021.668396

Friedrich, C. A., Morizot, D. C., Siciliano, M. J., & Ferrell, R. E. (1987). The reduction of aromatic alpha-keto acids by cytoplasmic malate dehydrogenase and lactate dehydrogenase. *Biochem Genet, 25*(9-10), 657-669. doi:10.1007/BF00556210

Furuhashi, M., & Hotamisligil, G. S. (2008). Fatty acid-binding proteins: role in metabolic diseases and potential as drug targets. *Nat Rev Drug Discov, 7*(6), 489-503. doi:10.1038/nrd2589

Gabelle, A., Roche, S., Geny, C., Bennys, K., Labauge, P., Tholance, Y., . . . Lehmann, S. (2011). Decreased sAbetaPPbeta, Abeta38, and Abeta40 cerebrospinal fluid levels in frontotemporal dementia. *J Alzheimers Dis, 26*(3), 553-563. doi:10.3233/JAD-2011-110515

Gendron, T. F., Chew, J., Stankowski, J. N., Hayes, L. R., Zhang, Y. J., Prudencio, M., . . . Petrucelli, L. (2017). Poly(GP) proteins are a useful pharmacodynamic marker for C9ORF72-associated amyotrophic lateral sclerosis. *Sci Transl Med, 9*(383). doi:10.1126/scitranslmed.aai7866

Ghidoni, R., Benussi, L., Glionna, M., Franzoni, M., & Binetti, G. (2008). Low plasma progranulin levels predict progranulin mutations in frontotemporal lobar degeneration. *Neurology, 71*(16), 1235-1239. doi:10.1212/01.wnl.0000325058.10218.fc

Goedert, M., Ghetti, B., & Spillantini, M. G. (2012). Frontotemporal dementia: implications for understanding Alzheimer disease. *Cold Spring Harb Perspect Med, 2*(2), a006254. doi:10.1101/cshperspect.a006254

Goedert, M., Spillantini, M. G., Jakes, R., Rutherford, D., & Crowther, R. A. (1989). Multiple isoforms of human microtubule-associated protein tau: sequences and localization in

neurofibrillary tangles of Alzheimer's disease. *Neuron, 3*(4), 519-526. doi:10.1016/0896-6273(89)90210-9

Goedert, M., Spillantini, M. G., Potier, M. C., Ulrich, J., & Crowther, R. A. (1989). Cloning and sequencing of the cDNA encoding an isoform of microtubule-associated protein tau containing four tandem repeats: differential expression of tau protein mRNAs in human brain. *EMBO J, 8*(2), 393-399. doi:10.1002/j.1460-2075.1989.tb03390.x

Gordon, E., Rohrer, J. D., & Fox, N. C. (2016). Advances in neuroimaging in frontotemporal dementia. *J Neurochem, 138 Suppl 1*, 193-210. doi:10.1111/jnc.13656

Gorno-Tempini, M. L., Hillis, A. E., Weintraub, S., Kertesz, A., Mendez, M., Cappa, S. F., . . . Grossman, M. (2011). Classification of primary progressive aphasia and its variants. *Neurology, 76*(11), 1006-1014. doi:10.1212/WNL.0b013e31821103e6

Gotzl, J. K., Brendel, M., Werner, G., Parhizkar, S., Sebastian Monasor, L., Kleinberger, G., . . . Haass, C. (2019). Opposite microglial activation stages upon loss of PGRN or TREM2 result in reduced cerebral glucose metabolism. *EMBO Mol Med, 11*(6). doi:10.15252/emmm.201809711

Gouna, G., Klose, C., Bosch-Queralt, M., Liu, L., Gokce, O., Schifferer, M., . . . Simons, M. (2021). TREM2-dependent lipid droplet biogenesis in phagocytes is required for remyelination. *J Exp Med, 218*(10). doi:10.1084/jem.20210227

Gratuze, M., Leyns, C. E. G., & Holtzman, D. M. (2018). New insights into the role of TREM2 in Alzheimer's disease. *Mol Neurodegener, 13*(1), 66. doi:10.1186/s13024-018-0298-9

Greaves, C. V., & Rohrer, J. D. (2019). An update on genetic frontotemporal dementia. *J Neurol, 266*(8), 2075-2086. doi:10.1007/s00415-019-09363-4

Guerreiro, R., Wojtas, A., Bras, J., Carrasquillo, M., Rogaeva, E., Majounie, E., . . . Alzheimer Genetic Analysis, G. (2013). TREM2 variants in Alzheimer's disease. *N Engl J Med, 368*(2), 117-127. doi:10.1056/NEJMoa1211851

Guilarte, T. R., Rodichkin, A. N., McGlothan, J. L., Acanda De La Rocha, A. M., & Azzam, D. J. (2022). Imaging neuroinflammation with TSPO: A new perspective on the cellular sources and subcellular localization. *Pharmacol Ther, 234*, 108048. doi:10.1016/j.pharmthera.2021.108048

Haass, C. (2004). Take five--BACE and the gamma-secretase quartet conduct Alzheimer's amyloid beta-peptide generation. *EMBO J, 23*(3), 483-488. doi:10.1038/sj.emboj.7600061

Haass, C., Kaether, C., Thinakaran, G., & Sisodia, S. (2012). Trafficking and proteolytic processing of APP. *Cold Spring Harb Perspect Med, 2*(5), a006270. doi:10.1101/cshperspect.a006270

Haass, C., Koo, E. H., Mellon, A., Hung, A. Y., & Selkoe, D. J. (1992). Targeting of cell-surface beta-amyloid precursor protein to lysosomes: alternative processing into amyloid-bearing fragments. *Nature, 357*(6378), 500-503. doi:10.1038/357500a0

Haass, C., & Neumann, M. (2016). Frontotemporal dementia: from molecular mechanisms to therapy. *J Neurochem, 138 Suppl 1*, 3-5. doi:10.1111/jnc.13619

Haass, C., Schlossmacher, M. G., Hung, A. Y., Vigo-Pelfrey, C., Mellon, A., Ostaszewski, B. L., . . . et al. (1992). Amyloid beta-peptide is produced by cultured cells during normal metabolism. *Nature, 359*(6393), 322-325. doi:10.1038/359322a0

Haass, C., & Selkoe, D. (2022). If amyloid drives Alzheimer disease, why have anti-amyloid therapies not yet slowed cognitive decline? *PLoS Biol, 20*(7), e3001694. doi:10.1371/journal.pbio.3001694

Haass, C., & Selkoe, D. J. (1993). Cellular processing of beta-amyloid precursor protein and the genesis of amyloid beta-peptide. *Cell, 75*(6), 1039-1042. doi:10.1016/0092-8674(93)90312-e

Haass, C., & Selkoe, D. J. (2007). Soluble protein oligomers in neurodegeneration: lessons from the Alzheimer's amyloid beta-peptide. *Nat Rev Mol Cell Biol, 8*(2), 101-112. doi:10.1038/nrm2101

Halliday, G., Bigio, E. H., Cairns, N. J., Neumann, M., Mackenzie, I. R., & Mann, D. M. (2012). Mechanisms of disease in frontotemporal lobar degeneration: gain of function versus loss of function effects. *Acta Neuropathol, 124*(3), 373-382. doi:10.1007/s00401-012-1030-4

Hammond, T. R., Dufort, C., Dissing-Olesen, L., Giera, S., Young, A., Wysoker, A., . . . Stevens, B. (2019). Single-Cell RNA Sequencing of Microglia throughout the Mouse Lifespan and in the Injured Brain Reveals Complex Cell-State Changes. *Immunity, 50*(1), 253-271 e256. doi:10.1016/j.immuni.2018.11.004

Hanhoff, T., Lucke, C., & Spener, F. (2002). Insights into binding of fatty acids by fatty acid binding proteins. *Mol Cell Biochem, 239*(1-2), 45-54. Retrieved from https://www.ncbi.nlm.nih.gov/pubmed/12479567

Hansen, D. V., Hanson, J. E., & Sheng, M. (2018). Microglia in Alzheimer's disease. *J Cell Biol, 217*(2), 459-472. doi:10.1083/jcb.201709069

Hardy, J., & Selkoe, D. J. (2002). The amyloid hypothesis of Alzheimer's disease: progress and problems on the road to therapeutics. *Science, 297*(5580), 353-356. doi:10.1126/science.1072994

Hardy, J. A., & Higgins, G. A. (1992). Alzheimer's disease: the amyloid cascade hypothesis. *Science, 256*(5054), 184-185. doi:10.1126/science.1566067

Harman, D. (2006). Alzheimer's disease pathogenesis: role of aging. *Ann N Y Acad Sci, 1067*, 454-460. doi:10.1196/annals.1354.065

Hassan, A., Araguas Rodriguez, P., Heidmann, S. K., Walmsley, E. L., Aughey, G. N., & Southall, T. D. (2020). Condensin I subunit Cap-G is essential for proper gene expression during the maturation of post-mitotic neurons. *Elife, 9*, e55159. doi:10.7554/eLife.55159

Hasselmann, J., Coburn, M. A., England, W., Figueroa Velez, D. X., Kiani Shabestari, S., Tu, C. H., . . . Blurton-Jones, M. (2019). Development of a Chimeric Model to Study and Manipulate Human Microglia In Vivo. *Neuron, 103*(6), 1016-1033 e1010. doi:10.1016/j.neuron.2019.07.002

Haynes, S. E., Hollopeter, G., Yang, G., Kurpius, D., Dailey, M. E., Gan, W. B., & Julius, D. (2006). The P2Y12 receptor regulates microglial activation by extracellular nucleotides. *Nat Neurosci, 9*(12), 1512-1519. doi:10.1038/nn1805

Higginbotham, L., Ping, L., Dammer, E. B., Duong, D. M., Zhou, M., Gearing, M., . . . Seyfried, N. T. (2020). Integrated proteomics reveals brain-based cerebrospinal fluid biomarkers in asymptomatic and symptomatic Alzheimer's disease. *Sci Adv, 6*(43). doi:10.1126/sciadv.aaz9360

Holtman, I. R., Raj, D. D., Miller, J. A., Schaafsma, W., Yin, Z., Brouwer, N., . . . Eggen, B. J. (2015). Induction of a common microglia gene expression signature by aging and neurodegenerative conditions: a co-expression meta-analysis. *Acta Neuropathol Commun, 3*, 31. doi:10.1186/s40478-015-0203-5

Holtman, I. R., Skola, D., & Glass, C. K. (2017). Transcriptional control of microglia phenotypes in health and disease. *J Clin Invest, 127*(9), 3220-3229. doi:10.1172/JCI90604

Holtzman, D. M., Bales, K. R., Tenkova, T., Fagan, A. M., Parsadanian, M., Sartorius, L. J., . . . Paul, S. M. (2000). Apolipoprotein E isoform-dependent amyloid deposition and neuritic degeneration in a mouse model of Alzheimer's disease. *Proc Natl Acad Sci U S A, 97*(6), 2892-2897. doi:10.1073/pnas.050004797

Holtzman, D. M., Fagan, A. M., Mackey, B., Tenkova, T., Sartorius, L., Paul, S. M., . . . Hyman, B. T. (2000). Apolipoprotein E facilitates neuritic and cerebrovascular plaque

formation in an Alzheimer's disease model. *Ann Neurol, 47*(6), 739-747. Retrieved from https://www.ncbi.nlm.nih.gov/pubmed/10852539

Hopperton, K. E., Mohammad, D., Trepanier, M. O., Giuliano, V., & Bazinet, R. P. (2018). Markers of microglia in post-mortem brain samples from patients with Alzheimer's disease: a systematic review. *Mol Psychiatry, 23*(2), 177-198. doi:10.1038/mp.2017.246

Hsieh, F. Y., Bloch, D. A., & Larsen, M. D. (1998). A simple method of sample size calculation for linear and logistic regression. *Stat Med, 17*(14), 1623-1634. doi:10.1002/(sici)1097-0258(19980730)17:14<1623::aid-sim871>3.0.co;2-s

Hu, F., Padukkavidana, T., Vaegter, C. B., Brady, O. A., Zheng, Y., Mackenzie, I. R., . . . Strittmatter, S. M. (2010). Sortilin-mediated endocytosis determines levels of the frontotemporal dementia protein, progranulin. *Neuron, 68*(4), 654-667. doi:10.1016/j.neuron.2010.09.034

Hughes, C. S., Sorensen, P. H., & Morin, G. B. (2019). A Standardized and Reproducible Proteomics Protocol for Bottom-Up Quantitative Analysis of Protein Samples Using SP3 and Mass Spectrometry. *Methods Mol Biol, 1959*, 65-87. doi:10.1007/978-1-4939-9164-8_5

Huin, V., Barbier, M., Bottani, A., Lobrinus, J. A., Clot, F., Lamari, F., . . . Le Ber, I. (2020). Homozygous GRN mutations: new phenotypes and new insights into pathological and molecular mechanisms. *Brain, 143*(1), 303-319. doi:10.1093/brain/awz377

Huttenrauch, M., Ogorek, I., Klafki, H., Otto, M., Stadelmann, C., Weggen, S., . . . Wirths, O. (2018). Glycoprotein NMB: a novel Alzheimer's disease associated marker expressed in a subset of activated microglia. *Acta Neuropathol Commun, 6*(1), 108. doi:10.1186/s40478-018-0612-3

Ittner, L. M., Ke, Y. D., Delerue, F., Bi, M., Gladbach, A., van Eersel, J., . . . Gotz, J. (2010). Dendritic function of tau mediates amyloid-beta toxicity in Alzheimer's disease mouse models. *Cell, 142*(3), 387-397. doi:10.1016/j.cell.2010.06.036

Jack CR Jr, B. D., Blennow K, et al. . (2016). A:T:N- An unbiased descriptive classification scheme for Alzheimer disease biomarkers *Neurology*. doi:doi-10.1212

Jack, C. R., Jr., & Vemuri, P. (2018). Amyloid-beta - a reflection of risk or a preclinical marker? *Nat Rev Neurol, 14*(6), 319-320. doi:10.1038/s41582-018-0008-9

Jack, C. R., Knopman, D. S., Jagust, W. J., Shaw, L. M., Aisen, P. S., Weiner, M. W., . . . Trojanowski, J. Q. (2010). Hypothetical model of dynamic biomarkers of the Alzheimer's pathological cascade. *The Lancet Neurology, 9*(1), 119-128. doi:10.1016/s1474-4422(09)70299-6

Jain, N., & Ulrich, J. D. (2022). TREM2 and microglia exosomes: a potential highway for pathological tau. *Mol Neurodegener, 17*(1), 73. doi:10.1186/s13024-022-00581-5

Jiahuan, X., Ying, Z., Hongyu, J., Zhijing, W., Shibo, G., Chengyue, D., . . . Wei, W. (2022). Serum sTREM2: A Potential Biomarker for Mild Cognitive Impairment in Patients With Obstructive Sleep Apnea. *Front Aging Neurosci, 14*, 843828. doi:10.3389/fnagi.2022.843828

Jin, H., Tang, Y., Yang, L., Peng, X., Li, B., Fan, Q., . . . Li, H. (2021). Rab GTPases: Central Coordinators of Membrane Trafficking in Cancer. *Front Cell Dev Biol, 9*, 648384. doi:10.3389/fcell.2021.648384

Jonsson, T., Stefansson, H., Steinberg, S., Jonsdottir, I., Jonsson, P. V., Snaedal, J., . . . Stefansson, K. (2013). Variant of TREM2 associated with the risk of Alzheimer's disease. *N Engl J Med, 368*(2), 107-116. doi:10.1056/NEJMoa1211103

Josephs, K. A., Hodges, J. R., Snowden, J. S., Mackenzie, I. R., Neumann, M., Mann, D. M., & Dickson, D. W. (2011). Neuropathological background of phenotypical variability in frontotemporal dementia. *Acta Neuropathol, 122*(2), 137-153. doi:10.1007/s00401-011-0839-6

Jurga, A. M., Paleczna, M., & Kuter, K. Z. (2020). Overview of General and Discriminating Markers of Differential Microglia Phenotypes. *Front Cell Neurosci, 14*, 198. doi:10.3389/fncel.2020.00198

Kamate, M., Detroja, M., & Hattiholi, V. (2019). Neuronal ceroid lipofuscinosis type-11 in an adolescent. *Brain Dev, 41*(6), 542-545. doi:10.1016/j.braindev.2019.03.004

Kaneko, M., Sano, K., Nakayama, J., & Amano, N. (2010). Nasu-Hakola disease: The first case reported by Nasu and review: The 50th Anniversary of Japanese Society of Neuropathology. *Neuropathology, 30*(5), 463-470. doi:10.1111/j.1440-1789.2010.01127.x

Karbek, B., Ozbek, M., Bozkurt, N. C., Ginis, Z., Gungunes, A., Unsal, I. O., . . . Delibasi, T. (2011). Heart-type fatty acid binding protein (H-FABP): relationship with arterial intima-media thickness and role as diagnostic marker for atherosclerosis in patients with impaired glucose metabolism. *Cardiovasc Diabetol, 10*, 37. doi:10.1186/1475-2840-10-37

Karikari, T. K., Ashton, N. J., Zetterberg, H., & Blennow, K. (2022). Editorial: Blood Biomarkers of Neurodegenerative Diseases. *Front Mol Neurosci, 15*, 966139. doi:10.3389/fnmol.2022.966139

Kawahata, I., Bousset, L., Melki, R., & Fukunaga, K. (2019). Fatty Acid-Binding Protein 3 is Critical for α-Synuclein Uptake and MPP(+)-Induced Mitochondrial Dysfunction in Cultured Dopaminergic Neurons. *Int J Mol Sci, 20*(21). doi:10.3390/ijms20215358

Kayasuga, Y., Chiba, S., Suzuki, M., Kikusui, T., Matsuwaki, T., Yamanouchi, K., . . . Nishihara, M. (2007). Alteration of behavioural phenotype in mice by targeted disruption of the progranulin gene. *Behav Brain Res, 185*(2), 110-118. doi:10.1016/j.bbr.2007.07.020

Keating, S. S., San Gil, R., Swanson, M. E. V., Scotter, E. L., & Walker, A. K. (2022). TDP-43 pathology: From noxious assembly to therapeutic removal. *Prog Neurobiol, 211*, 102229. doi:10.1016/j.pneurobio.2022.102229

Keren-Shaul, H., Spinrad, A., Weiner, A., Matcovitch-Natan, O., Dvir-Szternfeld, R., Ulland, T. K., . . . Amit, I. (2017). A Unique Microglia Type Associated with Restricting Development of Alzheimer's Disease. *Cell, 169*(7), 1276-1290 e1217. doi:10.1016/j.cell.2017.05.018

Kim, E. Y., Kim, W. K., Kang, H. J., Kim, J. H., Chung, S. J., Seo, Y. S., . . . Bae, K. H. (2012). Acetylation of malate dehydrogenase 1 promotes adipogenic differentiation via activating its enzymatic activity. *J Lipid Res, 53*(9), 1864-1876. doi:10.1194/jlr.M026567

Kleinberger, G., Brendel, M., Mracsko, E., Wefers, B., Groeneweg, L., Xiang, X., . . . Haass, C. (2017). The FTD-like syndrome causing TREM2 T66M mutation impairs microglia function, brain perfusion, and glucose metabolism. *EMBO J, 36*(13), 1837-1853. doi:10.15252/embj.201796516

Kleinberger, G., Yamanishi, Y., Suarez-Calvet, M., Czirr, E., Lohmann, E., Cuyvers, E., . . . Haass, C. (2014). TREM2 mutations implicated in neurodegeneration impair cell surface transport and phagocytosis. *Sci Transl Med, 6*(243), 243ra286. doi:10.1126/scitranslmed.3009093

Knapskog, A. B., Henjum, K., Idland, A. V., Eldholm, R. S., Persson, K., Saltvedt, I., . . . Nilsson, L. N. G. (2020). Cerebrospinal fluid sTREM2 in Alzheimer's disease: comparisons between clinical presentation and AT classification. *Sci Rep, 10*(1), 15886. doi:10.1038/s41598-020-72878-8

Kober, D. L., & Brett, T. J. (2017). TREM2-Ligand Interactions in Health and Disease. *J Mol Biol, 429*(11), 1607-1629. doi:10.1016/j.jmb.2017.04.004

Krasemann, S., Madore, C., Cialic, R., Baufeld, C., Calcagno, N., El Fatimy, R., . . . Butovsky, O. (2017). The TREM2-APOE Pathway Drives the Transcriptional

Phenotype of Dysfunctional Microglia in Neurodegenerative Diseases. *Immunity, 47*(3), 566-581 e569. doi:10.1016/j.immuni.2017.08.008
Kuang, H., & Lin, J. D. (2019). GPNMB: expanding the code for liver-fat communication. *Nat Metab, 1*(5), 507-508. doi:10.1038/s42255-019-0069-0
Kunkle, B. W., Grenier-Boley, B., Sims, R., Bis, J. C., Damotte, V., Naj, A. C., . . . Environmental Risk for Alzheimer's Disease, C. (2019). Genetic meta-analysis of diagnosed Alzheimer's disease identifies new risk loci and implicates Abeta, tau, immunity and lipid processing. *Nat Genet, 51*(3), 414-430. doi:10.1038/s41588-019-0358-2
Kwart, D., Paquet, D., Teo, S., & Tessier-Lavigne, M. (2017). Precise and efficient scarless genome editing in stem cells using CORRECT. *Nat Protoc, 12*(2), 329-354. doi:10.1038/nprot.2016.171
Kwon, H. J., Hahn, K. R., Kang, M. S., Choi, J. H., Moon, S. M., Yoon, Y. S., . . . Kim, D. W. (2023). Tat-malate dehydrogenase fusion protein protects neurons from oxidative and ischemic damage by reduction of reactive oxygen species and modulation of glutathione redox system. *Scientific Reports, 13*(1), 5653. doi:10.1038/s41598-023-32812-0
Lambert, J. C., Ibrahim-Verbaas, C. A., Harold, D., Naj, A. C., Sims, R., Bellenguez, C., . . . Amouyel, P. (2013). Meta-analysis of 74,046 individuals identifies 11 new susceptibility loci for Alzheimer's disease. *Nat Genet, 45*(12), 1452-1458. doi:10.1038/ng.2802
Lambert, M. P., Barlow, A. K., Chromy, B. A., Edwards, C., Freed, R., Liosatos, M., . . . Klein, W. L. (1998). Diffusible, nonfibrillar ligands derived from Abeta1-42 are potent central nervous system neurotoxins. *Proc Natl Acad Sci U S A, 95*(11), 6448-6453. doi:10.1073/pnas.95.11.6448
Lee, G., & Leugers, C. J. (2012). Tau and tauopathies. *Prog Mol Biol Transl Sci, 107*, 263-293. doi:10.1016/B978-0-12-385883-2.00004-7
Lee, Y., Park, Y., Nam, H., Lee, J. W., & Yu, S. W. (2020). Translocator protein (TSPO): the new story of the old protein in neuroinflammation. *BMB Rep, 53*(1), 20-27. doi:10.5483/BMBRep.2020.53.1.273
Lehmer, C., Oeckl, P., Weishaupt, J. H., Volk, A. E., Diehl-Schmid, J., Schroeter, M. L., . . . Otto, M. (2017). Poly-GP in cerebrospinal fluid links C9orf72-associated dipeptide repeat expression to the asymptomatic phase of ALS/FTD. *EMBO Mol Med, 9*(7), 859-868. doi:10.15252/emmm.201607486
Lewcock, J. W., Schlepckow, K., Di Paolo, G., Tahirovic, S., Monroe, K. M., & Haass, C. (2020). Emerging Microglia Biology Defines Novel Therapeutic Approaches for Alzheimer's Disease. *Neuron, 108*(5), 801-821. doi:10.1016/j.neuron.2020.09.029
Lewczuk, P., Ermann, N., Andreasson, U., Schultheis, C., Podhorna, J., Spitzer, P., . . . Zetterberg, H. (2018). Plasma neurofilament light as a potential biomarker of neurodegeneration in Alzheimer's disease. *Alzheimers Res Ther, 10*(1), 71. doi:10.1186/s13195-018-0404-9
Leyrolle, Q., Laye, S., & Nadjar, A. (2019). Direct and indirect effects of lipids on microglia function. *Neurosci Lett, 708*, 134348. doi:10.1016/j.neulet.2019.134348
Li, B., Syed, M. H., Khan, H., Singh, K. K., & Qadura, M. (2022). The Role of Fatty Acid Binding Protein 3 in Cardiovascular Diseases. *Biomedicines, 10*(9). doi:10.3390/biomedicines10092283
Li, Q., & Barres, B. A. (2018). Microglia and macrophages in brain homeostasis and disease. *Nat Rev Immunol, 18*(4), 225-242. doi:10.1038/nri.2017.125
Li, Q., Cheng, Z., Zhou, L., Darmanis, S., Neff, N. F., Okamoto, J., . . . Barres, B. A. (2019). Developmental Heterogeneity of Microglia and Brain Myeloid Cells Revealed by

Deep Single-Cell RNA Sequencing. *Neuron, 101*(2), 207-223.e210. doi:10.1016/j.neuron.2018.12.006
Lim, N. K., Moestrup, V., Zhang, X., Wang, W. A., Moller, A., & Huang, F. D. (2018). An Improved Method for Collection of Cerebrospinal Fluid from Anesthetized Mice. *J Vis Exp*(133). doi:10.3791/56774
Lomen-Hoerth, C., Anderson, T., & Miller, B. (2002). The overlap of amyotrophic lateral sclerosis and frontotemporal dementia. *Neurology, 59*(7), 1077-1079. doi:10.1212/wnl.59.7.1077
Lopez-Rodriguez, A. B., Hennessy, E., Murray, C. L., Nazmi, A., Delaney, H. J., Healy, D., . . . Cunningham, C. (2021). Acute systemic inflammation exacerbates neuroinflammation in Alzheimer's disease: IL-1beta drives amplified responses in primed astrocytes and neuronal network dysfunction. *Alzheimers Dement, 17*(10), 1735-1755. doi:10.1002/alz.12341
Loving, B. A., & Bruce, K. D. (2020). Lipid and Lipoprotein Metabolism in Microglia. *Front Physiol, 11*, 393. doi:10.3389/fphys.2020.00393
Loy, C. T., Schofield, P. R., Turner, A. M., & Kwok, J. B. (2014). Genetics of dementia. *Lancet, 383*(9919), 828-840. doi:10.1016/S0140-6736(13)60630-3
Ma, L. Z., Tan, L., Bi, Y. L., Shen, X. N., Xu, W., Ma, Y. H., . . . Yu, J. T. (2020). Dynamic changes of CSF sTREM2 in preclinical Alzheimer's disease: the CABLE study. *Mol Neurodegener, 15*(1), 25. doi:10.1186/s13024-020-00374-8
Mackenzie, I. R., & Neumann, M. (2012). FET proteins in frontotemporal dementia and amyotrophic lateral sclerosis. *Brain Res, 1462*, 40-43. doi:10.1016/j.brainres.2011.12.010
Mackenzie, I. R., & Neumann, M. (2016). Molecular neuropathology of frontotemporal dementia: insights into disease mechanisms from postmortem studies. *J Neurochem, 138 Suppl 1*, 54-70. doi:10.1111/jnc.13588
Mahan, T. E., Wang, C., Bao, X., Choudhury, A., Ulrich, J. D., & Holtzman, D. M. (2022). Selective reduction of astrocyte apoE3 and apoE4 strongly reduces Abeta accumulation and plaque-related pathology in a mouse model of amyloidosis. *Mol Neurodegener, 17*(1), 13. doi:10.1186/s13024-022-00516-0
Mallick, R., Basak, S., & Duttaroy, A. K. (2021). Fatty acids and evolving roles of their proteins in neurological, cardiovascular disorders and cancers. *Prog Lipid Res, 83*, 101116. doi:10.1016/j.plipres.2021.101116
Mancuso, R., Van Den Daele, J., Fattorelli, N., Wolfs, L., Balusu, S., Burton, O., . . . De Strooper, B. (2019). Stem-cell-derived human microglia transplanted in mouse brain to study human disease. *Nat Neurosci, 22*(12), 2111-2116. doi:10.1038/s41593-019-0525-x
Marks, J. D., Syrjanen, J. A., Graff-Radford, J., Petersen, R. C., Machulda, M. M., Campbell, M. R., . . . Alzheimer's Disease Neuroimaging, I. (2021). Comparison of plasma neurofilament light and total tau as neurodegeneration markers: associations with cognitive and neuroimaging outcomes. *Alzheimers Res Ther, 13*(1), 199. doi:10.1186/s13195-021-00944-y
Marschallinger, J., Iram, T., Zardeneta, M., Lee, S. E., Lehallier, B., Haney, M. S., . . . Wyss-Coray, T. (2020). Lipid-droplet-accumulating microglia represent a dysfunctional and proinflammatory state in the aging brain. *Nat Neurosci, 23*(2), 194-208. doi:10.1038/s41593-019-0566-1
Masters, C. L., Bateman, R., Blennow, K., Rowe, C. C., Sperling, R. A., & Cummings, J. L. (2015). Alzheimer's disease. *Nat Rev Dis Primers, 1*, 15056. doi:10.1038/nrdp.2015.56

Mawuenyega, K. G., Sigurdson, W., Ovod, V., Munsell, L., Kasten, T., Morris, J. C., . . . Bateman, R. J. (2010). Decreased clearance of CNS beta-amyloid in Alzheimer's disease. *Science, 330*(6012), 1774. doi:10.1126/science.1197623

Mazaheri, F., Snaidero, N., Kleinberger, G., Madore, C., Daria, A., Werner, G., . . . Haass, C. (2017). TREM2 deficiency impairs chemotaxis and microglial responses to neuronal injury. *EMBO Rep, 18*(7), 1186-1198. doi:10.15252/embr.201743922

McDade, E., Wang, G., Gordon, B. A., Hassenstab, J., Benzinger, T. L. S., Buckles, V., . . . Dominantly Inherited Alzheimer, N. (2018). Longitudinal cognitive and biomarker changes in dominantly inherited Alzheimer disease. *Neurology, 91*(14), e1295-e1306. doi:10.1212/WNL.0000000000006277

McQuade, A., & Blurton-Jones, M. (2019). Microglia in Alzheimer's Disease: Exploring How Genetics and Phenotype Influence Risk. *J Mol Biol, 431*(9), 1805-1817. doi:10.1016/j.jmb.2019.01.045

McQuade, A., Coburn, M., Tu, C. H., Hasselmann, J., Davtyan, H., & Blurton-Jones, M. (2018). Development and validation of a simplified method to generate human microglia from pluripotent stem cells. *Mol Neurodegener, 13*(1), 67. doi:10.1186/s13024-018-0297-x

Meeter, L. H., Dopper, E. G., Jiskoot, L. C., Sanchez-Valle, R., Graff, C., Benussi, L., . . . van Swieten, J. C. (2016). Neurofilament light chain: a biomarker for genetic frontotemporal dementia. *Ann Clin Transl Neurol, 3*(8), 623-636. doi:10.1002/acn3.325

Meeter, L. H., Kaat, L. D., Rohrer, J. D., & van Swieten, J. C. (2017). Imaging and fluid biomarkers in frontotemporal dementia. *Nat Rev Neurol, 13*(7), 406-419. doi:10.1038/nrneurol.2017.75

Meeter, L. H., Patzke, H., Loewen, G., Dopper, E. G., Pijnenburg, Y. A., van Minkelen, R., & van Swieten, J. C. (2016). Progranulin Levels in Plasma and Cerebrospinal Fluid in Granulin Mutation Carriers. *Dement Geriatr Cogn Dis Extra, 6*(2), 330-340. doi:10.1159/000447738

Meilandt, W. J., Ngu, H., Gogineni, A., Lalehzadeh, G., Lee, S. H., Srinivasan, K., . . . Hansen, D. V. (2020). Trem2 Deletion Reduces Late-Stage Amyloid Plaque Accumulation, Elevates the Abeta42:Abeta40 Ratio, and Exacerbates Axonal Dystrophy and Dendritic Spine Loss in the PS2APP Alzheimer's Mouse Model. *J Neurosci, 40*(9), 1956-1974. doi:10.1523/JNEUROSCI.1871-19.2019

Mendez, M. F. (2017). Early-Onset Alzheimer Disease. *Neurol Clin, 35*(2), 263-281. doi:10.1016/j.ncl.2017.01.005

Mielke, M. M., Hagen, C. E., Wennberg, A. M. V., Airey, D. C., Savica, R., Knopman, D. S., . . . Dage, J. L. (2017). Association of Plasma Total Tau Level With Cognitive Decline and Risk of Mild Cognitive Impairment or Dementia in the Mayo Clinic Study on Aging. *JAMA Neurol, 74*(9), 1073-1080. doi:10.1001/jamaneurol.2017.1359

Minarik, P., Tomaskova, N., Kollarova, M., & Antalik, M. (2002). Malate dehydrogenases--structure and function. *Gen Physiol Biophys, 21*(3), 257-265. Retrieved from https://www.ncbi.nlm.nih.gov/pubmed/12537350

Mohan, S., Sampognaro, P. J., Argouarch, A. R., Maynard, J. C., Welch, M., Patwardhan, A., . . . Kao, A. W. (2021). Processing of progranulin into granulins involves multiple lysosomal proteases and is affected in frontotemporal lobar degeneration. *Mol Neurodegener, 16*(1), 51. doi:10.1186/s13024-021-00472-1

Mol, M. O., van der Lee, S. J., Hulsman, M., Pijnenburg, Y. A. L., Scheltens, P., Seelaar, H., . . . Netherlands Brain, B. (2022). Mapping the genetic landscape of early-onset Alzheimer's disease in a cohort of 36 families. *Alzheimer's Research & Therapy, 14*(1), 77. doi:10.1186/s13195-022-01018-3

Moon, M. G., Yoon, C. H., Lee, K., Kang, S. H., Youn, T. J., & Chae, I. H. (2021). Evaluation of Heart-type Fatty Acid-binding Protein in Early Diagnosis of Acute Myocardial Infarction. *J Korean Med Sci, 36*(8), e61. doi:10.3346/jkms.2021.36.e61

Moore, C. S., Ase, A. R., Kinsara, A., Rao, V. T., Michell-Robinson, M., Leong, S. Y., . . . Antel, J. P. (2015). P2Y12 expression and function in alternatively activated human microglia. *Neurol Neuroimmunol Neuroinflamm, 2*(2), e80. doi:10.1212/NXI.0000000000000080

Morenas-Rodriguez, E., Li, Y., Nuscher, B., Franzmeier, N., Xiong, C., Suarez-Calvet, M., . . . Dominantly Inherited Alzheimer, N. (2022). Soluble TREM2 in CSF and its association with other biomarkers and cognition in autosomal-dominant Alzheimer's disease: a longitudinal observational study. *Lancet Neurol, 21*(4), 329-341. doi:10.1016/S1474-4422(22)00027-8

Mouton PR, M. L., Calhoun ME, Dal Forno G, Price DL. (1998). Cognitive decline strongly correlates with cortical atrophy in Alzheimer's dementia. *Neurobiol Aging*.

Mullan, M., Crawford, F., Axelman, K., Houlden, H., Lilius, L., Winblad, B., & Lannfelt, L. (1992). A pathogenic mutation for probable Alzheimer's disease in the APP gene at the N-terminus of beta-amyloid. *Nat Genet, 1*(5), 345-347. doi:10.1038/ng0892-345

Munir, R., Lisec, J., Swinnen, J. V., & Zaidi, N. (2019). Lipid metabolism in cancer cells under metabolic stress. *Br J Cancer, 120*(12), 1090-1098. doi:10.1038/s41416-019-0451-4

Munoz Herrera, O. M., & Zivkovic, A. M. (2022). Microglia and Cholesterol Handling: Implications for Alzheimer's Disease. *Biomedicines, 10*(12). doi:10.3390/biomedicines10123105

Murphy, M. P., & LeVine, H., 3rd. (2010). Alzheimer's disease and the amyloid-beta peptide. *J Alzheimers Dis, 19*(1), 311-323. doi:10.3233/JAD-2010-1221

Nakano, Y., Suzuki, Y., Takagi, T., Kitashoji, A., Ono, Y., Tsuruma, K., . . . Hara, H. (2014). Glycoprotein nonmetastatic melanoma protein B (GPNMB) as a novel neuroprotective factor in cerebral ischemia-reperfusion injury. *Neuroscience, 277*, 123-131. doi:10.1016/j.neuroscience.2014.06.065

Naor, D., Nedvetzki, S., Golan, I., Melnik, L., & Faitelson, Y. (2002). CD44 in cancer. *Crit Rev Clin Lab Sci, 39*(6), 527-579. doi:10.1080/10408360290795574

Neal, M. L., Boyle, A. M., Budge, K. M., Safadi, F. F., & Richardson, J. R. (2018). The glycoprotein GPNMB attenuates astrocyte inflammatory responses through the CD44 receptor. *J Neuroinflammation, 15*(1), 73. doi:10.1186/s12974-018-1100-1

Neumann, M., Bentmann, E., Dormann, D., Jawaid, A., DeJesus-Hernandez, M., Ansorge, O., . . . Mackenzie, I. R. (2011). FET proteins TAF15 and EWS are selective markers that distinguish FTLD with FUS pathology from amyotrophic lateral sclerosis with FUS mutations. *Brain, 134*(Pt 9), 2595-2609. doi:10.1093/brain/awr201

Neumann, M., Sampathu, D. M., Kwong, L. K., Truax, A. C., Micsenyi, M. C., Chou, T. T., . . . Lee, V. M. (2006). Ubiquitinated TDP-43 in frontotemporal lobar degeneration and amyotrophic lateral sclerosis. *Science, 314*(5796), 130-133. doi:10.1126/science.1134108

Nilsberth, C., Westlind-Danielsson, A., Eckman, C. B., Condron, M. M., Axelman, K., Forsell, C., . . . Lannfelt, L. (2001). The 'Arctic' APP mutation (E693G) causes Alzheimer's disease by enhanced Abeta protofibril formation. *Nat Neurosci, 4*(9), 887-893. doi:10.1038/nn0901-887

Nimmerjahn, A., Kirchhoff, F., & Helmchen, F. (2005). Resting microglial cells are highly dynamic surveillants of brain parenchyma in vivo. *Science, 308*(5726), 1314-1318. doi:10.1126/science.1110647

Notter, T., Coughlin, J. M., Gschwind, T., Weber-Stadlbauer, U., Wang, Y., Kassiou, M., . . . Meyer, U. (2018). Translational evaluation of translocator protein as a marker of

neuroinflammation in schizophrenia. *Mol Psychiatry, 23*(2), 323-334. doi:10.1038/mp.2016.248

Ntymenou, S., Tsantzali, I., Kalamatianos, T., Voumvourakis, K. I., Kapaki, E., Tsivgoulis, G., . . . Paraskevas, G. P. (2021). Blood Biomarkers in Frontotemporal Dementia: Review and Meta-Analysis. *Brain Sci, 11*(2). doi:10.3390/brainsci11020244

Nugent, A. A., Lin, K., van Lengerich, B., Lianoglou, S., Przybyla, L., Davis, S. S., . . . Di Paolo, G. (2020). TREM2 Regulates Microglial Cholesterol Metabolism upon Chronic Phagocytic Challenge. *Neuron, 105*(5), 837-854 e839. doi:10.1016/j.neuron.2019.12.007

Nutma, E., Ceyzeriat, K., Amor, S., Tsartsalis, S., Millet, P., Owen, D. R., . . . Tournier, B. B. (2021). Cellular sources of TSPO expression in healthy and diseased brain. *Eur J Nucl Med Mol Imaging, 49*(1), 146-163. doi:10.1007/s00259-020-05166-2

Nutma, E., Fancy, N., Weinert, M., Marzin, M. C., Tsartsalis, S., Muirhead, R. C. J., . . . Owen, D. R. (2022). Translocator protein is a marker of activated microglia in rodent models but not human neurodegenerative diseases. *bioRxiv*, 2022.2005.2011.491453. doi:10.1101/2022.05.11.491453

Oeckl, P., Weydt, P., Thal, D. R., Weishaupt, J. H., Ludolph, A. C., & Otto, M. (2020). Proteomics in cerebrospinal fluid and spinal cord suggests UCHL1, MAP2 and GPNMB as biomarkers and underpins importance of transcriptional pathways in amyotrophic lateral sclerosis. *Acta Neuropathol, 139*(1), 119-134. doi:10.1007/s00401-019-02093-x

Oizumi, H., Yamasaki, K., Suzuki, H., Hasegawa, T., Sugimura, Y., Baba, T., . . . Takeda, A. (2021). Fatty Acid-Binding Protein 3 Expression in the Brain and Skin in Human Synucleinopathies. *Front Aging Neurosci, 13*, 648982. doi:10.3389/fnagi.2021.648982

Ojala, M., & Garriga, G. C. (2009, 6-9 Dec. 2009). *Permutation Tests for Studying Classifier Performance.* Paper presented at the 2009 Ninth IEEE International Conference on Data Mining.

Olszewska, D. A., Lonergan, R., Fallon, E. M., & Lynch, T. (2016). Genetics of Frontotemporal Dementia. *Curr Neurol Neurosci Rep, 16*(12), 107. doi:10.1007/s11910-016-0707-9

Painter, M. M., Atagi, Y., Liu, C. C., Rademakers, R., Xu, H., Fryer, J. D., & Bu, G. (2015). TREM2 in CNS homeostasis and neurodegenerative disease. *Mol Neurodegener, 10*, 43. doi:10.1186/s13024-015-0040-9

Palmqvist, S., Janelidze, S., Quiroz, Y. T., Zetterberg, H., Lopera, F., Stomrud, E., . . . Hansson, O. (2020). Discriminative Accuracy of Plasma Phospho-tau217 for Alzheimer Disease vs Other Neurodegenerative Disorders. *JAMA, 324*(8), 772-781. doi:10.1001/jama.2020.12134

Palmqvist, S., Tideman, P., Cullen, N., Zetterberg, H., Blennow, K., Alzheimer's Disease Neuroimaging, I., . . . Hansson, O. (2021). Prediction of future Alzheimer's disease dementia using plasma phospho-tau combined with other accessible measures. *Nat Med, 27*(6), 1034-1042. doi:10.1038/s41591-021-01348-z

Paloneva, J., Autti, T., Raininko, R., Partanen, J., Salonen, O., Puranen, M., . . . Haltia, M. (2001). CNS manifestations of Nasu-Hakola disease: a frontal dementia with bone cysts. *Neurology, 56*(11), 1552-1558. doi:10.1212/wnl.56.11.1552

Panman, J. L., Jiskoot, L. C., Bouts, M., Meeter, L. H. H., van der Ende, E. L., Poos, J. M., . . . Papma, J. M. (2019). Gray and white matter changes in presymptomatic genetic frontotemporal dementia: a longitudinal MRI study. *Neurobiol Aging, 76*, 115-124. doi:10.1016/j.neurobiolaging.2018.12.017

Paolicelli, R. C., Sierra, A., Stevens, B., Tremblay, M. E., Aguzzi, A., Ajami, B., . . . Wyss-Coray, T. (2022). Microglia states and nomenclature: A field at its crossroads. *Neuron, 110*(21), 3458-3483. doi:10.1016/j.neuron.2022.10.020

Papadopoulos, V., & Miller, W. L. (2012). Role of mitochondria in steroidogenesis. *Best Pract Res Clin Endocrinol Metab, 26*(6), 771-790. doi:10.1016/j.beem.2012.05.002

Parhizkar, S., Arzberger, T., Brendel, M., Kleinberger, G., Deussing, M., Focke, C., . . . Haass, C. (2019). Loss of TREM2 function increases amyloid seeding but reduces plaque-associated ApoE. *Nat Neurosci, 22*(2), 191-204. doi:10.1038/s41593-018-0296-9

Pavisic, I. M., Nicholas, J. M., O'Connor, A., Rice, H., Lu, K., Fox, N. C., & Ryan, N. S. (2020). Disease duration in autosomal dominant familial Alzheimer disease: A survival analysis. *Neurol Genet, 6*(5), e507. doi:10.1212/NXG.0000000000000507

Petersen, R. C., Thomas, R. G., Aisen, P. S., Mohs, R. C., Carrillo, M. C., Albert, M. S., . . . Foundation for, N. I. H. B. C. A. D. M. C. I. P. D. A. P. T. (2017). Randomized controlled trials in mild cognitive impairment: Sources of variability. *Neurology, 88*(18), 1751-1758. doi:10.1212/WNL.0000000000003907

Pettas, S., Karagianni, K., Kanata, E., Chatziefstathiou, A., Christoudia, N., Xanthopoulos, K., . . . Dafou, D. (2022). Profiling Microglia through Single-Cell RNA Sequencing over the Course of Development, Aging, and Disease. *Cells, 11*(15). doi:10.3390/cells11152383

Piccio, L., Buonsanti, C., Cella, M., Tassi, I., Schmidt, R. E., Fenoglio, C., . . . Cross, A. H. (2008). Identification of soluble TREM-2 in the cerebrospinal fluid and its association with multiple sclerosis and CNS inflammation. *Brain, 131*(Pt 11), 3081-3091. doi:10.1093/brain/awn217

Piccio, L., Deming, Y., Del-Aguila, J. L., Ghezzi, L., Holtzman, D. M., Fagan, A. M., . . . Cruchaga, C. (2016). Cerebrospinal fluid soluble TREM2 is higher in Alzheimer disease and associated with mutation status. *Acta Neuropathol, 131*(6), 925-933. doi:10.1007/s00401-016-1533-5

Pick, A. (1892). Uber die Beziehungen der senilen Hirnatrophie zur Aphasie. *Prag Med Wchnschr, 17*, 165-167.

Poliani, P. L., Wang, Y., Fontana, E., Robinette, M. L., Yamanishi, Y., Gilfillan, S., & Colonna, M. (2015). TREM2 sustains microglial expansion during aging and response to demyelination. *J Clin Invest, 125*(5), 2161-2170. doi:10.1172/JCI77983

Potokar, M., Jorgačevski, J., Lacovich, V., Kreft, M., Vardjan, N., Bianchi, V., . . . Zorec, R. (2017). Impaired αGDI Function in the X-Linked Intellectual Disability: The Impact on Astroglia Vesicle Dynamics. *Mol Neurobiol, 54*(4), 2458-2468. doi:10.1007/s12035-016-9834-1

Pozzo, E. D., Tremolanti, C., Costa, B., Giacomelli, C., Milenkovic, V. M., Bader, S., . . . Martini, C. (2019). Microglial Pro-Inflammatory and Anti-Inflammatory Phenotypes Are Modulated by Translocator Protein Activation. *Int J Mol Sci, 20*(18). doi:10.3390/ijms20184467

Price, B. R., Sudduth, T. L., Weekman, E. M., Johnson, S., Hawthorne, D., Woolums, A., & Wilcock, D. M. (2020). Therapeutic Trem2 activation ameliorates amyloid-beta deposition and improves cognition in the 5XFAD model of amyloid deposition. *J Neuroinflammation, 17*(1), 238. doi:10.1186/s12974-020-01915-0

Prinz, M., Masuda, T., Wheeler, M. A., & Quintana, F. J. (2021). Microglia and Central Nervous System-Associated Macrophages-From Origin to Disease Modulation. *Annu Rev Immunol, 39*, 251-277. doi:10.1146/annurev-immunol-093019-110159

Prinz, M., & Priller, J. (2014). Microglia and brain macrophages in the molecular age: from origin to neuropsychiatric disease. *Nat Rev Neurosci, 15*(5), 300-312. doi:10.1038/nrn3722

Ran, F. A., Hsu, P. D., Wright, J., Agarwala, V., Scott, D. A., & Zhang, F. (2013). Genome engineering using the CRISPR-Cas9 system. *Nat Protoc, 8*(11), 2281-2308. doi:10.1038/nprot.2013.143

Ransohoff, R. M., & El Khoury, J. (2015). Microglia in Health and Disease. *Cold Spring Harb Perspect Biol, 8*(1), a020560. doi:10.1101/cshperspect.a020560
Rappsilber, J., Ishihama, Y., & Mann, M. (2003). Stop and go extraction tips for matrix-assisted laser desorption/ionization, nanoelectrospray, and LC/MS sample pretreatment in proteomics. *Anal Chem, 75*(3), 663-670. doi:10.1021/ac026117i
Rascovsky, K., Hodges, J. R., Knopman, D., Mendez, M. F., Kramer, J. H., Neuhaus, J., . . . Miller, B. L. (2011). Sensitivity of revised diagnostic criteria for the behavioural variant of frontotemporal dementia. *Brain, 134*(Pt 9), 2456-2477. doi:10.1093/brain/awr179
Rauchmann, B.-S., Brendel, M., Franzmeier, N., Trappmann, L., Zaganjori, M., Morenas-Rodriguez, E., . . . Perneczky, R. (2022). MRI connectivity-based spread of microglial activation in early Alzheimer's disease. *medRxiv*, 2022.2002.2022.22271354. doi:10.1101/2022.02.22.22271354
Raulin, A.-C., Doss, S. V., Trottier, Z. A., Ikezu, T. C., Bu, G., & Liu, C.-C. (2022). ApoE in Alzheimer's disease: pathophysiology and therapeutic strategies. *Molecular Neurodegeneration, 17*(1), 72. doi:10.1186/s13024-022-00574-4
Reifschneider, A., Robinson, S., van Lengerich, B., Gnorich, J., Logan, T., Heindl, S., . . . Haass, C. (2022). Loss of TREM2 rescues hyperactivation of microglia, but not lysosomal deficits and neurotoxicity in models of progranulin deficiency. *EMBO J, 41*(4), e109108. doi:10.15252/embj.2021109108
Reisberg, B., & Gauthier, S. (2008). Current evidence for subjective cognitive impairment (SCI) as the pre-mild cognitive impairment (MCI) stage of subsequently manifest Alzheimer's disease. *Int Psychogeriatr, 20*(1), 1-16. doi:10.1017/S1041610207006412
Reisberg, B., Prichep, L., Mosconi, L., John, E. R., Glodzik-Sobanska, L., Boksay, I., . . . de Leon, M. J. (2008). The pre-mild cognitive impairment, subjective cognitive impairment stage of Alzheimer's disease. *Alzheimers Dement, 4*(1 Suppl 1), S98-S108. doi:10.1016/j.jalz.2007.11.017
Rhinn, H., Tatton, N., McCaughey, S., Kurnellas, M., & Rosenthal, A. (2022). Progranulin as a therapeutic target in neurodegenerative diseases. *Trends Pharmacol Sci, 43*(8), 641-652. doi:10.1016/j.tips.2021.11.015
Roberson, E. D., Scearce-Levie, K., Palop, J. J., Yan, F., Cheng, I. H., Wu, T., . . . Mucke, L. (2007). Reducing endogenous tau ameliorates amyloid beta-induced deficits in an Alzheimer's disease mouse model. *Science, 316*(5825), 750-754. doi:10.1126/science.1141736
Rupprecht, R., Papadopoulos, V., Rammes, G., Baghai, T. C., Fan, J., Akula, N., . . . Schumacher, M. (2010). Translocator protein (18 kDa) (TSPO) as a therapeutic target for neurological and psychiatric disorders. *Nat Rev Drug Discov, 9*(12), 971-988. doi:10.1038/nrd3295
Saade, M., Araujo de Souza, G., Scavone, C., & Kinoshita, P. F. (2021). The Role of GPNMB in Inflammation. *Front Immunol, 12*, 674739. doi:10.3389/fimmu.2021.674739
Safaiyan, S., Besson-Girard, S., Kaya, T., Cantuti-Castelvetri, L., Liu, L., Ji, H., . . . Simons, M. (2021). White matter aging drives microglial diversity. *Neuron, 109*(7), 1100-1117.e1110. doi:10.1016/j.neuron.2021.01.027
Sala Frigerio, C., Wolfs, L., Fattorelli, N., Thrupp, N., Voytyuk, I., Schmidt, I., . . . De Strooper, B. (2019). The Major Risk Factors for Alzheimer's Disease: Age, Sex, and Genes Modulate the Microglia Response to Aβ Plaques. *Cell Rep, 27*(4), 1293-1306.e1296. doi:10.1016/j.celrep.2019.03.099
Salter, M. W., & Stevens, B. (2017). Microglia emerge as central players in brain disease. *Nat Med, 23*(9), 1018-1027. doi:10.1038/nm.4397
Sanchez-Valle, R., Heslegrave, A., Foiani, M. S., Bosch, B., Antonell, A., Balasa, M., . . . Fox, N. C. (2018). Serum neurofilament light levels correlate with severity measures

and neurodegeneration markers in autosomal dominant Alzheimer's disease. *Alzheimers Res Ther, 10*(1), 113. doi:10.1186/s13195-018-0439-y

Satoh, J. I., Kino, Y., Yanaizu, M., Ishida, T., & Saito, Y. (2019). Microglia express GPNMB in the brains of Alzheimer's disease and Nasu-Hakola disease. *Intractable Rare Dis Res, 8*(2), 120-128. doi:10.5582/irdr.2019.01049

Schlepckow, K., Kleinberger, G., Fukumori, A., Feederle, R., Lichtenthaler, S. F., Steiner, H., & Haass, C. (2017). An Alzheimer-associated TREM2 variant occurs at the ADAM cleavage site and affects shedding and phagocytic function. *EMBO Mol Med, 9*(10), 1356-1365. doi:10.15252/emmm.201707672

Schlepckow, K., Monroe, K. M., Kleinberger, G., Cantuti-Castelvetri, L., Parhizkar, S., Xia, D., . . . Haass, C. (2020). Enhancing protective microglial activities with a dual function TREM2 antibody to the stalk region. *EMBO Mol Med, 12*(4), e11227. doi:10.15252/emmm.201911227

Schmitz, M., Llorens, F., Pracht, A., Thom, T., Correia, A., Zafar, S., . . . Zerr, I. (2016). Regulation of human cerebrospinal fluid malate dehydrogenase 1 in sporadic Creutzfeldt-Jakob disease patients. *Aging (Albany NY), 8*(11), 2927-2935. doi:10.18632/aging.101101

Schöll, M., Maass, A., Mattsson, N., Ashton, N. J., Blennow, K., Zetterberg, H., & Jagust, W. (2019). Biomarkers for tau pathology. *Mol Cell Neurosci, 97*, 18-33. doi:10.1016/j.mcn.2018.12.001

Sebastian Monasor, L., Muller, S. A., Colombo, A. V., Tanrioever, G., Konig, J., Roth, S., . . . Tahirovic, S. (2020). Fibrillar Abeta triggers microglial proteome alterations and dysfunction in Alzheimer mouse models. *Elife, 9*. doi:10.7554/eLife.54083

Seelaar, H., Rohrer, J. D., Pijnenburg, Y. A., Fox, N. C., & van Swieten, J. C. (2011). Clinical, genetic and pathological heterogeneity of frontotemporal dementia: a review. *J Neurol Neurosurg Psychiatry, 82*(5), 476-486. doi:10.1136/jnnp.2010.212225

Selkoe, D. J. (2001). Clearing the brain's amyloid cobwebs. *Neuron, 32*(2), 177-180. doi:10.1016/s0896-6273(01)00475-5

Selkoe, D. J., & Hardy, J. (2016). The amyloid hypothesis of Alzheimer's disease at 25 years. *EMBO Mol Med, 8*(6), 595-608. doi:10.15252/emmm.201606210

Shaw, L. M., Vanderstichele, H., Knapik-Czajka, M., Clark, C. M., Aisen, P. S., Petersen, R. C., . . . Alzheimer's Disease Neuroimaging, I. (2009). Cerebrospinal fluid biomarker signature in Alzheimer's disease neuroimaging initiative subjects. *Ann Neurol, 65*(4), 403-413. doi:10.1002/ana.21610

Shimamoto, C., Ohnishi, T., Maekawa, M., Watanabe, A., Ohba, H., Arai, R., . . . Yoshikawa, T. (2014). Functional characterization of FABP3, 5 and 7 gene variants identified in schizophrenia and autism spectrum disorder and mouse behavioral studies. *Hum Mol Genet, 23*(24), 6495-6511. doi:10.1093/hmg/ddu369

Shioda, N., Yabuki, Y., Kobayashi, Y., Onozato, M., Owada, Y., & Fukunaga, K. (2014). FABP3 protein promotes alpha-synuclein oligomerization associated with 1-methyl-1,2,3,6-tetrahydropiridine-induced neurotoxicity. *J Biol Chem, 289*(27), 18957-18965. doi:10.1074/jbc.M113.527341

Sims, R., van der Lee, S. J., Naj, A. C., Bellenguez, C., Badarinarayan, N., Jakobsdottir, J., . . . Schellenberg, G. D. (2017). Rare coding variants in PLCG2, ABI3, and TREM2 implicate microglial-mediated innate immunity in Alzheimer's disease. *Nat Genet, 49*(9), 1373-1384. doi:10.1038/ng.3916

Sitia, R., & Rubartelli, A. (2020). Evolution, role in inflammation, and redox control of leaderless secretory proteins. *J Biol Chem, 295*(22), 7799-7811. doi:10.1074/jbc.REV119.008907

Sleegers, K., Brouwers, N., Van Damme, P., Engelborghs, S., Gijselinck, I., van der Zee, J., . . . Van Broeckhoven, C. (2009). Serum biomarker for progranulin-associated

frontotemporal lobar degeneration. *Ann Neurol, 65*(5), 603-609. doi:10.1002/ana.21621
Smith, K. R., Damiano, J., Franceschetti, S., Carpenter, S., Canafoglia, L., Morbin, M., . . . Berkovic, S. F. (2012). Strikingly different clinicopathological phenotypes determined by progranulin-mutation dosage. *Am J Hum Genet, 90*(6), 1102-1107. doi:10.1016/j.ajhg.2012.04.021
Song, W., Hooli, B., Mullin, K., Jin, S. C., Cella, M., Ulland, T. K., . . . Colonna, M. (2017). Alzheimer's disease-associated TREM2 variants exhibit either decreased or increased ligand-dependent activation. *Alzheimers Dement, 13*(4), 381-387. doi:10.1016/j.jalz.2016.07.004
Song, W. M., & Colonna, M. (2018). The Microglial Response to Neurodegenerative Disease. *Adv Immunol, 139*, 1-50. doi:10.1016/bs.ai.2018.04.002
Spittau, B. (2017). Aging Microglia-Phenotypes, Functions and Implications for Age-Related Neurodegenerative Diseases. *Front Aging Neurosci, 9*, 194. doi:10.3389/fnagi.2017.00194
Stenmark, H. (2009). Rab GTPases as coordinators of vesicle traffic. *Nat Rev Mol Cell Biol, 10*(8), 513-525. doi:10.1038/nrm2728
Steyer, B., Bu, Q., Cory, E., Jiang, K., Duong, S., Sinha, D., . . . Saha, K. (2018). Scarless Genome Editing of Human Pluripotent Stem Cells via Transient Puromycin Selection. *Stem Cell Reports, 10*(2), 642-654. doi:10.1016/j.stemcr.2017.12.004
Suarez-Calvet, M., Araque Caballero, M. A., Kleinberger, G., Bateman, R. J., Fagan, A. M., Morris, J. C., . . . Dominantly Inherited Alzheimer, N. (2016). Early changes in CSF sTREM2 in dominantly inherited Alzheimer's disease occur after amyloid deposition and neuronal injury. *Sci Transl Med, 8*(369), 369ra178. doi:10.1126/scitranslmed.aag1767
Suarez-Calvet, M., Kleinberger, G., Araque Caballero, M. A., Brendel, M., Rominger, A., Alcolea, D., . . . Haass, C. (2016). sTREM2 cerebrospinal fluid levels are a potential biomarker for microglia activity in early-stage Alzheimer's disease and associate with neuronal injury markers. *EMBO Mol Med, 8*(5), 466-476. doi:10.15252/emmm.201506123
Suarez-Calvet, M., Morenas-Rodriguez, E., Kleinberger, G., Schlepckow, K., Araque Caballero, M. A., Franzmeier, N., . . . Alzheimer's Disease Neuroimaging, I. (2019). Early increase of CSF sTREM2 in Alzheimer's disease is associated with tau related-neurodegeneration but not with amyloid-beta pathology. *Mol Neurodegener, 14*(1), 1. doi:10.1186/s13024-018-0301-5
Sudre, C. H., Bocchetta, M., Heller, C., Convery, R., Neason, M., Moore, K. M., . . . On behalf of, G. (2019). White matter hyperintensities in progranulin-associated frontotemporal dementia: A longitudinal GENFI study. *Neuroimage Clin, 24*, 102077. doi:10.1016/j.nicl.2019.102077
Sun, H. Q., Kwiatkowska, K., Wooten, D. C., & Yin, H. L. (1995). Effects of CapG overexpression on agonist-induced motility and second messenger generation. *J Cell Biol, 129*(1), 147-156. doi:10.1083/jcb.129.1.147
Sun, W., Suzuki, K., Toptunov, D., Stoyanov, S., Yuzaki, M., Khiroug, L., & Dityatev, A. (2019). In vivo Two-Photon Imaging of Anesthesia-Specific Alterations in Microglial Surveillance and Photodamage-Directed Motility in Mouse Cortex. *Front Neurosci, 13*, 421. doi:10.3389/fnins.2019.00421
Swift, I. J., Sogorb-Esteve, A., Heller, C., Synofzik, M., Otto, M., Graff, C., . . . Rohrer, J. D. (2021). Fluid biomarkers in frontotemporal dementia: past, present and future. *J Neurol Neurosurg Psychiatry, 92*(2), 204-215. doi:10.1136/jnnp-2020-323520
Takada, L. T. (2015). The Genetics of Monogenic Frontotemporal Dementia. *Dement Neuropsychol, 9*(3), 219-229. doi:10.1590/1980-57642015DN93000003

Takahashi, K., Rochford, C. D., & Neumann, H. (2005). Clearance of apoptotic neurons without inflammation by microglial triggering receptor expressed on myeloid cells-2. *J Exp Med, 201*(4), 647-657. doi:10.1084/jem.20041611

Takalo, M., Wittrahm, R., Wefers, B., Parhizkar, S., Jokivarsi, K., Kuulasmaa, T., . . . Haass, C. (2020). The Alzheimer's disease-associated protective Plcgamma2-P522R variant promotes immune functions. *Mol Neurodegener, 15*(1), 52. doi:10.1186/s13024-020-00402-7

Tanaka, M., Yamakage, H., Muranaka, K., Yamada, T., Araki, R., Ogo, A., . . . Satoh-Asahara, N. (2022). Higher Serum Soluble TREM2 as a Potential Indicative Biomarker for Cognitive Impairment in Inadequately Controlled Type 2 Diabetes Without Obesity: The DOR-KyotoJ-1. *Front Endocrinol (Lausanne), 13*, 880148. doi:10.3389/fendo.2022.880148

Telano, L. N., & Baker, S. (2022). Physiology, Cerebral Spinal Fluid. In *StatPearls*. Treasure Island (FL).

Tellechea, P., Pujol, N., Esteve-Belloch, P., Echeveste, B., García-Eulate, M. R., Arbizu, J., & Riverol, M. (2018). Early- and late-onset Alzheimer disease: Are they the same entity? *Neurologia (Engl Ed), 33*(4), 244-253. doi:10.1016/j.nrl.2015.08.002

Thijssen, E. H., La Joie, R., Wolf, A., Strom, A., Wang, P., Iaccarino, L., . . . Treatment for Frontotemporal Lobar Degeneration, i. (2020). Diagnostic value of plasma phosphorylated tau181 in Alzheimer's disease and frontotemporal lobar degeneration. *Nat Med, 26*(3), 387-397. doi:10.1038/s41591-020-0762-2

Thornton, P., Sevalle, J., Deery, M. J., Fraser, G., Zhou, Y., Stahl, S., . . . Crowther, D. C. (2017). TREM2 shedding by cleavage at the H157-S158 bond is accelerated for the Alzheimer's disease-associated H157Y variant. *EMBO Mol Med, 9*(10), 1366-1378. doi:10.15252/emmm.201707673

Tijms, B. M., Gobom, J., Reus, L., Jansen, I., Hong, S., Dobricic, V., . . . Visser, P. J. (2020). Pathophysiological subtypes of Alzheimer's disease based on cerebrospinal fluid proteomics. *Brain, 143*(12), 3776-3792. doi:10.1093/brain/awaa325

Tomiyama, T., & Shimada, H. (2020). APP Osaka Mutation in Familial Alzheimer's Disease-Its Discovery, Phenotypes, and Mechanism of Recessive Inheritance. *Int J Mol Sci, 21*(4). doi:10.3390/ijms21041413

Turnbull, I. R., & Colonna, M. (2007). Activating and inhibitory functions of DAP12. *Nat Rev Immunol, 7*(2), 155-161. doi:10.1038/nri2014

Turnbull, I. R., Gilfillan, S., Cella, M., Aoshi, T., Miller, M., Piccio, L., . . . Colonna, M. (2006). Cutting edge: TREM-2 attenuates macrophage activation. *J Immunol, 177*(6), 3520-3524. doi:10.4049/jimmunol.177.6.3520

Tusher, V. G., Tibshirani, R., & Chu, G. (2001). Significance analysis of microarrays applied to the ionizing radiation response. *Proc Natl Acad Sci U S A, 98*(9), 5116-5121. doi:10.1073/pnas.091062498

Tyanova, S., Temu, T., Sinitcyn, P., Carlson, A., Hein, M. Y., Geiger, T., . . . Cox, J. (2016). The Perseus computational platform for comprehensive analysis of (prote)omics data. *Nat Methods, 13*(9), 731-740. doi:10.1038/nmeth.3901

Ulland, T. K., & Colonna, M. (2018). TREM2 - a key player in microglial biology and Alzheimer disease. *Nat Rev Neurol, 14*(11), 667-675. doi:10.1038/s41582-018-0072-1

Ulland, T. K., Song, W. M., Huang, S. C., Ulrich, J. D., Sergushichev, A., Beatty, W. L., . . . Colonna, M. (2017). TREM2 Maintains Microglial Metabolic Fitness in Alzheimer's Disease. *Cell, 170*(4), 649-663 e613. doi:10.1016/j.cell.2017.07.023

Ulrich, J. D., Finn, M. B., Wang, Y., Shen, A., Mahan, T. E., Jiang, H., . . . Holtzman, D. M. (2014). Altered microglial response to Abeta plaques in APPPS1-21 mice heterozygous for TREM2. *Mol Neurodegener, 9*, 20. doi:10.1186/1750-1326-9-20

Ulrich, J. D., Ulland, T. K., Colonna, M., & Holtzman, D. M. (2017). Elucidating the Role of TREM2 in Alzheimer's Disease. *Neuron, 94*(2), 237-248. doi:10.1016/j.neuron.2017.02.042

Ulrich, J. D., Ulland, T. K., Mahan, T. E., Nystrom, S., Nilsson, K. P., Song, W. M., . . . Holtzman, D. M. (2018). ApoE facilitates the microglial response to amyloid plaque pathology. *J Exp Med, 215*(4), 1047-1058. doi:10.1084/jem.20171265

Van Acker, Z. P., Perdok, A., Bretou, M., & Annaert, W. (2021). The microglial lysosomal system in Alzheimer's disease: Guardian against proteinopathy. *Ageing Res Rev, 71*, 101444. doi:10.1016/j.arr.2021.101444

Van Damme, P., Van Hoecke, A., Lambrechts, D., Vanacker, P., Bogaert, E., van Swieten, J., . . . Robberecht, W. (2008). Progranulin functions as a neurotrophic factor to regulate neurite outgrowth and enhance neuronal survival. *J Cell Biol, 181*(1), 37-41. doi:10.1083/jcb.200712039

van der Ende, E. L., Meeter, L. H., Stingl, C., van Rooij, J. G. J., Stoop, M. P., Nijholt, D. A. T., . . . van Swieten, J. C. (2019). Novel CSF biomarkers in genetic frontotemporal dementia identified by proteomics. *Ann Clin Transl Neurol, 6*(4), 698-707. doi:10.1002/acn3.745

van der Ende, E. L., Morenas-Rodriguez, E., McMillan, C., Grossman, M., Irwin, D., Sanchez-Valle, R., . . . Seelaar, H. (2021). CSF sTREM2 is elevated in a subset in GRN-related frontotemporal dementia. *Neurobiol Aging, 103*, 158 e151-158 e155. doi:10.1016/j.neurobiolaging.2021.02.024

van der Poel, M., Ulas, T., Mizee, M. R., Hsiao, C. C., Miedema, S. S. M., Adelia, . . . Huitinga, I. (2019). Transcriptional profiling of human microglia reveals grey-white matter heterogeneity and multiple sclerosis-associated changes. *Nat Commun, 10*(1), 1139. doi:10.1038/s41467-019-08976-7

van Duijn, C. M., Clayton, D., Chandra, V., Fratiglioni, L., Graves, A. B., Heyman, A., . . . et al. (1991). Familial aggregation of Alzheimer's disease and related disorders: a collaborative re-analysis of case-control studies. *Int J Epidemiol, 20 Suppl 2*, S13-20. doi:10.1093/ije/20.supplement_2.s13

Virgilio, E., De Marchi, F., Contaldi, E., Dianzani, U., Cantello, R., Mazzini, L., & Comi, C. (2022). The Role of Tau beyond Alzheimer's Disease: A Narrative Review. *Biomedicines, 10*(4). doi:10.3390/biomedicines10040760

Wagner, M., Lorenz, G., Volk, A. E., Brunet, T., Edbauer, D., Berutti, R., . . . Winkelmann, J. (2021). Clinico-genetic findings in 509 frontotemporal dementia patients. *Mol Psychiatry, 26*(10), 5824-5832. doi:10.1038/s41380-021-01271-2

Wang, H., & Wen, T. (2022). Modulation of Rab GDP-Dissociation Inhibitor Trafficking and Expression by the Transmembrane Protein 59 (TMEM59). *Separations, 9*(11), 341. Retrieved from https://www.mdpi.com/2297-8739/9/11/341

Wang, S., Mustafa, M., Yuede, C. M., Salazar, S. V., Kong, P., Long, H., . . . Colonna, M. (2020). Anti-human TREM2 induces microglia proliferation and reduces pathology in an Alzheimer's disease model. *J Exp Med, 217*(9). doi:10.1084/jem.20200785

Wang, Y., Cella, M., Mallinson, K., Ulrich, J. D., Young, K. L., Robinette, M. L., . . . Colonna, M. (2015). TREM2 lipid sensing sustains the microglial response in an Alzheimer's disease model. *Cell, 160*(6), 1061-1071. doi:10.1016/j.cell.2015.01.049

Ward, A., Crean, S., Mercaldi, C. J., Collins, J. M., Boyd, D., Cook, M. N., & Arrighi, H. M. (2012). Prevalence of apolipoprotein E4 genotype and homozygotes (APOE e4/4) among patients diagnosed with Alzheimer's disease: a systematic review and meta-analysis. *Neuroepidemiology, 38*(1), 1-17. doi:10.1159/000334607

Watterson, A., Arneaud, S. L. B., Wajahat, N., Wall, J. M., Tatge, L., Beheshti, S. T., . . . Douglas, P. M. (2022). Loss of heat shock factor initiates intracellular lipid

surveillance by actin destabilization. *Cell Rep, 41*(3), 111493. doi:10.1016/j.celrep.2022.111493
Weggen, S., & Beher, D. (2012). Molecular consequences of amyloid precursor protein and presenilin mutations causing autosomal-dominant Alzheimer's disease. *Alzheimers Res Ther, 4*(2), 9. doi:10.1186/alzrt107
Weiner, S., Sauer, M., Visser, P. J., Tijms, B. M., Vorontsov, E., Blennow, K., . . . Gobom, J. (2022). Optimized sample preparation and data analysis for TMT proteomic analysis of cerebrospinal fluid applied to the identification of Alzheimer's disease biomarkers. *Clin Proteomics, 19*(1), 13. doi:10.1186/s12014-022-09354-0
Weisheit, I., Kroeger, J. A., Malik, R., Klimmt, J., Crusius, D., Dannert, A., . . . Paquet, D. (2020). Detection of Deleterious On-Target Effects after HDR-Mediated CRISPR Editing. *Cell Rep, 31*(8), 107689. doi:10.1016/j.celrep.2020.107689
Weisheit, I., Kroeger, J. A., Malik, R., Wefers, B., Lichtner, P., Wurst, W., . . . Paquet, D. (2021). Simple and reliable detection of CRISPR-induced on-target effects by qgPCR and SNP genotyping. *Nat Protoc, 16*(3), 1714-1739. doi:10.1038/s41596-020-00481-2
Weissmann, R., Hüttenrauch, M., Kacprowski, T., Bouter, Y., Pradier, L., Bayer, T. A., . . . Wirths, O. (2016). Gene Expression Profiling in the APP/PS1KI Mouse Model of Familial Alzheimer's Disease. *Journal of Alzheimer's Disease, 50*, 397-409. doi:10.3233/JAD-150745
Whitwell, J. L. (2019). FTD spectrum: Neuroimaging across the FTD spectrum. *Prog Mol Biol Transl Sci, 165*, 187-223. doi:10.1016/bs.pmbts.2019.05.009
WHO, W. H. O. (2017). Global action plan on the public health response to dementia 2017–2025.
Wilson, E. N., Swarovski, M. S., Linortner, P., Shahid, M., Zuckerman, A. J., Wang, Q., . . . Andreasson, K. I. (2020). Soluble TREM2 is elevated in Parkinson's disease subgroups with increased CSF tau. *Brain, 143*(3), 932-943. doi:10.1093/brain/awaa021
Wirth, M., Madison, C. M., Rabinovici, G. D., Oh, H., Landau, S. M., & Jagust, W. J. (2013). Alzheimer's disease neurodegenerative biomarkers are associated with decreased cognitive function but not beta-amyloid in cognitively normal older individuals. *J Neurosci, 33*(13), 5553-5563. doi:10.1523/JNEUROSCI.4409-12.2013
Wisniewski, J. R., Zougman, A., & Mann, M. (2009). Combination of FASP and StageTip-based fractionation allows in-depth analysis of the hippocampal membrane proteome. *J Proteome Res, 8*(12), 5674-5678. doi:10.1021/pr900748n
Wood, E. M., Falcone, D., Suh, E., Irwin, D. J., Chen-Plotkin, A. S., Lee, E. B., . . . Grossman, M. (2013). Development and validation of pedigree classification criteria for frontotemporal lobar degeneration. *JAMA Neurol, 70*(11), 1411-1417. doi:10.1001/jamaneurol.2013.3956
Wunderlich, P., Glebov, K., Kemmerling, N., Tien, N. T., Neumann, H., & Walter, J. (2013). Sequential proteolytic processing of the triggering receptor expressed on myeloid cells-2 (TREM2) protein by ectodomain shedding and gamma-secretase-dependent intramembranous cleavage. *J Biol Chem, 288*(46), 33027-33036. doi:10.1074/jbc.M113.517540
Xiang, X., Werner, G., Bohrmann, B., Liesz, A., Mazaheri, F., Capell, A., . . . Haass, C. (2016). TREM2 deficiency reduces the efficacy of immunotherapeutic amyloid clearance. *EMBO Mol Med, 8*(9), 992-1004. doi:10.15252/emmm.201606370
Xiang, X., Wind, K., Wiedemann, T., Blume, T., Shi, Y., Briel, N., . . . Brendel, M. (2021). Microglial activation states drive glucose uptake and FDG-PET alterations in neurodegenerative diseases. *Sci Transl Med, 13*(615), eabe5640. doi:10.1126/scitranslmed.abe5640

Xu, F., Han, L., Wang, Y., Deng, D., Ding, Y., Zhao, S., . . . Chen, X. (2023). Prolonged anesthesia induces neuroinflammation and complement-mediated microglial synaptic elimination involved in neurocognitive dysfunction and anxiety-like behaviors. *BMC Medicine, 21*(1), 7. doi:10.1186/s12916-022-02705-6

Yao, R., Pan, R., Shang, C., Li, X., Cheng, J., Xu, J., & Li, Y. (2020). Translocator Protein 18 kDa (TSPO) Deficiency Inhibits Microglial Activation and Impairs Mitochondrial Function. *Front Pharmacol, 11*, 986. doi:10.3389/fphar.2020.00986

Zerr, I., Villar-Pique, A., Schmitz, V. E., Poleggi, A., Pocchiari, M., Sanchez-Valle, R., . . . Schmitz, M. (2019). Evaluation of Human Cerebrospinal Fluid Malate Dehydrogenase 1 as a Marker in Genetic Prion Disease Patients. *Biomolecules, 9*(12). doi:10.3390/biom9120800

Zetterberg, H. (2016). Neurofilament Light: A Dynamic Cross-Disease Fluid Biomarker for Neurodegeneration. *Neuron, 91*(1), 1-3. doi:10.1016/j.neuron.2016.06.030

Zetterberg, H., & Bendlin, B. B. (2021). Biomarkers for Alzheimer's disease-preparing for a new era of disease-modifying therapies. *Mol Psychiatry, 26*(1), 296-308. doi:10.1038/s41380-020-0721-9

Zetterberg, H., & Blennow, K. (2021). Moving fluid biomarkers for Alzheimer's disease from research tools to routine clinical diagnostics. *Mol Neurodegener, 16*(1), 10. doi:10.1186/s13024-021-00430-x

Zhang, Y., Kent, J. W., 2nd, Lee, A., Cerjak, D., Ali, O., Diasio, R., . . . Kissebah, A. H. (2013). Fatty acid binding protein 3 (fabp3) is associated with insulin, lipids and cardiovascular phenotypes of the metabolic syndrome through epigenetic modifications in a Northern European family population. *BMC Med Genomics, 6*, 9. doi:10.1186/1755-8794-6-9

Zhang, Y.-w., Thompson, R., Zhang, H., & Xu, H. (2011). APP processing in Alzheimer's disease. *Molecular Brain, 4*(1), 3. doi:10.1186/1756-6606-4-3

Zhong, L., Wang, Z., Wang, D., Wang, Z., Martens, Y. A., Wu, L., . . . Chen, X. F. (2018). Amyloid-beta modulates microglial responses by binding to the triggering receptor expressed on myeloid cells 2 (TREM2). *Mol Neurodegener, 13*(1), 15. doi:10.1186/s13024-018-0247-7

Zhou, C., Shang, W., Yin, S.-K., Shi, H., & Ying, W. (2021). Malate-Aspartate Shuttle Plays an Important Role in LPS-Induced Neuroinflammation of Mice Due to its Effect on STAT3 Phosphorylation. *Frontiers in Molecular Biosciences, 8*. doi:10.3389/fmolb.2021.655687

Zhou, X., Sun, L., Bastos de Oliveira, F., Qi, X., Brown, W. J., Smolka, M. B., . . . Hu, F. (2015). Prosaposin facilitates sortilin-independent lysosomal trafficking of progranulin. *J Cell Biol, 210*(6), 991-1002. doi:10.1083/jcb.201502029

Zhou, Y., Song, W. M., Andhey, P. S., Swain, A., Levy, T., Miller, K. R., . . . Colonna, M. (2020). Human and mouse single-nucleus transcriptomics reveal TREM2-dependent and TREM2-independent cellular responses in Alzheimer's disease. *Nat Med, 26*(1), 131-142. doi:10.1038/s41591-019-0695-9

Zhuang, L., Mao, Y., Liu, Z., Li, C., Jin, Q., Lu, L., . . . Chen, K. (2021). FABP3 Deficiency Exacerbates Metabolic Derangement in Cardiac Hypertrophy and Heart Failure via PPARalpha Pathway. *Front Cardiovasc Med, 8*, 722908. doi:10.3389/fcvm.2021.722908

List of abbreviations

3R tau isoforms	tau isoform with 3 microtubule-binding repeats
4R tau isoforms	tau isoform with 4 microtubule-binding repeats
A/T/N	amyloid/tau/neurodegeneration
ABC	ammonium bicarbonate
ABCA7	ATP-binding cassette transporter A7
ABI3	abscisic acid intensive 3
AD	Alzheimer's disease
ADAD	autosomal dominant AD
ADAM10	a disintegrin and metalloproteinase domain-containing protein 10
ADAM17	a disintegrin and metalloproteinase domain-containing protein 17
AGC	automatic gain control
AICD	APP intracellular domain
AKT	protein kinase B
ALS	amyotrophic lateral sclerosis
AMI	acute myocardial infarction
APOE	apolipoprotein E
APP	amyloid precursor protein
ARM	activated response microglia
ARTFL	Advancing research & treatment for frontotemporal lobar degeneration
Aβ	amyloid β
Aβ38	amyloid β 38 amino acids long
Aβ40	amyloid β 40 amino acids long

Aβ42	amyloid β 42 amino acids long
BAF	B allele frequencies
BCA	bicinchoninic acid
BIN1	myc box-dependent-interacting protein 1
bp	base pair
BSA	bovine serum albumin
bvFTD	behavioral variant FTD
C9ORF72	chromosome 9 open reading frame 72
CAPG	macrophage-capping protein
Cas9	CRISPR-associated endonuclease Cas9
CBD	corticobasal degeneration
CD2AP	CD2 associated protein
CFD	cutting frequency determination
CHMP2B	charged multivesicular body protein 2B gene
CJD	Creutzfeldt-Jakob disease
CLEC7A	C-type lectin domain family 7 member A
CLU	clusterin
CNC	Cognitively normal controls
CNS	central nervous system
CON	control
CR1	complement receptor 1
CR3A	complement receptor 3 alpha
CRISPR	clustered regularly interspaced short palindromic repeats
CSF	cerebrospinal fluid
CTSA	cathepsin A

CTSB	cathepsin B
CTSC	cathepsin C
CTSD	cathepsin D
CTSL	cathepsin L
CTSS	cathepsin S
CTSZ	cathepsin Z
CX3CL1	chemokine ligand 1
CX3CR1	CX3C chemokine receptor 1
DAM	disease-associated microglia
DAM1	disease-associated microglia 1 (TREM2-independent activation)
DAM2	disease-associated microglia 2 (TREM2-dependent activation)
DAP12	DNAX activation protein of 12kDa
DAPI	4',6-diamidino-2-phenylindole
DC-HIL	dendritic cell heparan sulfate proteoglycan integrin-dependent ligand
DDA	data dependent acquisition
DIA	data independent acquisition
DLB	dementia with Lewy bodies
DMSO	dimethyl sulfoxide
DNA	deoxyribonucleic acid
DNTPs	deoxynucleoside triphosphates
DPR	dipeptide repeat
DTT	dithiothreitol
EAE	experimental autoimmune encephalomyelitis
EDTA	ethylenediaminetetraacetic acid
ELISA	enzyme-linked immunosorbent assay

EMIF-AD MBD	European Medical Information Framework Alzheimer's Disease Multimodal Biomarker Discovery
EOAD	early-onset AD
ERK	extracellular-signal-regulated kinase
EWS	Ewing's sarcoma
f-FTD	familial FTD
FA	formic acid
FABP3	fatty acid binding protein 3
FASP	filter aided sample preparation
FDG-PET	(18F)-fluorodeoxyglucose (FDG)-PET
FET	FUS, EWS, and TAF15
FTD	frontotemoral dementia
FTD-ALS	amyotrophic lateral sclerosis with frontotemporal dementia
FTD-GRN	FTD caused by heterozygous mutation in the *GRN* gene
FTD-MND	FTD combined with motorneuron disease
FTLD	frontotemporal lobar degeneration
FTLD-FET	frontotemporal lobar degeneration with FET-positive inclusions
FTLD-tau	frontotemporal lobar degeneration with tau-positive inclusions
FTLD-TDP	frontotemporal lobar degeneration with TDP-43-positive inclusions
FTLD-U	frontotemporal lobar degeneration with ubiquitin-positive inclusions
FUS	fused in sarcoma
GDI1	GDP dissociation inhibitor-1
GENFI	The Genetic FTD initiative
GPNMB	glycoprotein non-metastatic melanoma protein B
GRN	progranulin encoding gene
gRNA	guide RNA

GWAS	genome-wide association studies
HBSS	Hank's balanced salt solution
hCSF	human CSF
HEPES	N-2-hydroxyethylpiperazine-N-2-ethane sulfonic acid
HGFIN	hematopoietic growth factor inducible neurokinin-1 type
hiMGL	human-iPSC-derived microglia
HPC	hematopoietic progenito cell
HPLC	high-performance liquid chromatography
HRE	hexanucleotide repeat expansion
HSF-1	heat shock factor 1
i.d.	inner diameter
IAA	iodoacetamide
IL-6	interleukin-6
INPP5D	inositol polyphosphate-5-phosphatase D
IP3	inositol trisphosphate
iPSC	induced pluripotent stem cell
ITAM	immunoreceptor tyrosine-based activation motif
ITGAM	integrin alpha M
ITGAX	integrin subunit alpha X
IVC	individually ventilated cages
kDa	kilodaltons
ko	knockout
LC-MS	liquid chromatography–mass spectrometry
LC-MS/MS	liquid chromatography tandem mass spectrometry
LEFFTDS	Longitudinal evaluation of familial frontotemporal dementia subject

LFQ	label-free quantification
LOAD	late-onset AD
LOF	loss-of-function
LOF	loss-of-function
LPL	lipoprotein lipase
LPS	lipopolysaccharide
LRP1	lipoprotein receptor-related protein 1
lv-PPA	logopenic variant PPA
LYZ2	lysozyme C-2 (mouse)
M-CSF	macrophage colony-stimulating factor
M6PR	mannose 6-phosohate receptor
MACS	magnetic-activated cell sorting
MAPT	microtubule associated protein tau
MCI	mild cognitive impairment
mCSF	mouse CSF
MDH1	malate dehydrogenase 1
MGnD	microglial neurodegenerative phenotype
MIMS	microglia inflamed in MS
MMF	medetomidine-midazolam-fentanyl
MND	motorneuron disease
MRI	magnetic resonance imaging
mRNA	messenger RNA
MS/MS	tandem mass spectrometry
MS4A6A	membrane-spanning 4-domains subfamily A6A
MS4A6E	membrane-spanning 4-domains subfamily A6E

NaCl	sodium chloride
NCL	neuronal ceroid lipofuscinosis
NCRAD	National centralized repository for Alzheimer's Disease and related dementias
NFL	neurofilament light
NFT	nerofibrillary tangle
nfv-PPA	non-fluent variant PPA
NHD	Nasu-Hakola disease
o.d.	outer diameter
p-tau	phosphorylated tau
p-tau181	phosphorylated tau, phosphorylated at site 181
p-tau217	phosphorylated tau, phosphorylated at site 217
P2RY12	P2Y purinoceptor 12
PAD	peripheral artery disease
PAM	proliferative-region-associated microglia
PBS	phosphate-buffered saline
PCR	polymerase chain reaction
PET	positron emission tomography
PGRN	progranulin (protein)
Pi	protease inhibitor
PI3K	phosphatidylinositol 3-kinases
PiB-PET	[18F] florbetapir, or Pitsburgh compound-B-PET
PICALM	phosphatidylinositol binding clathrin assembly protein
PLCG2	phospholipase C gamma 2
PLOSL	polycystic lipomembranous osteodysplasia leukoencephalopathy
PPA	primary progressive aphasia

PRR	pattern recognition receptors
PSAP	prosaposin
PSEN1	presenilin 1
PSEN2	presenilin 2
PSP	progressive supranuclear palsy
qPCR	quantitiative PCR
RFLP	restriction fragment length polymorphism technique
RIPA	radioimmunoprecipitatio assay
RNA	ribonucleic acid
ROS	reactive oxygen species
sAPPβ	soluble amyloid β
SCI	subjective cognitive impairment
scRNAseq	single-cell RNA sequencing
SDC	sodium deoxycholate
SDS	sodium dodecyl sulfate
SMC	subjective membory complaint
SNP	single-nucleotide polymorphism
SORL1	sortilin related receptor 1
SORT1	sortilin
SP3	single-pot, solid-phase-enhanced sample preparation
SPI1	transcription factor PU.1
SPP1	osteopontin
SQSTM1	sequestosome 1
SSEA4	stage-specific embryonic antigen-4
STET	sodium chloride-Tris-Cl-EDTA-Triton X-100

sTREM2	soluble TREM2
sv-PPA	semantic variant PPA
SYK	tyrosine-protein kinase SYK
TAF15	TATA-binding protein-associated factor 15
TARDBP	transactive response DNA-binding protein
TCA	tricarboxylic acid
TDP-43	transactive response DNA-binding protein 43
TGF-β	transforming growth factor β
TRA160	podocalyxin
TREM2	triggering receptor expressed on myeloid cells 2
TSPO	translocator protein
TSPO-PET	translocator protein 18kDa-positron emission tomography
Ub	ubiquitination
UHPLC	Ultra-High-Performance Liquid Chromatography
VCP	valosin containing protein
VTN	vitronectin
WAM	white matter-associated microglia
WT	wild-type
XLID	X-linked intellectual disability

List of figures

List of tables

Acknowledgements

I thought the acknowledgment part would be easy as the gratefulness that I am feeling is beyond obvious to me, but now I've come to realize that words of any language will not be enough to explain how thankful I am. I will try my best.

First, I would like to thank my mentor and thesis advisor, Christian Haass. It's impossible not to comment on the enthusiastic atmosphere that you create in the lab. It is fun and inspiring - just like science should be! In addition to your great enthusiasm, I really want to thank you for believing in me. Not only by offering me (then a bachelor student) the position as a PhD student, but especially for your constant encouragement of new thoughts, questions and ideas. No matter how good, bad or crazy the idea or question may be, you welcome them all and for that I am extremely thankful. My curiosity is part of who I am as a scientist and thanks to you I will never doubt to express it!

To the members of my thesis advisory committee, Stefan Lichtenthaler and Henrik Zetterberg, thank you for your support and guidance throughout my PhD studies. Your expertise has been invaluable to me and it will continue to be.

Many thanks to the Graduate School of Systemic Neuroscience (GSN) and the International Max Planck Research School for Molecular Life Sciences (IMPRS-LS) for giving me the opportunity to be part of the fast-track PhD program.

A very special thanks to all the members of the Haass Lab, also known as the lab family. It's truly been a pleasure to work with you all! I especially want to thank Alice Sülzen for being a fantastic colleague and friend. The warmest of thanks also to the smart, funny and slightly weird women Maria Mühlhofer and Sophie Robinson, who have not only helped me with my project and the writing of my thesis but they have also been a great support and the best desk-buddies one can ask for.

I would also like to thank all the former members of the lab, with a special thanks to Gernot Kleinberger and Nadine Pettkus who supervised me when I arrived in the lab back in 2016. Another former member of the Haass Lab who I'm very thankful to have met and worked with is Samira Parhizkar. Thank you for teaching me how to collect CSF from mice, for being my supervisor(-ish) and of course for being a great friend and support.

This project would not at all be possible without Stephan Müller, who has been like an extra supervisor to me and guided me through the world of proteomics. I am beyond grateful for all your help and support!

Big thanks to Alana Darcher, a great collaborator and an invaluable friend.

Many thanks to Manuela Schneider, Anne von Thaden, Gerda Mitteregger-Kretzschmar and the teams working at the mouse facilities at CSD and ZNP. You do not only make the mouse-related work possible, but your efforts and organization are very much appreciated as it has facilitated the planning and execution of my experiments.

I want to express my deepest gratitude to all the patients, families and research efforts that have made this project possible. Without you there would be no clinical research. I would also like to thank all other collaborators who were part of this project and made this possible.

Last but not least, I want to thank my friends and family. With a special thanks to my grandma, Varpu Pesämaa, my aunt, Ulla Andersson, and my dearest friend, Emelie Nyman - det finns inte nog med ord i denna värld för att beskriva hur fantastiska ni är!

Author contributions

I hereby declare that the following authors contributed to the data presented in this study as following specified:

Prof. Christian Haass and Ida Pesämaa, together with Dr. Stephan Müller and Prof. Stefan Lichtenthaler, designed the proteomics studies of mice, hiMGL and the human CSF from the ALLFTD cohort.

Prof. Henrik Zetterberg, as a member of the thesis advisory committee, co-supervised the project.

Ida Pesämaa and Dr. Stephan Müller performed the mass spectrometry-based proteomic analysis for this study.

Ida Pesämaa and Anna Berghofer prepared all samples prior to mass spectrometry analysis.

Sophie Robinson designed and generated the hiMGL lines used in this study. In addition, she performed the qPCR and imaging analysis of these cells. All under the supervision of Prof. Dominik Paquet.

Alana Darcher performed the machine learning-based analysis of the Panel 6 proteins.

Dr. Johan Gobom, Sophia Weiner assisted with the analysis of the data from the EMIF-AD MBD cohort.

Patient CSF was collected by the ALLFTD consortium and provided by National Centralized Repository for Alzheimer's Disease and Related Dementias (NCRAD).

All other experiments, including sample isolation from mice and hiMGL, sample processing, and data analysis were performed by Ida Pesämaa.

Yours sincerely,

Place, date

Ida Pesämaa Prof. Christian Haass